ELECTRICAL PROPERTIES OF EPITAXIAL FILMS OF PbTe , PbSe AND PbS

by Raymond Frank EGERTON , B. A.

A thesis submitted for the
Degree of Doctor of Philosophy
in the University of London

Materials Section
Department of Electrical Engineering
Imperial College of Science and Technology

September 1968

ABSTRACT

Epitaxial films of the semiconductors lead telluride, lead selenide and lead sulphide have been produced by vacuum evaporation on to cleaved mica.

Film structure was examined by electron microscopy. Transmission micrographs and diffraction patterns show that under suitable growth conditions the films are well-oriented with {111} planes parallel to the substrate, but contain double-positioning boundaries. Shadowed surface replicas were used to investigate the nucleation and growth of the films.

Electrical properties were studied by means of the Hall effect. Carrier concentrations were mostly within the range 10^{17} to 10^{19} cm^{-3}. Hall mobilities at room temperature were near to those of the bulk single crystals, and increased with decreasing temperature in a similar way to previously-reported films of these materials on alkali halide substrates.

The effect of ambients was investigated by making Hall measurements on freshly-deposited films in vacuum and during subsequent exposure to various gases. Oxygen was found to have a large effect, increasing the amount of p-type conduction. The results are discussed in terms of adsorption and diffusion processes.

Field-effect measurements were carried out on PbTe and PbSe films by applying an electric field through the mica substrate. The results indicate two possible models for surface states at the mica interface : (1) Acceptor and donor levels near the middle of the band gap, each of density 2×10^{12} cm^{-2} and about $\cdot 05$ eV apart ; (2) A uniform density of 2×10^{13} states $cm^{-2}\,eV^{-1}$ within $\pm 0 \cdot 05$ eV of mid-gap. The evidence is mainly in favour of the second model. The surface-state time constant was about 100 μsec at room temperature. Small-signal measurements gave field-effect mobilities of several hundred $cm^2\,volt^{-1}\,sec^{-1}$, which suggests that the films could be suitable for thin-film-transistor applications.

ACKNOWLEDGEMENTS

The author is grateful for the sympathetic guidance of Dr. C. Juhasz, and for the support and encouragement of Professor J.C. Anderson.

I should like to thank members of the Materials Section, particularly Mr. D.L. Lile and Dr. D.P. Martin, for useful discussions.

I am also indebted to Drs. M. Green, A.J. Crocker, M.J. Lee, B. Lewis and D.J. Stirland for their helpful advice, and to the Imperial College Centre for Computation and Automation for use of the I.B.M. 7090 computer.

Thanks are also due to the Science Research Council for financial support.

CONTENTS

		Page
ABSTRACT		3
Chapter 1	PROPERTIES OF PbTe, PbSe AND PbS	
1.1	Introduction : applications	9
MATERIALS :		
1.2	Polycrystalline samples	10
1.3	Polycrystalline films	11
1.4	Single crystals	12
1.5	Single - crystal films	13
PROPERTIES :		
1.6	Crystal structure and bonding	16
1.7	Dielectric constant	16
1.8	Energy gap	17
1.9	Band structure	20
1.10	Carrier mobility and scattering mechanisms	25
Chapter 2	FILM PREPARATION	
2.1	Vacuum system	31
2.2	Evaporation assemblies : a) System A	31
	b) System B	33
2.3	Source materials	37
2.4	Evaporation proceedure	38
2.5	Calibration of film thickness monitor	39
2.6	Calibration of substrate thermocouples	41

Page

Chapter 3 ELECTRON MICROSCOPY

3.1 Transmission micrographs and diffraction patterns 43

3.2 Surface replicas 48

a) Nucleation and growth 53

b) Effect of substrate temperature 60

3.3 PbTe on PbSe 64

3.4 Discussion 66

a) Nucleation processes 67

b) Application to PbTe on mica 69

c) Growth processes 73

d) Effect of substrate temperature 74

Chapter 4 HALL MEASUREMENTS

4.1 Experimental details 78

4.2 Theory 79

4.3 Results : carrier concentrations 82

4.4 Hall coefficient as a function of temperature 85

4.5 Variation of Hall mobilities with temperature :

Results 89

Discussion : causes of mobility reduction 94

a) Surface scattering 96

b) Boundary scattering 99

c) Potential barriers 103

d) Dislocations 107

e) Effects of stress 108

f) Cracking 110

g) Compensation effects 112

Page

Chapter 5 EFFECT OF AMBIENTS

LONG - TERM EFFECTS :

5.1 Experimental results 113

5.2 Discussion 117

SHORT - TERM EFFECTS :

5.3 Experimental details 120

5.4 Results : a) 1 - carrier films 120
b) 2 - carrier films 124
c) Films coated with insulator 124

5.5 Discussion : a) 1 - carrier films 128
b) 2 - carrier films 130

5.6 Comparison of adsorption and diffusion models 136

5.7 Mechanisms for diffusion 142

Chapter 6 FIELD - EFFECT MEASUREMENTS

THEORY :

6.1 The surface space-charge region 149

6.2 Surface states 154

6.3 Surface transport 156

6.4 Experimental methods 160

RESULTS :

6.5 Large-signal measurements 164

6.6 Small-signal measurements 168

a) Field-effect mobilities 172

b) Variation with temperature 175

c) Variation with frequency 175

d) Pulsed field effect 177

Page

6.7 Discussion

a) Large-signal field effect 182

b) Small-signal field effect 185

Chapter 7 SUMMARY AND CONCLUSIONS

7.1 Structure and growth of epitaxial PbTe, PbSe and PbS films 193

7.2 Electrical properties of epitaxial films 195

7.3 Interaction of the lead salts with oxygen 197

7.4 Surface states at lead-salt surfaces 201

APPENDIX A : Hall coefficient of an inhomogeneous semiconductor 204

APPENDIX B : Computer program for surface data analysis 208

APPENDIX C : Surface transport theory 212

APPENDIX D : Publication 216

REFERENCES 219

CHAPTER 1

PROPERTIES OF PbTe , PbSe AND PbS

1.1 Applications

Although the compound semiconductors lead telluride , lead selenide and lead sulphide * have not achieved the technological importance of the elements germanium and silicon, they are of some practical as well as theoretical interest.

In fact, PbS was probably the first semiconductor to be put to use, namely for the detection of radio waves. These 'cat's whisker' detectors were eventually superseded by vacuum tubes and later by the introduction of Ge and Si diodes.

Since then, the most important application has been in the detection of infra-red radiation. Polycrystalline films of all three materials are highly sensitive for wavelengths between 1 and 7 microns , with response times better than 10^{-4} sec.

Other uses which are still being considered are as a thermoelectric element for refrigeration purposes, and to provide the semiconductor for an active device (thin film transistor) in thin film integrated circuits.

This chapter contains a description of some of the basic physical and electrical properties of the lead salts, as they appear in the light of previous research. As with silicon and germanium, these properties only became clearly understood as relatively pure and perfect materials became available.

The different forms of material which have been used, and certain properties peculiar to each of them, will be described in sections 1.2 to 1.5 . In the second half of the chapter (1.6 to 1.10) , some of the basic material properties are discussed in greater detail .

---

* hereafter referred to collectively as 'the lead salts' .

1.2 Polycrystalline (bulk) samples

The materials available to early experimenters were either naturally-occurring minerals such as galena (PbS), which could be single-crystal but were often impure, or artificially-produced microcrystalline or compressed-powder samples. The latter types contained a large amount of internal surfaces (grain boundaries) and it was difficult to decide whether the observed properties were due to bulk or to surface effects. It was later established, by direct comparison of compressed-powder and single-crystal samples, that below room temperature a large part of the resistivity of the former is due to the grain boundaries (P 16).

However, the following points were established, which showed that the lead salts could be classed as semiconductors.

1) The resistivities (commonly 1 to 10^{-3} Ω cm at room temperature) are between those of typical metals and insulators, and decrease with increasing temperature under certain conditions.

2) They can exhibit rectification. The rectifying action of PbS was discovered as long ago as 1874 (B 10).

3) Thermoelectric power and Hall effect (P 20) are easily measurable (H 7).

4) The materials are capable of displaying photoconductivity.

In common with other compound semiconductors, the lead salts were found to exist with either an excess or a deficiency of metal content (W 1). With an excess of lead, the materials showed a negative Hall coefficient and (usually) negative thermoelectric power, indicating that the current carriers were electrons. With a deficiency of lead, the Hall coefficient and thermoelectric power were positive, signifying conduction by holes. The p-type (lead-deficient) material could be converted to n-type by heating in vacuum; on the other hand, n-type material could be changed to p-type by heating in oxygen or chalcogen vapour (H 7).

It is this deviation from stoichiometry (rather than the presence of foreign impurity atoms) which normally accounts for

the relatively high carrier concentration in these compounds, and makes the preparation of intrinsic material more difficult than for the case of an element, such as Ge or Si.

1.3 Polycrystalline films

The lead salts can be sublimed in vacuum at relatively low temperatures (500°C) without excessive dissociation, and it is therefore easy to produce thin films of the materials by condensing the vapour on a substrate such as glass. Thin layers can also be deposited by chemical means from solution (W 7).

These films consist of crystallites in different (sometimes random) orientations. The crystallite size depends on the preparation conditions and on the film thickness, but is commonly between 100 A° and several thousand A° (W 7). As in the case of powder samples, the resistivity is largely determined by the contact resistance between the grains of the film. Evidence for this was believed to come from measurements at high frequencies ($\sim 10^5$ Hz), where the electrical impedance of a film was found to be considerably less than the d.c. value, this being attributed to the capacitance of the inter-grain boundaries (C 1, H 12). However, Broudy and Levinstein calculated that this effect should begin to occur at much higher frequencies than those observed experimentally, and interpreted the results as being due to self-capacitance and large-scale inhomogeneities in the film.

If measured in vacuum by means of the Hall effect, films which had just been deposited from the vapour were found to be n-type, with carrier concentrations of the order of 10^{18} cm^{-3} and carrier mobilities about 100 cm^2 / volt sec (S 17). But if oxygen is gradually admitted to the film, the resistivity increases by more than an order of magnitude, and may then reach a maximum and subsequently decrease. When the resistivity is near the maximum value, the thermoelectric power changes sign and the film appears p-type. Photoconductivity is very low in

vacuum but rises during exposure to oxygen, attaining a maximum value just after the maximum in resistance (B 8) .

A great deal of discussion and argument has taken place over the mechanism of photoconductivity in thin films of the lead salts, particularly with regard to : (1) the effect of oxygen, which appears to be a unique sensitising agent, (2) the mechanism by which excess carriers are produced by radiation, and (3) the role of intercrystalline boundaries in the process. The various theories have been reviewed by several authors (S 21, M 14, M 15, P 7) .

1.4 Bulk single crystals

Natural crystals such as galena are of variable perfection and purity, and therefore not ideal for experimental work.

Single crystals of PbTe and PbSe were first grown artificially by Lawson (L 2) , using the Bridgman - Stockbarger method in which purified material (contained in a sealed evacuated tube) is allowed to solidify by gradually lowering through a temperature gradient. The first crystals were p-type due to doping by oxygen ; when care was taken to eliminate this, both n- and p-type samples could be produced* . The method was also applied successfully to PbS (L 3) .

The electrical properties of single crystals have been described by Putley (P 19) and by Allgaier and Scanlon (A 10) . The Hall effect (P 20) was used to measure the concentration and mobility of carriers. Samples were found to be extrinsic at room temperature (n or p of the order of 10^{18} cm^{-3}) , the Hall coefficient R_H being essentially constant down to the lowest temperature of measurement (4·2 °K) . Above room temperature, they showed intrinsic behaviour, but beyond about 400°C irreversible changes in carrier concentration occurred, due to dissociation or incorporation of oxygen.

* due to an excess of Pb or Te . The material can also be intentionally doped n- or p-type, for example with Br or Na (K 8, C 4).

The constancy of R_H down to very low temperatures shows that the ionisation energy of impurity states must be very small (B 11, S 16). It has been suggested (A 10) that at high carrier concentrations the impurity centres form an energy band which overlaps with the conduction (or valence) band, since R_H remains constant even when the Fermi level is expected to go into the majority carrier band.

The Hall mobility μ_H was found to increase with decreasing temperature, according to $\mu_H \propto T^{-m}$, where $m \sim 2{\cdot}5$. This law is valid from just below the intrinsic region down to at least $100^{\circ}K$. Below about $50^{\circ}K$, the mobility has been found to increase less rapidly and in many samples reaches a saturation value (F 1, A 10). Even so, values as high as 4×10^6 cm^2/v.s. have been reported for PbTe (K 2).

Graphs of $\log \mu_H$ against $\log(1/T)$ over the range $300^{\circ}K$ to $4{\cdot}2^{\circ}K$ are shown in fig. 1.1 for PbTe, PbSe and PbS from the results of Allgaier and Scanlon (A 10). Values of Hall mobility at liquid nitrogen and room temperatures are also given.

1.5 Single-crystal films

In 1948, Elleman and Wilman (E 5) reported thin films of PbS produced by subliming the purified compound in vacuum on to a cleaved rocksalt (NaCl) substrate, which was heated during the deposition. The films had a single crystallographic orientation, as shown by an electron diffraction pattern, although the crystallite size was less than about $300\,A^{\circ}$.

Films of PbTe, about 2 microns thick, grown by vacuum evaporation on to heated mica substrates were described by Makino in 1964 (M 3). They were found to be in a single orientation, with $\{111\}$ planes parallel to the substrate surface, as determined from X-ray and electron diffraction. The electrical properties of these films were also measured (M 4). All samples were found to be n-type, with carrier concentrations mostly in the range 10^{17} to 10^{18} cm^{-3}. The Hall mobility was quite high; values up to 1000 cm^2/volt sec at room temperature and up to

Figure 1.1 HALL MOBILITIES of BULK SINGLE CRYSTALS

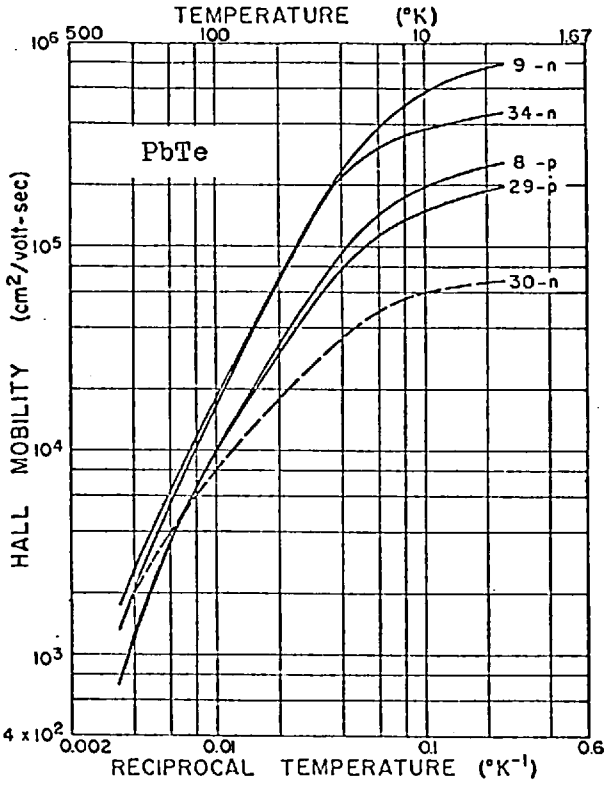

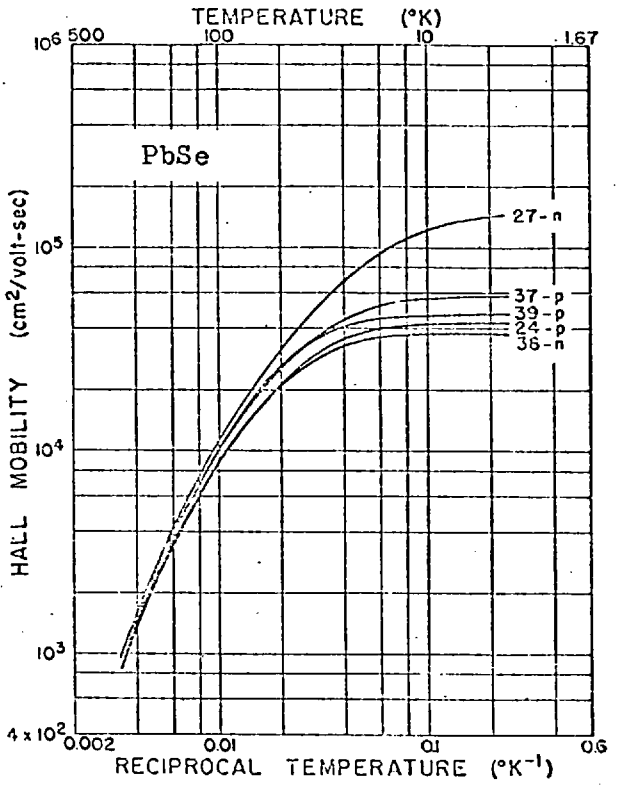

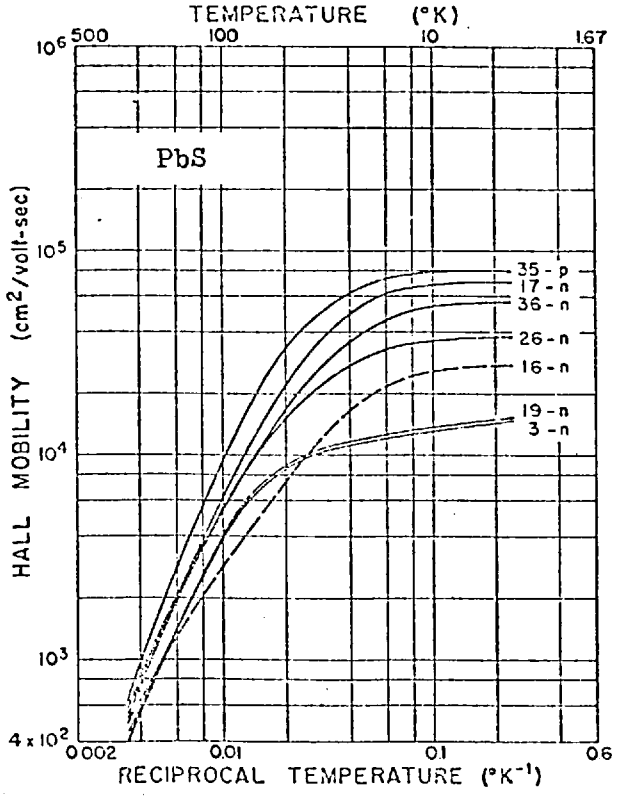

MOBILITY VALUES
(cm^2/volt sec)

material	295°K	77°K
n-PbTe	1600	25,000
p-PbTe	750	18,000
n-PbSe	1000	15,000
p-PbSe	930	14,000
n-PbS	560	9,000
p-PbS	610	15,000
galena	430	6,000

All data from Allgaier and Scanlon, Phys. Rev. 111, 1029 (1958)

18,000 cm^2 / volt sec at 77^oK were obtained. The mobility varied approximately as $\mu_H \propto T^{-2.5}$. These films therefore behaved electrically very much like bulk single crystals. This is in contrast with other semiconductor thin films, where the mobility below room temperature is mainly determined by crystal defects, even in so-called epitaxial films where electron diffraction pictures show that the material is in a single orientation.

Similar work on PbTe and PbSe, using NaCl and KCl substrates, appeared in Russian journals at about the same time (S 11, S 12, S 13, P 1). Soon afterwards, bulk-like properties were reported for PbTe, PbSe and PbS films on alkali-halide substrates (Z 7, B 19, G 3).

Several parameters seem to be important in obtaining films of good electrical characteristics, namely vacuum pressure, rate and time of deposition, substrate temperature and the nature of the substrate material. These are discussed later.

In contrast with the corresponding polycrystalline films, photoconductivity in epitaxial films of the lead salts is not easily observable (Z 7). It has been detected in epitaxial PbS (B 17, C 12) but was of much smaller magnitude and shorter time constant then in the polycrystalline case. Again, oxygen appears to be necessary for measurable photoconductive response; no effect was observed with freshly-deposited films which were measured in vacuum.

- - - - - - - - - -

The remainder of this chapter is devoted to the basic properties of single-crystal material. In many cases, measurement of these (e.g. band structure) is only possible with highly-perfect single crystals.

1.6 Crystal structure and bonding

X-ray measurements show that PbTe, PbSe and PbS all have the sodium chloride crystal structure, the dimensions of the unit cell being about 6 A^o. Precise values of the lattice constants determined by various authors are given below.

	PbTe	PbSe	PbS	reference
LATTICE CONSTANTS a_o (in A^o)	6·50	6·1243	5·9362	(A 1)
	6·34	6·14	5·9233	(W 8)
		6·110		(E 1)

The crystal structure, and the fact that the lattice constants agree fairly well with the sum of the ionic radii (anion + cation) might suggest that the bonding between lead and chalcogen is ionic. In fact, the lead salts have traditionally been referred to as ionic semiconductors. But recent work on carrier scattering in single crystals implies that the bonding is mainly covalent. This is confirmed by measurements of the frequency of nuclear magnetic resonance in the three compounds (W 4).

1.7 Dielectric constant

For field effect calculations it is necessary to know the static relative permittivity K of the semiconductor. In the case of the lead salts, this cannot be measured by standard methods because the conductivity, even of intrinsic materials, is too high. However, the refractive index n for infra-red radiation can be measured (M 15) and has a value of about 5. The optical (relative) permittivity ϵ is then obtained from : $\epsilon = n^2$. Values of for PbTe, PbSe and PbS are given in table [1.1] (next page).

1.7

Since the lead salts are not ferroelectric, κ was assumed for a long time to be of the same order as ϵ. Calculation of the carrier mobilities at very low temperature, however, showed that the observed values can only be explained if a value of several hundred is assumed for κ (A 10, M 12). Moreover, κ can be calculated from measured transverse and longitudinal optical phonon frequencies by use of the Lyddane-Sachs-Teller equation (L 14) :

$$\frac{\kappa}{\epsilon} = \left(\frac{\omega_L}{\omega_T}\right)^2$$

Values obtained for PbTe, PbSe and PbS are shown below.

Table [1.1]

		PbTe	PbSe	PbS
OPTICAL	ϵ	33	23	17
and STATIC	κ	400	280	175

RELATIVE PERMITTIVITIES

The value of $\kappa = 400$ for PbTe has been confirmed by capacitance measurements on junction diodes at $77^{\circ}K$ and $4{\cdot}2^{\circ}K$ (K 1), although magneto-optical measurements (B 15) at microwave frequencies (in the presence of free carriers) gave even higher values ($\kappa \sim 3200$ for $p \sim 10^{17}$ in PbTe).

1.8 Energy gap

The most reliable way of measuring the energy gap between conduction and valence bands in the lead salts has proved to be the optical method, employing the relation : $h\nu = E_g^*$

where ν is the cut-off frequency for photoconductivity or absorption of infra-red radiation, and E_g^* is the 'optical gap' i.e. the energy separation between the two bands at a particular value of the electron wave-vector k.

Values of E_g^* from measurements by Gibson (G 2), re-calculated by Smith (S 22) and extrapolated to 0^oK are shown below.

	PbTe	PbSe	PbS
E_{go}^* (eV)	0·18	0·14	0·22

An alternative method for obtaining the energy gap is to measure the variation of conductivity σ or Hall coefficient R_H with temperature in the intrinsic range. Assuming that the mobility is given by $\mu \propto T^{-2.5}$ in the intrinsic region,

$$\begin{aligned} \sigma &\propto T^{-1} \exp(-E_g/2kT) \\ R_H &\propto T^{-1.5} \exp(+E_g/2kT) \end{aligned} \qquad (1.1)$$

where E_g is the 'thermal energy gap' i.e. the energy separation of the extrema of the two bands, which may not be at the same point in k-space. Since the main temperature dependence occurs in the exponential factors in equations (1.1), a graph of $\log \sigma$ (or $\log R_H$) against $1/T$ should be linear, the slope being equal to E_{go}, where $E_g = E_{go} + \alpha T$. This assumes that E_g varies linearly with temperature (i.e. α = constant) and that the mobility ratio of holes and electrons is independent of temperature. These assumptions have been discussed by Smith (S 22). There is also the danger of irreversible effects (annealing and dissociation of the sample) (S 4, P 19) and the possibility of thermal generation of defects at high temperatures (M 11).

In practice, the graphs obtained are not precisely straight lines; values for E_{go} are variable and usually larger than those from optical measurements. Values obtained by Putley (P 18) from measurements in the range 500 - 800 ^oK were as follows :

	PbTe	PbSe	PbS
E_{go} (eV)	0·63	0·50	1·17

Later measurements, in which irreversible effects were suppressed by

using lower temperatures or encapsulating the sample, gave lower values of E_{go} : 0·34 eV (S 16) and 0·35 eV (M 11) for PbTe . However, these are still higher than the optical values (E_{go}^*) .

On theoretical grounds, the thermal energy gap E_g should be less than or equal to the optical gap E_g^* . Recent work on the band structure of the lead salts indicates that the energy gap is direct, so that the values of E_g and E_g^* should be identical.

An explanation for the discrepancy was suggested by Tauber et al (T 2) , who measured the optical gap of PbTe as a function of temperature between 80°K and 520°K . The curve (fig. 1.2) consists of two regions. Below 400°K , E_g^* increases linearly with T , according to $E_g^* = (0{\cdot}19 + 4{\cdot}1 \times 10^{-4}\ T)$ eV , in fairly good agreement with previous work (G 2 , S 3, S 1) . Above 400°K , E_g is practically constant. When this high-temperature portion of the curve is extrapolated to T = 0°K , a value between 0·33eV and 0·36eV is obtained, which agrees well with the more recent determinations of E_{go} from thermal data. If $E_g = E_g^*$, this agreement is to be expected, since thermal measurements are normally done at temperatures above 400°K . Below 400°K , the energy gap should then still be given correctly by the optical data. This is confirmed by recent work (S 26) on bismuth-doped PbTe , where the carrier concentration was so low that the intrinsic region occurred near room temperature. This gave E_{go} = 0·17 eV , in reasonable agreement with the optical value.

Energy gaps at liquid N_2 and room temperatures, obtained from infra-red measurements on epitaxial films (Z 7) are given in

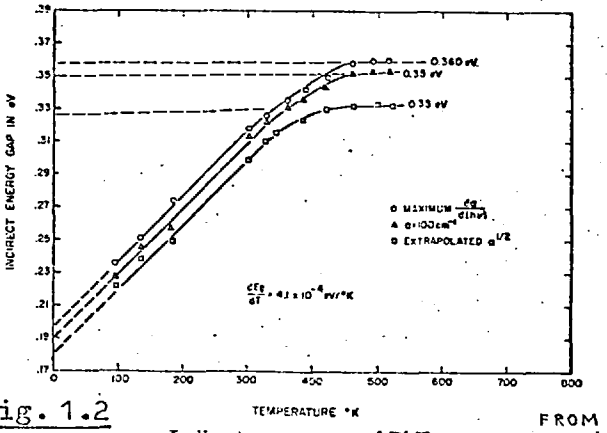

Fig. 1.2 Indirect energy gap of PbTe as a function of temperature. FROM REF. (T 2)

1.8

table [1.2] .

Table [1.2] Energy gaps (in eV) from optical data, ref. (Z 7) .

T	PbTe	PbSe	PbS
300°K	0·31	0·27	0·41
77°K	0·20	0·15	0·28

1.9 Band structure

Because the lead salt semiconductors have the NaCl crystal structure, the first Brillouin zone is a truncated octahedron, as shown in fig. 1.3 with certain points and axes labelled. The energy gap in these materials is direct i.e. the extrema of the conduction and valence bands occur at the same point in k-space, namely the L-point on the Brillouin zone boundary. Constant energy surfaces for both bands are prolate ellipsoids, with major axes parallel to ⟨111⟩ , as shown in fig. 1.4 .

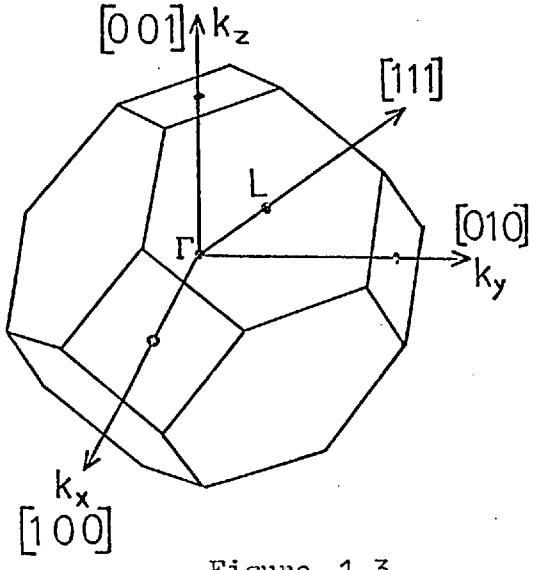

Figure 1.3

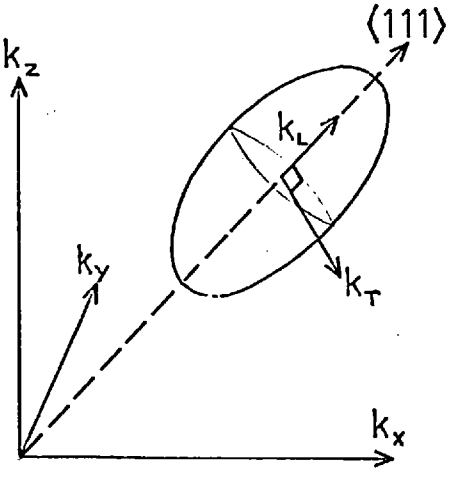

Figure 1.4

Because the energy surfaces are non-spherical, the effective mass is a tensor (dependent on direction). However, two 'principal effective masses' m_L and m_T can be defined with reference to the ellipsoid axes (fig. 1.4). The longitudinal effective mass m_L is given by :

$$\frac{1}{m_L} = \hbar^{-2}\left(\frac{\partial^2 E}{\partial k_L^2}\right) \qquad (1.2)$$

and the transverse effective mass m_T by :

$$\frac{1}{m_T} = \hbar^{-2}\left(\frac{\partial^2 E}{\partial k_T^2}\right) \qquad (1.3)$$

where the vector $\underline{k}_L$ is in a direction parallel to $\langle 111 \rangle$ and $\underline{k}_T$ is perpendicular to $\underline{k}_L$.

The ratio m_L / m_T is known as the mass anisotropy ratio K , and is approximately equal to the ellipsoid anisotropy K′ (C 8) , which is the ratio of the major and minor axes of the constant-energy surface. Values of K , m_L and m_T obtained from recent work on PbTe , PbSe and PbS are shown in table [1.3] .

TABLE I. 3 *Band edge parameters in* PbTe, PbSe, *and* PbS *at* 4 °K from ref.(C 9)

	m_T^*	K	m_L^*	ε'_{gt} (ev)	ε_g (ev)	E'_{pt} (ev)	$\lvert g_{\parallel} \rvert$
PbTe							
Conduction	.024 ± .003	10 ± 1.5	.24 ± .05	.16 ± .04		6.3 ± .4	45 ± 8
Valence	.022 ± .003	14 ± 2	.31 ± .05	.14 ± .04	.19	6.4 ± .4	51 ± 8
PbSe							
Conduction	.040 ± .008	1.75 ± .2	.07 ± .015	.22 ± .04		5.2 ± .5	27 ± 7
Valence	.034 ± .007	2.0 ± .2	.068 ± .015	.18 ± .03	.16	5.5 ± .4	32 ± 7
PbS							
Conduction	.080 ± .01	1.3 ± .1	.105 ± .015	.29 ± .04		3.4 ± .4	12 ± 3
Valence	.075 ± .01	1.4 ± .1	.105 ± .015	.33 ± .04	.28	4.9 ± .4	13 ± 3

* EFFECTIVE MASSES IN UNITS OF M_0 = MASS OF FREE ELECTRON

There are two other effective masses, both of which are directly related to electrical properties. The inertial effective mass m_i enters into equations which describe the dynamics of holes and electrons (e.g. transport properties). It may therefore be defined by the equation :

$$\mu = \frac{q \tau}{m_i} \tag{1.4}$$

where μ is the conductivity mobility and τ the relaxation time. The density-of-states effective mass m_d occurs in expressions which involve the equilibrium statistics of the carriers, and is given (Z 9) by :

$$g(E) = \frac{4\pi}{h^3} (2 m_d)^{\frac{3}{2}} E^{\frac{1}{2}} \tag{1.5}$$

Here, $g(E)$ is the density-of-states function and E is the particle energy, measured from the band edge.

The quantities m_i and m_d contain an average over direction ; they are related to the band-structure effective masses by the equations (S 20):

$$\frac{3}{m_i} = \frac{1}{m_L} + \frac{2}{m_T} \tag{1.6}$$

$$m_d = N_v^{\frac{2}{3}} (m_L m_T^2)^{\frac{1}{3}} \tag{1.7}$$

where N_v is the number of equivalent valleys (band maxima or minima) . Because of symmetry, $N_v = 4$ (S 20 , C 7) for extrema at the L-point .

As well as being dependent on direction, the effective mass is also a function of energy i.e. the E v. k relationship is non-parabolic (except in special directions) . This is caused by interband interaction (K 3, C 2 , A 7) , due to the small energy gap. The effect on the density-of-states function is shown in fig. 1.5 . As a result of interband interaction, the effective mass depends on the carrier concentration, and also on temperature (see section 1.10) . The variation of m_T , K and m_d with temperature and carrier concentration for PbTe is given in figures 1.6 and 1.7 .

Fig. 1.5

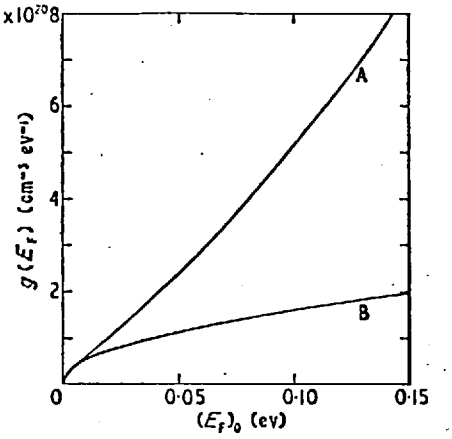

from ref. (R 4)

The density of states as a function of the energy at 0°K: A, in the principal valence band of PbTe; B, in a parabolic band with the same band edge effective mass.

Fig. 1.6

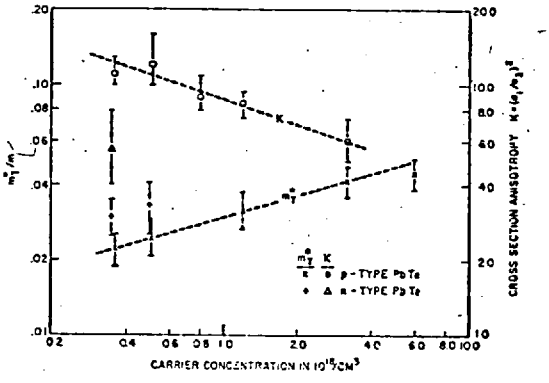

from ref. (C 8)

Figure 1.6 The transverse effective mass m_T^* and the ellipsoid cross-section anisotropy K for p- and n-type PbTe as a function of carrier concentration. The broken lines serve only to connect the points.

Fig. 1.7

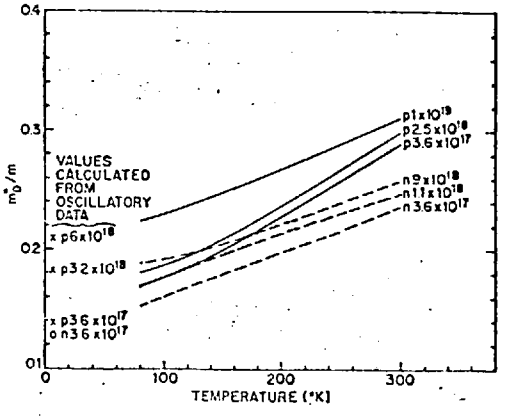

from ref. (C 8)

Figure 1.7 The density of states effective mass m_D^* for n- and p-type PbTe of various carrier concentrations as a function of temperature. m_D^* was determined from the thermoelectric power, high field Hall coefficient and the energy dependence of scattering. The values shown at 4·2°K are calculated from the SdH values of m_T^* and K, assuming four valleys.

Values of m_d and m_i for PbTe at room temperature (with a carrier concentration of 10^{18} cm^{-3}) are shown in table [1.4] . The values of m_d are from Cuff et al (C 8) and are in reasonable agreement with those of Johnson (J 2) . m_i has been calculated from m_d using equation (1.13) (page 14), assuming that m_L (from C 9) does not vary with temperature (C 8, R 4) .

Table [1.4]

m_d and m_i for PbTe at 300°K

	m_d / m_o	m_i / m_o
CONDUCTION BAND	0·24	0·09
VALENCE BAND	0·29	0·11

In addition to the band extrema at the L - point, there is evidence in the case of PbTe of a second valence band, having a higher effective mass, and with a maximum probably at $k = 0$ (A 6, R 3, A 8, D 4, S 29, S 3, D 5, A 9, T 2, C 6) . Some earlier work (S 28, C 7) suggested that the valence band had a second maximum very close in energy (at 4 °K) to the maximum at the L - point. However, more recent investigations have established that there are two valence bands with an energy separation ΔE given by : $\Delta E = \Delta E_o - aT$ where ΔE_o is between 0·14 and 0·19 eV and a is between $(2{\cdot}0$ and $4{\cdot}1) \times 10^{-4}$ eV/ °K (D 5 , A 2, A 9, A 15) . Tauber et al (T 2) assume that the second valence band V_2 is at a fixed energy (0·36 eV) from the conduction band, and that $E_o = 0{\cdot}165$ eV , $a = 4{\cdot}1 \times 10^{-4}$ eV/ °K which gives $E \sim 0{\cdot}04$ eV at 300°K. Above 400°K , the principal valence band maximum V_1 would be further away (in energy) from the conduction band than V_2 ; thermal and optical transitions would then occur between the conduction band and V_2 . This explains the constant value of E_g above 400°K and the difference in E_{go} obtained from optical and thermal measurements (section 1.8) .

Some of the methods which have been used to investigate the band structure of the lead salts are similar to those

employed to study the Fermi surface in metals (P 12). They include cyclotron resonance (S 29, N 2), de Haas - van Alphen effect (S 28), magnetoresistance (A 5, A 6, C 7, K 2) and Shubnikov - de Haas effect (C 7, C 8). Measurements of optical properties (D 4, P 2, D 5), thermoelectric coefficients (G 1, S 20, A 2, D 6, C 6) and the dependence of the Hall coefficient on temperature and magnetic field (A 6, A 8, A 9, A 7, C 6) have also been used.

The first theoretical predictions of the band structure of PbS (B 3) gave results which are now known to be incorrect. But more recent calculations for PbTe (C 3) and for PbS and PbSe (R 1), using the A.P.W. method (Z 9, p. 87) including relativistic effects and spin - orbit coupling, show that the band structure should be similar for all three compounds, the energy gap being direct, at the L - point. The results show no evidence of a second valence band at $k = 0$; the principal valence band does have a second maximum along a $\langle 110 \rangle$ direction, which is close in energy to the maximum at L, but this is not likely to have the spherical symmetry proposed experimentally (S 28). Calculations of Lin and Kleinman (L 9) also indicate $\langle 111 \rangle$ ellipsoids at the L - point, with K between 8 and 14 for PbTe, and closer to unity for PbSe and PbS. Agreement was obtained with experimental optical and electrical data.

1.10 Carrier mobility and scattering mechanisms

a) Above 77°K

Values of electron and hole mobilities for single crystals of PbTe, PbSe and PbS were given in figure 1.1. As remarked previously, the mobility in these compounds is found to obey a power-law temperature dependence ($\mu \propto T^{-m}$ where m is approximately 2·5) from around 50°K up to room temperature or above.

This temperature dependence proved difficult to explain, particularly as the materials were originally thought to be polar

(ionic) in character ; this implies that lattice scattering should be mainly by optical phonons. Attempts were made (P 10, H 8, S16) to fit the experimental mobility data to polar scattering theory (F 5, H 12, L 11) . This involves the Debye temperature θ_D , which is around 150 - 200 ^oK for the lead salts (A 1) .

For $T \ll \theta_D$, the temperature dependence of the mobility is given by :

$$\mu \propto \exp(\theta_D/T) - 1 \quad . \qquad (1.8)$$

For $T \gg \theta_D$, the expression from perturbation theory reduces to :

$$\mu \propto T^{-\frac{1}{2}} \qquad (1.9)$$

Neither of these expressions gives the correct variation with temperature, and even when combined with other common types of carrier scattering, it was impossible to account for the experimental data except over a limited temperature range.

Various authors have derived a $\mu \propto T^{-2.5}$ law theoretically ; by obtaining solutions to a many-electron Schrödinger equation (T 4) and by considering one- and two-phonon processes for acoustical scattering (G 1, R 2) . Inter- and intra-valley scattering (H 4) and scattering from acoustical and optical phonons (E 4) have also been considered. But none of these treatments were wholly satisfactory.

Eventually, it was established that scattering is mainly by acoustical phonons (G 1, K 2, D 1, J 2, C 8) . In general, the mean free path l of a carrier depends on its energy E and on temperature T , and can be written (G 1) : $l = \phi(T)\ F(E)$ where the functions ϕ and $F(E)$ depend on the scattering mechanism. Considering the carrier as a particle, the relaxation time τ is given by :

$$\tau = {}^{l}/_{c} \propto l E^{-\frac{1}{2}} = \phi(T)\ F(E)\ E^{-\frac{1}{2}}$$

where c is the thermal velocity of the carrier and $E = \frac{1}{2} m c^2$ The energy and temperature dependence of l and τ is given in the table (next page) for various scattering mechanisms.

scattering centres	$l(E,T)$	$\tau(E,T)$
acoustical phonons	T^{-1}	$E^{-\frac{1}{2}}\ T^{-1}$
optical phonons ($T \gg \theta_D$)	$E\ T^{-1}$	$E^{\frac{1}{2}}\ T^{-1}$
ionised impurities	E^2	$E^{3/2}$
neutral impurities	constant	$E^{-\frac{1}{2}}$

$F(E)$ is seen to be of the form E^r, the value of r being dependent on the scattering mechanism. The parameter r also enters into expressions for the thermoelectric coefficient α, the Hall factor (see page 80) and the ratio $\left(\frac{K}{\sigma}\right)$ of the thermal and electrical conductivity due to the carriers. Investigation of these quantities therefore enables the scattering mechanism to be distinguished. The results for PbTe (G 1, K 2, D 1, J 2, C 8) show that r is approximately zero, indicating scattering predominantly by acoustical phonons.

There is still the problem of explaining the observed temperature dependence of mobility, since acoustical scattering is expected theoretically to give $\mu \propto T^{-1.5}$ rather than $\mu \propto T^{-2.5}$. This was eventually solved by taking into account the interaction between conduction and valence bands (K 3, C 2, A 7).

Interband interaction occurs when the energy gap between the bands is small, as in the lead salts and in indium antimonide. As a result, the energy bands are non-parabolic, and also the effective masses in both bands depend on the width of the energy gap (R 2). In the lead salts, the energy gap E_g increases with increasing temperature (the causes of this are discussed in references (P 5) and (R 2)); consequently, the effective mass becomes an increasing function of temperature. The conductivity mobility must then be written :

$$\mu(T) = \frac{q \langle \tau(E) \rangle}{m_i(T)} \qquad (1.10)$$

where $\langle \tau(E) \rangle$ is the relaxation time averaged over carrier energy.

For acoustical scattering (Z 9) :

$$\tau(E) \propto \frac{1}{T\, g(E)} \qquad (1.11)$$

where $g(E)$ is the density-of-states function.

If the carrier concentration is not too high (so that the average carrier energy is much less than E_g), non-parabolicity may be neglected and $g(E)$ can be written (R 4) in the usual form, namely:

$$g(E) = \frac{4\pi}{h^3} (2 m_d)^{\frac{3}{2}} E^{\frac{1}{2}}$$

From (1.10) & (1.11) ,

$$\mu \propto q \left(m_i\, m_d^{3/2}\, T\, \langle E \rangle^{\frac{1}{2}} \right)^{-1} \qquad (1.12)$$

The temperature dependence of m_d has been determined by thermoelectric power measurements (S 20, Z 8) and is given by :

$$m_d \propto T^{0.4 \pm .05}$$

The temperature dependence of m_i can be found by expressing m_i and m_d in terms of m_L and m_T (defined in 1.9) . Experimental evidence (C 8, D 6) shows that m_L is a factor of 10 larger than m_T , and is approximately independent of temperature. Equations (1.6) and (1.7) then give :

$$\frac{3}{m_i} = \frac{1}{m_L} + \frac{2}{m_T} \doteqdot \frac{2}{m_T}$$

$$m_d = N_v^{\frac{2}{3}} \left(m_L\, m_T^2 \right)^{\frac{1}{3}}$$

$$\therefore \quad m_i = m_d^{3/2}\, m_L^{-\frac{1}{2}} \left(\frac{3}{2\, N_v} \right) \qquad (1.13)$$

and

$$m_i \propto T^{0.6 \pm .075} \qquad (1.14)$$

When Boltzmann statistics are applicable, $E^{\frac{1}{2}} \doteqdot \sqrt{kT}$ and substitution for m_i and m_d in equation (1.12) gives :

$$\mu \propto T^{-(2.7 \pm .15)} \qquad (1.15)$$

(For a wide band-gap semiconductor, where m_i and m_d are

independent of T , (1.12) gives the usual form $\mu \propto T^{-3/2}$) .

At low temperatures, where the semiconductor is completely degenerate ($E_F \gg kT$), $\langle E^{\frac{1}{2}} \rangle = E_F^{\frac{1}{2}}$ and eqn. (1.12) gives ;

$$\mu \propto T^{-(2{\cdot}2 \pm {\cdot}15)} \qquad (1.16)$$

Temperature variation of the effective mass therefore provides a satisfactory explanation of the dependence of carrier mobility on temperature.

Closer agreement with the $\mu \propto T^{-2{\cdot}5}$ law for a non-degenerate semiconductor is obtained by replacing eqn. (1.11) by $\tau(E) \propto T^{-1} E^{-R}$, where $R = 0{\cdot}3$ to $0{\cdot}4$. This value of R was determined from thermomagnetic measurements, and is taken to indicate a small percentage of optical-mode scattering (C 8) .

1.10b Mobility below $77^{\circ}K$

Below liquid nitrogen temperature, the mobility starts to increase less rapidly with decreasing temperature, and below $10^{\circ}K$ it is more or less constant, as seen from figure 1.1 (page 14) This cannot be due to ionised-impurity scattering (which occurs in Si and Ge at low temperatures) because the Conwell-Weisskopf formula predicts that μ should decrease with increasing temperature ; the values of mobility are in any case greatly in excess of those predicted.

Allgaier and Scanlon (A 10) suggest that the scattering centres at these very low temperatures may be dislocations, and have demonstrated that the mobility is reduced if dislocations are introduced by subjecting the sample to mechanical force.

Other workers (K 2, S 2) have found that in PbTe the Hall mobility decreases with increasing carrier concentration according to $\mu_H \propto n^{-\frac{1}{3}}$ for $n > 10^{18}$ cm^{-3} , which was interpreted (K 2) , from the energy dependence of τ , as being due to neutral impurity scattering.

1.10 b

For lower carrier concentrations, the low-temperature mobility has been observed to increase with increasing doping (K 2, S 2, F 1) ; possible explanations include scattering by vacancies and inhomogeneities in the sample.

FILM PREPARATION

This chapter describes the techniques used to prepare epitaxial films of PbTe, PbSe and PbS for the present study.

2.1 Vacuum system

The vacuum equipment consisted of an Edwards F403 diffusion pump containing silicone 705 oil, backed by a 1SC150B rotary pump. A liquid nitrogen cold trap, mounted between the high vacuum valve and baseplate, was used to prevent backstreaming of oil vapour and to reduce the partial pressure of condensable gases. Pressure in the evaporation chamber was measured by an ionisation guage, and was below 2×10^{-6} τ after several hours pumping.

2.2 Evaporation assemblies

Two different evaporation assemblies have been used.

a) System A

This is shown diagrammatically in fig. 2.1 . The evaporation source for the semiconductor consisted of a cylindrical tube, $2\frac{1}{2}$ cms. long and 4 mm. internal diameter, made of high purity silica and surrounded by a spiral of 1 mm. diameter tantalum wire which was heated by a current of about 8 amps. The source tube is believed to approximate to a Knudsden cell, reducing the amount of preferential evaporation of the more volatile component of the lead compound. The temperature at which the latter sublimed was about 650° C.

A similar source mounted nearby could be used to evaporate silicon monoxide. A shutter could be rotated to cover both sources.

The substrate assembly was about 10 cm. above the source. The mica substrate, approximately 2" X 1" , was clamped at one end, the top surface having been coated with a suspension of graphite in alcohol, in which was embedded the tip of an iron-constantan thermocouple. This was covered by a second piece of mica, above which was the substrate heater, which consisted of a 2" x $1\frac{1}{4}$" strip of molybdenum foil (2 thou thickness). This was connected

Figure 2.1 EVAPORATION ASSEMBLY, System A

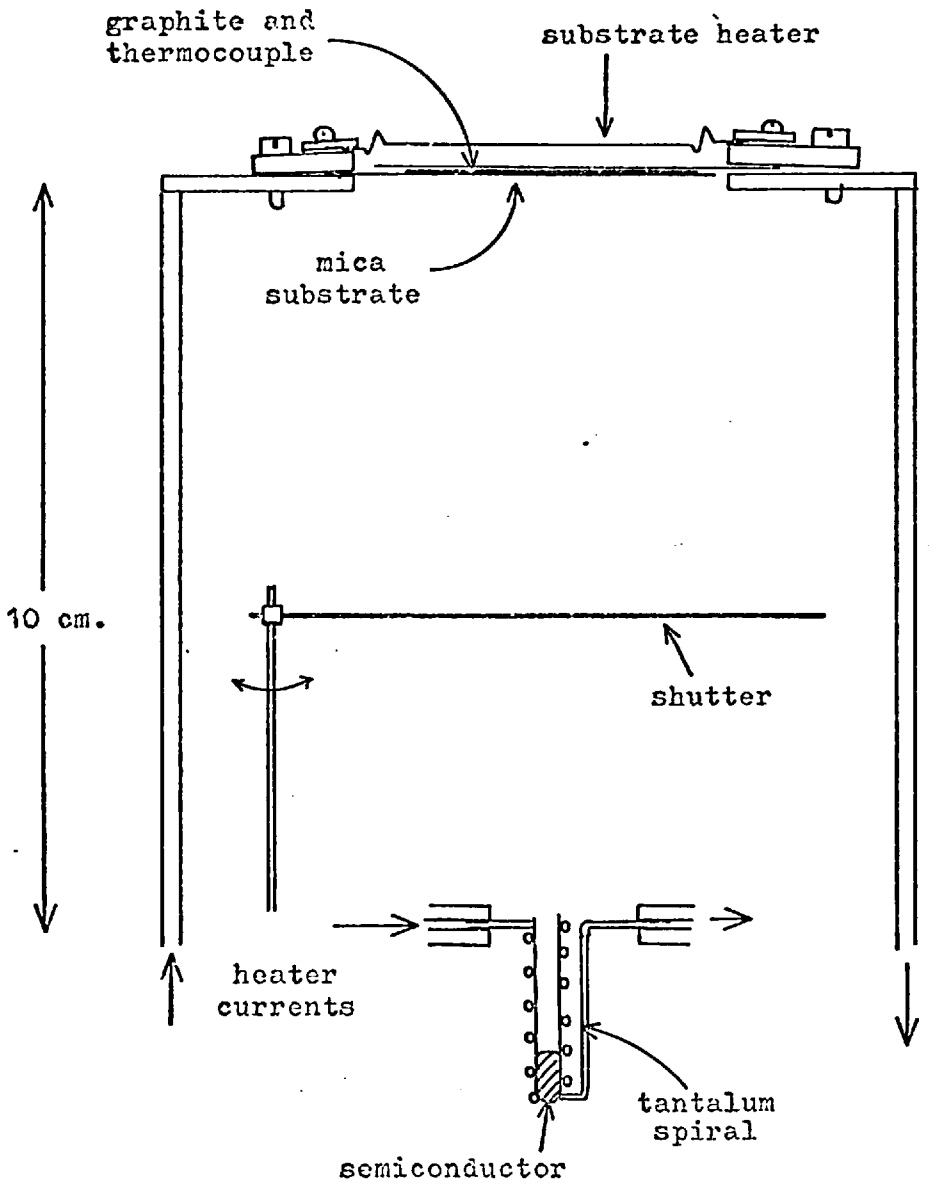

to a 100 amp transformer and supplied radiation which was absorbed by the graphite coating on the back of the substrate. A quartz crystal was mounted near to the substrate and connected to an Edwards film thickness monitor, so that the evaporation rate and film thickness could be measured during growth of the film.

The evaporation system was surrounded by a Meissner spiral, through which liquid nitrogen could be circulated during an evaporation in order to obtain a lower pressure (less than 5×10^{-7} torr) in the chamber. However, this did not produce any significant difference in film properties, and was not normally used.

The entire evaporation assembly was enclosed by a 12" diameter glass bell jar, which sealed to the baseplate by means of a Viton A 'L' gasket.

b) System B

This is shown in fig. 2.2 , and was built to replace system A, in order to make electrical measurements on samples directly after preparation, without breaking the vacuum. It also differs from the previous system by using masks to define the shape of the sample.

There are four evaporation sources, screened from each other by aluminium partitions. A shutter is held above these , and can be rotated to cover any particular source.

The mask and substrate assemblies are mounted onto the underside of a top-plate made of half-inch duralumin, which forms a vacuum seal to the cylindrical glass bell jar by means of a Viton gasket. The mask holder can be seen in fig. 2.3 , and consists of a stainless steel plate on which are mounted four molybdenum masks, one above each evaporation source.

As before, the substrates are 2" X 1" pieces of $2\frac{1}{2}$ thou mica, painted on one side with graphite, to absorb radiation. Up to six of these can be accommodated. They are clamped at one end to the substrate holder, a stainless steel disk which can be rotated to bring a particular substrate over the required evaporation source or into the gap of an electro-magnet.

Figure 2.2 EVAPORATION CHAMBER (system B)

Figure 2.3 Mask and substrate assemblies (system B)

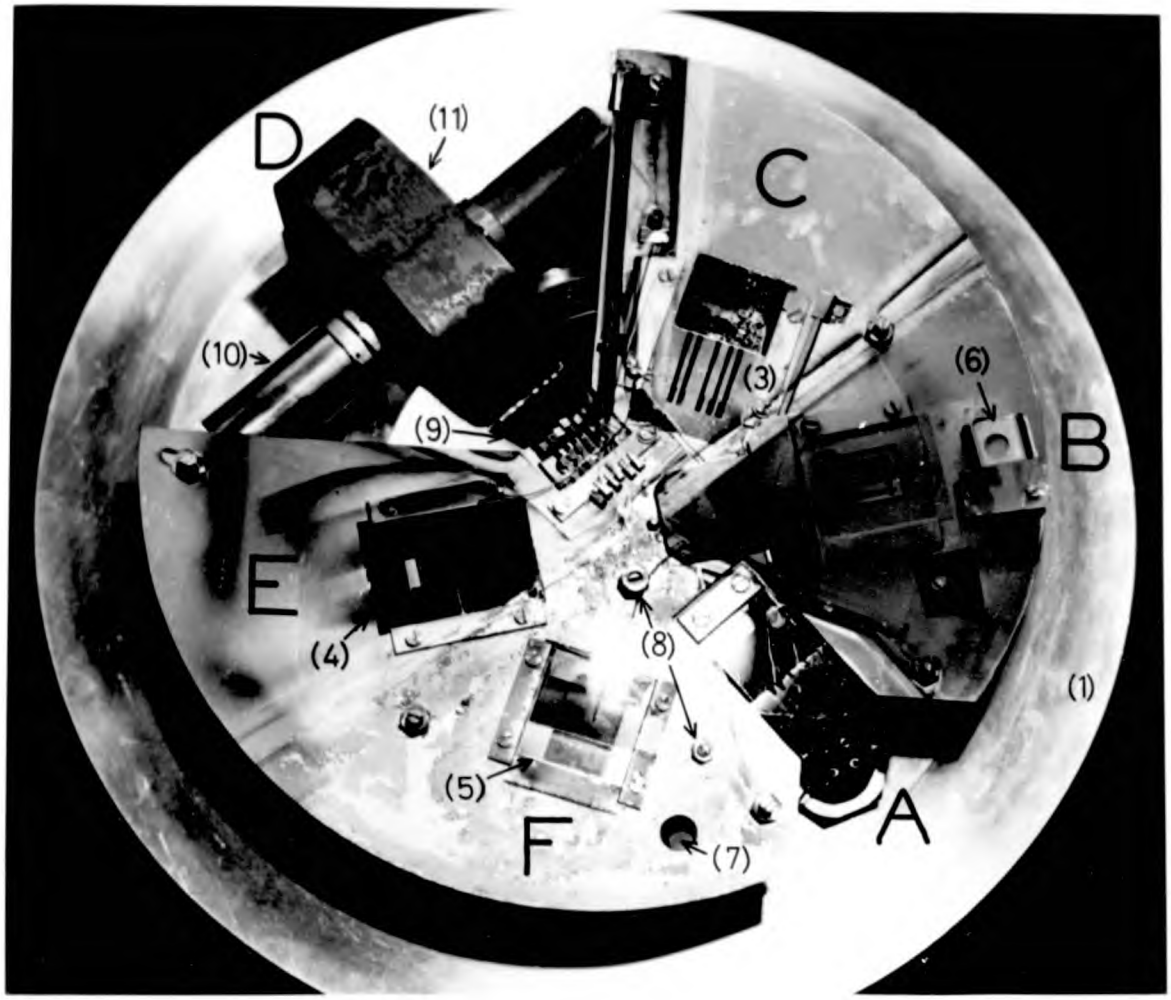

KEY : (1) vacuum top-plate (2),(3),(4),(5) evaporation masks for the semiconductor, Cu/Ag, nickel and insulator sources

(6), (7) quartz crystals for semiconductor and insulator

(8) locating pins (9) contacts to film

(10) liquid nitrogen reservoir (11) electromagnet

Substrates are inserted at position (A) (fig. 2.3). After replacing the top-plate and evacuating the chamber, the required substrate is then positioned above the semiconductor source (position B). Two locating pins (shown in fig. 2.3) enable the substrate to be accurately positioned with respect to the evaporation mask. They also ensure that the substrate is brought vertically downwards to within 3mm. of the molybdenum mask. The tip of an iron-constantan thermocouple then touches the mica surface at a point near to the sample area.

A substrate heater, consisting of a molybdenum wire threaded through alumina tubes, enables the substrate to be heated from above by radiation. This type of heater has greater thermal mass than a molybdenum strip; fluctuations in substrate temperature are therefore reduced. Also, less heat is conducted away through the leads. A double radiation shield made of 2 thou molybdenum sheet prevents radiation upwards.

A quartz oscillator crystal, mounted underneath the mask holder, is used for monitoring the evaporation rate and film thickness. The revolving shutter may be used to cover the evaporation mask with or without the crystal being exposed to the evaporant, as shown in fig. 2.4 .

Figure 2.4

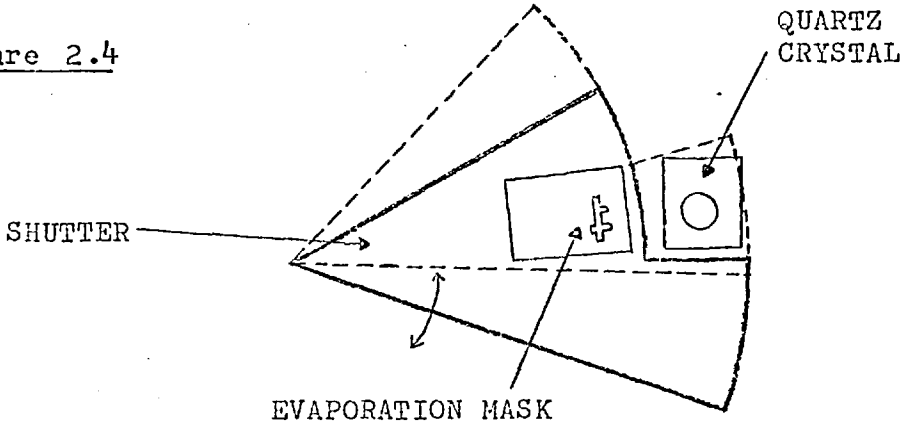

If the substrate is rotated to position (C), copper or silver can be evaporated from a molybdenum boat to form leads which connect to the semiconductor sample. However, these gave contact trouble at the external connections and were subsequently replaced by graphite strips, painted onto the surface of the mica

just after mounting the substrate.

Also, there is a tungsten wire source for evaporation of nickel (port E) which was intended to be used to prepare thin film thermocouples for direct measurement of the substrate surface temperature. These were also found to be unreliable. In particular, the resistance became high when lead telluride was deposited onto the heated substrate, probably due to attack by tellurium vapour.

The remaining port (F) contains a Drumheller source for evaporating silicon monoxide. Alternatively, magnesium fluoride can be evaporated from a tantalum boat. During deposition of the insulator, the substrate can be heated from above by radiation, if required. Rate and thickness can be monitored by means of a second quartz crystal mounted above the mask holder.

Measurements of the Hall coefficient and resistivity of the sample can be made by rotating the substrate into the gap of the electromagnet (position D), where it is brought down onto a row of five contacts which connect to an external circuit.

The magnet takes a D.C. current of 3·2 amps from a 12 volt battery and gives a flux of 1·56 K Gauss in the $\frac{1}{2}$-inch gap. To prevent outgassing, the energising coil is outside the vacuum chamber (see fig. 2.2) and the magnetic flux is conducted through two steel plates which form a vacuum seal to the top-plate by means of Viton 'O' rings.

2.3 Source materials

The materials used were as follows:

material	source	specifications
lead telluride *	Zenith Radio	$p \sim 2 \times 10^{18}$ cm
lead selenide lead sulphide	Koch-Light Laboratories Ltd.	5N purity
silicon monoxide	'Kemet' Union Carbide Ltd.	95% SiO 5% Si + SiO_2
magnesium fluoride	B.D.H. Ltd.	zone-refined
mica	Mica & Micanite Ltd.	ruby muscovite 5 thou thickness

* The author would like to thank Dr. A.J. Crocker, of the Zenith Radio Research Laboratories (U.K.), for supplying the PbTe.

2.4 Evaporation Procedure

The following remarks apply to films prepared with either of the evaporation assemblies.

The source tube was cleaned by heating in vacuum (to remove any remaining deposit of the lead compound) and then rinsed with distilled water.

To obtain a substrate surface as clean and reproducible as possible, the mica was cleaved in half just before pump-down, and mounted in the apparatus with the cleaved face towards the source.

Evaporation of the semiconductor was carried out at a pressure of less than 5×10^{-6} torr.

The source was allowed to warm up for several minutes. With the shutter masking the substrate but leaving the quartz crystal uncovered, the evaporation rate could be adjusted to the required value ; 4 A°/sec was used initially, but it was found possible to increase this to 10 A°/sec without noticeable change in film properties. The substrate heater was turned on and the substrate temperature allowed to reach equilibrium. After removing the shutter, the evaporation rate and substrate thermocouple reading could be kept constant by slight adjustment of the heater currents ; this was done manually. The shutter was replaced over the source when the film thickness reached a predetermined value, usually 2000 - 4000 A°. If an overlayer of silicon monoxide or magnesium fluoride was required, this was deposited in a similar manner to the semiconductor. Usually, the substrate heater was not operated during evaporation of the insulator, but the sample received considerable radiation heating from the source. The sample could then be annealed for several minutes at about 400°C (surface temperature) , which gave improved electrical mobility, the insulator layer preventing dissociation of the semiconductor. It was then allowed to cool slowly.

2.5 Calibration of the Film Thickness Monitor.

Film thickness was determined by measuring the height of the step produced by the edge of an evaporation mask, using interferometry. It is usually necessary to coat both sides of the step with a thin layer of a highly reflecting metal, such as silver or aluminium. The film surface is then pressed against a half-silvered plate and illuminated with parallel light from a sodium lamp, as shown in fig. 2.5a . By correct adjustment of the contact pressure, multiple-beam interference fringes are formed at right angles to the step, as indicated in fig. 2.5b. These are viewed and measured by means of an eyepiece containing a graduated scale.

The film thickness t is given by :

$$t = \frac{\lambda}{2} \cdot \frac{\bar{d}}{\bar{s}}$$

where λ is the wavelength of sodium light $\sim$ 5900 A°
$\bar{d}$ and $\bar{s}$ are the values of displacement and separation of the fringes, averaged over six or more fringes.

t can probably be measured to within 200 A° by a single measurement. Films on mica substrates are more difficult to measure accurately than those on glass, because the mica tends to deform under the applied pressure, which gives curved fringes. Also, the material tend to relax under the stress, giving rise to slow drift in the fringe system.

The film thickness monitor needs to be calibrated for a particular source and crystal and a given material. The substrate temperature is also important, since the condensation coefficient may vary with temperature.

The sensitivity of the thickness monitor is obtained by dividing the frequency shift by the measured film thickness. Some of the values obtained for different evaporants are given on the next page.

Figure 2.5 FILM THICKNESS MEASUREMENT

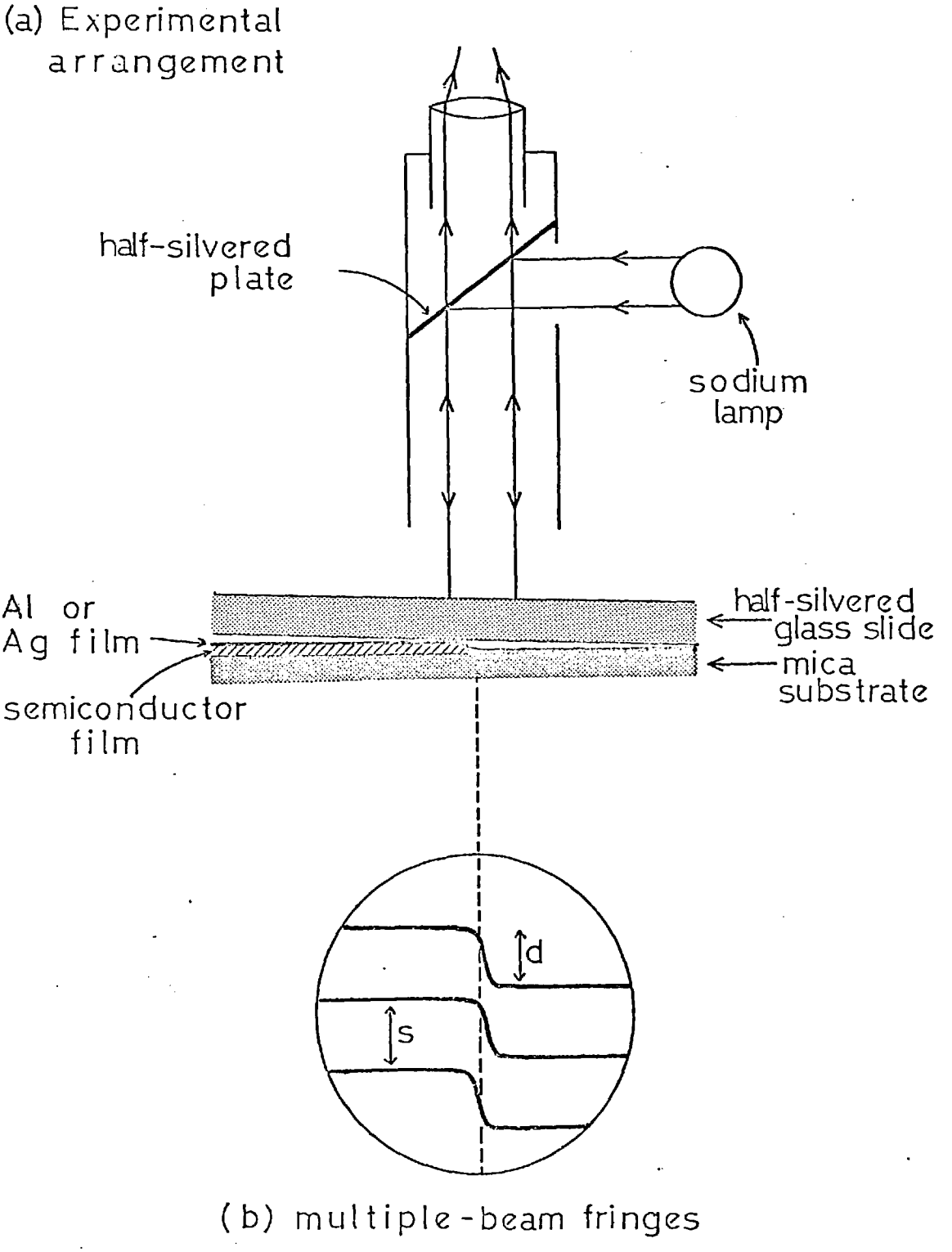

evaporation system	material	substrate surface temp.	sensitivity
A	PbTe	275	4·5
	PbTe	20	5·9
B	PbTe	300	7·2
	PbSe	300	7·7
	Si O	20	3·1
		°C	Hz / A°

2.6 Calibration of Substrate Thermocouples

The temperature measured by a thermocouple embedded in the graphite coating (as in system A) is probably close to the temperature at the mica surface exposed to the evaporant.

The thermocouple used in system B was just touching the underside of the mica substrate and was found to give a lower reading than a similar thermocouple embedded in the graphite on the back.

It is possible to estimate the temperature at the front face of the mica by observing the melting point of small crystals of various salts placed on the surface. Fig. 2.6 shows a calibration curve of surface temperature against thermocouple reading (from D.P. Martin, ref. M7) using this method, together with a diagram showing the experimental arrangement. Since the thermal conditions in the two cases are similar, this calibration curve was used for system B, to correct the substrate thermocouple readings.

Figure 2.6 SUBSTRATE THERMOCOUPLE CALIBRATION

(a) Calibration curve

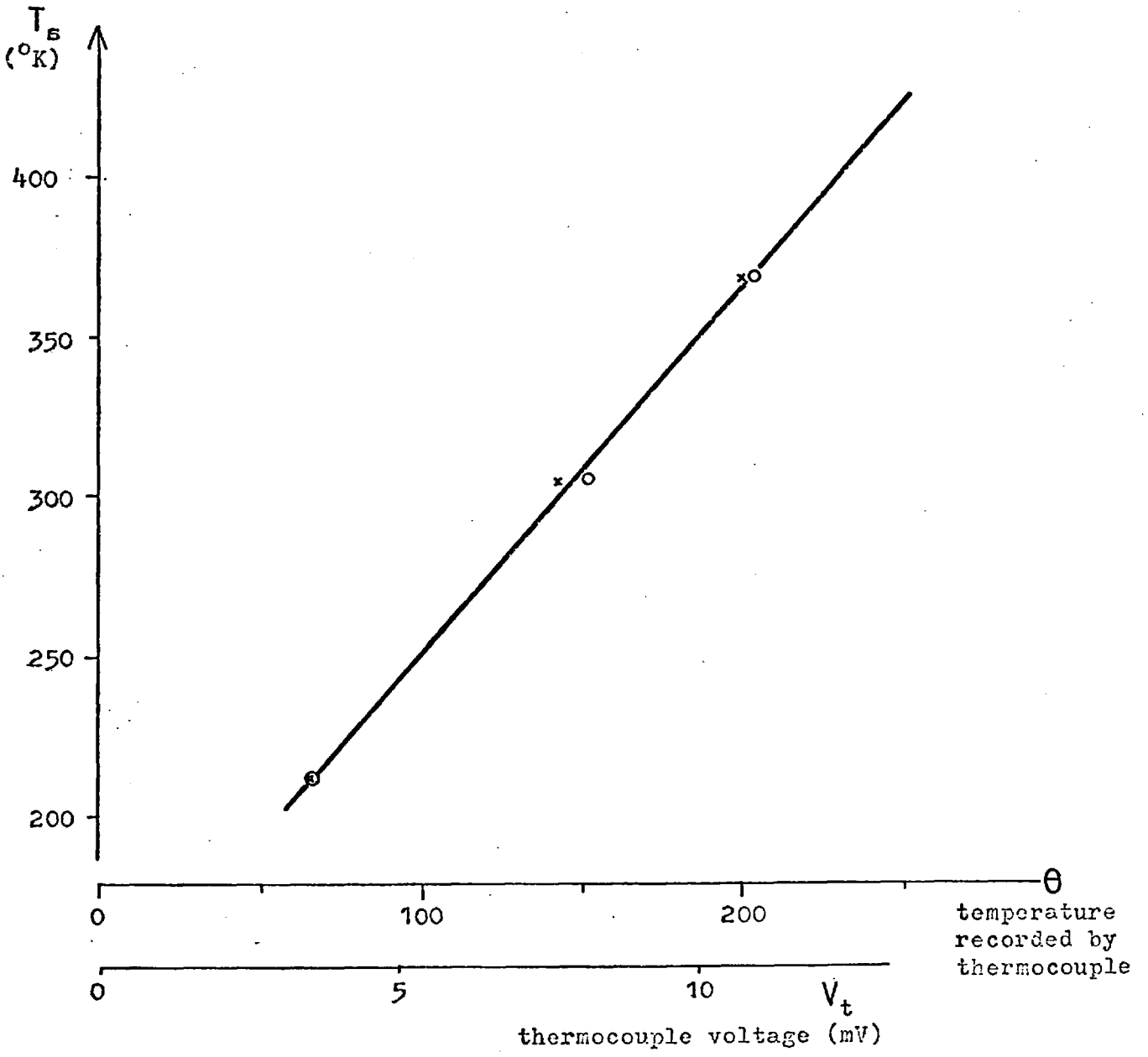

(b) Experimental arrangement

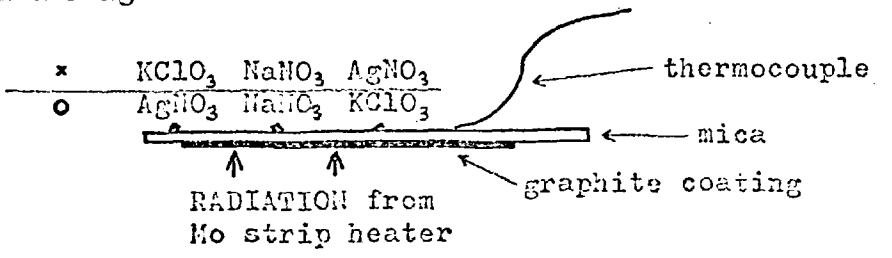

CHAPTER 3

ELECTRON MICROSCOPY

3.1 Transmission micrographs and diffraction patterns

Films of PbTe, PbSe and PbS grown for the purpose of studying their electrical properties were normally between 2000 A° and 4000 A° thick. Due to the high electron absorption of these materials, the thickness must be reduced to less than 1000 A° (and preferably below 500 A°) in order to study the structure of the films in an electron microscope. Also, the films have to be detached from the mica substrate.

Both of these operations can be achieved by immersing the sample in a suitable etch, which preferentially attacks the film - substrate interface. The following solvents were found to be satisfactory.

MATERIAL	SOLVENTS USED
PbTe	HF, HNO_3 or a mixture
PbSe	HNO_3
PbS	HCl or HNO_3

Having separated the film from the substrate, the former can be thinned down by further etching if required. Pieces of film were transferred to distilled water and caught on C.400 or C.200 microscope grids. The specimens were examined using a 'JEM 7' electron microscope.

Figure 3.1 shows a typical transmission micrograph of an epitaxial PbTe film deposited on to a heated mica substrate. The dark bands are extinction contours, which result from very slight bending of the specimen. They do not represent real structure in the film, but indicate that the crystal orientation is uniform over appreciable areas. The fine lines visible in the picture are believed to be due to double-positioning boundaries,

Figure 3.1 Transmission micrograph of PbTe on mica

which are perpendicular to the plane of the film, and are regions where the crystalline order is interrupted.

These can be seen at higher magnification (X 15,000) in fig. 3.2 a . Fig. 3.2 b is a diffraction pattern of this same area of film, and shows hexagonal symmetry, indicating that the plane of the specimen (which was originally paralled to the substrate surface) is of the type (111) . The fact that the diffraction pattern consists of sharp spots signifies that there is no angular misorientation about the normal to the film plane. This is further demonstrated by the electron diffraction pattern shown in fig. 3.2 c , which shows Kikuchi lines (dark bands across the pattern), representing good crystal perfection. The micrograph of the corresponding area (fig. 3.2 d) shows the double-positioning boundaries more clearly, and also small spots within the enclosed areas which may represent dislocations running perpendicular to the plane of the film.

Figure 3.3 shows X - ray diffraction photographs, obtained by the Laue back-reflection method, with spots which are due to a {111} film of lead telluride. The hexagonal symmetry in this case indicates that the semiconductor actually occurs in two different orientations, 180° apart (about the normal to the film plane). This results from the fact that the double-positioning boundaries are reflection planes, the material on either side being in twinned orientation.

The electron diffraction patterns of single-crystal films (fig. 3.2) show no evidence of extra phases e.g. free lead. To check that the film material was PbTe , a thin layer of aluminium was evaporated over part of a specimen. The resulting diffraction pattern showed an F.C.C. system of rings due to the aluminium, as well as a spot pattern from the semiconductor ; the two lattice constants could therefore be directly compared. Assuming the lattice spacing in the Al film to be equal to the bulk value of $4{\cdot}05\ A^{\circ}$ (W 8) , the diffraction pattern from the semiconductor was consistent with an NaCl structure having a lattice constant of $a_o = 6{\cdot}45 \pm {\cdot}02\ A^{\circ}$, in agreement with

Figure 3.2 SELECTED AREA DIFFRACTION PATTERNS AND MICROGRAPHS

(X 15,000) for PbTe deposited on to heated mica

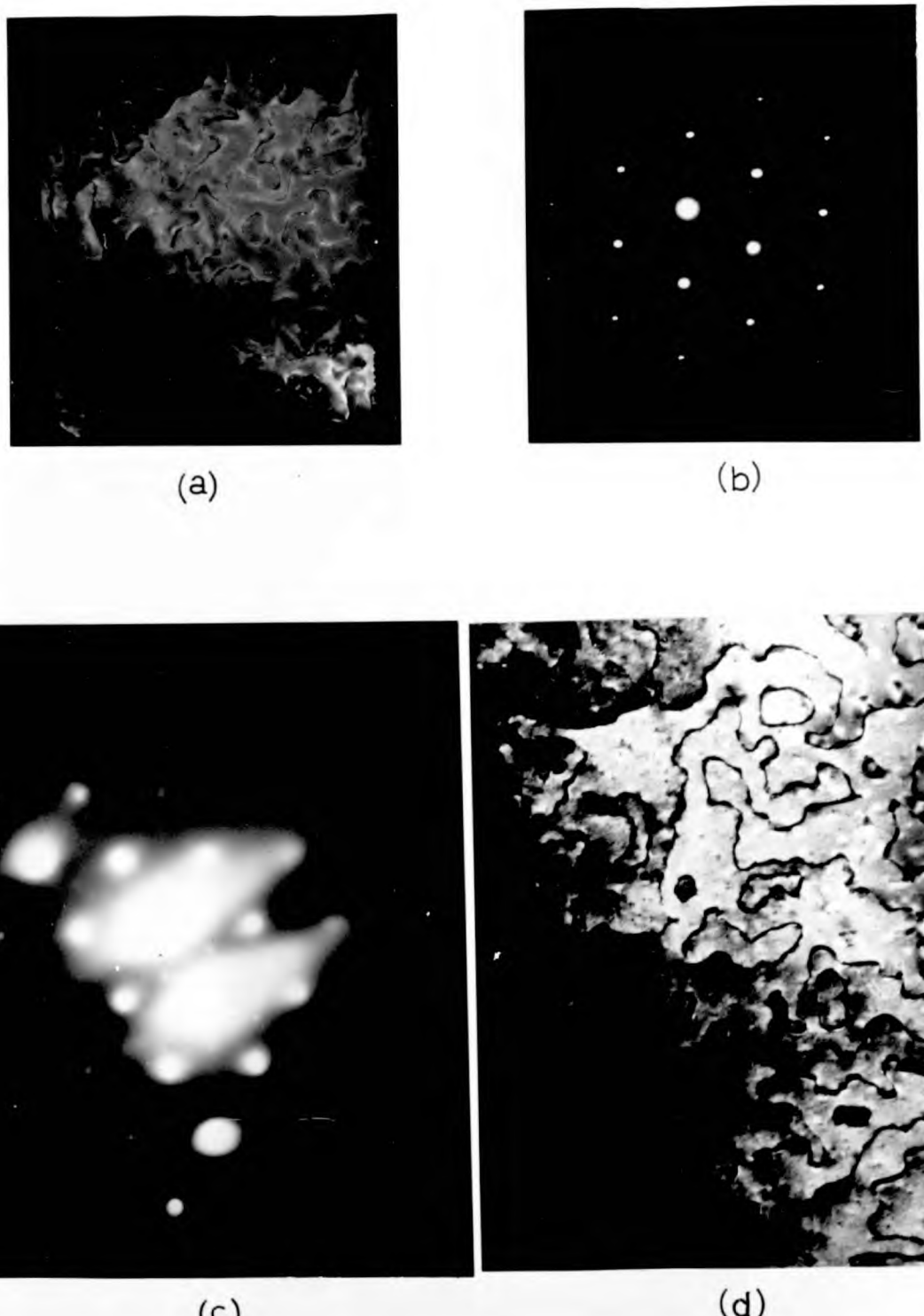

(a) (b)

(c) (d)

Figure 3.3 X-RAY (Laue) BACK-REFLECTION PHOTOGRAPHS

(unfiltered Cu radiation, film 5 cm. from specimen)

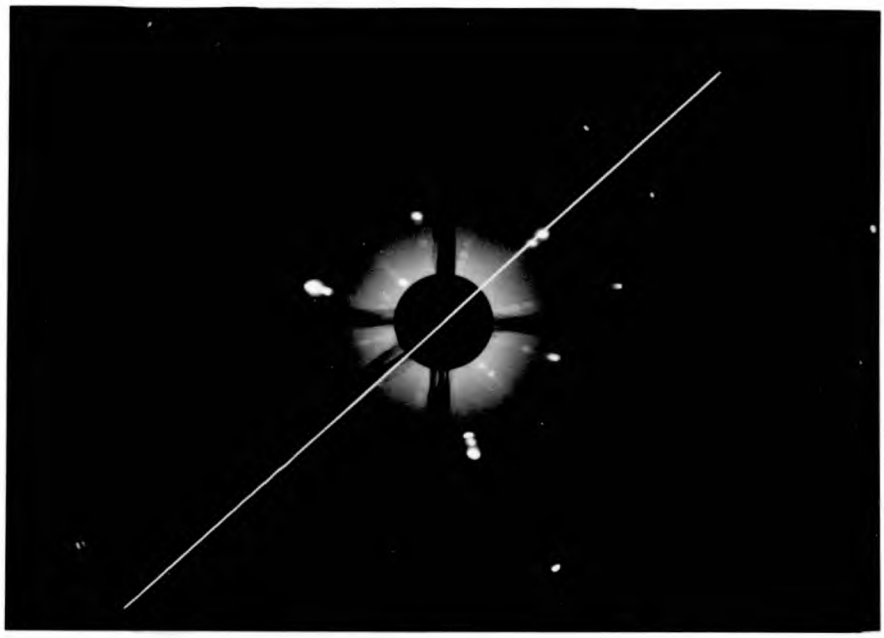

(a) MICA SUBSTRATE ALONE

(the reflection symmetry plane is marked)

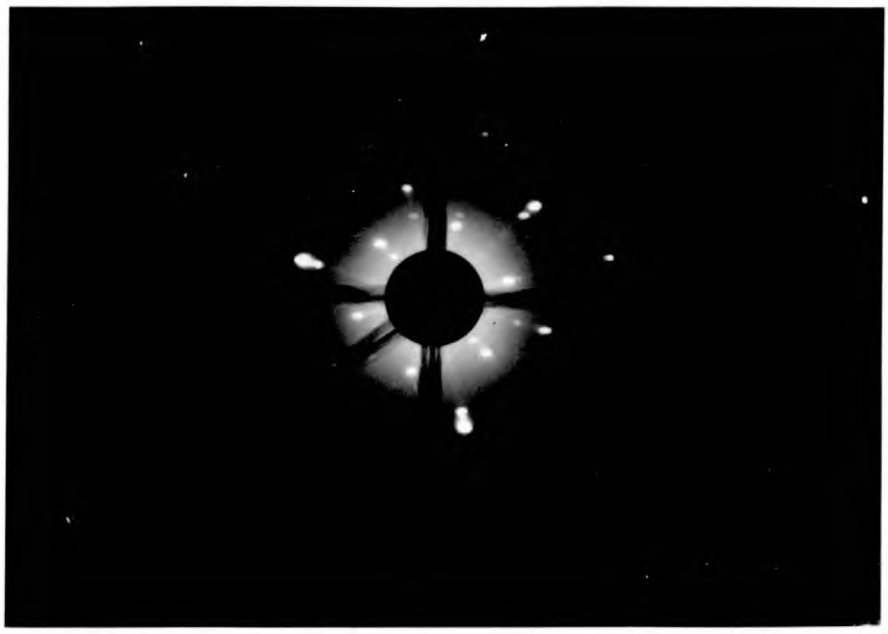

(b) PbTe ON MICA SUBSTRATE

(the six centre spots are due to PbTe)

previous data for PbTe (see page 16) .

Electron diffraction patterns for PbSe and micrographs of the relevant areas are shown in fig. 3.4 . When PbSe is evaporated on to mica at room temperature, the diffraction pattern (3.4 a) indicates good orientation of the deposit, although the 'crystallite size' (as seen from 3.4 b) is very small. For a high substrate temperature during deposition, the diffraction pattern (fig. 3.4 c) is more complicated, due to a mixture of phases or orientations, whereas the crystallite sizes are larger.

The diffraction patterns for PbS (figure 3.5) show a different behaviour. For material deposited at room temperature, a ring pattern is obtained, indicating a mixture of orientations, possibly with {100} and {111} parallel to the substrate but with random alignment about the azimuth. With a substrate temperature of about 275 °C , there is a certain amount of preferential orientation. At 320 °C deposition temperature, the diffraction pattern shows spots which indicate that the {100} plane is parallel to the surface. The diffuse circle in the centre is due to a carbon support film. For a growth temperature of 365 °C , the film plane is entirely {100} . The tetrad axis of the PbS is then parallel to the six-fold axis of the surface layer of the mica (section 3.4 b) ; this allows 3 - fold positioning of the deposit, giving a diffraction pattern with 12 - fold symmetry . There is also a small amount of {100} material not aligned about the perpendicular axis, as shown by faint rings near the centre of the pattern.

3.2 Surface replicas

Since mica is much less chemically-reactive than the lead salts, the semiconductor can only be separated from the substrate by destroying part of the film. There is consequently a danger that features apparent in transmission micrographs may be artefacts produced by the etch.

An alternative technique, which avoids this difficulty,

Figure 3.4 Selected area diffraction patterns and micrographs (x50,000) of PbSe on mica

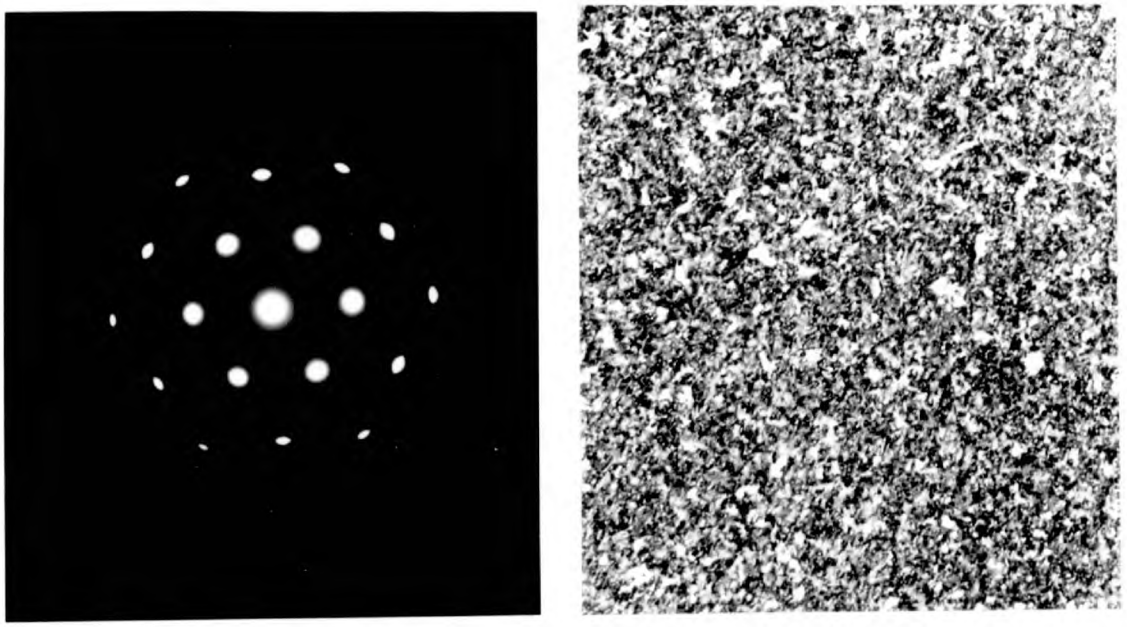

(a) deposited at 20°C (b)

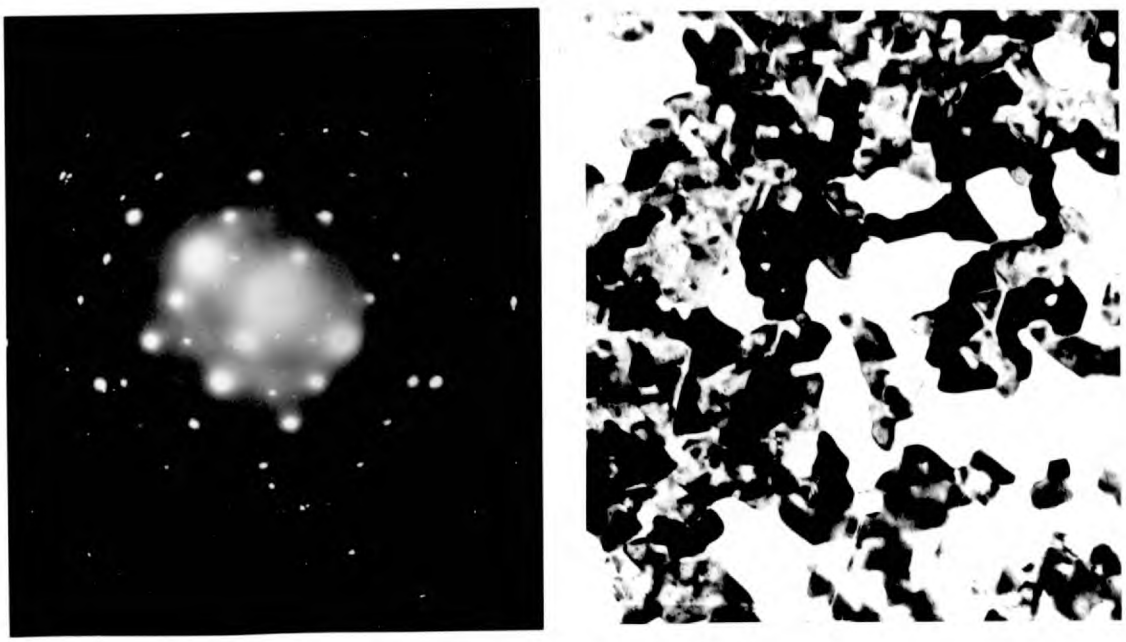

(c) deposited at 370°C (d)

Figure 3.5 Diffraction patterns of PbS films on mica

$T_S = 20°C$

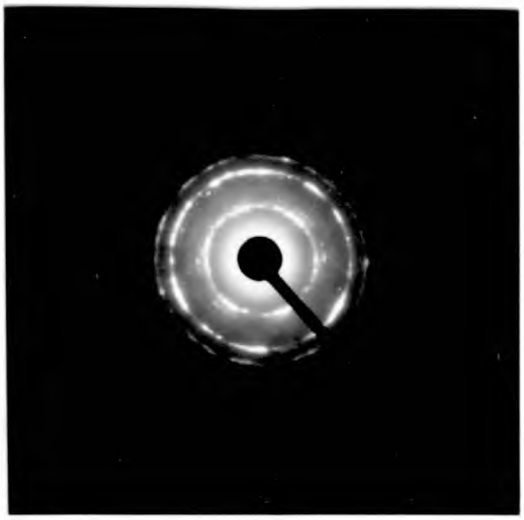

$T_S = 275°C$

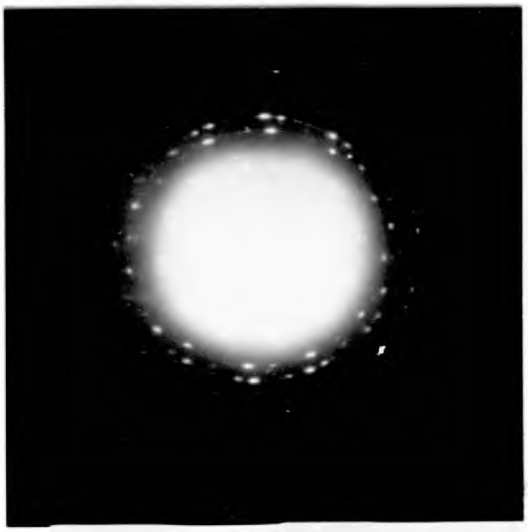

$T_S = 320°C$

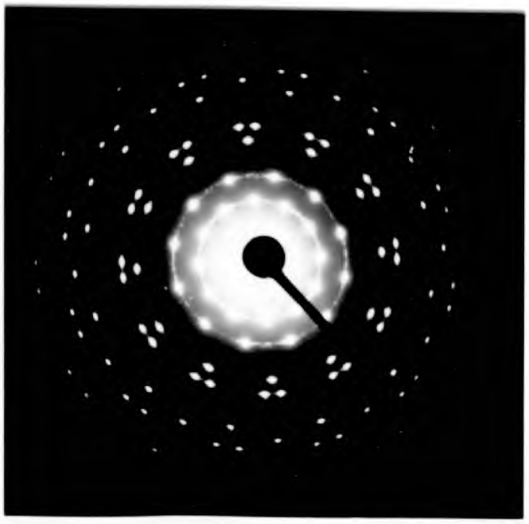

$T_S = 365°C$

is to study the surface structure of the films by making a replica. The most suitable replicating material for high-resolution work is evaporated carbon, which is amorphous (with a very small grain size).

The carbon was evaporated on to the specimen in a vacuum of about 10^{-5} torr from a source consisting of two pointed carbon rods held together under light pressure. A current of about 100 amp was passed between the two rods for a few seconds, giving a film thickness of 100 - 200 A^{o}. The specimen was then immersed in an acid which would dissolve the semiconductor, thereby separating the carbon film from the substrate. The carbon replica was mounted on a grid and viewed in transmission in the electron microscope. The image obtained shows thickness gradient contrast, because the thickness of carbon film presented to the electron beam is highest at steps on the surface (see figure 3.6 a). Surface features therefore appear in outline; an example of this type of replica is shown in figure 3.11 (page 59)

Either before or after depositing the carbon film, the specimen can be 'shadowed' by evaporating a mixture of platinum and carbon at an oblique angle, as shown in fig. 3.6 c. The same type of carbon source was used, but with a small piece of platinum foil between the carbon rods. After immersion in acid, platinum remains attached to the carbon replica, and greatly reduces the electron-transparency of the film. Only these areas of specimen which were shielded from the evaporation beam appear bright in the image formed on the microscope screen. An example of a shadowed replica is shown in fig. 3.6 d. The effect is similar to that produced by oblique illumination of specimens in an optical microscope, and is more realistic when seen as a negative of the original image, since the shadowed areas then appear dark (figures 3.13 c and 3.13 d, page 63). Shadowing increases the contrast obtained from a replica, and was therefore employed in most of the present work. There is also the advantage that the height of surface protrusions can be estimated from the

Figure 3.6 SURFACE REPLICAS

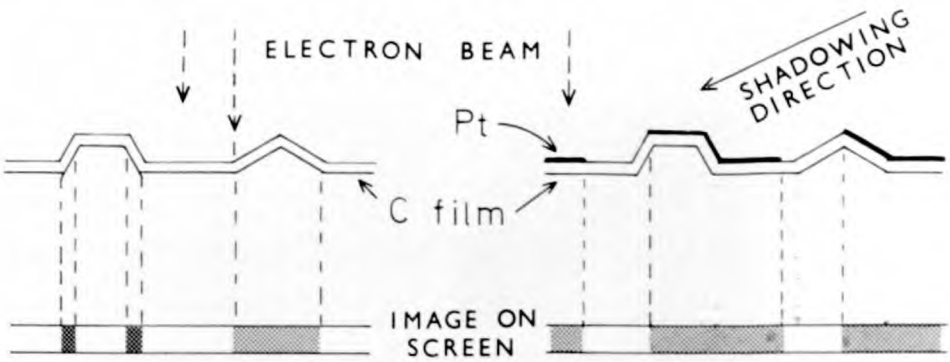

(a) Unshadowed replica (b) Shadowed replica

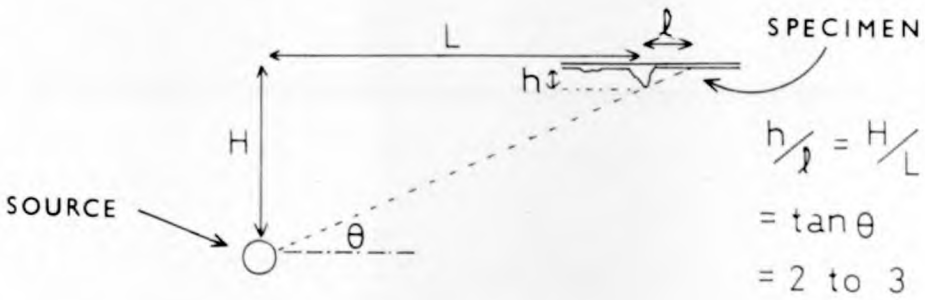

(c) Arrangement for evaporating Pt/C mixture

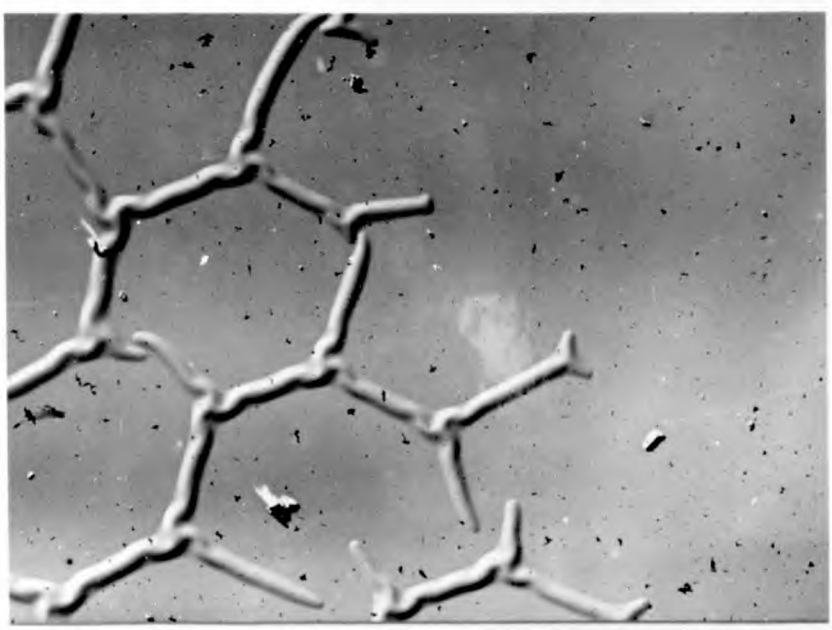

(d) Carbon film on mica, shadowed with Pt/C (x4000)

shadow length, if the angle θ is known (see fig. 3.6 c) .

The replica method is particularly useful for discontinuous films, and was used to examine the early stages of growth of the present films.

3.2 a Nucleation and growth of PbTe , PbSe and PbS on mica

Figure 3.7 shows stages in the growth of a PbTe film deposited on to mica at 300 °C .

The first picture (a) shows an area of film with an average thickness of about 5 A° . The lead telluride is in the form of tetrahedral nuclei about 300 A° across, in either of two different orientations as indicated below.

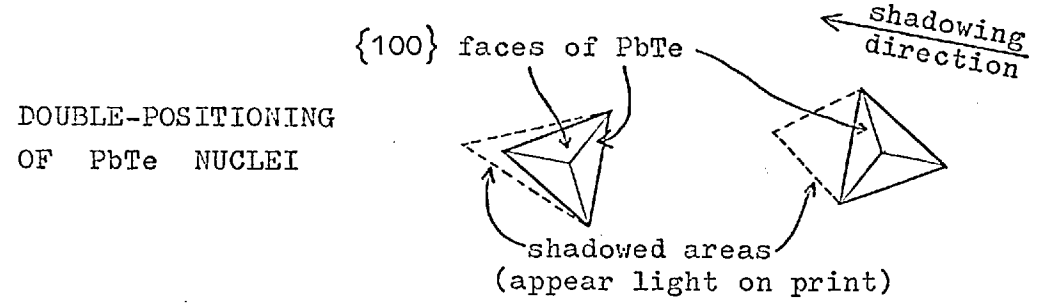

As the film thickness increases, the nuclei grow in dimension, their density remaining practically the same (fig. b). At an average film thickness of 100 A° , they begin to overlap with one another (fig. c) . When this happens, their shape becomes distorted, and the nuclei undergo a liquid-like coalescence. This is shown at higher magnification (X 75,000) in figure 3.7 d . With further increase in thickness (fig. e) the nuclei completely lose their angular shape ; at the same time, the film becomes electrically continuous.

In figure 3.7 f , the areas between the original nuclei have all filled in , but depressions are left in the surface ; these are irregular in shape but tend to show the 60° angles of the original outlines of the nuclei. At a film thickness of 3000 A° (fig. g) these are still present. It is not possible to estimate the depth of the surface depressions from

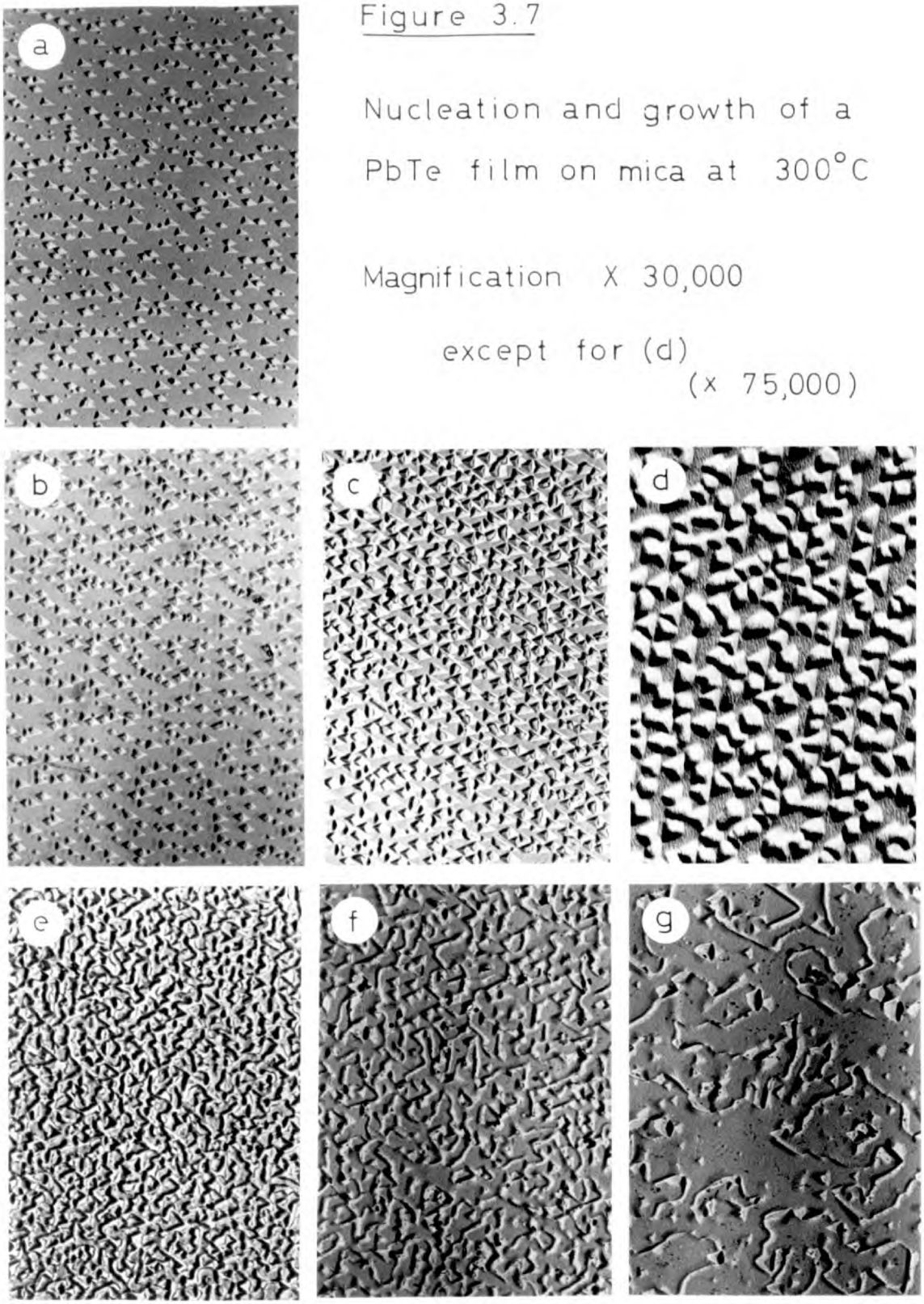

Figure 3.7

Nucleation and growth of a PbTe film on mica at 300°C

Magnification X 30,000

except for (d)
(x 75,000)

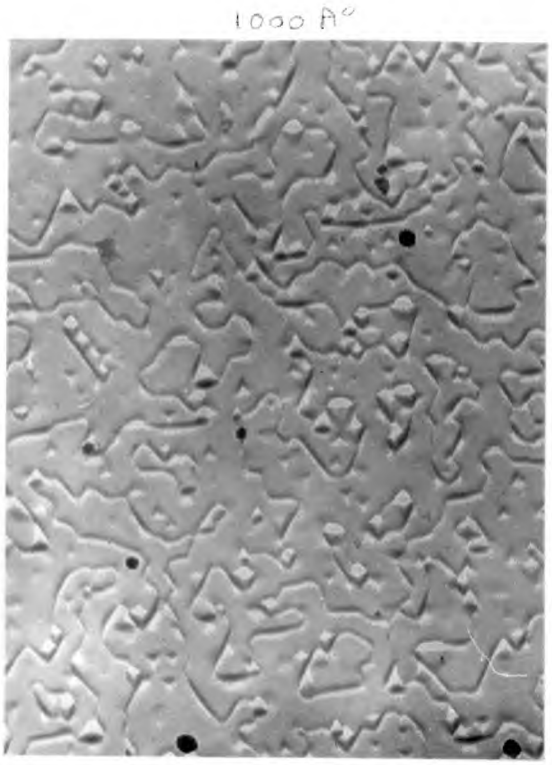

Figure 3.8

PbTe films of different thickness, grown on mica at 310°C

Replicas X 25,000

1μ

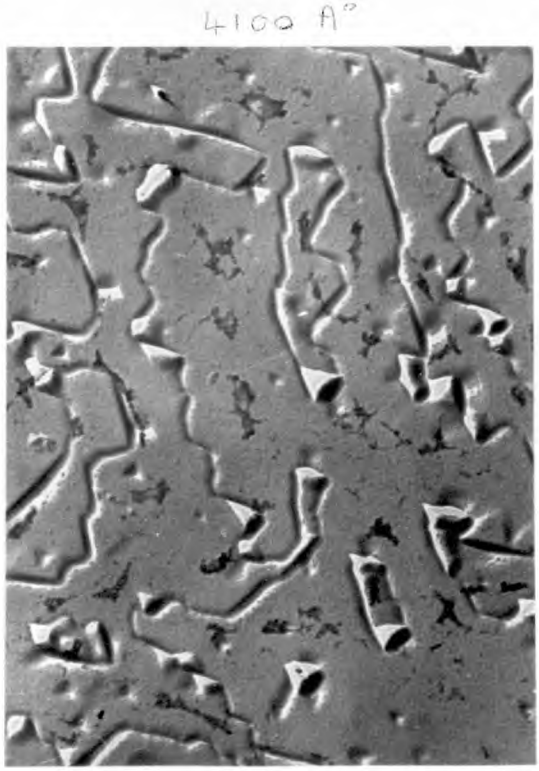

the shadowing, but they are believed to correspond to the double-positioning boundaries observed in transmission micrographs (figs. 3.1 and 3.2) .

The micrographs in figure 3.7 were obtained by looking at different areas near the edge of a Hall sample, where the film has a thickness gradient produced by the edge of an evaporation mask (see 2.2 b) . (This is due to the finite aperture of the source, and possibly also to scattering of evaporant by the edge of the mask) . The thinner areas of film are therefore due to a lower (effective) deposition rate. However, discontinuous films produced at normal evaporation rates (e.g. 5 A^{o} / sec) appeared very similar ; it is therefore assumed that the nucleation behaviour is not very rate dependent.

Replicas which had some PbTe still attached to the carbon film gave a spot diffraction pattern for all thicknesses, indicating that the semiconductor film remains well-oriented with respect to the substrate during all stages of growth.

Figure 3.8 shows replicas of three continuous PbTe films of different thickness , deposited on to mica at 310 ^{o}C . The number of boundaries visible at the surface decreases with increasing film thickness.

Figure 3.9 is a micrograph of PbTe deposited on a heated alumina substrate * . A similar surface structure is present, with 60^{o} angles between boundaries, suggesting that the film plane is again {111} . The micrograph also shows evidence of cracks, probably caused by the difference in expansion coefficient between the film and substrate (see 4.5 f) .

The nucleation of PbSe is similar to that of PbTe . Figure 3.10 a shows a micrograph of a discontinuous PbSe film deposited on to mica at 370 ^{o}C . The film was coated with carbon, which forms a continuous support film, and immersed briefly in an

---

* The author is grateful to Dr. E.A.D. White for supplying the single - crystal Al_2O_3 platelets.

Figure 3.9 PbTe on alumina (shadowed replica)

X 30,000 1 μ

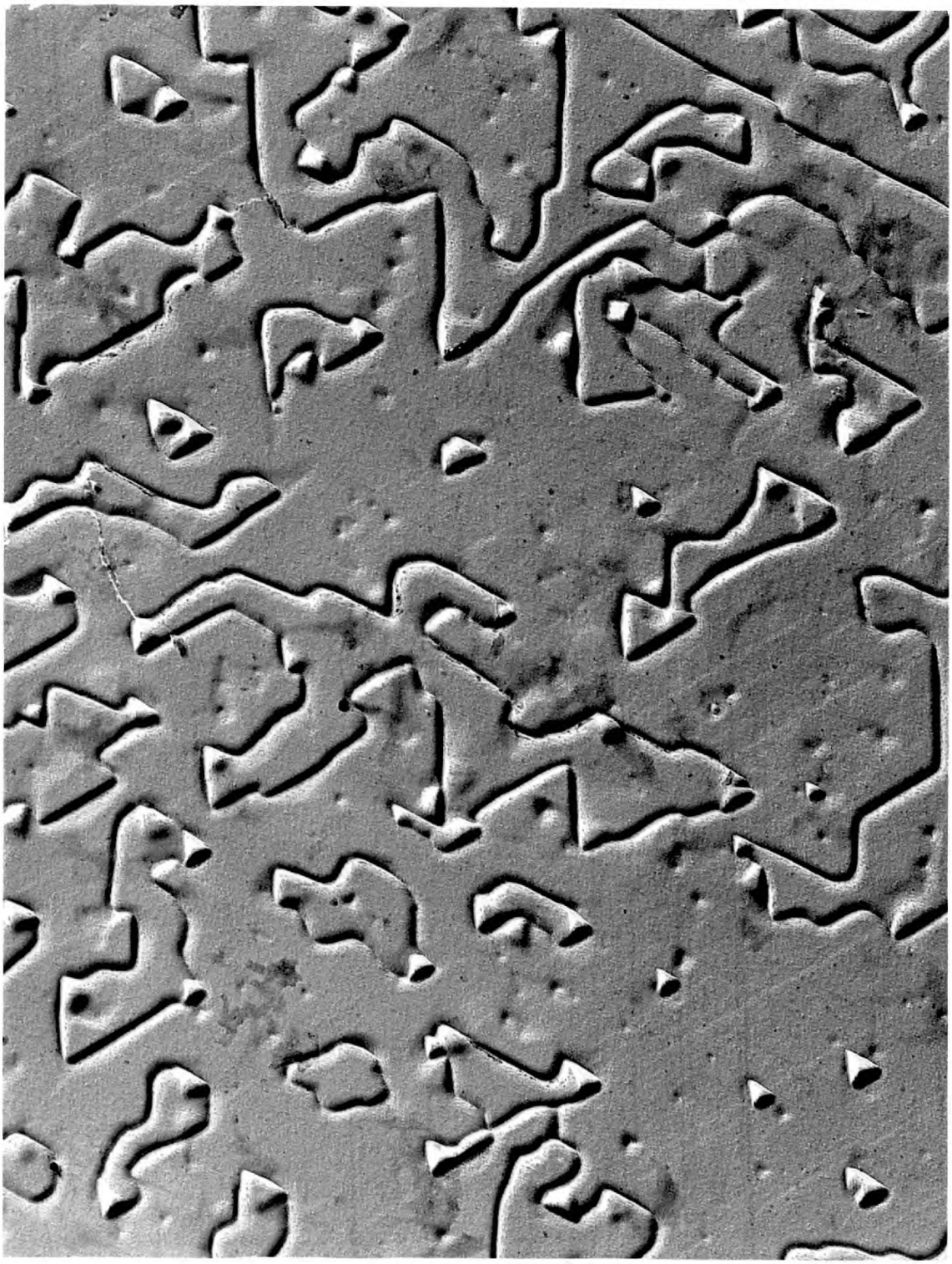

Figure 3.10 PbSe films grown on mica

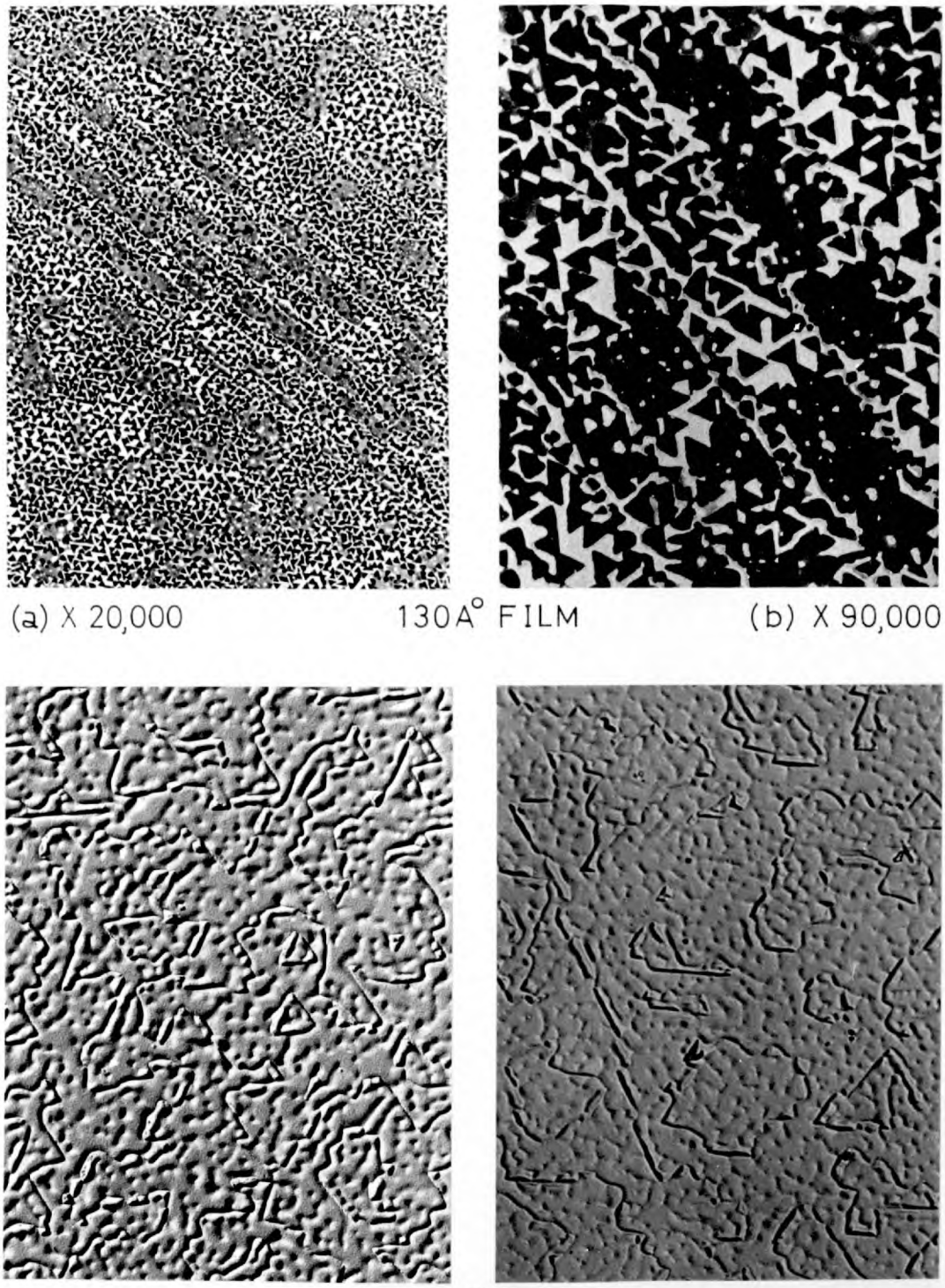

(a) X 20,000 130A° FILM (b) X 90,000

(c) C replica 3000A° FILM X 20,000 (d) SiO replica

Figure 3.11 NUCLEATION OF PbS

X 40,000

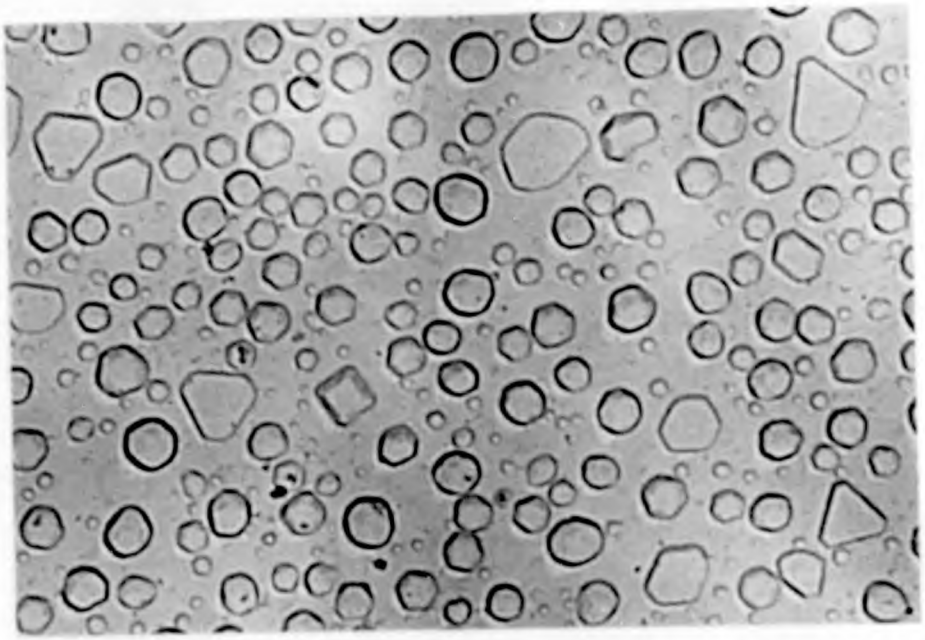

(a) Unshadowed carbon replica

(b) Carbon replica shadowed with Pt

etch, leaving some PbSe present, which shows up the outline of the nuclei. The sample area shown contained cleavage steps on the mica surface, which have been 'decorated' by the deposit. At higher magnification (figure 3.10 b), the nuclei adjacent to the steps are seen to be of small size and irregular shape. The flat grey areas visible in this picture are probably due to PbSe with the {100} plane parallel to the surface (P 13). Replicas of 3000 A^{o} films (figs. 3.10 c and 3.10 d ; deposition temperature = 350°C) are fairly similar to the case of PbTe . Fig. 3.10 d is from a silicon monoxide replica , which was lightly shadowed with Pt / C .

Replicas of discontinuous PbS films are more complicated, as would be expected from the diffraction patterns. Figure 3.11 shows carbon replicas of a discontinuous PbS film, deposited on to mica at 320 °C . The specimen shown in fig. 3.11 a was not shadowed, and displays thickness gradient contrast. The shape of the nuclei suggests a mixture of orientations, including both {100} and {111} parallel to the substrate. A notable feature is that most of the nuclei are flat, plate - like structures .

3.2 b Effect of substrate temperature

A number of PbTe films were deposited on mica substrates at different temperatures, using the same evaporation rate (300 A^{o} / minute) and time (10 mins) . Substrate surface temperatures were obtained from the calibration curve for thermocouple readings, fig. 2.6 . Shadowed carbon replicas were made of the surfaces of the films, and these are shown in figure 3.12 .

At a deposition temperature of 40 °C , the surface has a granular appearance. At 170 °C , there is in addition a system of lines and 60° corners. At 230 °C , these lines have become longer and more widely-spaced. The granular structure is now seen to consist of small triangular pits, with smooth areas in between . At 250 °C , most of these pits have disappeared, leaving flat areas between the boundaries, which now resemble the

Figure 3.12 PbTe films grown at different substrate temperatures

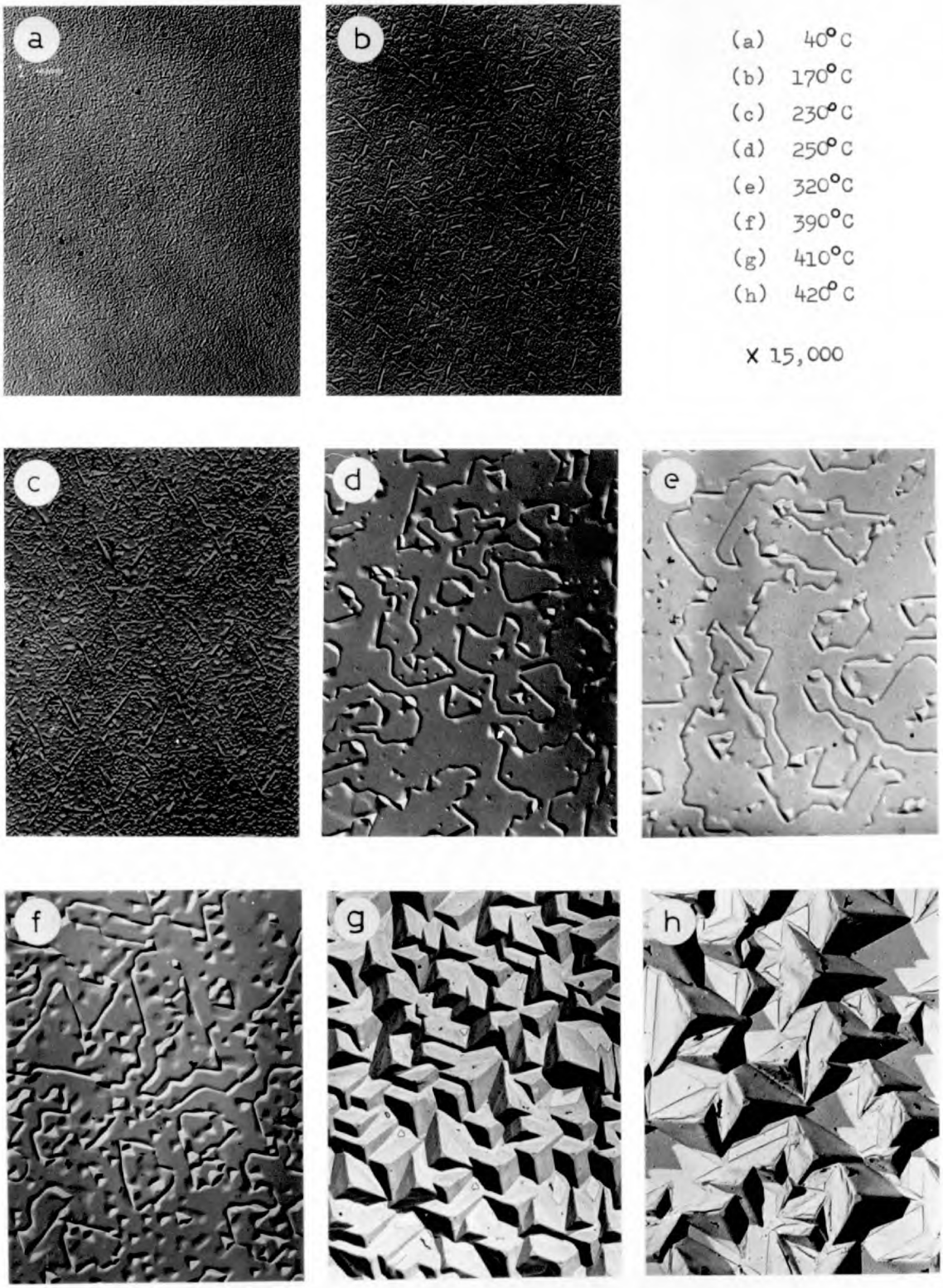

surface structure observed in previous micrographs at 300 °C substrate temperature. At 320 °C, the structure is much the same, except that the boundaries enclose rather larger areas. At 390 °C, the boundary pattern is the same, but rather large triangular pits occur in between.

At 410 °C substrate temperature, the surface appears quite different, consisting almost entirely of {100} faces in the form of tetrahedral peaks. At about 420 °C the tetrahedra have become larger and are separated by flat areas, which are regions of bare substrate. This allows the average film thickness to be calculated; for fig. 3.12 h this is estimated to be 1000 A°, whereas the 'expected thickness' (evaporation rate × time) is 3000 A°. This means that the sticking coefficient (s) has decreased to about $\frac{1}{3}$ at this temperature. (Film thickness measurements gave $s \doteqdot .75$ at 275 °C for a 3000 A° film; see 2.5). The tetrahedra are fairly sharply faceted, the sides being 100 except for a small area of {111} face which truncates the top of them. They are similar in shape to the nuclei observed at lower deposition temperatures, but several thousand times as large (in volume).

The rough nature of the surface at T_s = 410 °C is shown at lower magnification in figure 3.13 a. Whereas films grown at lower temperature have a bright (shiny) appearance, a substrate temperature of 410 °C gives samples which appear dull and 'milky' when viewed (without magnification) in visible light. This is not surprising, since the micrographs show that the surface roughness (distance between peaks) is of the same order as the optical wavelength.

Figure 3.13 b shows a thinner region of film near the edge of a sample grown at 410 °C. Here, the carbon support film was stripped from the mica substrate leaving most of the PbTe attached. The nuclei therefore appear in outline, and this shows up the sharp edges of the tetrahedra.

Figure 3.13 c is a replica of a fully-discontinuous PbTe

Figure 3.13 PbTe films deposited at high temperature

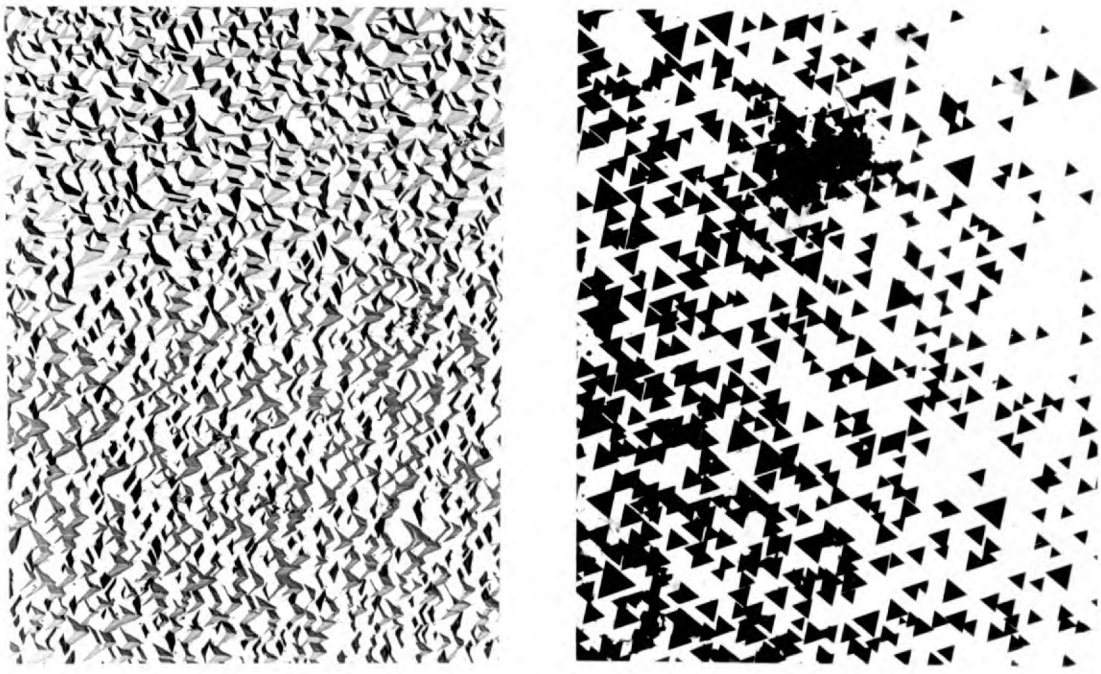

(a) $T_S = 410°C$ (x 4000) (b)

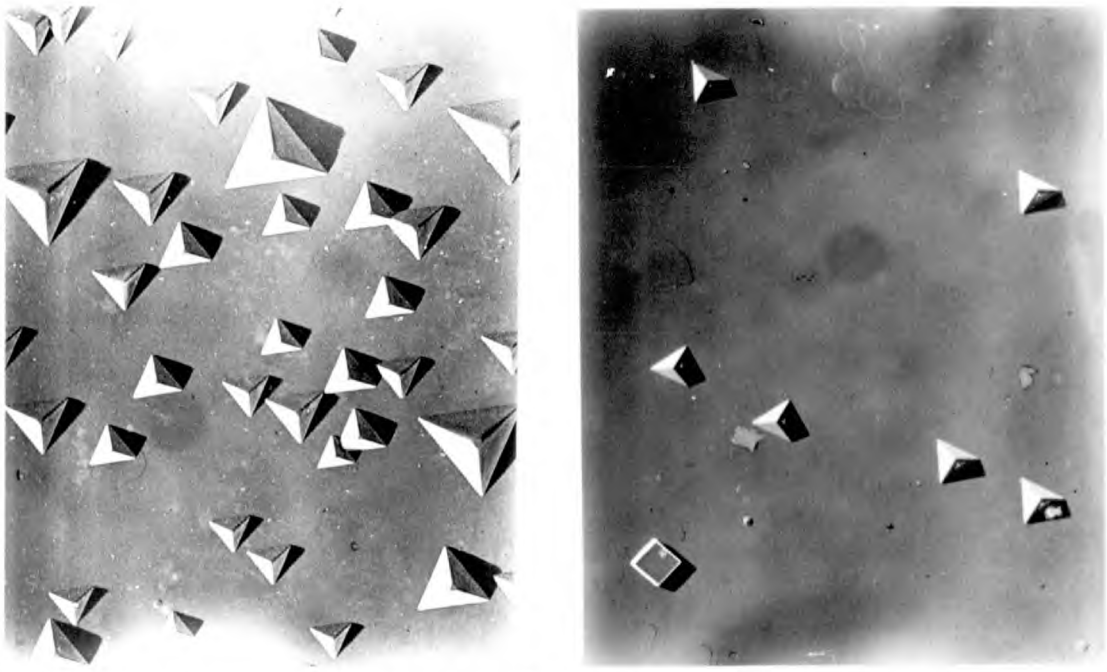

(c) $T_S = 420°C$ (x 15000) (d)

film grown at a substrate temperature of about 420 °C . The tetrahedral faces are maintained even where two nuclei interpenetrate. Figure 3.13 d shows another area of the same film, including a square-sided nucleus which had {100} parallel to the substrate. This type was fairly rare in the PbTe specimens, but occurs frequently in PbSe films (P 13).

3.3 PbTe on PbSe

Figure 3.14 shows a diffraction pattern from a double film produced by evaporating about 240 A° of PbSe on to mica, followed by 120 A° of PbTe , the substrate temperature being kept at 300 °C . The electron diffraction pattern consists of double or multiple spots, but maintains hexagonal symmetry, indicating that the PbSe and PbTe lattices are in the same orientation.

A micrograph of the same area (fig. 3.14 b) shows that the film is partially discontinuous, with areas of substrate devoid of semiconductor. But in the regions where PbSe was present initially, PbTe has deposited epitaxially . As a result, these regions show a two-dimensional system of Moiré fringes on the bright-field micrograph, due to the different lattice spacing of PbSe and PbTe .

Figure 3.14 c shows another area of the sample at higher magnification (x 200,000). In this case, the Moiré fringes are mainly one - dimensional .

By measuring the radial separation of spots (between PbSe and PbTe) on the diffraction pattern (fig. a) , the difference in lattice constant is estimated as 5% . This is within the range 3·2% to 6·2% given by measurements on bulk specimens (section 1.6) and is consistent with the assumption that the difference in lattice spacing is accommodated by misfit dislocations at the interface, as found for PbSe and PbS (M8).

The spacing D of Moiré fringes for parallel lattices

Figure 3.14 PbTe on PbSe

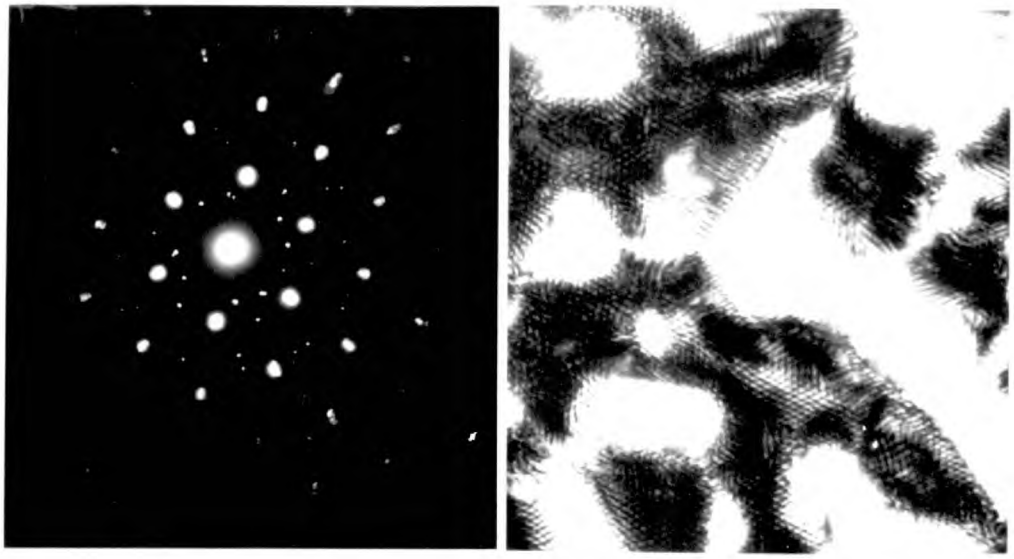

(a) Diffraction pattern (b) Selected area X 100,000

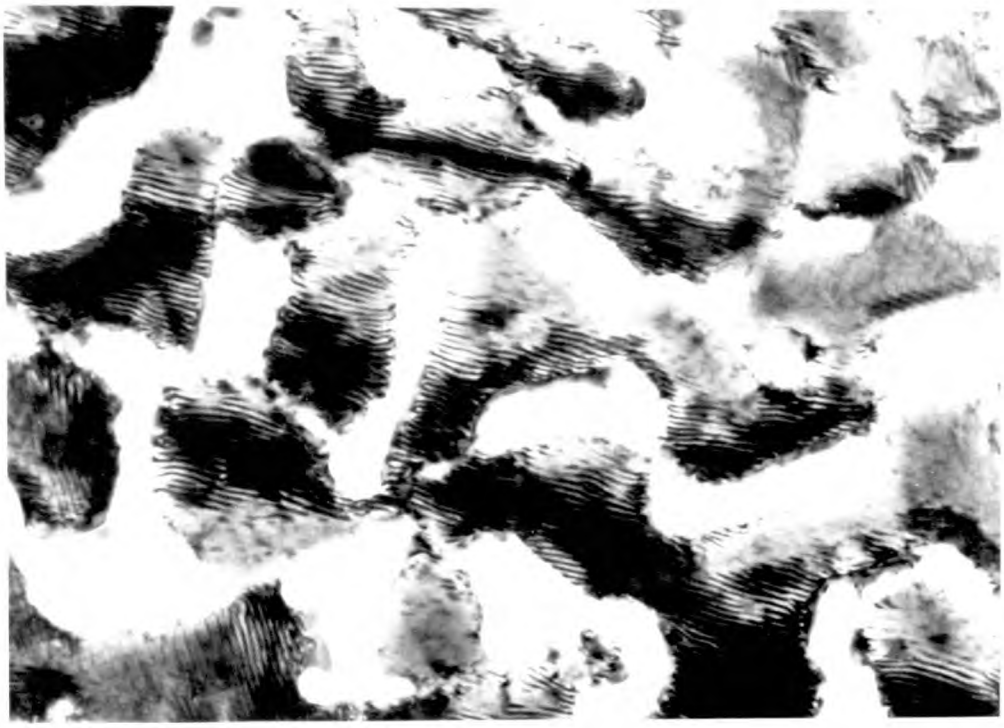

(c) Moiré fringes 1000 Å X 200,000

is given (H 9, K 4) by :

$$D = \frac{d_1 \, d_2}{\Delta d} \qquad (3.1)$$

where d_1 and d_2 are the spacings of the diffracting planes in the two materials and $\Delta d = |d_1 - d_2|$
For similar planes in both materials, and for $d_1 \doteqdot d \doteqdot d_2$,

$$\frac{\Delta d}{d} = \frac{\Delta a_o}{a_o} \doteqdot 5 \times 10^{-2} \quad \text{from above}$$

where a_o is the approximate lattice constant of both materials.

The Moiré fringe spacing in figure 3.14 c is about 42 A^o . Equation (3.1) then gives :

$$d \doteqdot 42 \times 5 \times 10^{-2} \doteqdot 2{\cdot}1 \; A^o$$

This indicates that the diffracting planes which gave rise to the fringes in fig. 3.14 c were of the type (220) , since these planes have a spacing of $a_o/\sqrt{8} \doteqdot 2{\cdot}1 \; A^o$.

3.4 Discussion

The diffraction patterns for PbTe and PbSe show that these materials can be grown epitaxially on mica even at room temperature. This is in contrast to the majority of other systems, where a substrate temperature of several hundred degrees centigrade is normally required for perfect orientation of the deposit * . Thin films of the lead salts are also unusual in having semiconductor properties similar to those of the bulk materials ** .

Good electrical properties and epitaxy down to room temperature are also obtained by evaporating these materials on to NaCl and other alkali halide substrates (Z 7, S 11). However, there is the important difference that in the latter case the deposit occurs with {100} parallel to the substrate.

---

* An exception is Ag on NaCl , which can be epitaxial at room temperature.

** Other examples are SnTe (Z 7) and Ag_2Te (P 3) .

The aim of this discussion is to try to account for some of the above observations.

3.4 a Nucleation processes

Present theories of thin-film nucleation (H 10, W 2, L 6, H 1) assume that the evaporant arrives at the substrate in the form of isolated atoms. These will prefer to take up positions of lowest energy, namely at 'atomic sites' where the binding energy is E_a . The value of this adsorption energy will depend on the type of bonding in the substrate and in the material being deposited. Where only physical (Van der Waals) forces are present between the two materials, E_a is typically 0·1 eV / atom . Where chemical (ionic or covalent) bonding is involved, E_a may be 1 eV / atom or more.

Very soon after arriving on the substrate surface, atoms of the material being deposited acquire an equilibrium energy which depends on the substrate temperature. Due to this thermal energy, a single atom on the surface will eventually re-evaporate. This will occur after an average lifetime τ_a , given by :

$$\tau_a = \nu_o^{-1} \exp (E_a / kT) \qquad (3.2)$$

where ν_o is an atomic vibrational frequency, of the order of 10^{12} to 10^{13} sec^{-1} . As a further result of their thermal energy, deposited atoms ('adatoms') are mobile, and can change atomic sites at a rate v per second, where :

$$v = \nu_1 \exp (-E_d / kT) \qquad (3.3)$$

ν_1 is another vibrational frequency, often assumed equal to ν_o , and E_d is the activation energy for surface diffusion , i.e. the energy barrier height between low-energy atomic sites.

When there are appreciable numbers of atoms on the substrate surface, those which collide can become temporarily bound together. As soon as a cluster of atoms reaches a certain critical size, it becomes stable ; in the majority of practical

systems, these critical clusters contain only a few atoms. Growth (by the addition of atoms) can then proceed from these centres, which eventually become large enough to be visible in an electron microscope. These nuclei grow further in size and number until they overlap and the film becomes continuous. During this coalescence stage, defects such as dislocations, low-angle and double-positioning boundaries are introduced into the film, due to differences in orientation or atomic positions between neighbouring nuclei.

In cases where epitaxy occurs, the orientation of the deposit is determined by the substrate and is usually that for which the energy of the smallest stable cluster of atoms is a minimum. For large clusters, this means the lowest interfacial energy ; for small clusters, the energy must be calculated as the sum of the separate bond energies. When the nuclei have grown sufficiently to become visible in the electron microscope, their shape is largely determined by the external faces which have minimum free energy (providing the mobility of adatoms is sufficiently high , as discussed in 3.4 d).

Good epitaxy is therefore expected to depend on the following conditions.

1) A small value of E_d will lead to a high surface mobility v (eqn. (3.3)) so that adatoms can move sufficiently far in times comparable with the evaporation time to take up positions of minimum energy.

2) E_a should be large compared with E_d , since the number of sites visited by a single adatom before re-evaporation is given (from (3.2) and (3.3)) by :

(assuming $\nu_0 = \nu_1$)

$$m_a = \exp(E_a - E_d / kT) \qquad (3.4)$$

A large value of m_a will ensure that the final positions of the atoms are those of lowest energy, and will lead to a smaller number of nuclei.

3) The adsorption energy (E_a) itself should be fairly high, since this is more likely to give a substantial difference in energy between alternative equilibrium sites on the substrate surface, and therefore favour a single orientation of the deposit.

3.4 b Application to PbTe on mica

The nucleation theories outlined above can be expected to apply to semiconducting compounds such as the lead salts, with the difference that the migrating species consists of molecules rather than single atoms. From energy considerations, it might be expected that a molecule of PbTe becomes bound to the substrate with both Pb and Te atoms adjacent to the surface, as shown in fig. 3.15 a, since this could involve a larger number of bonds per molecule. But when nuclei are formed, these occur in {111} orientation, such that the atomic plane next to the substrate surface consists entirely of one type of atom (Pb or Te). This would therefore involve re-orientation of single molecules, as shown in fig. 3.15 b .

Figure 3.15

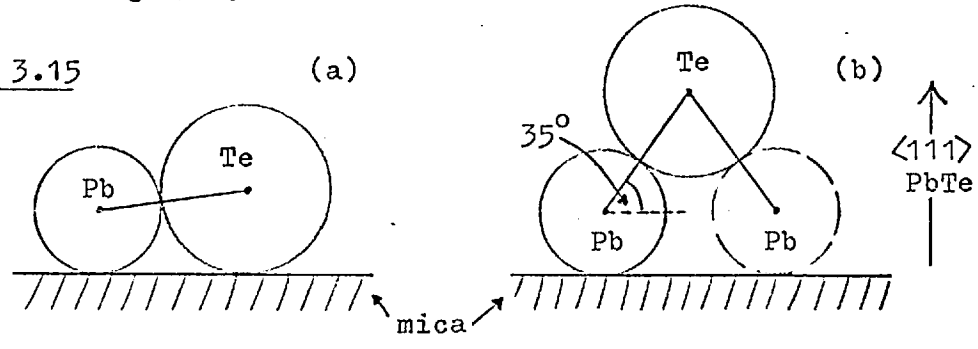

Lewis and Stirland (L7) have investigated the nucleation of PbTe on NaCl . Here, the deposit is {100}, so that both Pb and Te atoms can remain in contact with the substrate. The adsorption energy E_a was estimated as 0·78 eV / molecule. This fairly high value is close to the self-binding energy of a single molecule on a PbTe surface, which is about one third of the bulk cohesion energy (heat of sublimation). The diffusion energy was assumed to be low, because of the good orientation observed.

There is cause to believe that the nucleation conditions for PbTe on mica are similar, and that the requirements for epitaxy (discussed in 3.4 a) are well-satisfied. The reasons are as follows.

1) At room temperature, the surface mobility is sufficient for all molecules to become oriented, suggesting a low value of E_d.

2) $E_a - E_d$ must be considerable ($> .5$ eV) because of the fairly low density of nuclei ($\sim 10^{10}$ cm^{-2} in figs. 3.7 a and 3.7 b) at $T_s = 300\,^{\circ}C$.

3) At a deposition temperature of $420\,^{\circ}C$, the sticking coefficient (s) is still appreciable, and in view of the large sizes and distances between nuclei, PbTe molecules must be able to migrate over considerable distances (of the order of 1 micron). This, too, indicates that E_a is considerably larger than E_d. The formation of sharply-defined crystal faces is also an indication of high mobility of the molecules.

Examination of figures 3.7 a and 3.7 b shows that double positioning gives rise to the two orientations of nuclei in approximately equal numbers. This suggests that the layer of surface atoms on the mica substrate presents a hexagonal symmetry to the deposit. Figure 3.16 shows a diagram of the cleavage plane of muscovite mica (W 8). The surface consists of oxygen atoms forming the bases of silicate tetrahedra which are linked together at the corners to form a continuous sheet structure. In the bulk of the material, these sheets are linked to potassium atoms by fairly weak, mainly ionic forces which arise because a variable but limited proportion of silicon atoms within the tetrahedra are replaced by aluminium (E 6). When the mica is cleaved, a potassium atom at the cleavage plane may vapourise or remain attached to either of the two faces. The resulting arrangement of potassium atoms is therefore not known, and may be irregular. However, the oxygen atoms form hexagonal rings, which can account for the equal numbers of PbTe nuclei in the two orientations.

Figure 3.16 MICA SURFACE STRUCTURE

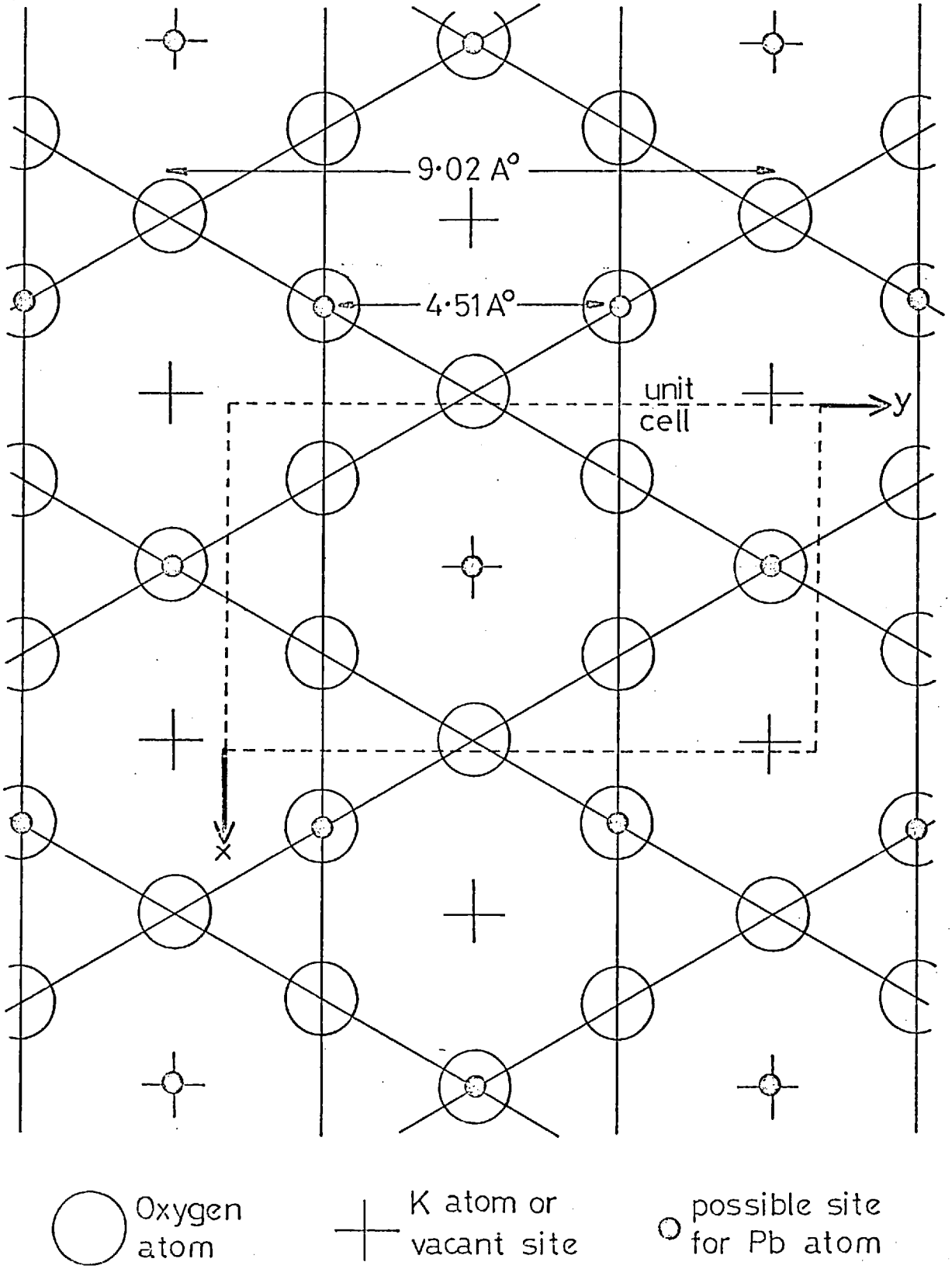

In view of the chemical affinities, it is likely that the bonding takes place between oxygen and lead, rather than between oxygen and tellurium atoms. The atomic plane adjacent to the substrate would then consist of Pb atoms, and the strength of the Pb - O bond (4·3 eV in single molecules, ref. P 14) would account for a high adsorption energy. A low diffusion energy is perhaps understandable, since a PbTe molecule could migrate with the Pb atom remaining in contact with oxygen atoms, which form a 2-dimensional structure.

From the Laue photograph (figure 3.3), the orientation of the PbTe deposit (purely from symmetry considerations) is either :

(A) (111) PbTe ‖ (001) mica , $[1\bar{1}0]$ PbTe ‖ [100] mica

or (B) (111) PbTe ‖ (001) mica , $[1\bar{1}0]$ PbTe ‖ [010] mica

From X-ray and reflection electron diffraction data, Makino (M 3) concluded that PbTe evaporated on to heated mica exists in orientation (A) . There is then a difference of about 13% between the spacing of potassium sites in the mica and the separation of Pb atoms on the (111) plane of PbTe .

However, Poh (P 13) has examined similar films by X-ray diffraction and electron microscopy, and deduced that the deposit occurs in orientation (B) . In this case, there exists an approximately exact relation between the atomic spacing in the two lattices along a common direction, since the nearest-neighbour distance * in the (111) PbTe plane is half the b_o dimension of the unit cell of mica (see fig. 3.16). It is then possible to place Pb (or Te) atoms at similar sites on the mica surface over a considerable area without straining the PbTe lattice. A possible arrangement is shown in fig. 3.16 .

There is no guarantee that this orientation (B) will provide the lowest energy for a stable cluster of PbTe molecules . In fact, there are cases ({100} films of Cu , Ag or Au on

---

* assuming a_o = 6·37 A° for PbTe, which lies between the two experimentally-determined values ; see page 16 .

NaCl) where the chosen orientation is not the one for least atomic misfit ; the exact nature of the bonding and the size of the atoms involved must be taken into account. However, it seems probable that good epitaxy is in general more likely to occur when atomic spacings in the two materials differ by only a small percentage (M 10) . In the present case, this hypothesis is attractive, since it could explain the fact that epitaxy of PbSe and PbS on mica is less perfect, nucleation occurring on more than one plane. In orientation (B) , the misfits are 4% and 7% for PbSe and PbS .

3.4 c Growth processes

The double-positioning boundaries which occur in PbTe films on mica are incoherent twin boundaries, which result from a lattice rotation of 180° about a {111} axis. The twin plane is {111} . (They can also be regarded as a special case of a high-angle grain boundary, the angle being 60°) . Similar boundaries have been observed in other systems, e.g. {111} Au on mica and MoS_2 (P 4, J 1, S 30), and originate when two nuclei in twinned orientations coalesce.

The boundary represents an increase in energy compared with a single orientation, and there will be a tendency for the combined nucleus to recrystallise in one of the two orientations, by migration of the boundary out of the system. The time needed for this to occur depends on the relative sizes and positions of the two islands before coalescence (J 1) . In practice, some D.P. boundaries are left when the film becomes continuous. These link together to form complete loops enclosing a domain of single orientation. Their shape is irregular, but they tend to intersect the external surface of the film along $\langle 1\bar{1}0 \rangle$ directions (the boundary plane is then $\{11\bar{2}\}$) . A decrease in the total length of a boundary (with a consequent decrease in interfacial energy) can take place by a reduction in the number of corners and by the gradual shrinkage and eventual disappearance of certain domains. The boundaries therefore appear straighter and their number decreases with increasing film thickness, as can be seen in fig. 3.8 .

Since boundary movement is a thermally-activated process, the number of boundaries remaining in the film will be less at higher growth temperatures (compare figures 3.12 b to e) .

3.4 d The effect of substrate temperature

Micrographs of films deposited at a temperature above 400 °C (e.g. figs. 3.12 f , 3.13 a) show that the external surface breaks up into a corrugated structure, which is similar in appearance to the effect obtained from thermal etching of certain materials such as cleaved rocksalt. This suggests that despite the increase in surface area, there is a net decrease in energy compared with a flat {111} surface, the PbTe molecules being sufficiently mobile at these temperatures to give a configuration closer to equilibrium. Films grown at even higher temperature (figs. 3.13 c and 3.13 d) consist of isolated nuclei, whose dimensions can exceed 1 micron. Similar large structures have been observed in the case of copper evaporated on to a {111} silver surface (K 5) .

The height of the PbTe nuclei can be estimated from the shadowing (fig. 3.6 c), and this shows that the faces of the tetrahedra are {100} and not {111} as previously observed for some metals, e.g. Au nuclei on MoS_2 (J 1) . This indicates that for PbTe the surface of minimum free energy is {100} , rather than {111} as in F.C.C. metals, this difference being due to the differences in crystal bonding in the two cases. However, close examination shows that all the nuclei have a small area of {111} face truncating the tetrahedron. Assuming that the nuclei represent an approximation to the thermal equilibrium shape, this would suggest that although the free energy is lowest for the {100} surface, the {111} surface is not much higher. This hypothesis is reasonable, since PbTe cleaves (when crushed) mainly along the {100} face , but only to the extent of 90% (G 4) . Moreover, crystals grown from PbTe vapour can exhibit {111} as well as {100} faces (C 5) .

The preference for {100} surfaces in PbTe films is

apparent even at lower deposition temperatures (figs. 3.12 b to f), particularly in regions where D.P. boundaries intersect the external surface. Here, the surface forms a V-shaped valley, whose sides appear to be 100 surfaces. This would tend to stabilise the system of D.P. boundaries, and in fact these do not decrease in number between 320 and 390 °C (see figs. 3.12 e & f). At 390 °C, an increase in the amount of {100} surface also occurs by the formation of triangular pits (fig. 3.12 f), corresponding to the beginning of the transition to a completely faceted surface (fig. 3.12 g).

At lower deposition temperatures, the micrographs show a large number of small surface pits, which probably occur at the intersection of line defects (dislocations) with the external surface. The number of these decreases with increasing deposition temperature (figs. 3.12 a to d).

Figure 3.17 shows results obtained by Poh (P 13) from electrical measurements on the same PbTe samples as were used for the microscopy. Films deposited at 100 °C or below have very low Hall mobility, but the mobility starts to increase at about 170 °C. From the corresponding micrograph (fig. 3.12 b), the surface pits are then about 170 A° apart, which is close to the calculated carrier mean free path of 180 A° at this temperature (section 4.5 a, equation (4.11)). It is therefore likely that the low electrical mobilities at low deposition temperatures are due to scattering of carriers by defects such as dislocations.

Above about 250 °C deposition temperature, the Hall mobility starts to fall (fig. 3.17), the reason for which is not readily apparent from the surface replicas (fig. 3.12). A similar effect in epitaxial films of PbS on NaCl was observed by Zemel (Z 4), who suggested that the decrease in Hall mobility was due to the formation of microcracks in the film when this is cooled from the deposition temperature. Figure 3.17 indicates that for $T_s > 250$ °C, the mobilities measured at room

Figure 3.17 Hall mobilities of p-type PbTe films (measured in air) as a function of deposition temperature.

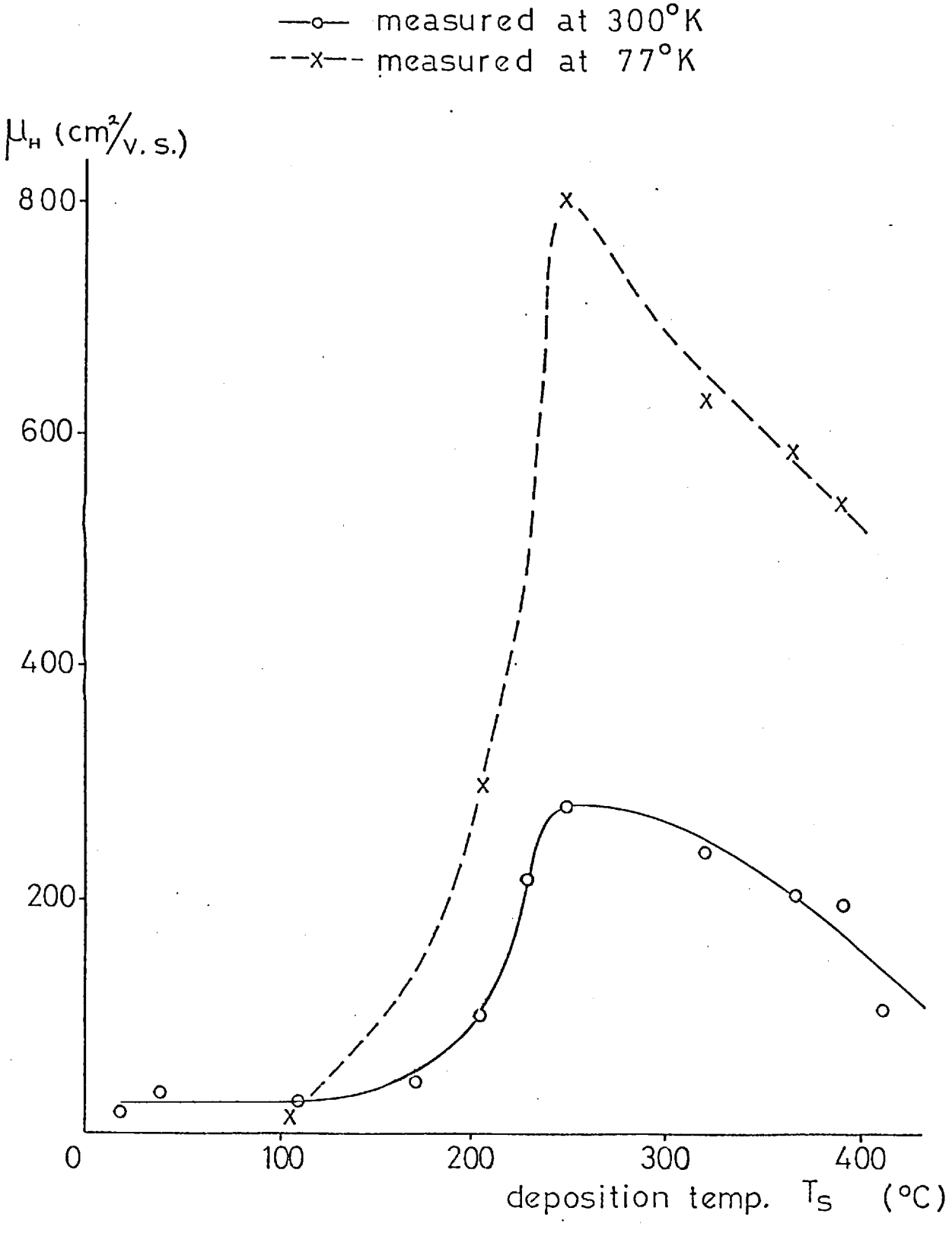

temperature and at 77 °K decrease in roughly the same proportion with increasing deposition temperature, which is consistent with this explanation (section 4.5 f) . A relatively small number of cracks could be effective in reducing the mobility, and these would not necessarily show up in the small areas selected for microscopy. Cracking effects are discussed further in chapter 4 .

CHAPTER 4

HALL MEASUREMENTS

4.1 Experimental details

Films were prepared in the deposition system B by evaporation through a mask, to give a standard Hall sample shape as shown in fig. 4.1 b (next page). In the case of films deposited in system A (without a mask), an equivalent form of sample was made by scratching through the film, as in fig. 4.1 a. The approximate dimensions are shown in the diagram; actual values could be measured to within $\pm$ ·02 mm. by means of a travelling microscope.

Electrical contact to the film was made by soldering with indium or In / Bi alloy *. Contact resistance did not present a serious problem, except in the case of a few low-carrier-concentration samples below room temperature.

Connection was made to five pins on a sample holder by means of 2- thou diameter annealed silver wire. The sample was enclosed by a tight-fitting copper can and placed inside a 'Thermos' tube (which could be filled with liquid nitrogen when required) between the pole-pieces of a 2K Gauss permanent magnet. The magnetic field was calibrated with a 'Norma' (model 251 F) fluxmeter.

A constant d.c. current (typically 250 μA) was passed between contacts 1 and 4 of the sample (see fig. 4.1) and the voltage V , inversely proportional to the film conductivity, measured between contacts 2 and 3. Voltage measurements were performed by a ('Solartron') digital voltmeter, whose input impedance varied between 10 MΩ and 5000 MΩ, depending on the range. To measure the Hall voltage, the voltmeter was connected between contacts 3 and 5 and the maximum and minimum readings recorded as the sample was rotated in the magnetic field. The Hall voltage V_H is then half the

* 33% Bismuth ; melting point 75°C

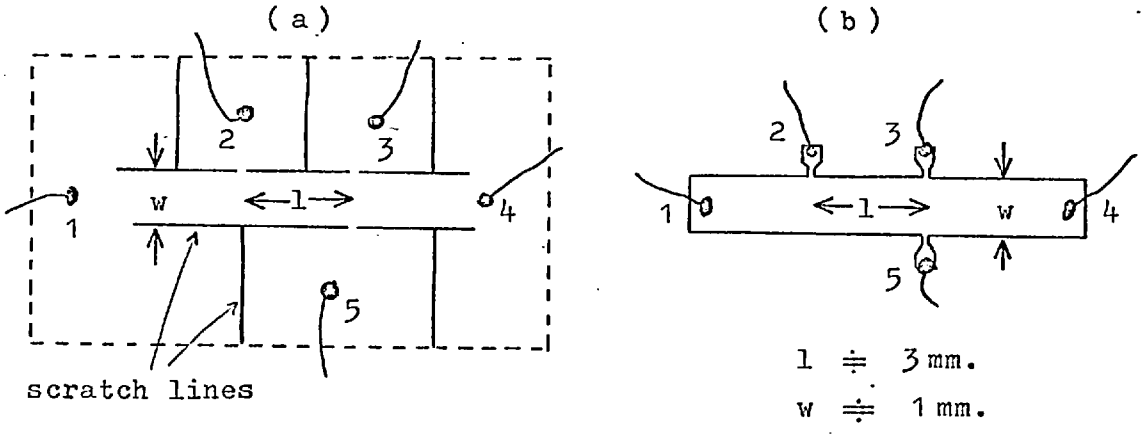

Figure 4.1 Hall samples

difference between the two readings.

The magnetic field of 2 K Gauss corresponds to the low-field region (ref. S23, p. 106) where the Hall coefficient is independent of field, since the highest values of Hall mobility μ_H in the samples gave $(\mu_H B)^2 \sim 0{\cdot}1$. In addition, the Hall coefficient of certain samples was measured with fields up to 12 K Gauss and found to be independent of magnetic field.

The temperature of the sample could be reduced to 77°K by immersion in liquid nitrogen. By pouring out the nitrogen and replacing the sample holder inside the 'Thermos' tube, the sample was allowed to warm up slowly and Hall measurements could be made as a function of temperature. The temperature inside the sample holder was measured by means of a copper-constanton thermocouple.

The results given in this chapter were all obtained from measurements using the apparatus described above, with the sample in air. Hall measurements could also be made on films kept under vacuum in system B. These are described in chapter 5.

4.2 Theory

The Hall coefficient (denoted R_H or R) and the conductivity (σ) of a sample are calculated from the following

formulae :

$$R_H = \frac{V_H\, t}{B\, I} \quad , \quad \sigma = \frac{l\, I}{w\, t\, V} \tag{4.1}$$

where l and w are the sample dimensions (fig. 4.1)

V_H and V are the Hall and conductivity voltages

B is the magnetic field strength

and t is the film thickness, determined by interferometry (as described in 2.5)

If conduction is by both electrons and holes, R_H and σ are given (P20, S23) in the low-field region by :

$$R_H = \frac{rf}{q} \frac{p\mu_p^2 - n\mu_n^2}{(p\mu_p - n\mu_n)^2} \tag{4.2}$$

$$\sigma = q(p\mu_p + n\mu_n) \tag{4.3}$$

where p and n are the hole and electron concentrations

μ_p and μ_n the hole and electron conductivity mobilities

and q is the magnitude of the electronic charge

r is a small factor which depends on the scattering mechanism and statistics of the carriers, and is given by $\langle\tau^2\rangle / \langle\tau\rangle^2$ (see B2 p. 101 , S23 p. 118) . For acoustical mode scattering, r varies between 1·18 and 1·0 , depending on the degree of degeneracy.

f is another small factor, equal to $\frac{3K(K+2)}{(2K+1)^2}$ (S23 , p. 151 . K is defined in secn. 1.9)

For the lead salts , $K = 4$ and $f = 0{\cdot}89$.

In calculations from the experimental results, the Hall factor (rf) has been taken as urity.

In the extrinsic region, where nearly all the carriers are of one type, the expressions for R_H and σ simplify.

If conduction is predominantly by holes ($p \gg n$) , (4.2) reduces to :

$$R_H \doteqdot \frac{rf}{qp} \doteqdot \frac{1}{qp} \tag{4.4}$$

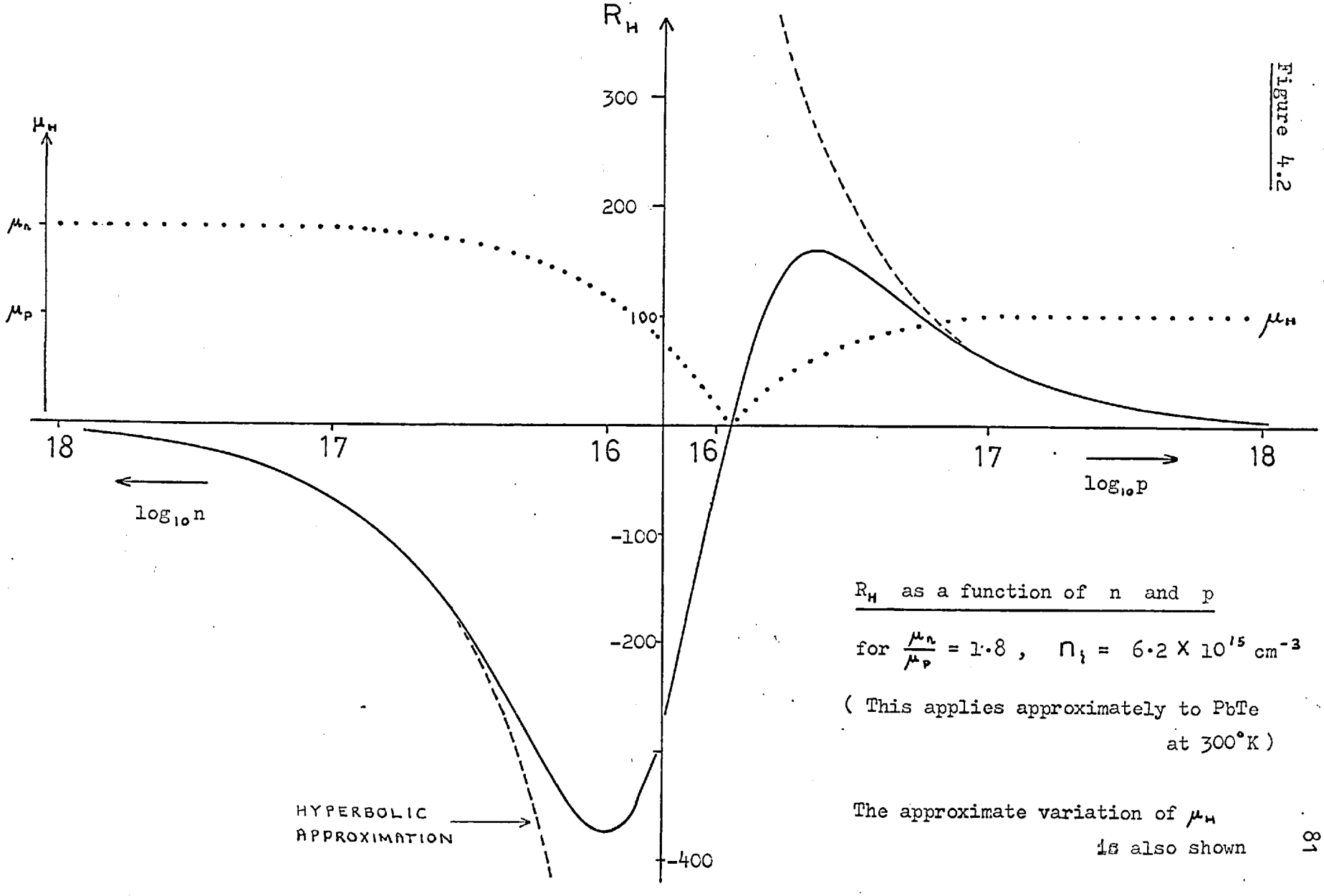

Figure 4.2

R_H as a function of n and p

for $\frac{\mu_n}{\mu_p} = 1{\cdot}8$, $n_i = 6{\cdot}2 \times 10^{15}\ cm^{-3}$

(This applies approximately to PbTe at 300°K)

The approximate variation of μ_H is also shown

When conduction is mainly due to electrons ($n >> p$), (4.2) becomes :

$$R_H \doteqdot \frac{-rf}{qp} \doteqdot \frac{-1}{qn} \qquad (4.5)$$

R_H as a function of carrier concentration (calculated from equation (4.2)) for PbTe is shown in fig. 4.2 . The approximations (4.4) and (4.5) are also plotted (broken lines), and are seen to be valid (to within 10%) for $p > 5 \times 10^{16}$ cm^{-3} and $n > 2{\cdot}5 \times 10^{16}$ cm^{-3} respectively .

The Hall mobility μ_H is defined by $\mu_H = |R_H \sigma|$ (4.6)

From (4.2) and (4.3) ,

$$\mu_H = rf \left| \frac{p\mu_p^2 - n\mu_n^2}{p\mu_p - n\mu_n} \right|$$

For $p >> n$, $\mu_H \doteqdot rf\mu_p$ (4.7)

For $n >> p$, $\mu_H \doteqdot rf\mu_n$ (4.8)

In the case of PbTe , (4.7) and (4.8) are accurate to within 10% for $p > 5 \times 10^{16}$ and $n > 3 \times 10^{16}$ respectively . Similar approximations will apply to PbSe and PbS .

In the extrinsic range, Hall measurements therefore give a direct measure of the density and mobility of the majority carriers. In principle, it is possible to calculate these quantities for mixed conduction, from equations (4.2) and (4.3) . However, this involves assuming values for b ($= \mu_n / \mu_p$) and n_i^2 ($= np$) and is unlikely to be very accurate.

4.3 Experimental results : carrier concentrations

About 70 films (including 13 PbSe and 6 PbS) were prepared in the evaporation system A and measured in air . Hall coefficients and mobilities of a few of these are shown in table [4.1].

Both n- and p-type films were obtained, except for

Table [4.1] TABLE OF FILM PROPERTIES

Electrical properties were measured on films of 2000 A° to 6000 A° thickness ; the samples below are all 4000 A° films.

MATERIAL	SAMPLE NUMBER	GROWTH TEMP.	CARRIER CONCENTRATION	HALL MOBILITY 300°K	77°K
n - PbTe	6 a	250	1.0×10^{18}	1100	4,600
	21	240	3.1×10^{17}	1000	10,000
	22	240	5.2×10^{17}	1100	10,000
	* 39	240	7.0×10^{17}	1240	16,600
	40	260	7.6×10^{17}	1200	7,000
	* 41	260	5.0×10^{17}	1400	17,000
	68	240	6.3×10^{18}	900	3,000
p - PbTe	38	260	3.5×10^{17}	330	1,200
	70	260	1.9×10^{17}	540	2,200
n - PbSe	49	280	2.5×10^{18}	700	4,750
	52	300	2.5×10^{18}	1020	7,300
	* 75	300	1.4×10^{18}	870	10,000
p - PbSe	58 A	250	5.0×10^{17}	680	3,100
	72	300	2.2×10^{18}	310	2,300
n - PbS	62	210	2.4×10^{18}	200	500
	* 76	210	1.2×10^{19}	250	800
		°C	cm^{-3}	cm^2 / volt sec	

* indicates samples annealed beneath SiO layer

Figure 4.3 Change in carrier concentration with time, for PbSe

(evaporation rate = 200 A°/minute)

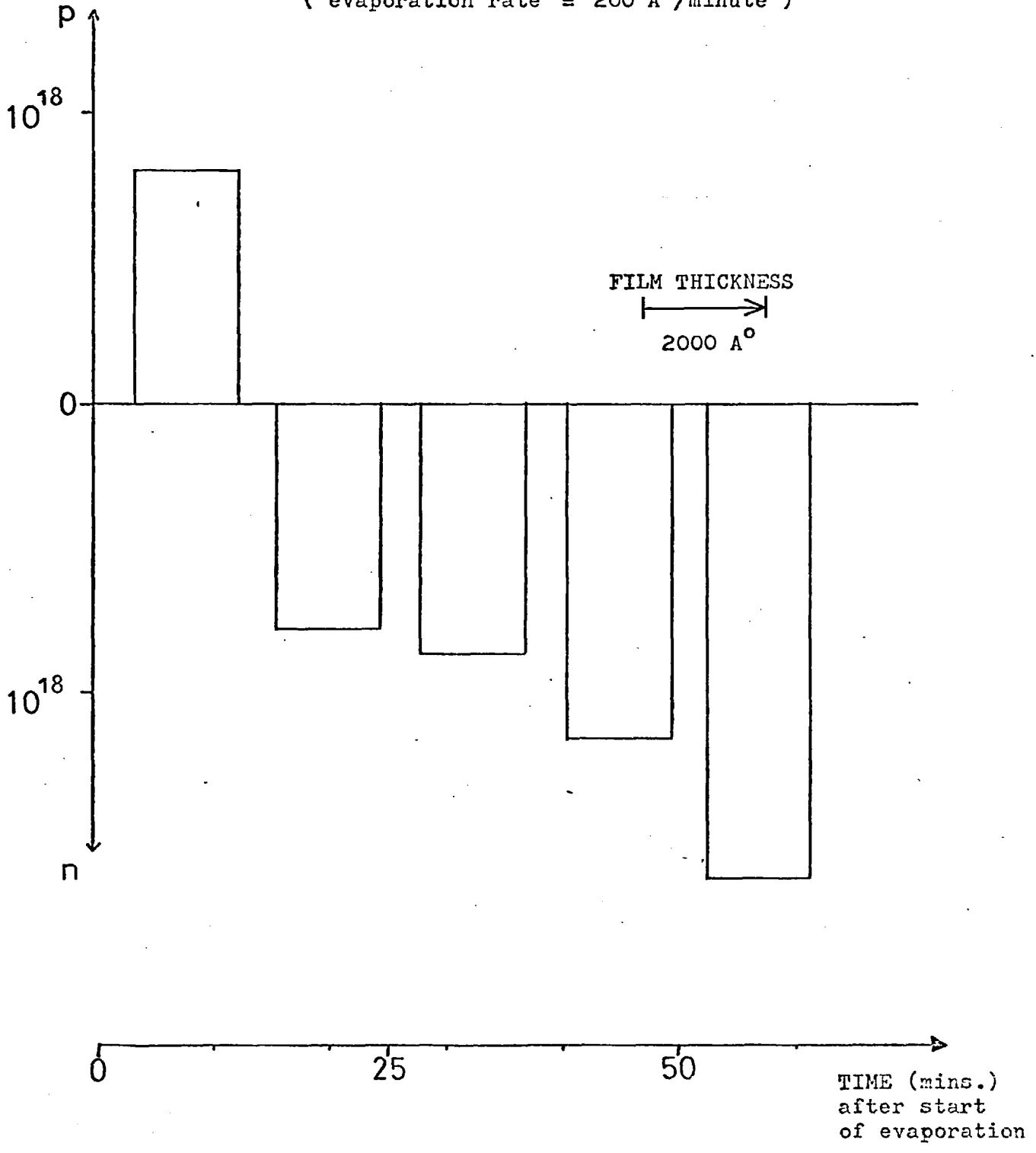

PbS, which was always n-type. About 80% of the PbTe and 50% of the PbSe samples were n-type.

Control over the carrier concentration was not possible, although it was noticed that when the source material was used for more than one evaporation, successive films were more likely to be n-type. This suggests that some dissociation of the lead compound is occurring in the source.

According to Brebrick and Strauss (B12), lead telluride evaporates mainly as PbTe molecules, but with a proportion of molecular Te_2 which depends on the composition of the solid evaporant. Thus, a p-type source material will lose tellurium preferentially at the beginning of an evaporation, but to a lesser extent as the remaining material becomes n-type. As the vapour condenses on the substrate, the initial deposit will be p-type, but the film may later change to n-type if tellurium is also being lost by preferential re-evaporation from the substrate. This is in agreement with the results shown in fig. 4.3. A sliding mask was used to prepare five Hall samples at different stages during the evaporation of the same source material; the first sample to be deposited was p-type and the rest increasingly n-type. The semiconductor in this case was PbSe, but the vapour products of PbSe and PbTe are similar (P14).

Even in a vacuum of 10^{-6} torr, there is also the possibility of impurities entering the film from the surroundings. In the case of a 4000 A° film, a single monolayer of electrically active impurity atoms would be sufficient to produce a carrier concentration of 10^{19} cm^{-3}.

4.4 Hall coefficients as a function of temperature

The Hall coefficient of typical PbTe, PbSe and PbS films on mica is shown in figures (4.4) and (4.5) as a function of reciprocal temperature, between 77°K and 300°K. In most cases, R_H is seen to be roughly constant over this temperature

Figure 4.4 HALL COEFFICIENTS as a function of TEMPERATURE for PbTe films on mica

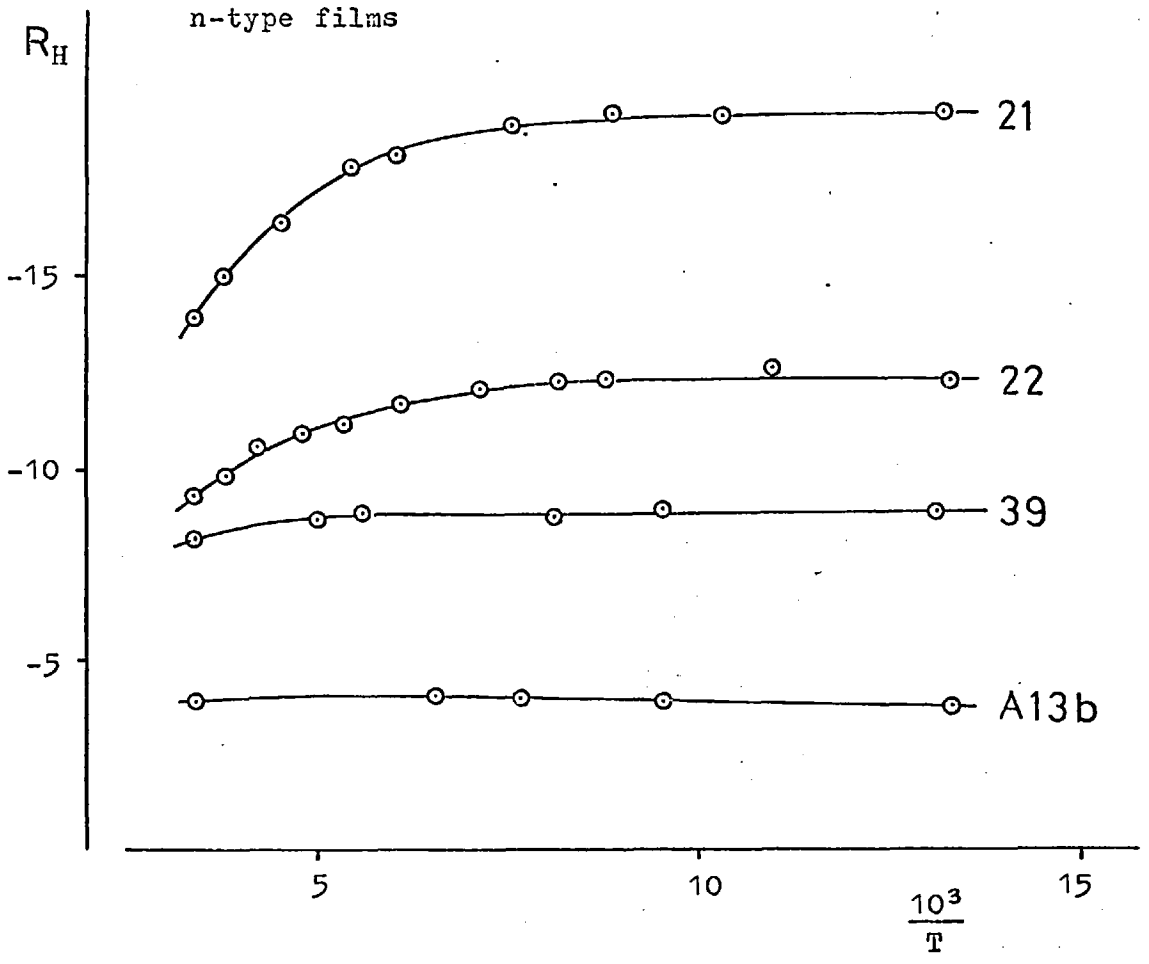

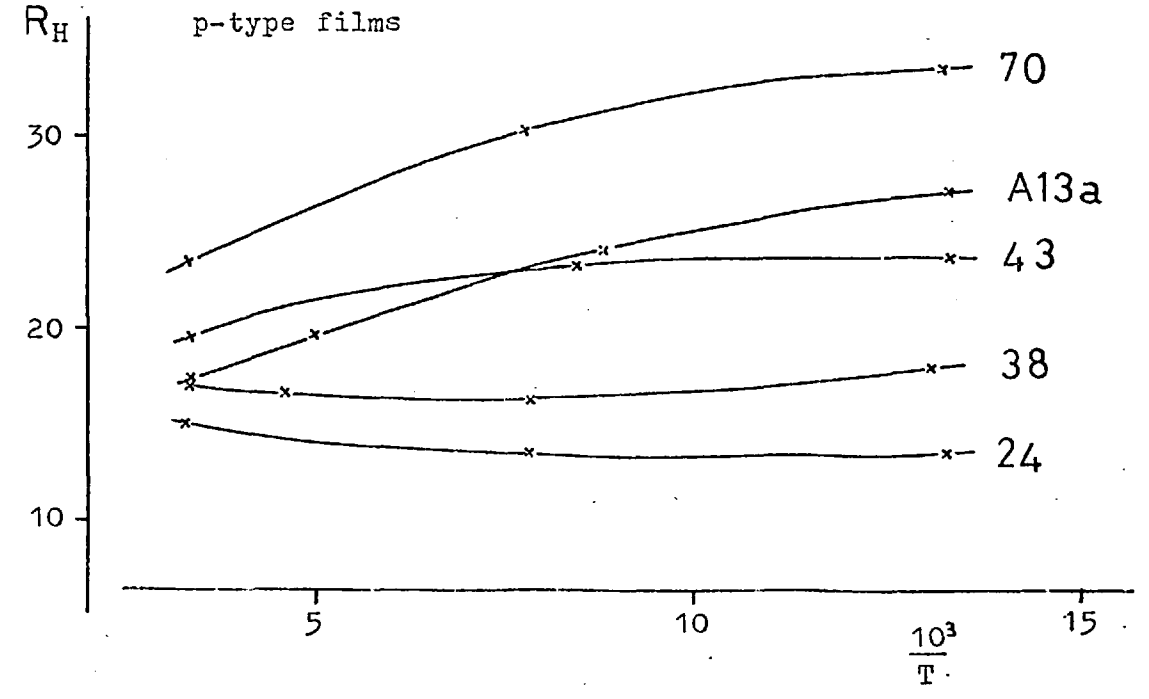

Figure 4.5 HALL COEFFICIENTS as a function of TEMPERATURE for PbSe and PbS films on mica

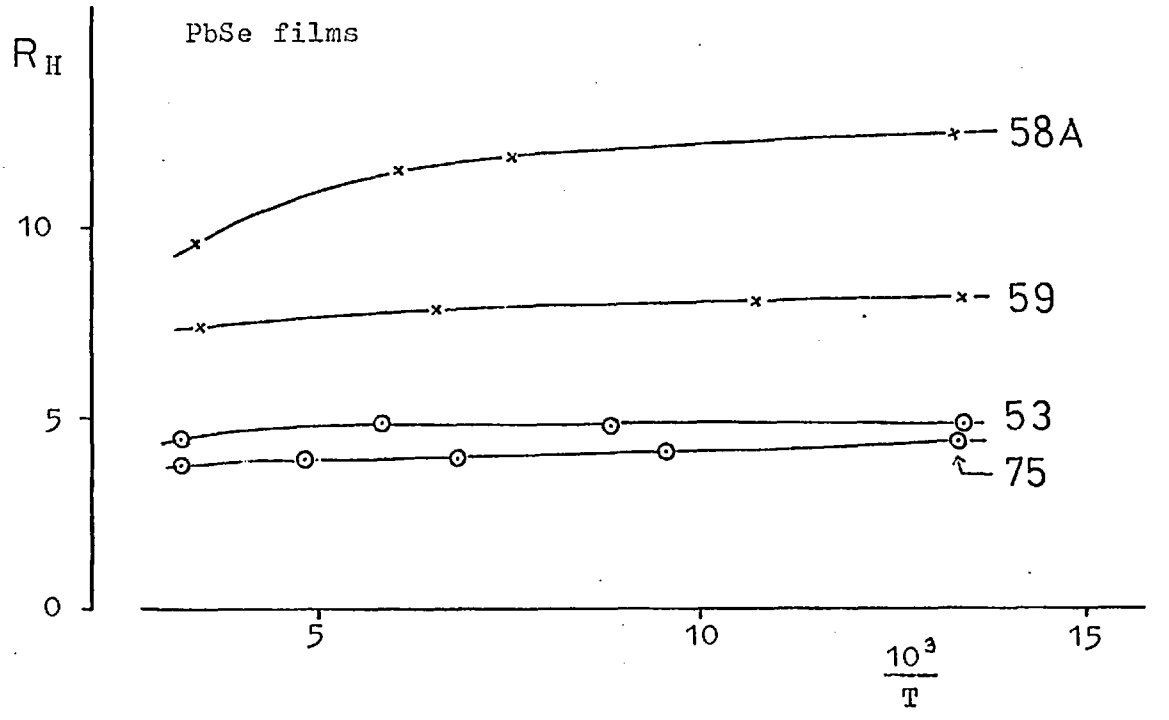

× p - type

⊙ n - type

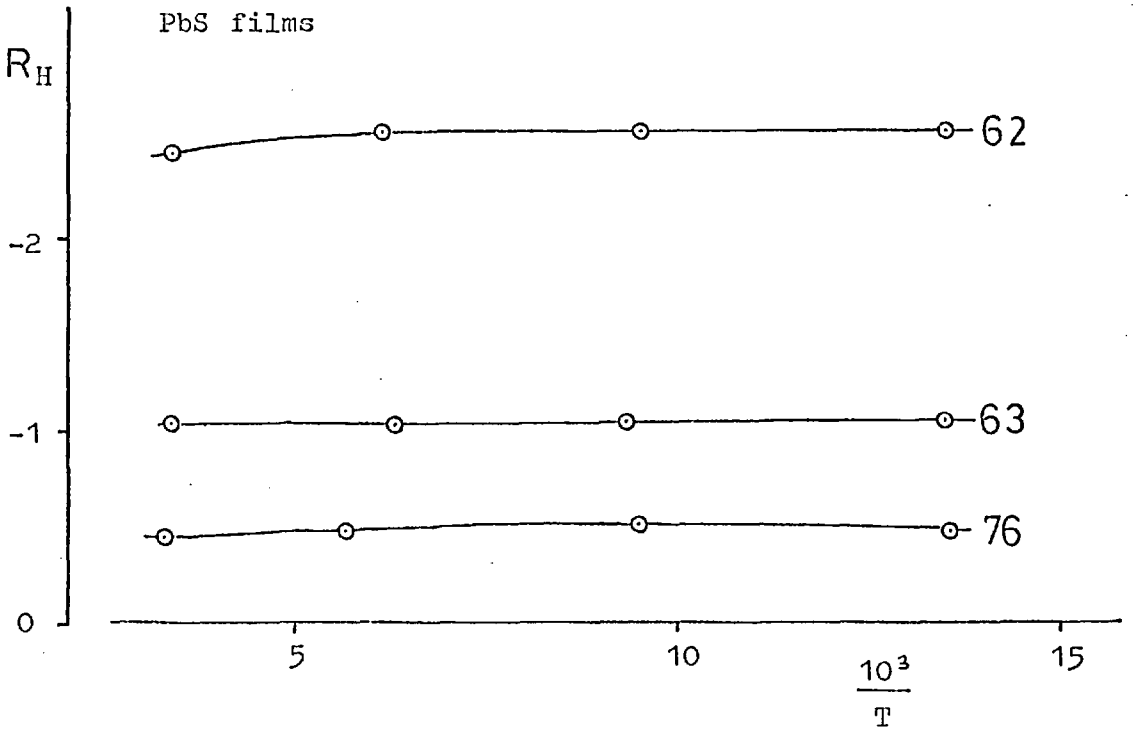

range, as in the case of extrinsic bulk samples (A10, P19).

In principle, R_H can increase with increasing temperature by up to 18%, as the parameter r in the Hall factor (equation 4.2) changes from 1 to $3\pi/8$ (A10). This is due to the transition from Fermi-Dirac to Boltzmann statistics, and occurs around the degeneracy temperature (usually below room temperature). The effect has been observed in bulk single crystals (A10).

However, the present results generally indicate some decrease in R_H at the higher temperatures, this being particularly noticeable in n-type PbTe samples. The curves in fig. 4.4a might suggest that bipolar conduction is becoming important at room temperature. But since the samples shown all had apparent carrier concentrations of 3×10^{17} or more, the magnitude of the effect can only be explained by assuming that the intrinsic carrier concentration n_i is about 10^{17} cm^{-3}, which is a factor of 10 higher than the accepted value for PbTe.

A similar decrease in R_H with increasing temperature is evident from the curves of Makino and Hoshina (M4) for n-PbTe on mica. Zemel et al. (Z7) also observed substantial variations in R_H with temperature for epitaxial PbTe, PbSe and PbS films on alkali halide substrates.

These effects, which occur in epitaxial films but not in good bulk single crystals, could be due to the following causes.

a) If the film has a thin layer at the surface of opposite doping to the rest of the sample, the carrier concentration in the majority of the film will be less than that estimated from equation (4.4) or (4.5), due to compensation of the Hall voltages from the two layers. Bipolar conduction will then occur at a lower temperature than expected. This is a plausible explanation in the case of n-type films, the surface exposed to the air

being p-type due to the effect of oxygen (see chapter 5). This compensation effect would also cause the Hall mobility to be significantly less than the bulk value (see section 4.5 g).

b) Trapping and release of carriers from states on the surface or in the bulk of the film. Such effects have been reported in photoconducting PbS films (P11) and appear to be a common feature of polycrystalline films of semiconductors. If the trap density is high, R_H increases exponentially with reciprocal temperature ; in epitaxial films, a lower density of traps might cause R_H to vary at higher temperatures. In the case of PbS , the traps were believed to be acceptor states caused by the penetration of oxygen.

c) Modification of the band structure of the semiconductor due to stress. There is evidence that the present films are under stress, which is tensile (see 4.5 e). The effect of this on the band structure, with particular regard to p-type PbTe , is discussed in section 4.5 e . It is worth mentioning here that a tensile stress has the effect of increasing the energy gap in the lead salts, which would decrease n_i by about 40% and reduce the amount of bipolar conduction at room temperature.

4.5 Variation of Hall mobilities with temperature.

Graphs of Hall mobility against reciprocal temperature (plotted on a log - log scale) are given for a number of different films of each of the three lead compounds in figures (4.6) , (4.7) , (4.8) and (4.9) . The bulk mobility, from data of Allgaier and Scanlon (A10) is also shown.

For the better films, mobilities are close to the bulk values at room temperature. Moreover, $\mu_H \propto T^{-m}$, where $m \sim 2{\cdot}5$ near room temperature, as for bulk single crystals. There is some departure from bulk behaviour at lower temperatures, the mobility increasing less rapidly with decreasing T (except

Figure 4.6

HALL MOBILITIES of n-type PbTe films, as a function of TEMPERATURE from 300°K to 77°K

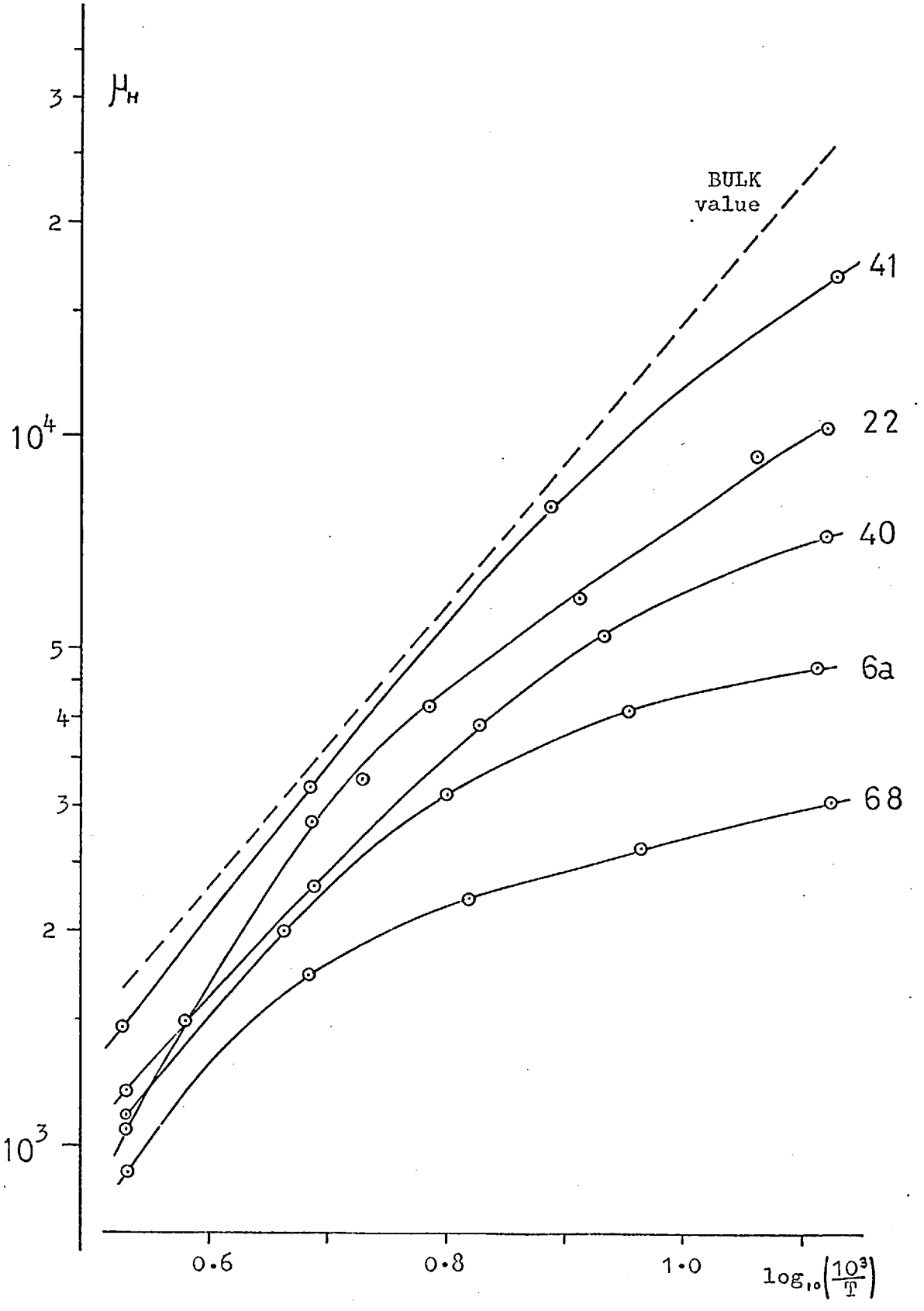

Figure 4.7 HALL MOBILITIES of p-type PbTe films, as a function of TEMPERATURE from 300°K to 77°K

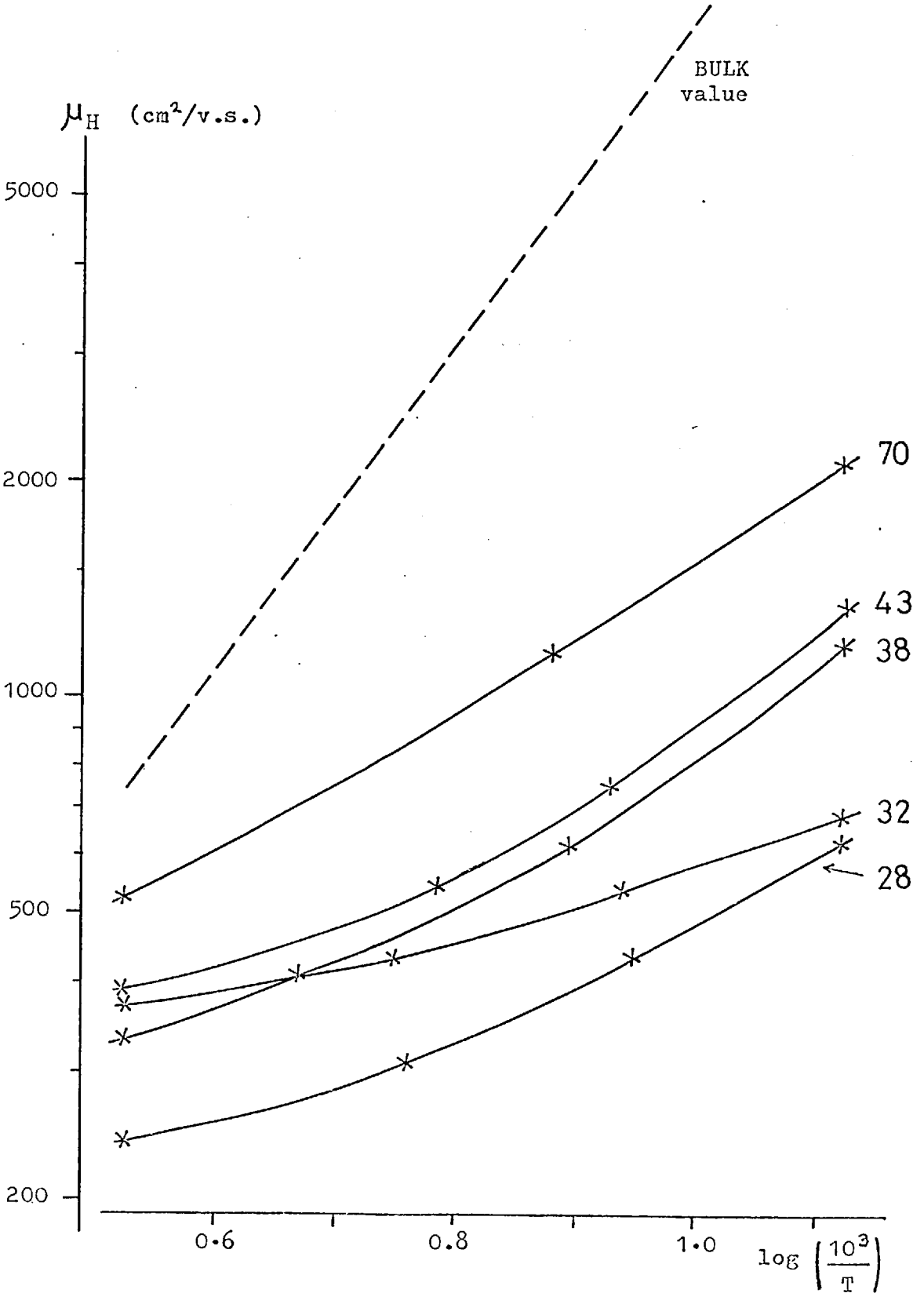

Figure 4.8 Hall mobilities of PbSe films on mica, as a function of temperature from 300°K to 77°K

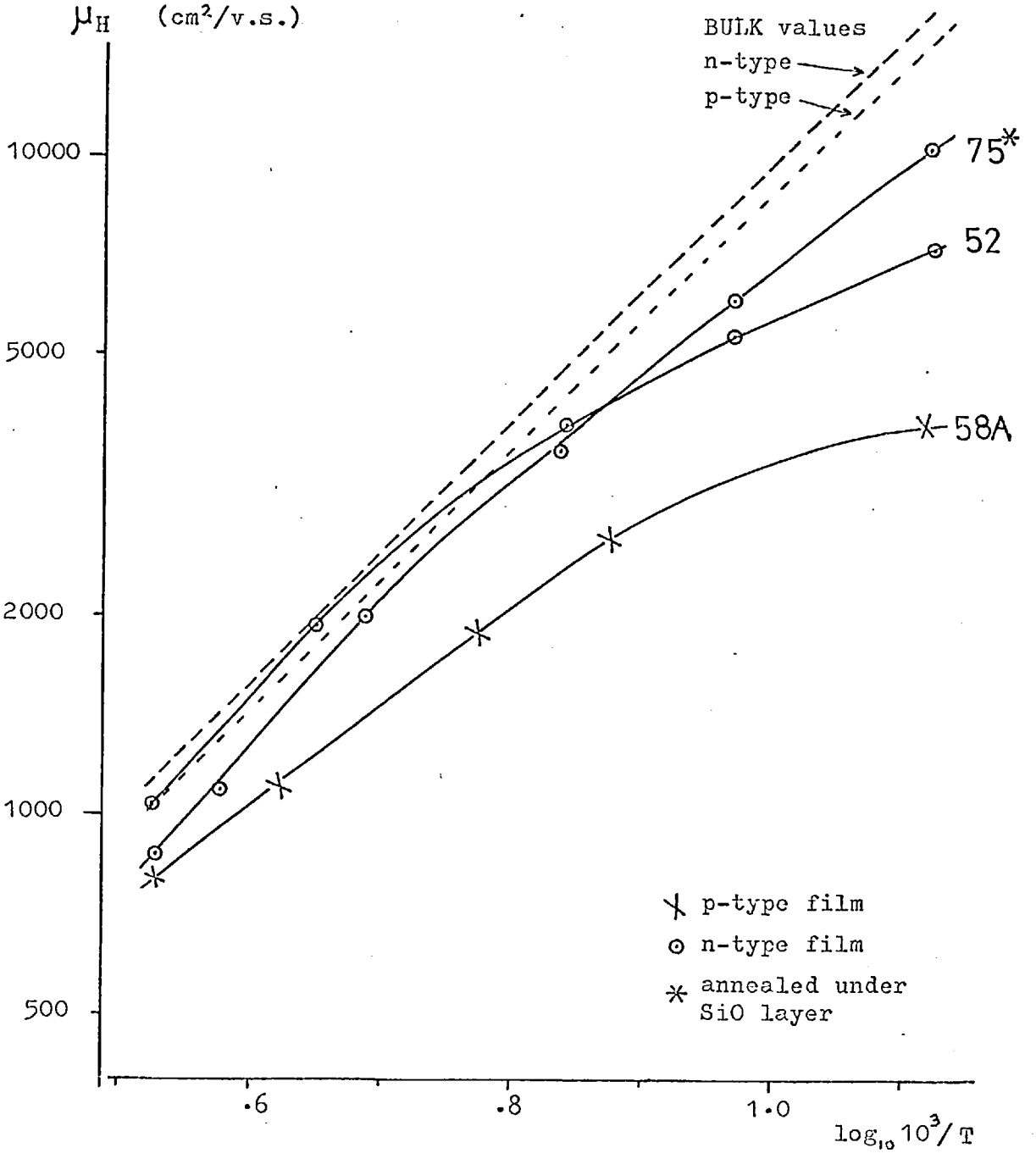

Figure 4.9 Hall mobilities of PbS films (n-type) as a function of temperature from 300°K to 77°K

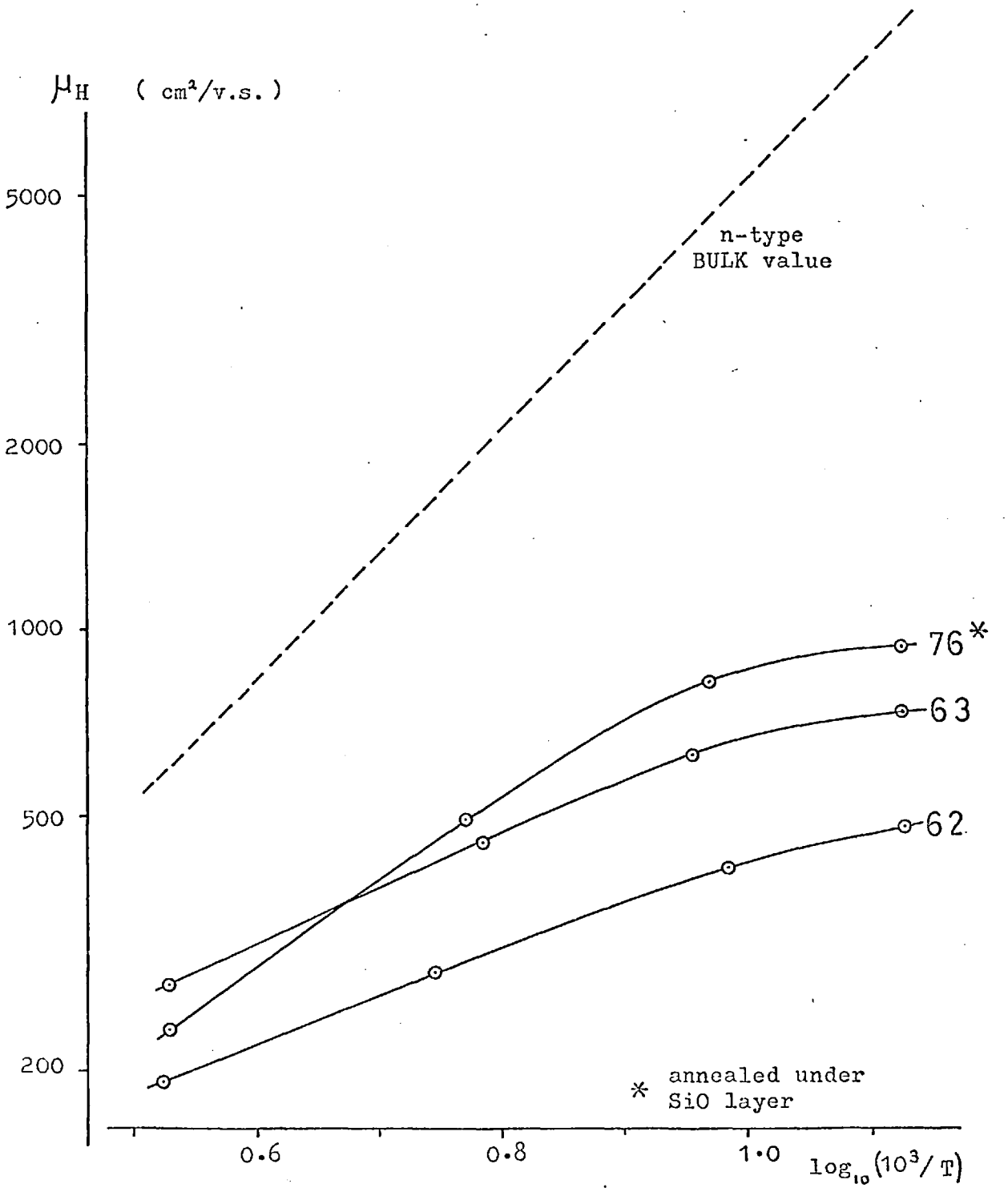

in the case of p-type PbTe).

After deposition, some of the films were coated with an evaporated layer of SiO and annealed in vacuum at about 400°C , as described in 2.4 . This had the effect of improving the electrical mobility (as seen from the graphs of μ_H) , particularly at low temperatures. A similar proceedure has been used to obtain high mobilities in InSb films (J5) .

Only one sample was measured down to liquid-helium temperature ; the result is shown in fig. 4.10 . In this case, the Hall coefficient, which was constant between room temperature and 77°K , was assumed to be the same at 4·2°K , by analogy with bulk behaviour .

Discussion of Hall mobilities

For bulk single crystals of the lead salts, the Hall mobility varies with temperature according to $\mu_H \propto T^{-2.5}$ over the range 77°K to 300°K , which is due to carrier scattering mainly by acoustic lattice vibrations (see 1.10)

In the case of epitaxial films of these materials, there is some departure from this law ; possible reasons for this will now be considered , with the following aims :

1) To gain some understanding of the conduction processes in epitaxial films

2) To explain why carrier mobilities are closer to bulk values than in epitaxial films of other semiconductors

3) To discover the best conditions for obtaining high mobilities, and to correlate the measured electrical properties with the film structure as revealed by microscopy .

The mechanisms to be examined are :
a) Surface scattering, b) scattering from boundaries, c) the effect of potential barriers, d) dislocation scattering, e) stress effects, f) cracking, and g) compensation of Hall voltage.

a) arises because of the small thickness of the films; b), c) and

Figure 4.10 HALL MOBILITY AS A FUNCTION OF TEMPERATURE (from 300°K to 4·2°K) FOR SAMPLE 41 (n-type PbTe under SiO)

The graph also shows the effect of ageing in air.

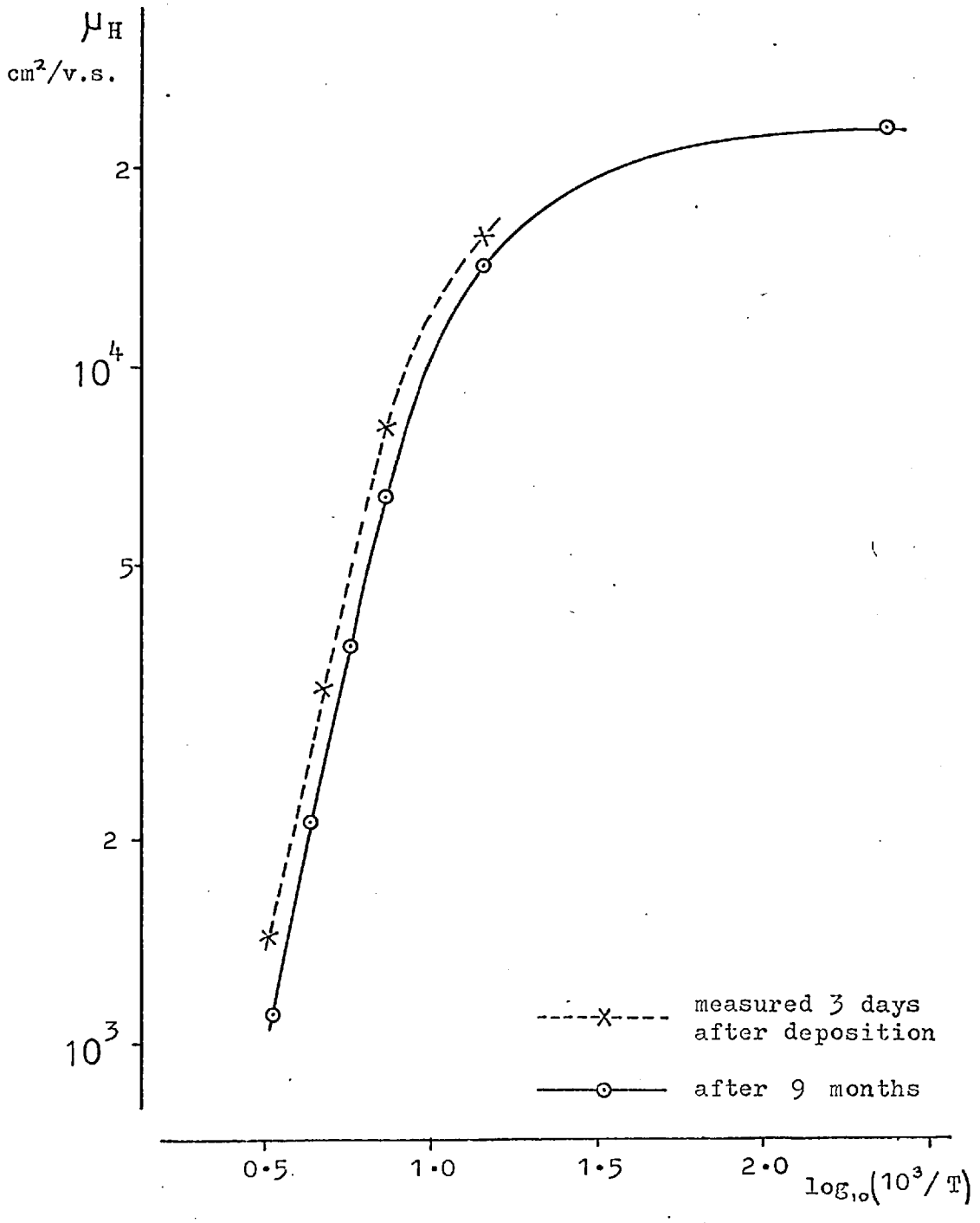

d) result from imperfections in the crystal structure (due to the growth mechanism of the films). e) and f) are a result of the deposition conditions, and g) is an effect due to contact with the atmosphere. For convenience of discussion, mainly the experimental data for n-type PbTe will be considered ; the effects in PbSe and PbS should be similar. The conclusions will be summarised in chapter 7 .

4.5a Surface scattering

Carriers in a semiconductor have an amount of kinetic energy which depends on temperature in the non-degenerate case, and on carrier concentration if the material is highly degenerate. They make frequent collisions ($\sim 10^{13}$ per second) with scattering centres, which in the bulk of the material are lattice vibrations (phonons). In addition, carriers which collide with an external surface may have their drift velocity randomized in direction. This is known as diffuse surface scattering, and is important when the mean free path of the carriers is comparable with the smallest dimension of the sample i.e. the thickness in the case of films. The effect of this additional scattering on the electrical mobility can be calculated from the theories outlined in appendix C .

It is interesting to see whether this effect could explain the reduced mobility (compared with bulk values) in the present films, particularly at low temperatures.

To calculate the mean free path (l) of the carriers, either the Boltzmann (non-degenerate) or the metallic (highly degenerate) approximation can be used.

Using Boltzmann statistics,

$$\tfrac{1}{2} m_i \overline{c^2} = \tfrac{3}{2} k T \qquad (4.9)$$

$$\mu = \frac{q \tau}{m_i} = \frac{q}{m_i} \cdot \frac{l}{\bar{c}} \qquad (4.10)$$

$$l = \frac{\mu}{q} \left(3 m_i k T\right)^{1/2} \frac{\bar{c}}{(\overline{c^2})^{1/2}} = \frac{\mu}{q} \cdot \left(\frac{9\pi}{8} m_i k T\right)^{1/2} \qquad (4.11)$$

where m_i is the inertial effective mass (section 1.9)

c is the thermal velocity of a carrier

l is the carrier mean free path, assumed to be independent of c. This is justified for acoustical scattering (section 1.10a)

τ is the relaxation time

Using degenerate statistics,

$$\tfrac{1}{2} m_i c^2 = \tfrac{1}{2} m_i c_F^2 = E_F = \frac{\hbar^2}{2 m_d} (3\pi^2 n)^{2/3} \qquad (4.12)$$

(ref. Z9)

Using (4.10),

$$l = \frac{\mu}{q} \hbar (3\pi^2 n)^{1/3} \left(\frac{m_i}{m_d}\right)^{1/2} \qquad (4.13)$$

where E_F and c_F are the Fermi energy and velocity

n is the carrier concentration, and $\hbar = h/2\pi$ where h is Planck's constant.

m_d is the density-of-states effective mass (1.10a)

For extrinsic PbTe at room temperature (assuming $n \sim 10^{18} cm^{-3}$, $\mu \sim 1000\ cm^2/v.s.$ and $m_i \sim 0{\cdot}1\ m_o$ (table 1.4))
Boltzmann statistics give $l = 140$ A°
Degenerate statistics give $l = 125$ A°

For PbTe, the Boltzmann approximation is fairly accurate at room temperature, for $n < 10^{19}\ cm^{-3}$ (R4). But at 77°K, material with $n \sim 10^{18}\ cm^{-3}$ is fairly degenerate. Using each of the approximations, the average carrier mobility was calculated for a 3000 A° PbTe film, employing ref. (M5), page 314. This assumes that the energy bands are flat throughout the semiconductor and that the scattering is completely diffuse from both surfaces. The results are shown in fig. 4.11.

Comparison with fig. 4.6 shows that diffuse surface scattering gives the right form of temperature dependence and could explain a substantial proportion of the deviation from bulk mobility in the 'better' films.

Surface scattering would lead to a large mobility

Figure 4.11 Mobility reduction for a 3000 A° PbTe film due to diffuse surface scattering (assuming flat bands)

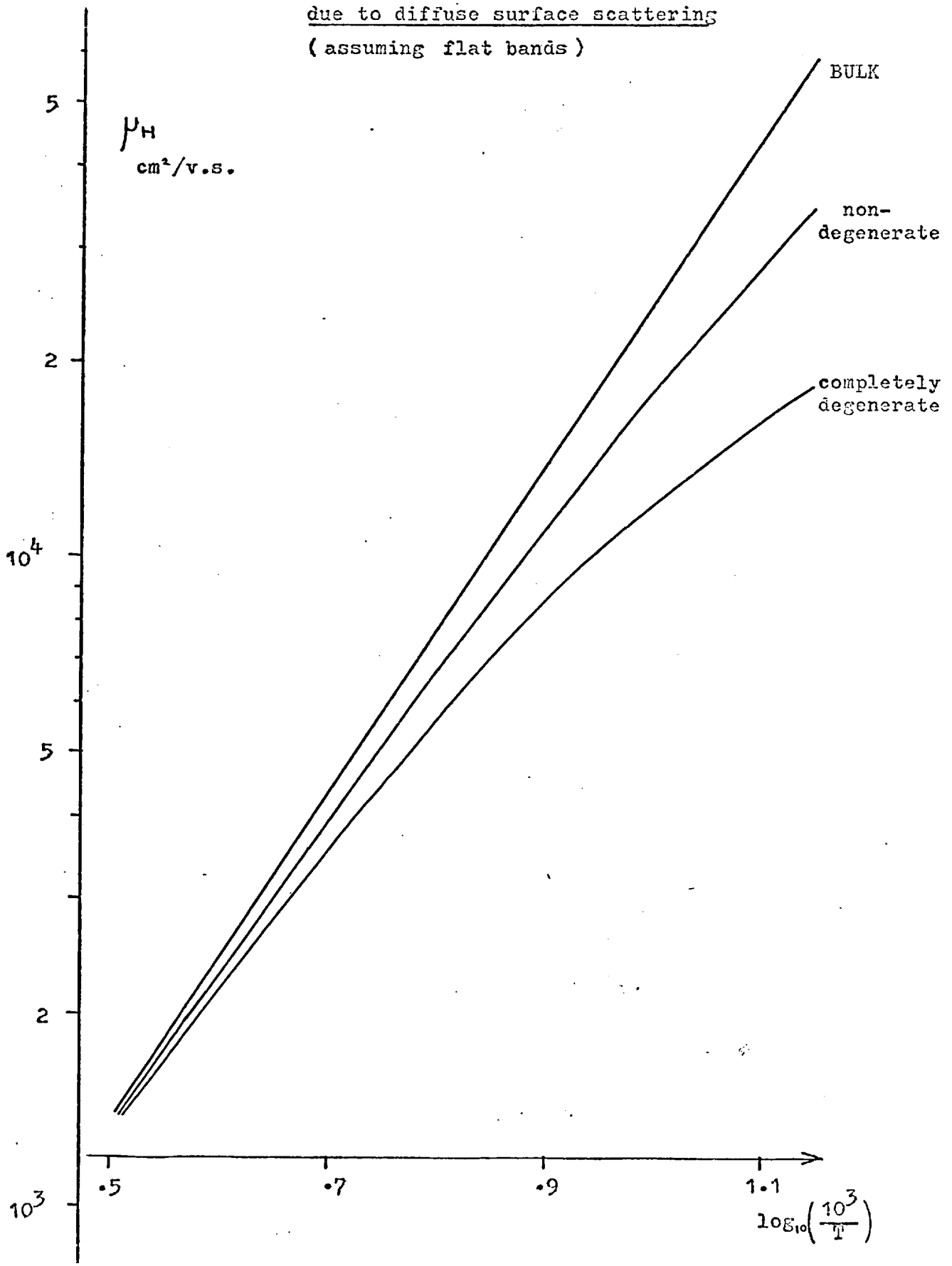

reduction at liquid helium temperature ; here, the metallic approximation should be accurate (the Fermi level being more than 10 k T into the majority carrier band) . The predicted value of mobility for the n-type PbTe sample 41 (fig. 4.10) is 34,000 $cm^2/v.s.$ The measured Hall mobility at 4·2°K is 23,000 $cm^2/v.s.$ Values for bulk single crystals at this temperature are typically 10^5 to 10^6 (A10) .

Although diffuse surface scattering gives a mobility reduction of the right order of magnitude for the highest-mobility films , it does not account for the fact that other films of the same thickness have lower mobility. In addition, n-type PbTe films on mica reported by Makino and Hoshina (M4) show similar mobilities at 77°K ; there, the film thickness was about 2 micron and surface scattering would be ineffective in reducing the mobility.

4.5b Boundary scattering

Electron microscopy (chapter 3) shows that although the films are epitaxial, they contain defects including double-positioning boundaries. If the crystal bonding across the interface is non-coherent, a boundary can be regarded as containing dislocations, which will affect the electrical properties of the film due to scattering and trapping of carriers. The scattering effect of the boundaries is treated in this section ; carrier trapping is considered in 4.5c .

The mean free path l_B associated with boundary scattering should be a constant (independent of temperature) for a given film , equal to the average distance which carriers travel between collisions at a boundary. A mobility due to this process alone may be defined (by analogy with (4.10)) :

$$\mu_B = \frac{q}{m_i}\left(\frac{l_B}{\bar{c}}\right)$$

$\bar{c}$ can be obtained from either of equations (4.9) or (4.12) .

4.5 b

For a non-degenerate semiconductor, (4.9) gives

$$\mu_B = q\, l_B \left(\frac{9\pi}{8} m_i kT \right)^{-1/2} \qquad (4.13)$$

and from (1.14), $m_i \propto T^{0.6}$ $\qquad \mu_B \propto T^{-0.8}$ $\qquad (4.14)$

For a completely degenerate material, (4.12) gives

$$\mu_B = \frac{q\, l_B}{\hbar} \left(3\pi^2 n\right)^{-1/3} \left(\frac{m_d}{m_i}\right)^{1/2} \qquad (4.15)$$

Using (1.13) and (1.14),

$$\mu_B \propto T^{-0.1} \quad \text{i.e.} \quad \mu_B = \text{constant, approximately} \qquad (4.16)$$

The degenerate approximation is expected to be the more accurate at temperatures around $100^\circ K$.

The mobility μ due to both boundary and lattice scattering can be written approximately (S23, p. 114) as :

$$\frac{1}{\mu} = \frac{1}{\mu_L} + \frac{1}{\mu_B}$$

where μ_L is the mobility due to lattice scattering alone. This is given (see 1.10) by :

$$\mu_L = \mu_L(300) \left(\frac{T}{300}\right)^{-\frac{5}{2}} = A\, T^{-2.5}$$

where $\mu_L(300)$ is the value of μ_L at $300^\circ K$.

Therefore, $$\frac{1}{\mu} = \frac{T^{2.5}}{A} + \frac{1}{\mu_B} \qquad (4.17)$$

In fig. 4.12 a, $1/\mu_H$ has been plotted against $T^{2.5}$ for the five n-type PbTe samples previously shown in fig. 4.6. A line representing bulk mobility (zero boundary scattering) is also shown ; this has been corrected for the effect of stress (see 4.5 e), taking a value of 1620 cm^2 / v.s. for μ_L at $300^\circ K$ in the absence of stress.

Fig. 4.12 $\frac{1}{\mu_H}$ and $\left(\frac{1}{\mu_H} - \frac{1}{\mu_L}\right)$ plotted against $T^{5/2}$ for n-type PbTe films.

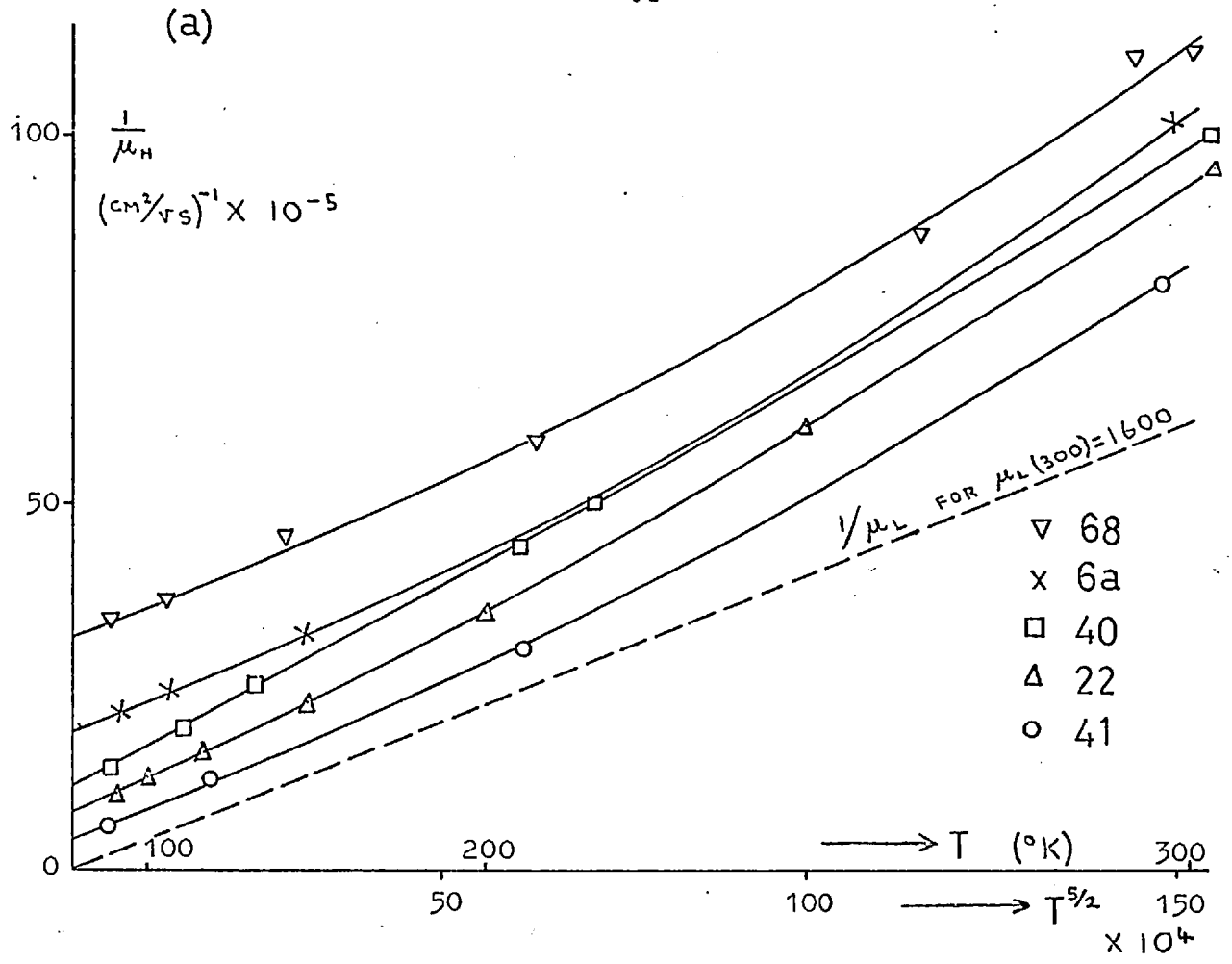

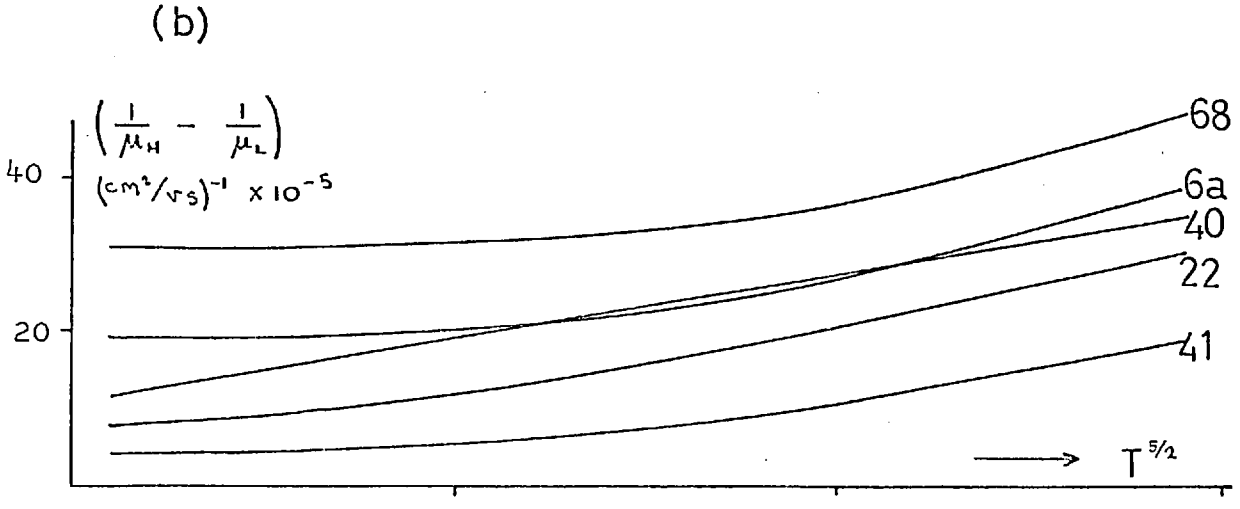

In each case, $1/\mu_H$ is approximately a straight line with gradient equal to that of the bulk line, for $T < 200°K$. $1/\mu_B$ is the vertical distance between the experimental curve and the line representing bulk mobility, and has been plotted separately in fig. 4.12 b. Between 77°K and 200°K, $1/\mu_B$ is roughly constant, as specified by equation (4.16). The increase in $1/\mu_B$ between 200°K and 300°K could be due to the material becoming non-degenerate, when $1/\mu \propto T^{0.8}$ from (4.14).

Zemel (Z7) invoked boundary scattering to account for the mobility of PbTe films on NaCl substrates. He assumed that the extra scattering was due to low-angle grain boundaries and obtained a value of l_B which was in rough agreement with the spacing between voids in a partially discontinuous film of PbS.

Values of μ_B for the five films in fig. 4.12 were obtained from the intercepts on the $T = 0$ axis, and are shown below together with values of $2l_B$ calculated from (4.15).

sample	μ_B	$2l_B$	D
41	25,000	10,000	8000
22	12,500	5,000	
40	9,100	3,600	5000
6a	5,000	2,000	
68	3,200	1,300	
	$cm^2/v.s.$	A°	A°

Surface replicas were made of two of the samples, and the average spacing D of boundaries estimated from the electron micrographs. It is not easy to estimate the 'grain size' because the boundaries form very irregular shapes (see for example fig. 3.8). The expected value of D is $2l_B$ (J4) and reference to the above table shows that the agreement is reasonable for the two films in question.

The five films discussed are representative of the range of mobilities obtained; in each case, boundary scattering provides a reasonable explanation of the temperature variation of mobility.

4.5 c Potential barriers

The trapping effect of dislocations associated with a non-coherent grain boundary can be thought of as being due to 'dangling bonds' at the interface. These give rise to acceptor states in germanium (P6), although donor levels have been found in the case of high-angle boundaries in InSb (M2).

In the following treatment, it will be assumed that carrier trapping creates a depletion region on each side of the boundary, i.e. the energy levels are acceptors in the case of an n-type semiconductor, as shown in fig. 4.13. A space-charge layer of this type will act as a potential barrier to electrons in the conduction band of the semiconductor which have energies less than the barrier height $E_B = q V_B$. The situation is similar to that which can exist at the boundary between a semiconductor and a metal, and has been treated theoretically (M16 p. 176, T5 p. 77, E2 p. 292) under two assumptions:

1) Diode theory

This is valid when the width of the barrier is less than the mean free path of carriers in the bulk, so that few collisions occur in the space-charge region. Carriers which are able to cross the boundary do so with their thermal velocity c, the net current flow being the difference between the fluxes of particles in both directions and is given by:

$$J = \tfrac{1}{2} q n_o \overline{c_x} \exp\left(\frac{-q V_B}{k T}\right)\left[\exp\left(\frac{q V}{k T}\right) - 1\right] \qquad (4.18)$$

where $\overline{c_x}$ is the mean thermal velocity perpendicular to the boundary and is given by:

$$\overline{c_x} = \left(\frac{2 k T}{\pi m_i}\right)^{1/2}$$

V is the applied voltage, which appears as a potential drop across the barrier region

n_o is the carrier concentration in the bulk of the semiconductor (away from the barrier region)

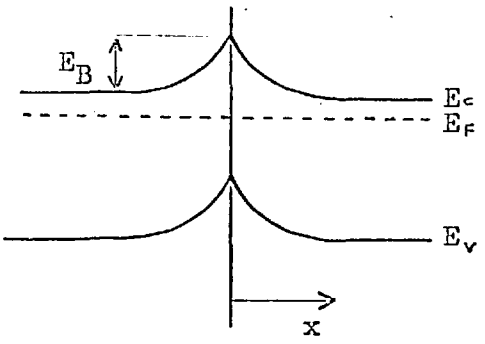

Fig. 4.13 Energy band diagram of a potential barrier in an n-type semiconductor.

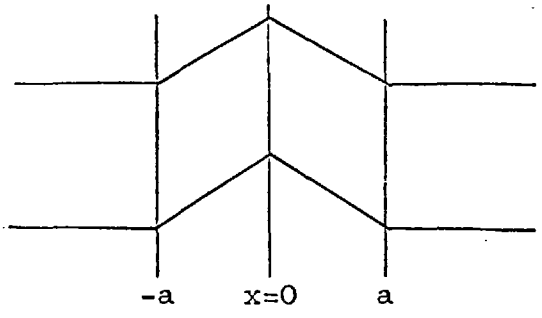

Fig. 4.14 Triangular barrier

2) Diffusion theory

This holds when the barrier width is large compared with the mean free path. Carriers then collide frequently in the barrier region and cross the boundary under the action of an electric field and carrier concentration gradient, with a drift velocity v_d. The current is found by solving the equation :

$$J = q n \mu \mathcal{E} + q D \frac{dn}{dx} \qquad (4.19)$$

where $D = \frac{kT}{q} \mu$

$\mathcal{E}$ and n are the electric field and carrier concentration in the barrier region, and μ is the carrier conductivity mobility

If the barrier is assumed to be triangular (fig.4.14),

$$\mathcal{E} = \frac{V_B}{a} = \text{constant}$$

and $$J = q n_o \mu \cdot \exp\left(\frac{-q V_B}{k T}\right)\left[\exp\left(\frac{q V}{k T}\right) - 1\right] \qquad (4.20)$$

When the voltage drop across each boundary is small ($qV/kT << 1$), both equations (4.18) and (4.20) can be written :

$$J = C \cdot \exp\left(\frac{-q V_B}{k T}\right) \cdot V$$

where $$C = \frac{q}{kT} \cdot \tfrac{1}{2} q n_o c_x = q^2 n_o \left(2\pi k m_i\right)^{-\frac{1}{2}} T^{-\frac{1}{2}} \qquad (4.21)$$

i.e. $C \propto T^{-0.8}$ (using eqn. (1.14)) for the diode model ,

and $C = q^2 n_o \frac{\mu \xi}{k T} \propto T^{-1}$ for the diffusion theory .(4.22)

The barrier has a resistivity per unit area of :

$$\rho_b = V/J = C^{-1} \exp\left(\frac{q V_B}{k T}\right)$$

The main temperature dependence of ρ_b occurs in the exponential term. Both theories predict that in cases where conduction is completely dominated by the effect of grain boundaries, the effective mobility is given by :

$$\mu \propto \frac{1}{\rho_b} \propto \exp\left(\frac{-q V_B}{k T}\right) \qquad (4.23)$$

This exponential temperature dependence has frequently been observed in polycrystalline films (see, for example, P7 , P11 , L8).

For epitaxial films, where the barrier height or the distance between boundaries are presumed to be lower, the effective mobility ~~mobility~~ has to be calculated by combining their effect with that due to bulk scattering. The simplest assumption to make is that the barriers and the semiconductor grains are electrically in series ; this appears to be fully justified in the case of the diffusion model. The applied voltage is then the sum of the voltage drops across the two components. The total resistivity ρ' (resistance per unit area perpendicular to the current flow) can then be written :

$$\rho' = (\rho\, d) + \rho_b$$

where ρ is the bulk resistivity of the semiconductor
d is the average grain size

This is equivalent to :

$$\frac{1}{\mu} = \frac{1}{\mu_L} + \frac{1}{\mu_B} \qquad (4.24)$$

where μ is the effective mobility , μ_L is the mobility due to lattice scattering, given by $\mu_L = A T^{-2.5}$.

$$\mu_B = B \exp\left(\frac{-q V_B}{k T}\right) \qquad (4.25)$$

where $B = \frac{d}{q n_o} C \propto T^{-n}$ $\quad 0{\cdot}8 \leqslant n \leqslant 1{\cdot}0$ from (4.21) and (4.22)

Equation (4.24) is the same as (4.17), but now μ_B is expected to increase with temperature, following an exponential law (apart from the small temperature dependence of B ; see (4.25)). The experimental results (fig. 4.12) indicate that μ_B decreases slightly with increasing temperature. This can only be accounted for by assuming $V_B = 0$, which invalidates the present theory. It would therefore appear that if energy barriers exist in the present films, they have no effect on the carriers. Evidence from fig. 4.10 supports this; if the mobility reduction at 77°K were due to potential barriers, (4.24) would predict a decrease in μ_H at even lower temperatures, which is not observed.

A possible reason for the small effect of barriers is the high static permittivity of the lead salt semiconductors, which would reduce the barrier height for a given charge at the interface. As an example, a 1° (low-angle) boundary would have a charge density of about 10^{12} charges/ cm^2. For a carrier concentration of 10^{18} cm^{-3} in PbTe, the barrier height would be $0{\cdot}3\ kT$ at room temperature (·01 eV). A rough estimate of the barrier thickness can be obtained from the Debye length (defined in 6.1), which is 250 A° for PbTe at room temperature and 70 A° at 77°K. The mean free path is 140 A° at room temperature and up to 2000 A° at 77°K. Therefore at lower temperatures the diode theory would be expected to be the more accurate. For D, the distance between barriers, equal to 1 micron, equations (4.25) and (4.21) give :

$$\mu_B = \frac{q}{2kT} D c_x \exp\left(\frac{-q V_B}{k T}\right) = 32{,}000 \exp(-0{\cdot}3)$$

$$= 24{,}000\ cm^2/vs \text{ at } 300°K$$

and $\mu_B = 63{,}000 \exp(-1{\cdot}2) = 19{,}000$ at 77°K

In this case, the reduction in measured mobility would be

negligible at room temperature (since $\mu_B >> \mu_L$), and would amount to only 50% at 77°K .

4.5 d Dislocation scattering

An expression for the mobility due to unionised dislocations distributed uniformly within a semiconductor is (D2) :

$$\frac{1}{\mu_D} = \frac{T}{\alpha_d} \quad , \quad \alpha_d = \frac{3\pi}{32} \frac{E_1^2 \, b^2}{k \hbar} \cdot \left(\frac{m_i}{q}\right) \cdot N \left(\frac{1-2\nu}{1-\nu}\right)^2 \qquad (4.26)$$

where N is the density (per unit area) of dislocations
b is the length of the Burgers vector
ν is Poisson's ratio for the semiconductor
E is the deformation potential constant

The mobility due to both dislocation and lattice scattering will be given approximately by :

$$\frac{1}{\mu} = \frac{1}{\mu_L} + \frac{1}{\mu_D}$$ where μ_D replaces μ_B in eqn. (4.17) .

However, the experimental results (fig. 4.12) indicate that μ_B is roughly constant below 200°K and decreases above this temperature, whereas (4.26) predicts that μ_D should decrease with increasing temperature over the whole range, in disagreement with fig. 4.12 .

This suggests that dislocations are not important scattering centres in the present films, which is surprising because carrier scattering in bulk single crystals of PbTe at very low temperatures (4·2°K) has been attributed to dislocations (A10), the dislocation density in similar samples being estimated as 7×10^6 cm^{-2} (S2) . The dislocation density observed in epitaxial PbS films was as high as 2×10^{10} cm^{-2} (M9), and since μ_D is inversely proportional to N , this would give

$\mu_D \sim 4 \times 10^5 \cdot 7 \times 10^6 / 2 \times 10^{10} = 140$ cm^2/v.s. for epitaxial PbS at 4·2°K . Substitution in equations (4.26)

also gives low values for μ_D . It would appear that either the dislocation density in the present films is not as high as that measured in PbS or that dislocations which are present are not as effective in scattering carriers as assumed by equation (4.26).

Gobrecht et al (G3) observed an increase in mobility, measured at 77°K , when epitaxial PbSe films were annealed at 200°C to 300°C and attributed this to the removal of dislocations. An improvement in the low-temperature mobility was also observed in the present case, after annealing (in vacuum) films coated with SiO , which could be due to the above cause or to a decrease in the number of boundaries within the film.

4.5 e Effect of stress

Because the films were grown at a substrate temperature of 250°C to 300°C and subsequently cooled to room temperature, they are likely to be under stress due to the different expansion coefficients of the semiconductor and substrate. Direct evidence of this was obtained when the mica substrate was cleaved down to below 10 microns for field-effect measurements ; curvature of the semiconductor surface was clearly visible in areas where the film had been deposited, indicating that the film was under considerable tensile stress. It is of interest to estimate the magnitude of this stress, and its effect on the electrical properties.

The induced strain at a temperature T (due to the difference in expansion coefficients) is :

$$\epsilon = (\alpha_1 - \alpha_2)(T_g - T) \qquad (4.27)$$

where α_1 and α_2 are the coefficients of linear expansion (averaged over the temperature range) of mica and PbTe respectively , and T_g is the growth temperature.

Assuming $T_g = 270°C$, $T = 20°C$

$\alpha_1 = 10 \times 10^{-6}$, $\alpha_2 = 20 \times 10^{-6}$ (N3)

$\epsilon = 2{\cdot}5 \times 10^{-3}$ at room temperature

and $\epsilon = 4{\cdot}5 \times 10^{-3}$ for $T = 77°K$

The stress in the plane of the film is given by :

$$Q = 3K\left(\frac{1-2\nu}{1-\nu}\right)\epsilon$$

where K is the bulk modulus for PbTe and can be taken (A14) as $4{\cdot}8 \times 10^{-5}$ Kg cm^{-2} . ν is Poisson's ratio, assumed to be $\sim {\cdot}25$

$\therefore$ $Q = 2{\cdot}4 \times 10^{3}$ Kg cm^{-2} = 2·4 Kbar at 300°K

and $Q = 4{\cdot}3 \times 10^{3}$ Kg cm^{-2} = 4·3 Kbar at 77°K

Equation (4.27) assumes that the stress in the film is zero at the growth temperature. However, Wilcock (W5) found that there was an intrinsic stress in PbTe which was deposited on to mica at room temperature. For an evaporation rate of 5 A° / sec , this was 0·4 Kbar . With a heated substrate, the intrinsic stress is unlikely to be as high as this (W6) , so the value of Q is not greatly affected.

These values of stress are sufficient to cause an appreciable change in electrical properties. Using data of Averkin and Dermenzhi (A13) , the resulting (percentage) change in conductivity and effective mass for PbTe are as follows :

		% change in σ	% change in m_d
n - PbTe ($n \sim 10^{18}$)	300°K	- 12	4·5
	77°K	- 21	8·2
p - PbTe ($p \sim 10^{18}$)	300°K	- 19	5·5
	77°K	- 30	9·9

Values for PbSe and PbS are similar to those for n-type PbTe (A14 , P5) . The coefficients for p - PbTe are higher because of the presence of a second valence band.

For n-type PbTe , the Hall coefficient does not change much with pressure (A13), so the reduction in conductivity due to tensile stress is reflected in a decrease in the Hall mobility. In the present case, this would be reduced from 1600 to 1400 at room temperature, and from 25,000 to 20,000 at 77°K (units are cm^2 / volt sec) .

It was originally thought that stress effects might explain the $\log \mu_H$ against $\log 1/T$ curves for p-type PbTe (fig. 4.7). These are concave upwards for all seven samples measured, in contrast with the curves for n-type films and for p-type PbSe, which are concave downwards, as expected when there is scattering from structural defects. Moreover, p-type films of PbTe on NaCl substrates, which are believed to be unstressed at room temperature (Z7), have curves which are concave downwards. Lead telluride has a second valence band (see 1.9) whose maximum is at an energy ΔE below the principal valence band. ΔE decreases with increasing temperature, and with tensile stress. The values of stress calculated above could be sufficient to cause the second band to have a significant effect on the Hall coefficient and mobility at room temperature. However, since the second band is known to have a lower hole mobility than the first (A9, R4), the result would be a downward curvature in fig. 4.7 (at higher temperature), in contradiction with the results. Therefore, the curves in fig. 4.7 remain unexplained.

4.5f Cracking.

If the stress in a film is sufficiently high, the strain can be relieved by the formation of cracks. This will decrease the conductivity, since carriers must avoid the cracks, particularly those running perpendicular to the current flow. The lines of current flow are therefore distorted, which reduces the effective width of the sample. Since the effect is a geometric one, the conductivity will be reduced by a constant fraction, independent of temperature. The Hall coefficient will not be affected, since the Hall voltage does not depend on the sample width (eqn. 4.1). As a result, the $\log \mu_H$ v. $\log 1/T$ curve should be displaced uniformly downwards (Z4). This is shown in fig. 4.15 for a PbTe film on an alumina substrate, where cracking is believed to have occurred on cooling to liquid nitrogen temperature (the strain in this case should be larger

Figure 4.15 Hall mobility as a function of temperature for PbTe on alumina, showing the effect of cracking

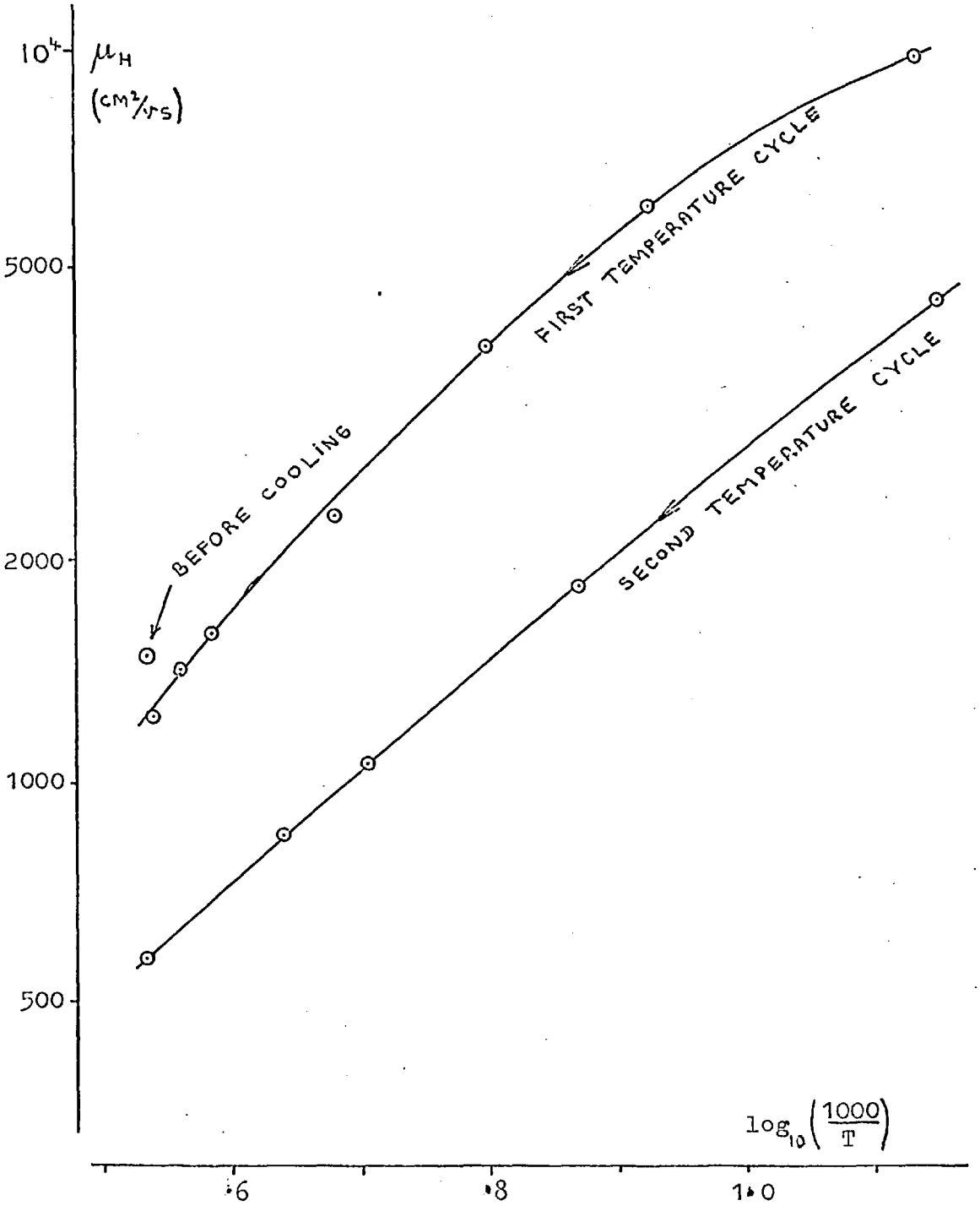

than for a mica substrate, due to the lower expansion coefficient of Al_2O_3) .

When first measured at room temperature, the Hall mobility was 1500 cm^2 / volt sec . After cooling to 77°K and returning to room temperature, the mobility was 1200 cm^2 / v.s. Upon cooling again to 77°K and making a second set of measurements up to room temperature, the values of μ_H were about half the previous values.

Similar effects were observed with mica substrates when the PbTe film was thicker than about 5000 A° , and are also reported for PbTe on glass (L8) . There is some direct evidence for the existence of cracks from electron microscopy (see fig. 3.9 and reference P13) .

4.5 g Compensation effects

Another mechanism which would lead to a more or less uniform reduction in mobility over the temperature range 77°K to 300°K is that of compensation of Hall voltage from a layer of opposite conductivity type. A p-type layer is believed to occur at the surface of n-type PbTe , PbSe and PbS due to the effect of atmospheric oxygen. Even some of the films coated with silicon oxide showed a reduction in Hall mobility after storing for some time in air (see figure 4.10) . In such cases, it was found possible to restore the mobility to higher values by annealing the sample (in air) at 100°C , which probably removed the p-type layer by diffusion into the semiconductor .

CHAPTER 5

THE EFFECT OF AMBIENTS

Long - term effects

5.1 Experimental results

Films prepared in the deposition system A had to be exposed to air before measurement. The Hall samples were stored in air and measured from time to time over a period of months. Changes in the Hall coefficients were observed ; these are summarised in table 5.1 (next page) .

Hall measurements on particular samples up to 1 year after preparation are shown in fig. 5.1 . The largest changes were found in PbTe films which were initially n-type ; here the process can be divided into three stages. There is first of all a gradual increase in $|R_H|$; then, after a period of a few months, R_H changes from negative to large positive values. The third stage, which is observed in some samples, is a subsequent decrease in R_H . In the case of n-type PbS , the change is much slower and corresponds to the first stage in n - PbTe . P - type samples (PbTe and PbSe) showed little variation, the Hall coefficient remaining positive.

To test whether water vapour had any effect on this ageing process, certain samples were kept in a dessicator. Other samples were stored in a chamber connected to a rotary vacuum pump. In neither case did this have any significant effect on the changes taking place. (see fig. 5.1) . However, in the case of an n-type film stored in a high-vacuum system, there was a slight decrease in $|R_H|$.

Unusual effects were observed in n-type PbSe films ; fig. 5.2 shows the Hall coefficient between 77°K and 300°K for a typical specimen. When measured soon after deposition, R_H was negative and roughly constant over the whole temperature range,

as expected for a uniform doping of 4×10^{18} cm^{-3} . After storing in air for 3 days, R_H became positive at room temperature and passed through zero at 210°K . After 4 days, the temperature at which $R_H = 0$ moved lower ; after 8 weeks, however, this temperature increased to about 290°K . After 40 weeks , R_H was negative up to room temperature .

Table [5.1] Change in R_H over a period of 1 year

MATERIAL	AGEING CHARACTERISTICS
n - PbTe	R_H becomes positive at all temperatures
n - PbSe	R_H becomes more negative at 77°K R_H at 300°K becomes positive
n - PbS	R_H increases , but R_H remains negative for all T
p - PbTe	R_H increases slightly (remains + ive)
p - PbSe	R_H decreases a small amount
n - type PbTe , PbSe and PbS with SiO overlayer	Not much change in R_H ; remains negative ~~positive~~

Figure 5.1 R_H (at 77°K) as a function of time for PbTe, PbSe and PbS samples

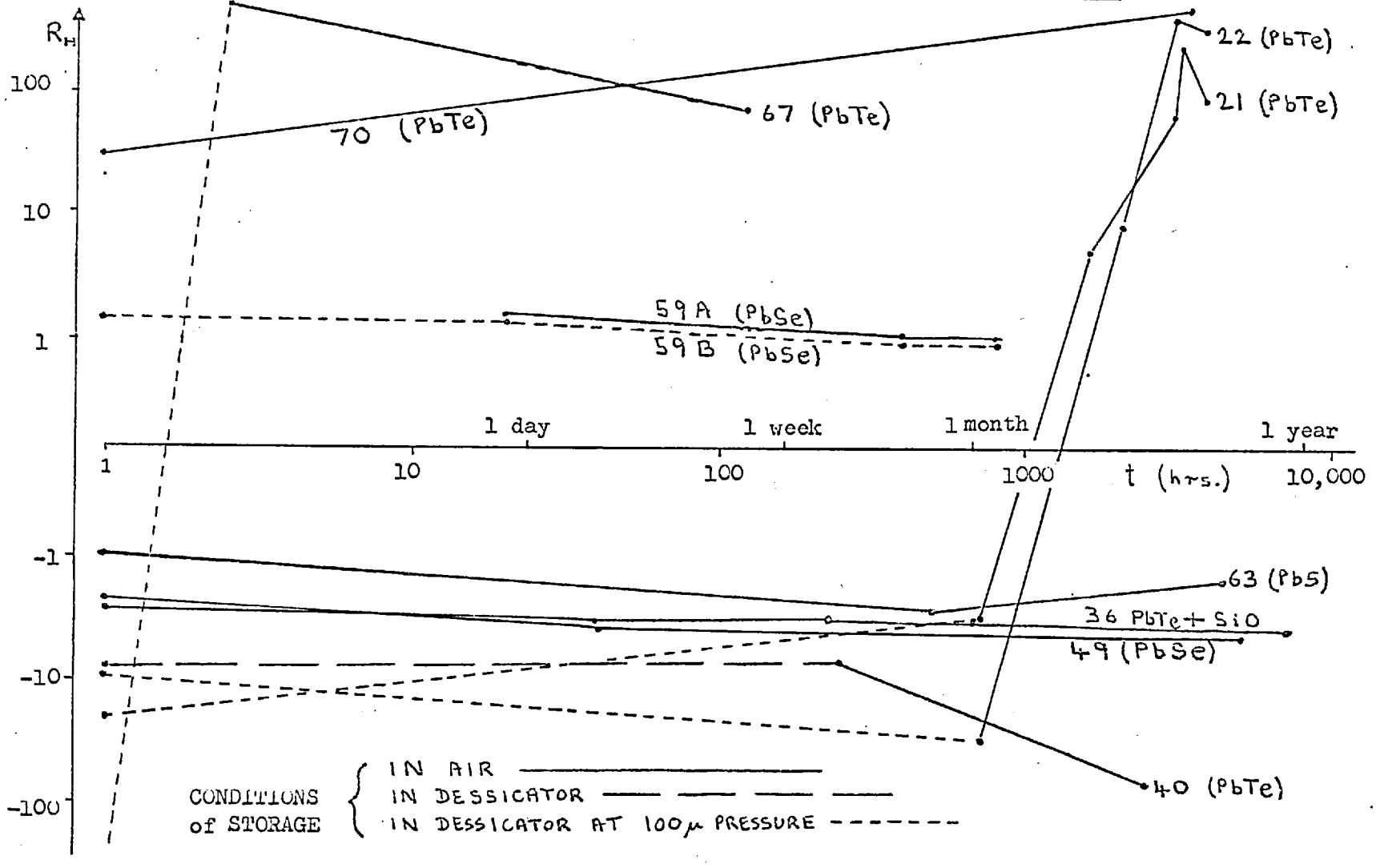

Figure 5.1

Figure 5.2 R_H v. $\log\left(\frac{1000}{T}\right)$ as a function of time after deposition, for PbTe sample (53).

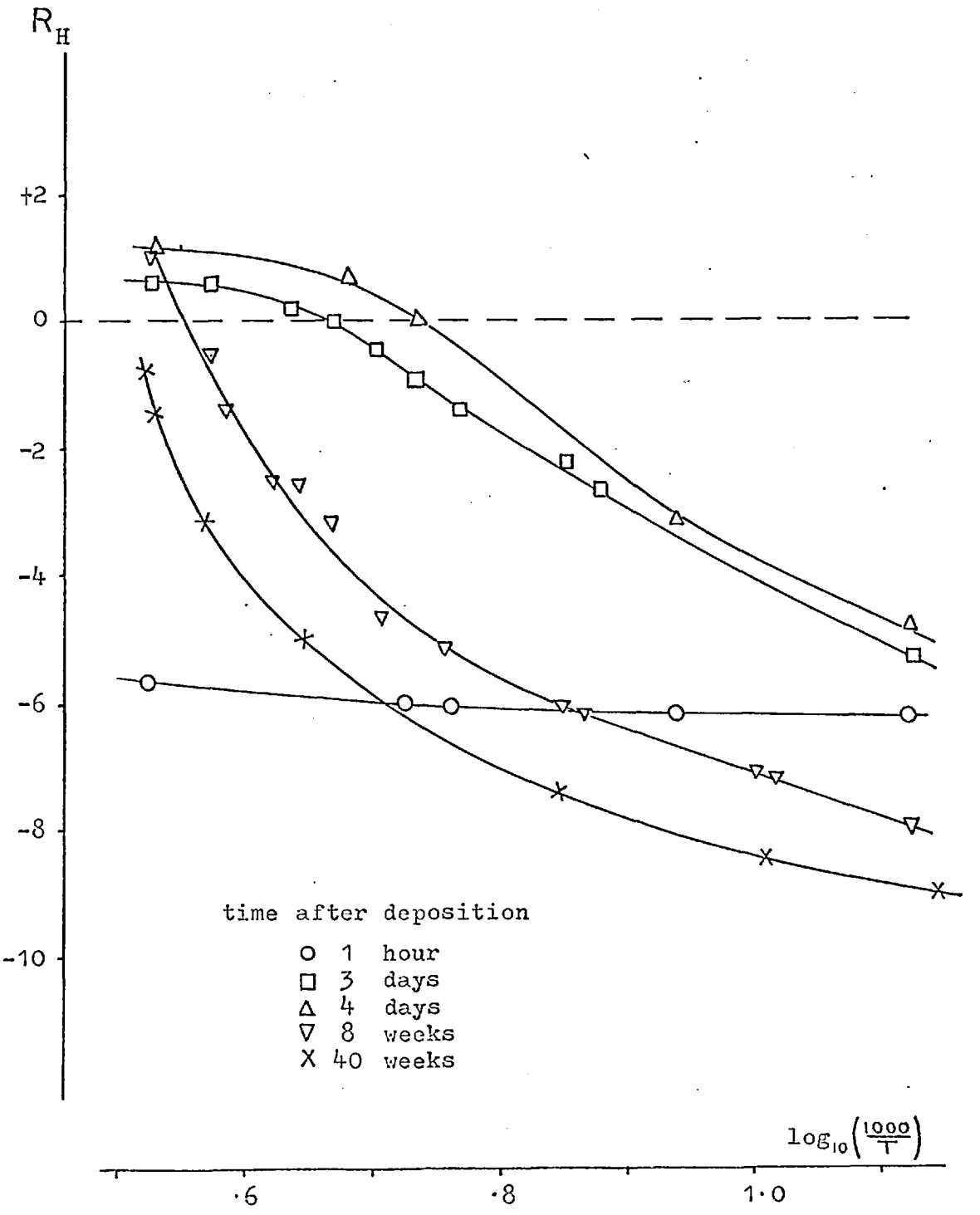

5.2 Discussion

The Hall coefficient changes described in 5.1 are explained qualitatively by assuming that p-type impurity is being added to the film (compare fig. 5.1 , particularly for n - PbTe , with fig. 4.2) . The most likely source of this is atmospheric oxygen, since oxygen is known to be an effective p-type dopant for the lead salts in the form of polycrystalline films (B8,J3,E3) and single crystals (L3) . One possibility is that oxygen enters the film by diffusion from the external surface. The diffusion coefficient of oxygen in these materials has not been measured, but the coefficient of self-diffusion of lead in PbTe , PbSe and PbS is as follows (Z4) :

MATERIAL	$D(300^{\circ}K)$ $cm^2\ sec^{-1}$
PbTe	$2{\cdot}9 \times 10^{-15}$
PbSe	$5{\cdot}5 \times 10^{-20}$
PbS	$5{\cdot}0 \times 10^{-28}$

The diffusion coefficient increases from PbS to PbTe , which is in qualitative agreement with the relative rates of change of R_H in the three types of sample. To a first approximation, the number of oxygen atoms (N' per unit area) which have entered the semiconductor at a time t is given (B9) by :

$$N' = \tfrac{1}{2} N_s (Dt)^{\frac{1}{2}} \qquad (5.1)$$

where N_s is the concentration at the surface .
If N_s is taken as the concentration of oxygen in the gas phase, the rate of penetration would depend on the ambient pressure. But reducing the pressure to 100 μ Hg (by a factor of 1000) had no effect on the ageing rate, as previously stated. A possible explanation is that oxygen is present at the surface as an oxide or as an adsorbed layer which is at least a monolayer thick, even at low pressures. N_s and dN/dt would then be independent of pressure.

A diffusion process involves an impurity gradient within the film, perpendicular to the substrate surface. There is some experimental evidence for this.

1) Field-effect measurements, made by applying an electric field through the mica substrate (see chapter 6) showed n-type conductivity modulation in certain PbTe films, even though the sample gave a positive Hall coefficient. As there is not likely to be an inversion layer at the mica interface (see 6.7 a), this suggests that the semiconductor adjacent to the substrate was n-type, with the rest of the film p-type.

2) The sign reversal (with temperature) of the Hall coeff. observed in the n-type PbSe films was previously discovered in bulk crystals of PbTe and PbSe (P19, U1) and appears to be associated with a possible impurity gradient within the sample. In fact, no explanation has been offered which assumes that the doping is uniform. The effect was also observed in PbSe epitaxial films by Zemel (Z4), who put forward an explanation based on impurity gradients. This relies on the observation that the Hall mobility of the lead salts increases less rapidly with decreasing temperature when the carrier concentration is high, which is believed to be due to the energy dependence of the effective mass, and to the presence of a second valence band in the case of PbTe (A9, R4). The semiconductor is assumed to consist of an n-type layer and a p-type layer of higher doping. The Hall voltages from the two layers therefore partially cancel one another. The resulting Hall coefficient is positive at room temperature due to the higher p-type doping, but reverses its sign at lower temperature as μ_p/μ_n decreases. As diffusion proceeds, the concentration of carriers in both layers is assumed to decrease so that R_H remains positive down to lower T.

Zemel (Z4) supposed that the doping profile was 'built in' during growth of the film. Clearly this does not apply in the present case, because R_H is well-behaved when measured soon after deposition, so that the presumed impurity gradient only

becomes significant after 1 or 2 days exposure to the atmosphere.

Zemel's explanation required a very substantial p-type doping level (10^{19} cm^{-3} or more in PbTe) to be effective. In the present case, an alternative explanation might be that the diffusing impurity (e.g. oxygen) creates deep acceptor states which only become ionised at higher temperatures (there is evidence (P11) in PbS of levels 0·1 eV above the valence band, caused by oxygen). If this happens mainly in a p-type surface region, whereas the bulk of the film is n-type, $|R_H|$ would decrease at higher temperatures and perhaps reverse sign. However, it is hard to explain why the Hall reversal temperature eventually increases, using either of these models.

Finally, the effect of an evaporated overlayer of silicon oxide should be mentioned. N-type PbTe and PbSe films which were coated in vacuum with SiO still had negative Hall coefficients after 2 years' storage in air, although there was some increase in $|R_H|$ (20% to 100%). The SiO layer would be expected to help to prevent oxygen entering the semiconductor, but due to the existence of pinholes etc. (the SiO films were less than 2000 A^o thick and were deposited at room temperature) this protection might not be perfect. The Hall mobility sometimes decreased after storage (typically 10-20 % over the whole temperature range 77°K to 300°K) as previously shown in fig. 4.10 . This could have been due to the formation of a p-type layer at the surface, which was removed by annealing (see section 4.5g) .

5.3 Measurements

In order to study more closely the effect of ambients on the films, the evaporation system was modified to allow Hall measurements to be made 'in situ' . After preparation, the sample could be rotated into the gap of an electromagnet and the Hall coefficient and resistivity measured at room temperature. A description of the magnet assembly etc. is given in 2.2 b .

Measurements could be made on the films within a few minutes after deposition , in vacuum and upon admission of various ambient gases. Nitrogen, hydrogen and water vapour were found to have little effect on the films. The only gas which had a rapid effect was oxygen, and no difference was observed between the effects of pure oxygen and air.

The results can conveniently be classified according to the initial condition of the semiconductor.

a) One-carrier films, where the semiconductor was heavily n-type in vacuum and remained n-type after admitting air or oxygen.

b) Two-carrier systems, where the film was initially lightly - doped and was p-type after exposure to air

c) Films coated with an evaporated layer of insulator.

These categories will be treated in turn.

5.4 Results

a) One - carrier films

Fig. 5.3 shows the effect of air on a 3000 A^{o} n-type PbTe film . When measured soon after deposition (at a pressure of less than 4×10^{-6} torr) the apparent carrier concentration was 4×10^{18} cm^{-3} and the Hall mobility 1200 cm^{2} / volt sec . Upon storage in vacuum for 2 hours , the Hall coefficient and resistivity both increased by a factor of two ; the Hall mobility was therefore unaltered. Upon admitting air to the deposition chamber

Figure 5.3 HALL COEFFICIENT and RESISTIVITY during exposure to air, for n-type PbTe (sample A 24)

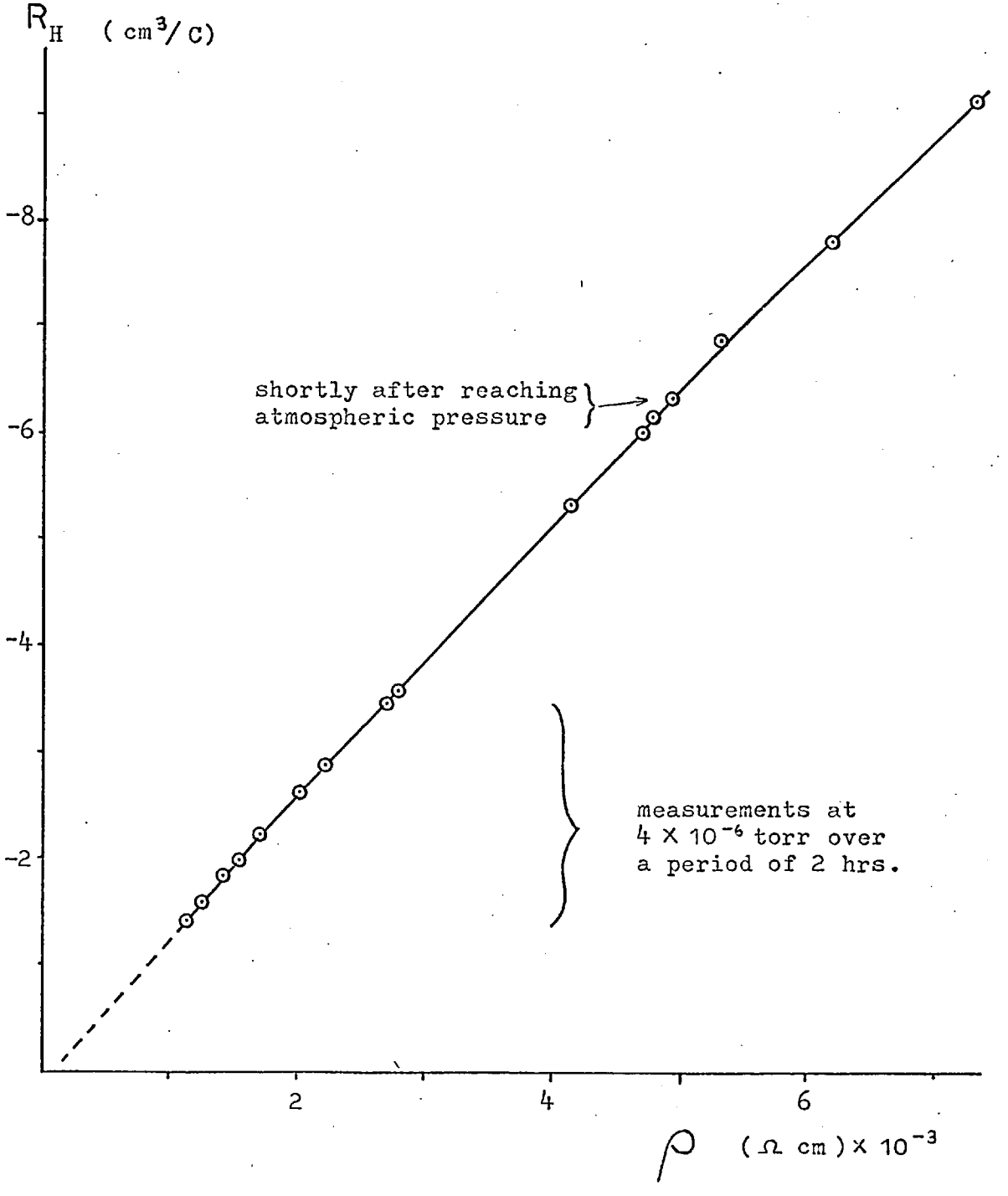

R_H and ρ increased further, with only a slight decrease in μ_H. Admitting a pulse of air caused the resistivity to rise for a few seconds and then to decay, as shown in fig. 5.4 Some of the experimental points in fig. 5.3 were measured whilst the values of R_H and were still changing. The values attained after a few minutes at atmospheric pressure are therefore less than the maximum value recorded, due to the relaxation effect. This phenomenon sometimes extended over a period of hours, R_H and ρ decreasing by a further 10% or 20% at atmospheric pressure.

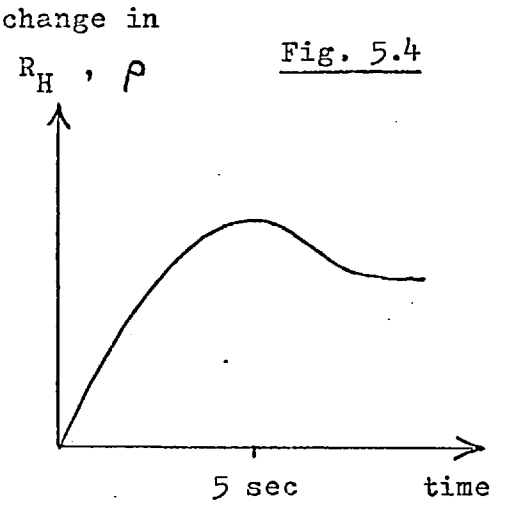

Fig. 5.4

Figure 5.3 is typical of the results obtained from six n-PbTe samples (all 3000A° films) which had measured carrier concentrations of between 3×10^{18} and 6×10^{18} cm^{-3} in vacuum, and between 1.0×10^{18} and 1.4×10^{18} in air. In each case, the graph of R_H against ρ is approximately a straight line, which on extrapolation passes very near to the origin.

If the deposition chamber was re-evacuated after letting up to air, the Hall coefficient and resistivity of the sample decreased, the mobility again remaining constant. In this way, R_H and ρ could be reduced to about half their values in air, i.e. roughly 3 times the initial values in vacuum.

Figure 5.5 shows results from a PbTe film of 1000 A° thickness. The initial and final values of R_H and ρ are similar to those for a 3000 A° film.

Figure 5.6 shows similar measurements on a 3000 A° film of PbSe. In this case, the initial and final values of R_H and ρ are both lower than those for the PbTe samples.

Figure 5.5 HALL COEFFICIENT AND RESISTIVITY during exposure to oxygen , for n-type PbTe films

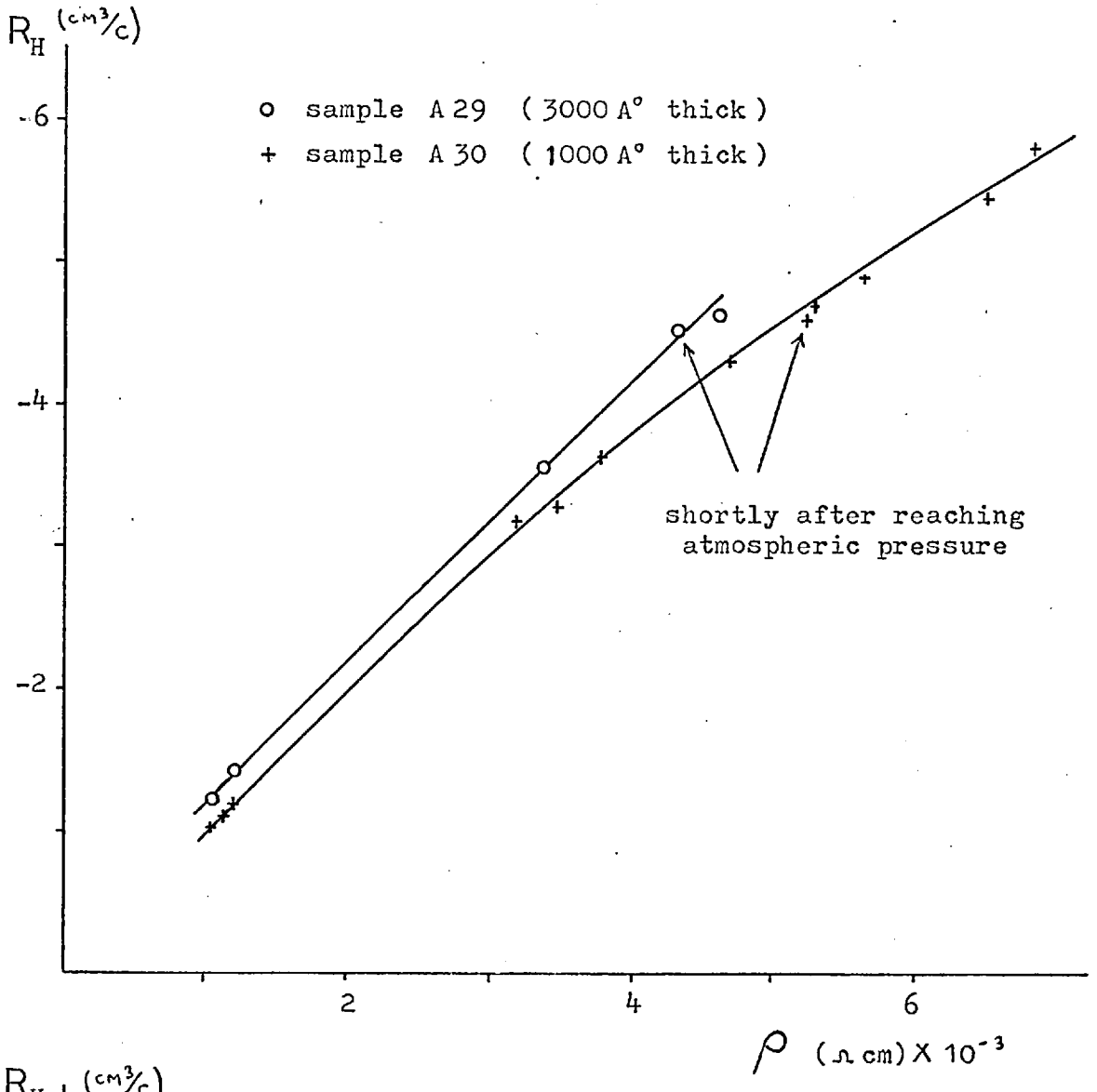

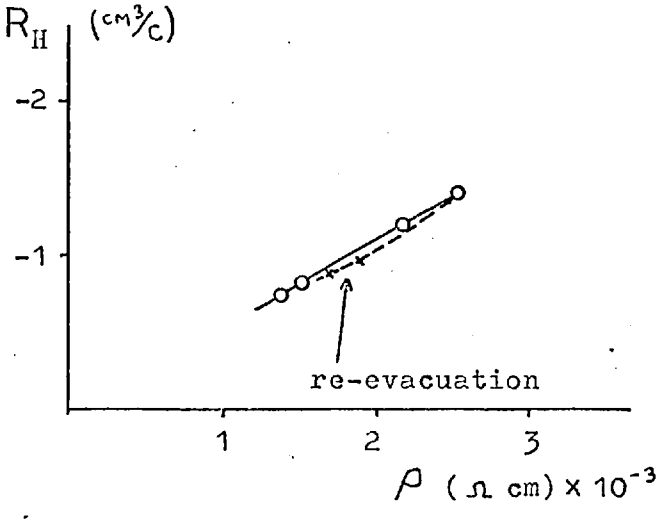

Figure 5.6

Hall coefficient and resistivity during exposure to air for n-type PbSe (sample B 10)

5.4 b Two - carrier films

Similar experiments were carried out on lead telluride films which were lightly - doped before exposure to air. Fig. 5.7 shows results obtained with sample A38 a , which was high-resistivity p- type in vacuum. In this case, admission of oxygen caused a net decrease in resistivity and Hall coefficient, but both of these quantities increased at first and went through a maximum before decreasing. After reaching atmospheric pressure, R_H and ρ had decreased by a factor of about 3 . However, the values obtained by re-evacuating the chamber do not lie along the original curve ; instead, R_H is higher for the same resistivity.

During the course of these experiments, it was found possible to control the initial carrier concentration by annealing the samples in vacuum at about $410\,^{\circ}C$. This causes preferential evaporation of tellurium from the film, and is irreversible i.e. the effect is always in the direction of n -type doping. The samples were cooled slowly to room temperature, and because of the fairly high self-diffusion coefficients at elevated temperatures, the doping in the resulting film should be uniform .

Figures 5.8 , 5.9 , and 5.10 show results for samples which were p-type after preparation and were then made lightly n-type by the annealing treatment before exposure to air. In each case, the effect of oxygen is sufficient to cause R_H to change sign, so that the samples are again p-type at atmospheric pressure. In fig. 5.9 , $|R_H|$ and ρ both go through a maximum before decreasing ; in fig. 5.8 only ρ goes through a maximum, and in fig 5.10 R_H and ρ decrease monotonically. Again, the points are not repeated upon re-evacuation from atmospheric pressure.

5.4 c Films coated with an insulator layer

Certain lead telluride samples were coated with an evaporated layer of insulator (Si O or MgF_2) as described in section 2.4 , and the effect of oxygen noted. The results are

Figure 5.7 HALL COEFFICIENT and RESISTIVITY of PbTe sample A 38 a during exposure to air

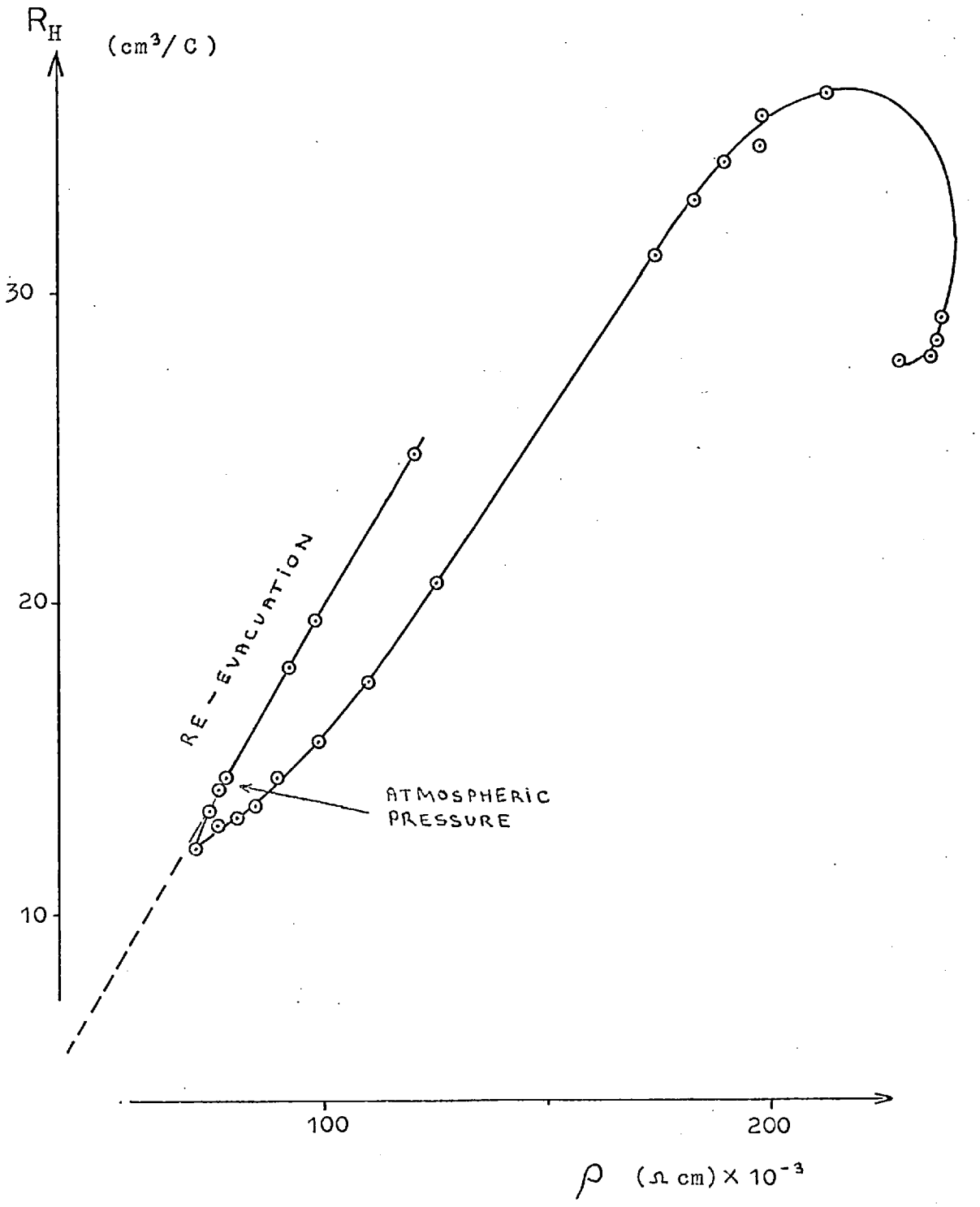

Fig. 5.8 PbTe sample A 38 b : exposure to air

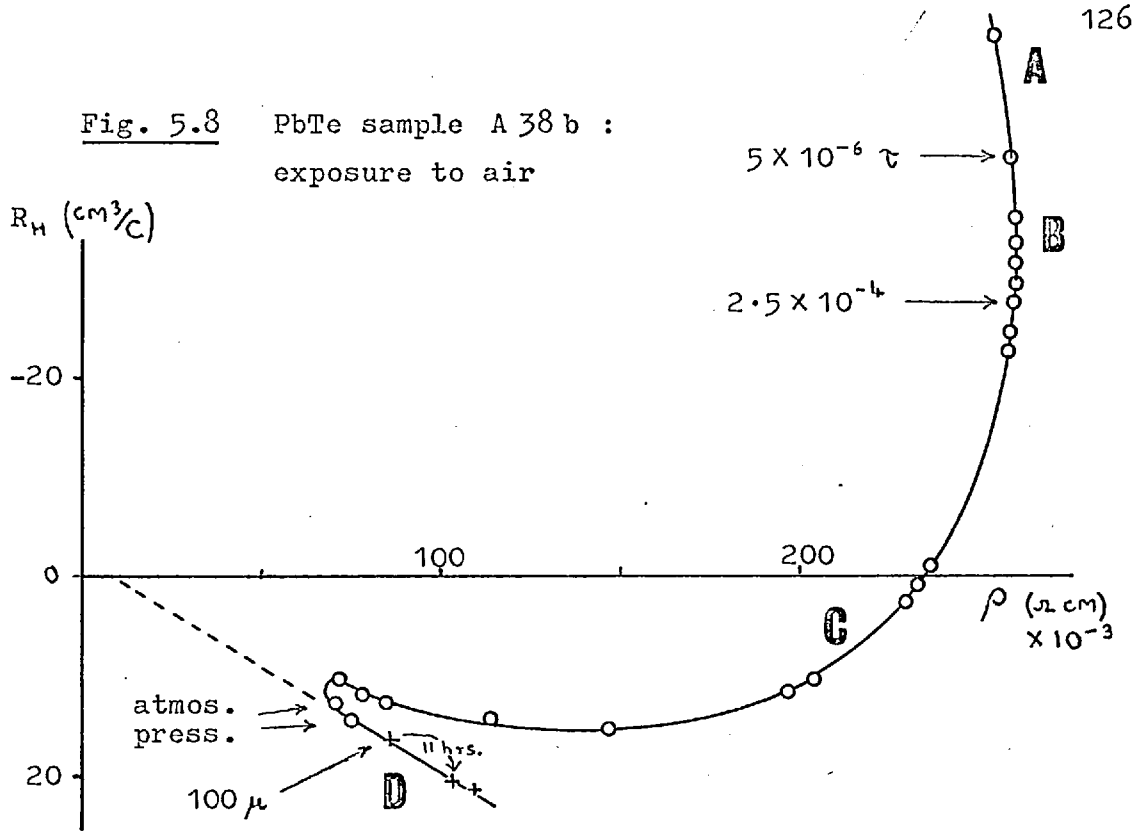

Fig. 5.9 PbTe sample A 39 ; exposure to air

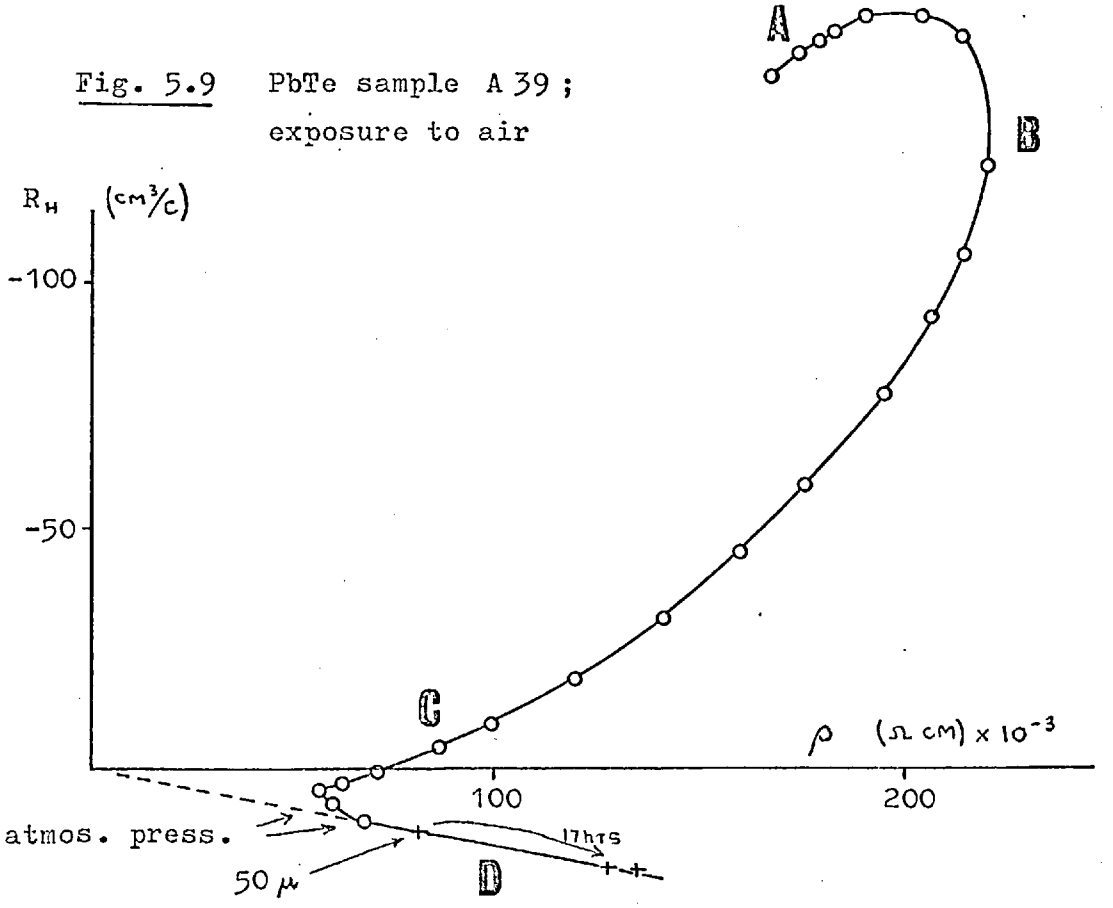

Figure 5.10 HALL COEFFICIENT and RESISTIVITY of PbTe sample A 40 during exposure to air

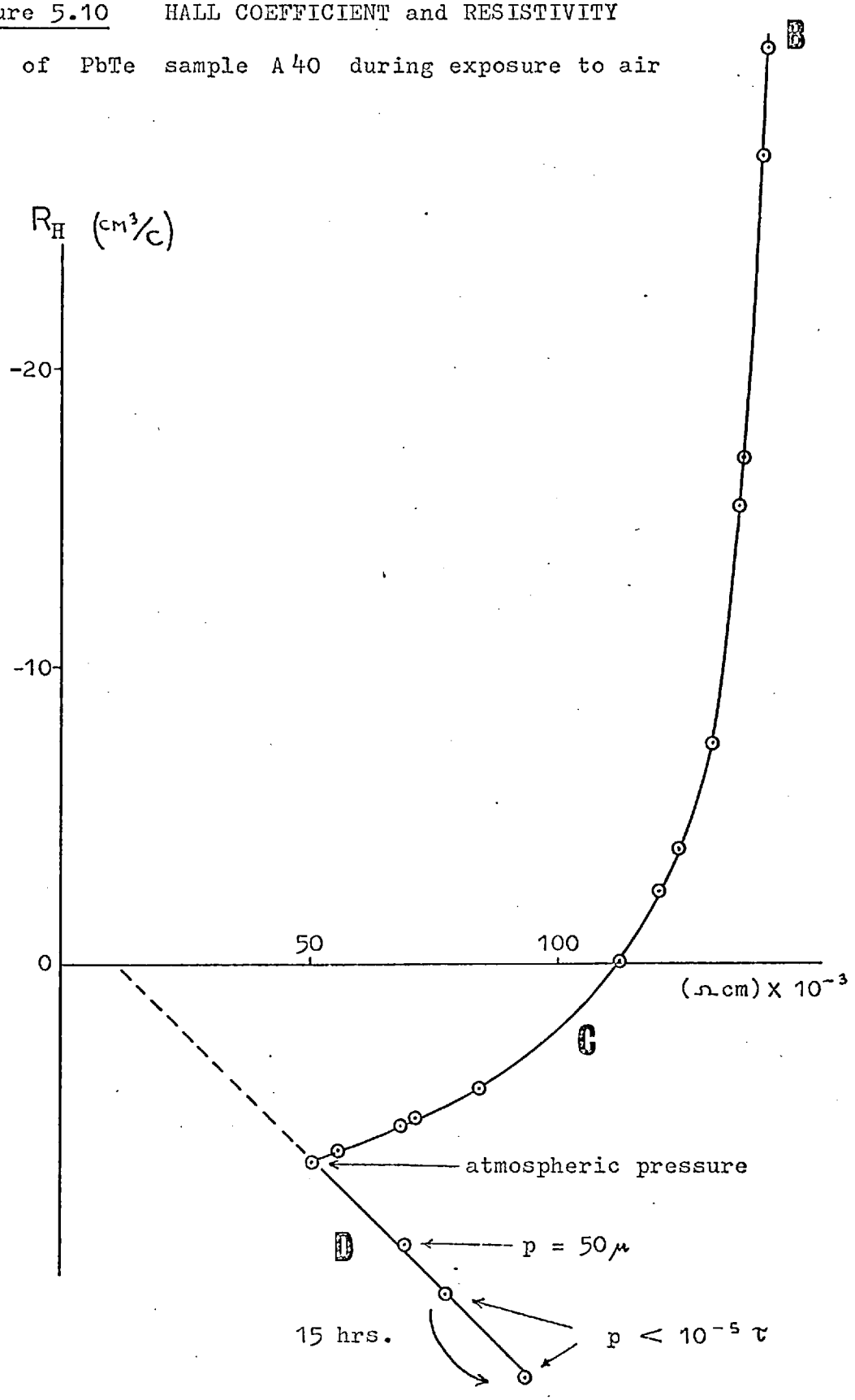

as follows.

1) Depositing the insulator on to films which had not been exposed to air gave no change in electrical properties in many cases. But in some samples, there was an n-type shift in doping, which could have been due to the introduction of chemical impurity from the source material or to radiation heating from the very hot source, resulting in evaporation of tellurium from the film.

2) Exposing the above samples to air resulted in a p-type shift in carrier concentration, but this was not as large as (roughly one third) the change observed in uncoated films of equivalent doping. The insulator therefore protects the PbTe from oxygen to a certain extent, as previously noted in 5.2 .

3) Evaporating insulator on to films which had previously been exposed to air gave no change in the electrical properties of the semiconductor, and when these samples were then exposed to air, there was again no change.

5.5 Discussion

a) One - carrier films

Before discussing the results presented in section 5.4 a , recent experiments of Brodsky and Zemel (B13) will be described.

These authors prepared epitaxial films of PbSe by evaporation on to NaCl substrates . The samples were exposed to air and then mounted in an apparatus where the Hall coefficient and resistivity could be measured simultaneously (at room temperature) as the pressure was reduced. The change in these parameters was slow but the rate was increased when an ion gauge (intended for monitoring the pressure) was turned on. When values of R_H and ρ were plotted against one another, the points were found to lie roughly on a straight line which passed near the origin of the graph. This means that the Hall mobility ($\mu_H = R_H/\rho$) remained approximately constant.

The change in R_H and ρ was attributed to the removal

of adsorbed oxygen from the surface of the semiconductor. The ion gauge was assumed to create some gaseous product (atomic hydrogen or carbon monoxide) which accelerates this process. By removing electrons from inside the semiconductor, the oxygen was believed to create a surface space-charge region (see 6.1), which is an accumulation layer in the case of p-type films. Reducing the ambient pressure therefore decreases the amount of band bending near the surface.

For p-type films, the change in surface conductance (= film thickness X change in conductivity) was quite large ($3 \times 10^{-3}\ \Omega^{-1}$). The surface band bending was assumed to be approximately zero at low ambient pressures, and would then be about 0·25 eV (10 kT at room temperature) at atmospheric pressure. Assuming completely diffuse surface scattering (see 6.3), the effective mobility of excess carriers in the space-charge region was estimated to be less than one fifth of the bulk mobility. (The calculation is similar to that outlined in section 4.5 a except that surface mobilities rather than average mobilities are required). Only a small decrease in ρ would then be possible due to the accumulation layer, and the Hall mobility would decrease with decreasing resistivity. The almost constant measured value of Hall mobility was therefore taken to indicate that excess carriers had bulk mobility and that surface scattering was specular. Further calculation showed that the slight decrease (with decreasing resistivity) observed in μ_H could be due to the change in effective mass with energy.

The above conclusions rest on the assumption that the band bending is given by the solution of Poisson's equation with uniform doping (secn. 6.1) i.e. that the oxygen does not cause a change in the concentration of impurity centres within the semiconductor.

Applying this adsorption model to the present results on n-type PbTe films immediately leads to difficulties. The

change in surface conductance in this case is even higher ($20 \times 10^{-3}\ \Omega^{-1}$) , which implies very large band bending. Assuming that the bands are flat in vacuum, the impurity concentration can be taken as $3{\cdot}5 \times 10^{18}$ cm^{-3} in a typical case. The effect of oxygen must now be to create a depletion layer at the surface ; the maximum amount of depletion (before inversion occurs) can be calculated using the computer program described in appendix B , which gives an answer of $1{\cdot}6 \times 10^{-3}\ \Omega^{-1}$ for the change in surface conductance. To account for the magnitude of the experimental change, it is therefore necessary to assume that there is an accumulation layer at the surface in vacuum, with a downward band bending of ~~around~~ at least 20 kT . This would make the semiconductor highly degenerate, with a surface charge of 10^{14} cm^{-2} and a surface electric field (5×10^{5} volt / cm) approaching the breakdown strength of most materials. Since values as high as this are not normally observed in semiconductors, the explanation based on adsorption needs further evidence before it can be acceptable.

5.5 b Two - carrier films

The results obtained from the low-carrier-concentration films (5.4 b) will now be discussed in a similar manner to those from the high-doping samples (5.4 a) . The treatment involves surface space charge concepts, which are defined in chapter 6 .

If the effect of oxygen is one of adsorption with charge transfer at the external surface, the interpretation is made easier by re-plotting the experimental curves in terms of the parameters σt and $R\sigma^2 t$ (t is the film thickness). The reason for this is that the surface quantities $\Delta\sigma$ and $\Delta R\sigma^2$ (defined in 6.3) representing excess carriers in the space-charge region are additive with respect to the bulk parameters σt and $R\sigma^2 t$ (see appendix A) . This has been done for sample A 38 b (from fig. 5.8) and the result is shown in fig. 5.11 (solid curve) . In this curve, the surface conductance σt

Fig. 5.11 PbTe sample A38b : exposure to air

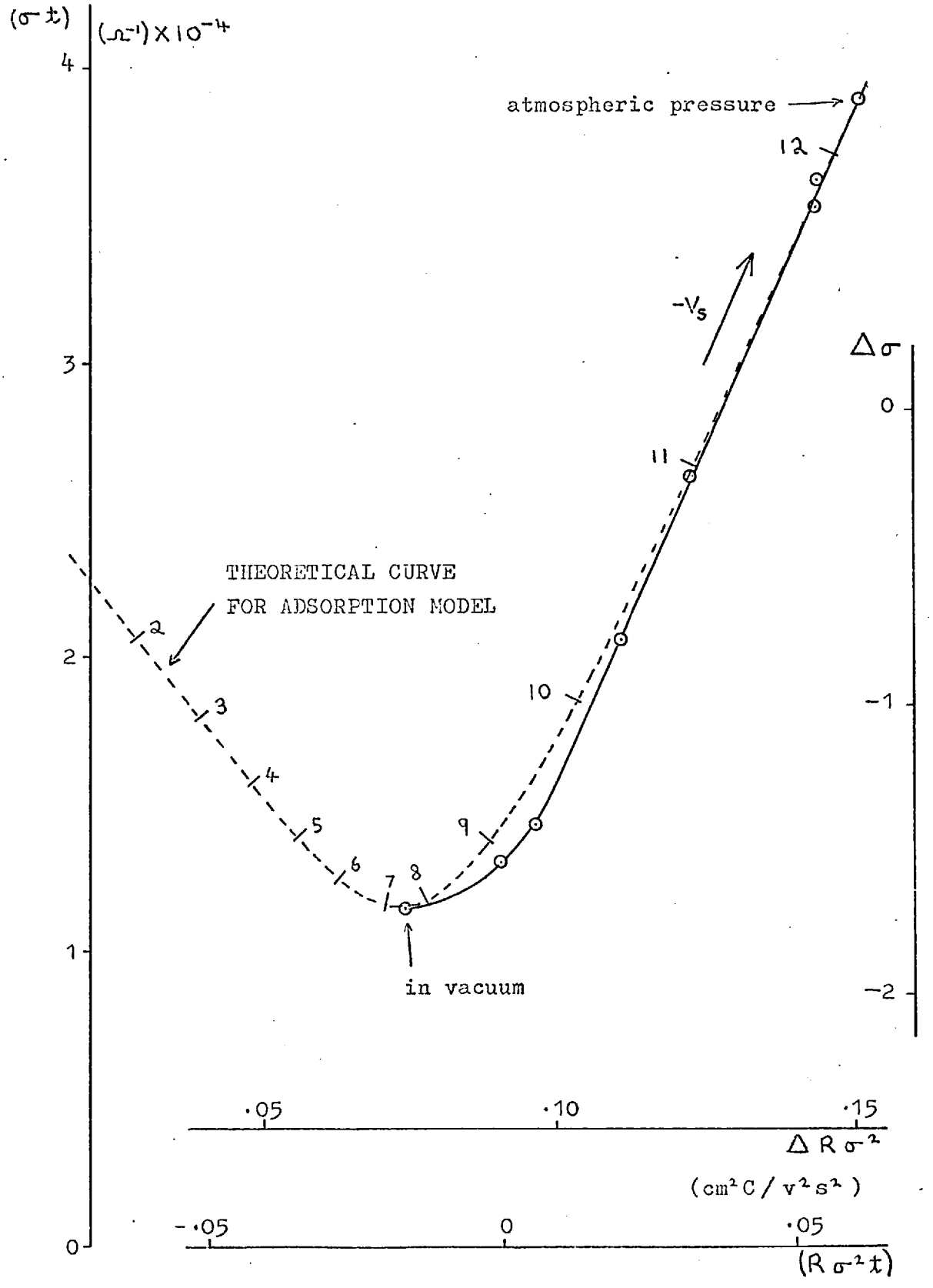

goes through a minimum value, which resembles the behaviour obtained from field-effect measurements when $\Delta\sigma$ is plotted against the surface space charge Q_{sc} . In fact, provided that $\mu_{ps} = \mu_{ns} = \text{constant} = \mu_s$,

eqn. (6.21) gives $\Delta R\sigma^{-2} = q\,\mu_s\,(\Delta P - \Delta N) \propto Q_{sc}$

so that $\Delta R\sigma^{-2}$ is a measure of the surface space charge.

Moreover, theoretical values of $\Delta\sigma$ and $\Delta R\sigma^{-2}$ can be calculated by solving Poisson's equation. This is done by the computer program described in appendix B . For the computer calculation, 'bulk' (as opposed to surface) values of the mobility μ_b and carrier concentration n_b for the particular sample are required. μ_b may be obtained from the gradient of the experimental σt v. $t R\sigma^{-2}$ curve away from the conductivity minimum, since

$$\frac{d(\sigma t)}{d(R\sigma^{-2}t)} = \frac{d(\Delta\sigma)}{d(\Delta R\sigma^{-2})} = \frac{q\,d(\mu_{ps}\Delta P + \mu_{ns}\Delta N)}{q\,d(\mu_{ps}^2\Delta P - \mu_{ns}^2\Delta N)}$$

$$\doteqdot \frac{1}{\mu_{ps}} \quad \text{if} \quad \Delta P \gg \Delta N$$

$$\doteqdot \frac{-1}{\mu_{ns}} \quad \text{if} \quad \Delta N \gg \Delta P$$

Surface and bulk mobilities μ_s and μ_b can be assumed approximately equal even if surface scattering is diffuse, since for low carrier concentration and surface potential the mobility reduction is not severe in PbTe (see fig. 6.9) .

n_b is given by : $\sigma_b = q\,\mu_b\,n_b$ (1-carrier approximation)

when there is no band bending. Since the flat-band point on the experimental curve is not yet known, the flat-band conductivity σ_b has to be estimated ; as a first approximation, it can be taken as the conductivity in vacuum.

The calculated curve of $\Delta\sigma$ against $\Delta R\sigma^{-2}$ may then be superimposed over the experimental one. The flat-band point is now known approximately and may give a value for n_b different

from the one previously assumed. This new value can then be used to calculate a second theoretical curve, and the procedure repeated until consistency is achieved. As a check on the value assumed for μ_b, the value of $R\sigma^2 t$ at the flat-band point should be approximately $q\mu_b^2 n_b$.

Figure 5.11 shows the 'best fit' obtained with a calculated curve (shown dotted) for $n_b = 1{\cdot}5 \times 10^{17}$ cm^{-3}, $\mu_b = 350$ cm^2/v.s. The results imply that the surface potential is $v_s \doteqdot -7$ in vacuum and $v_s \doteqdot -12$ in air. The charge transferred by oxygen to the space-charge region would be about 10^{13} charges/cm^2.

However, there is a difference in shape between the two curves in fig. 5.11. The experimental curve has a shallower minimum, and this is also true for other samples which were measured. It may therefore be necessary to assume that the process is not purely one of charge transfer at the surface, and that diffusion processes are important.

The qualitative features of the R_H against ρ curves, figures (5.7 to 5.10) can still be interpreted in terms of band bending, whether this is due to adsorption or diffusion or a mixture of the two.

Figure 5.12 shows different stages of band bending for an n-type semiconductor. The corresponding regions are labelled on the experimental curves, figs. 5.8, 5.9 and 5.10. Diagram A (in fig. 5.12) shows a depletion layer at the external surface, and probably represents the condition of samples A 39 and A 38b in vacuum. In the case of sample A39, a reduction in the number of electrons in the film (due to the presence of oxygen) causes $|R_H|$ to increase initially, but subsequently to decrease due to the increasing concentration of holes near the surface. For sample A 38 b, R_H decreases from the start, presumably due to higher initial band bending or lower doping. In both these cases, oxygen causes the resistivity to increase at first,

Fig. 5.12 Band bending due to oxygen in an n-type PbTe film

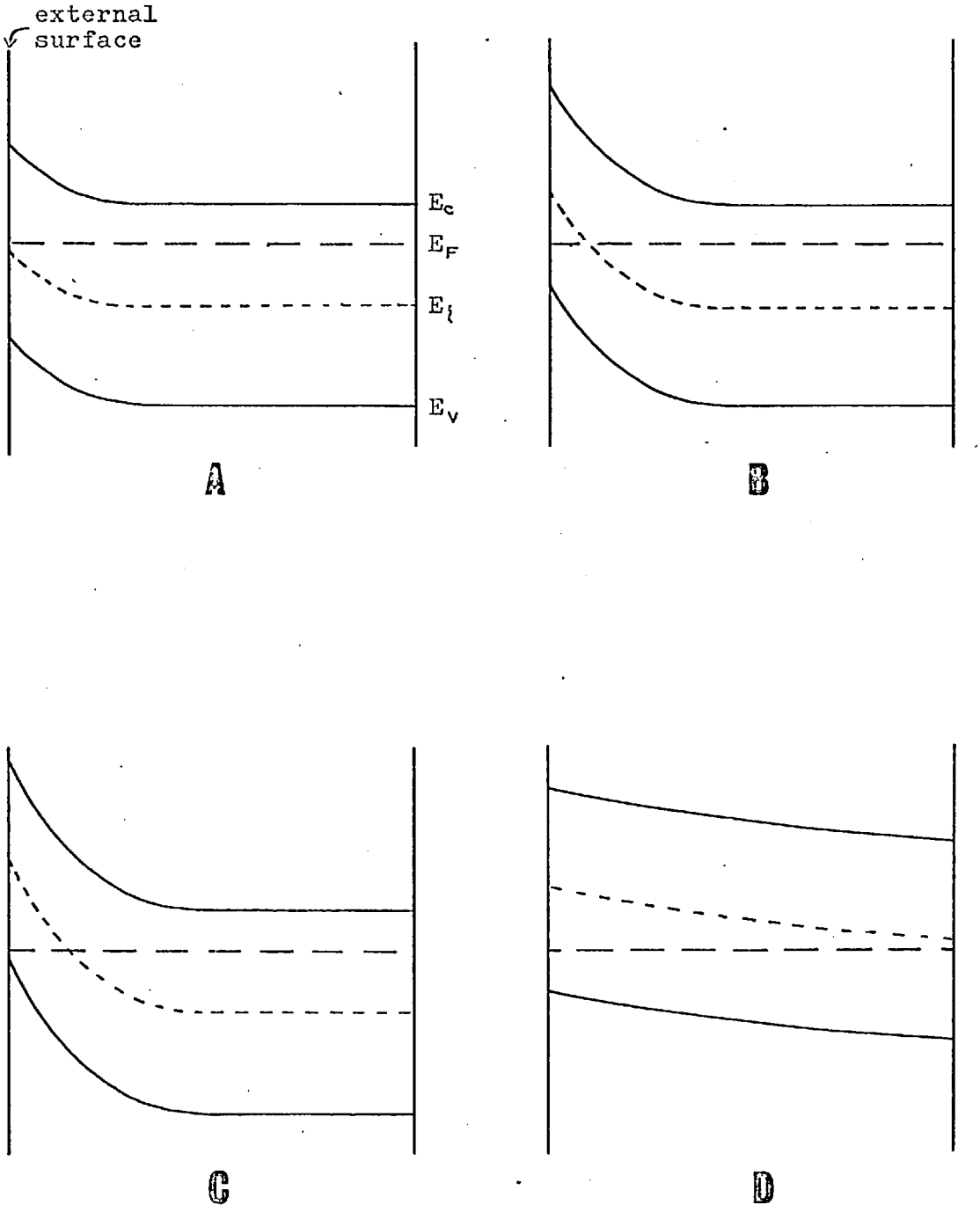

but ρ soon reaches a maximum corresponding to the minimum in surface conductance (fig. 5.11). This is the situation in diagram B (fig. 5.12); if the precess is one of adsorption alone, the band bending at this point is given by $v_s \doteqdot -2u_b$ (ref. M5), as shown. Diagram B also corresponds to the initial condition of sample A 40 in vacuum (fig. 5.10). Further band bending causes both ρ and R_H to decrease; eventually R_H passes through zero (diagram C) and becomes positive. If the oxidation proceeds far enough, R_H reaches a (positive) maximum and then starts to decrease (fig. 5.8), indicating that conduction now takes place mainly in the surface region and is due to holes.

If the sample is allowed to remain at atmospheric pressure for a few hours, ρ starts to increase and R_H becomes more positive, so that the points do not lie on the original curve (figs. 5.8 to 5.10). It does not seem possible to account for this non-reversible effect in terms of an adsorption model. However, the effect can be explained if diffusion is assumed to take place in the interior of the semiconductor film. This can be assumed to result in the gradual conversion of the majority of the semiconductor from n-type to p-type, due to the removal or compensation of the original n-type impurity centres. The Hall coefficient and resistivity then increase because of recombination of some of the holes with electrons. The final result of this process would be that the whole of the film becomes p-type, with the energy bands almost flat, as in diagram D (fig. 5.12). If the ambient pressure were then reduced, the sample would behave as a p-type film, R_H and ρ both increasing along a straight line passing through the origin, with a gradient equal to the hole mobility. Reference to figures (5.8 to 5.10) shows that the observed behaviour upon re-evacuation is in reasonable agreement with this prediction. In fig. 5.8, the points obtained after re-pumping lie on a line of gradient 200 cm^2 / v.s. which can be compared with the estimated hole mobility of 180 cm^2 / v.s. for this sample (assuming a mobility ratio μ_n / μ_p of 2·0 for PbTe).

The fact that the sample A38a (fig. 5.7) also shows this non-reversible behaviour would indicate that in this case part of the film was originally of n-type doping.

5.6 Comparison of adsorption and diffusion models

Both adsorption and diffusion processes would be expected to have similar effects on the Hall coefficient and resistivity of the semiconductor ; both involve electric fields and carrier concentration gradients near the surface. The differences between them are as follows.

In adsorption, the active species (oxygen) remains at the surface of the semiconductor, and charge (in the form of electrons or holes) is transferred across the interface, resulting in band bending. The shape of the bands (energy v. distance) is determined by electrostatics and can be calculated by solving Poisson's equation. The depth of penetration of the space charge depends on the surface potential and on the doping in the semiconductor. In the simplest case, the speed of the process is determined by the rate of arrival and the sticking coefficient of oxygen at the surface.

For diffusion, the effect penetrates into the semiconductor by an amount which depends on the relevant diffusion coefficient and on time. Band bending is caused by a change in the concentration of impurity centres. The diffusion profile can be calculated (L5), allowing for the fact that the diffusing species may be charged (ionised), but an exact solution is difficult. The shape of the band bending is different from that due to adsorption, and this makes conclusions regarding the surface scattering more difficult.

It is worth pointing out that the present results for PbTe do not give information about the specularity of the surface. In the case of highly n-type samples, oxygen creates a depletion layer (unless there is downward band bending in vacuum) and few carriers reach the surface ; in the low-doping films, the

concentration of carriers at the surface is insufficient to give rise to much surface scattering.

One possibility of distinguishing experimentally between adsorption and diffusion is to examine the kinetics of the process. Three results which are relevant are as follows.

1) In the case of a lightly-doped n-type PbTe sample which was kept under high vacuum (pressure $\sim 1\frac{1}{2} \times 10^{-6}$ torr) for several hours after deposition, $|R_H|$ was observed to decrease linearly with time (see fig. 5.13). This probably indicates that adsorption of oxygen on the surface is the rate-limiting process at these low pressures, but does not preclude subsequent diffusion from being responsible for the change in electrical properties. Assuming that the rate is determined by adsorption, the sticking coefficient of oxygen (defined as the fraction of oxygen molecules striking the surface which remain there) can be estimated. If each oxygen atom remaining on the surface effectively removes one electron from the semiconductor and if the partial pressure of oxygen in the vacuum system is 1% of the total pressure, the sticking coefficient at room temperature is between 10^{-7} and 10^{-8}. This is of the same order as the value previously obtained for clean (100) surfaces of PbTe (G4).

2) A similar sample was suddenly exposed to air at atmospheric pressure and the conductivity monitored as a function of time. The change was not linear with time, but when σ is plotted against $t^{\frac{1}{2}}$, the graph is approximately linear over parts of the range (see fig. 5.15). The curve is similar in shape to those obtained from the effect of oxygen on polycrystalline PbSe films (J3), except that the times involved in the latter case were much longer. For PbSe, it appeared likely that the increase in σ was due to a diffusion process; in the case of PbTe, the higher rate would then be due to a larger diffusion coefficient.

3) The third measurement concerns the variation of

Fig. 5.13 PbTe sample (A43b) kept under vacuum

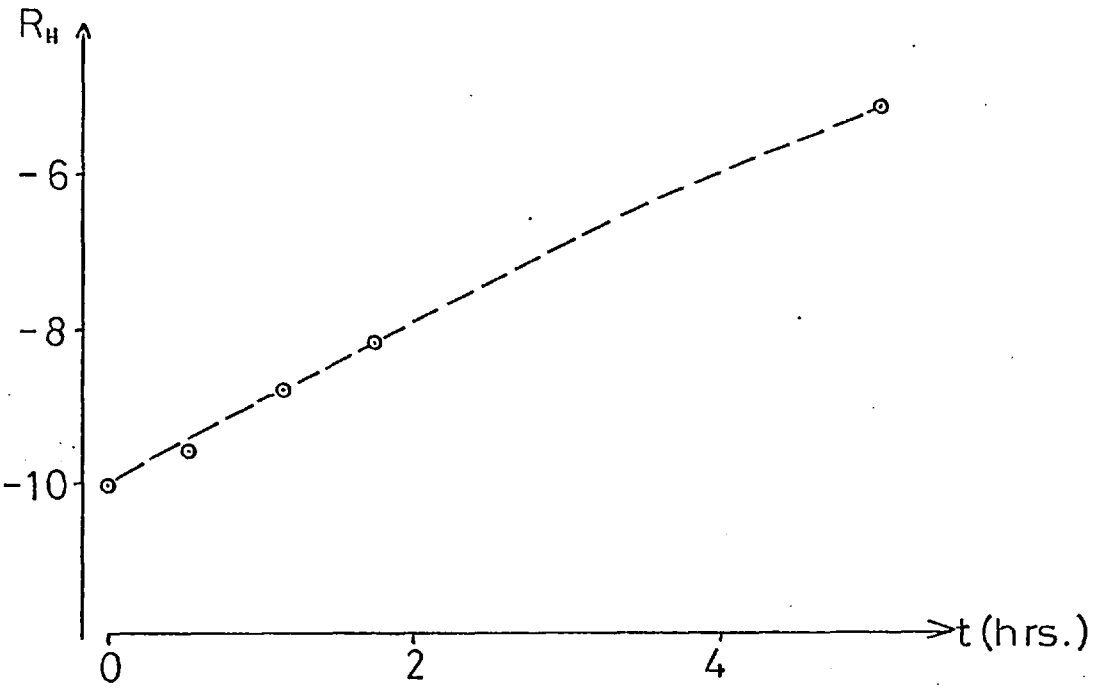

Fig. 5.14 Effect of temperature on oxidation rate

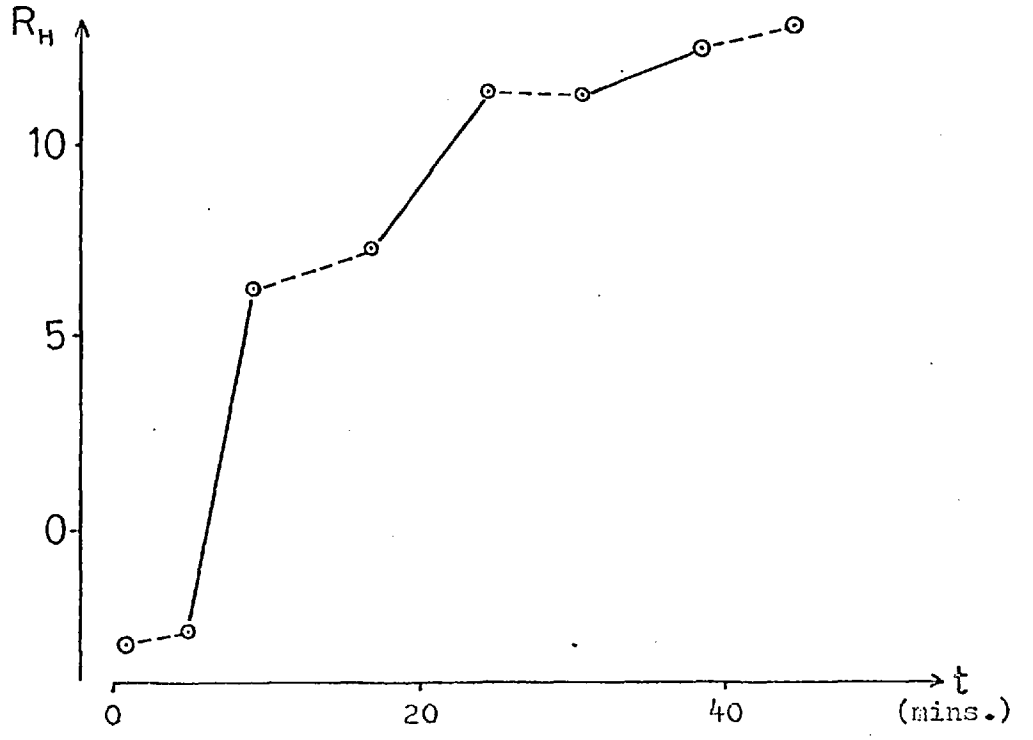

R_H in units of cm^3/coulomb

Figure 5.15 Change in conductivity with time for PbTe (sample A 47 b) upon exposure to the atmosphere

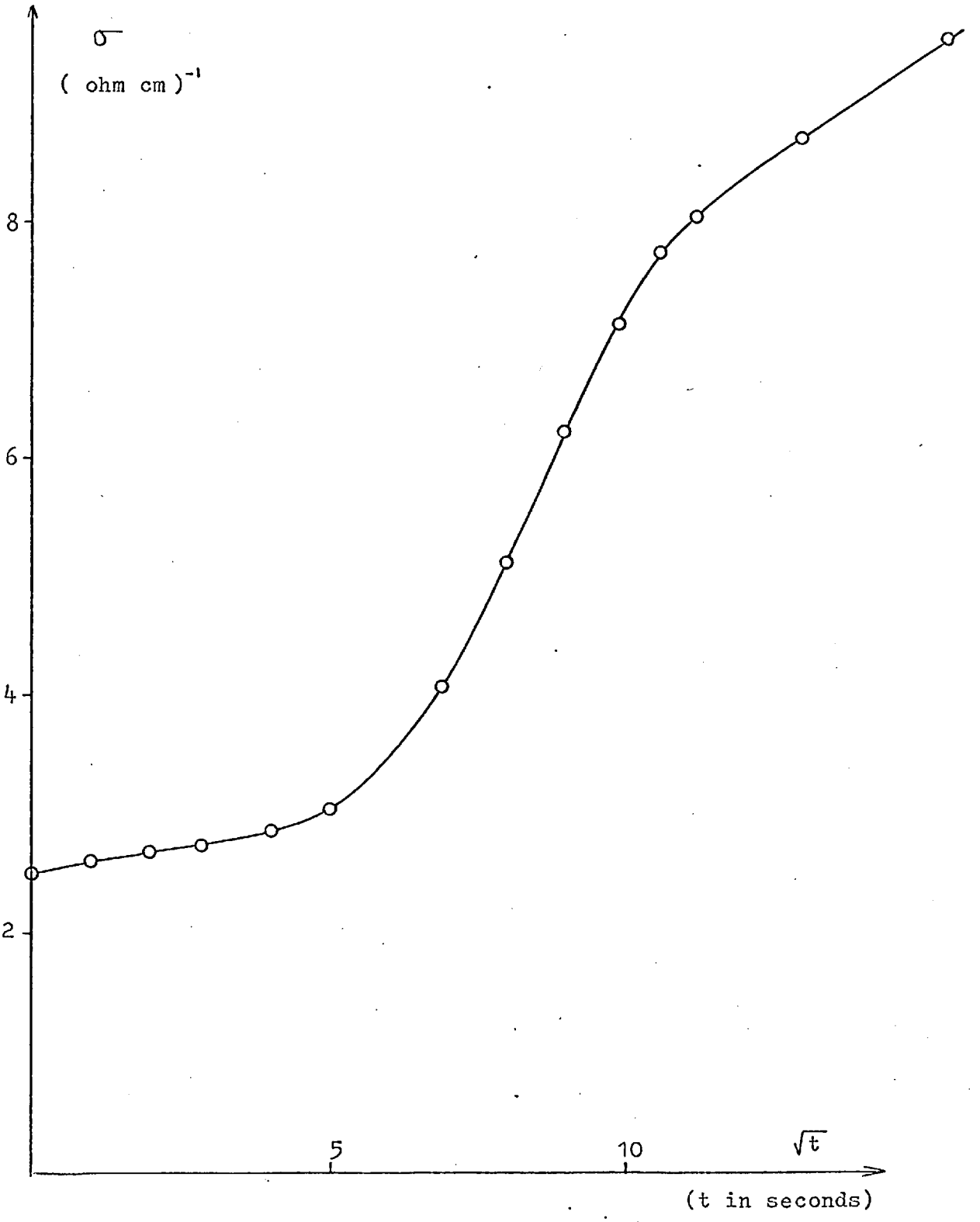

oxidation rate with temperature. Figure 5.14 shows the Hall coefficient of a PbTe sample, kept at a constant pressure of 3×10^{-3} torr by means of an air leak, which was heated to about $100^{\circ}C$ and cooled to room temperature for alternate periods of time. Clearly, the rate of change of R_H increases rapidly with temperature; this could be accounted for by assuming

$$\frac{dR_H}{dt} \propto \exp\left(\frac{-E}{kT}\right) \qquad (5.2)$$

where E is estimated very roughly as 0·5 eV. If a diffusion mechanism is involved, and this is the rate-limiting process at 3×10^{-3} torr, the rate of uptake of oxygen would be proportional to $D^{\frac{1}{2}}$ (equation 5.1) where D is the diffusion coefficient. The activation energy for diffusion would therefore (from(5.2)) be about 1 eV. On the other hand, if adsorption is the rate-limiting process, eqn. (5.2) indicates that the sticking coefficient s must be given by:

$$s \propto \exp\left(\frac{-E}{kT}\right) \qquad (5.3)$$

This is the interpretation given by Green and Lee (G4), who measured the rate of uptake of oxygen by crushed PbTe and obtained a value of E = 0·31eV for the (100) surface.

Although none of the above results are conclusive, the evidence suggests that diffusion plays a role in the effect of oxygen on PbTe films. A plausible explanation would be the following:

a) Diffusion within the semiconductor takes place over a period of hours and causes the non-reversible effects noted in 5.4b and 5.5b.

b) This process continues over a period of months, and is responsible for the long-term ageing effects described in 5.1 and 5.2.

c) The rapid effect observed when oxygen is initially

admitted to clean surfaces is due to adsorption and charge transfer at the surface .

This interpretation is satisfactory, except that it does not explain the following points :

1) To account for the observed changes in surface conductance for the highly-doped n-type films in terms of a surface space-charge region , the band bending would have to be extremely high and there would have to be a high surface potential in vacuum (section 5.5a) . This conclusion comes from calculations based on existing space-charge theory, including degeneracy in the bulk and in the space-charge region but neglecting surface quantization and impurity band effects. Quantization is expected to be significant for surface charges greater than 10^{12} cm^{-2} (see 6.1) , whereas the charge densities required by the adsorption mechanism are more than an order higher than this. However, the effect of such quantization would be to make the required surface potentials even larger. At high doping densities, the impurity centres probably form an energy band (see 1.4) but it is not obvious what effect this might have on the calculations. Conduction within such a band has been observed in germanium (H1 , K7) at low temperatures but the mobility was comparatively low.

2) The large band bending would result in an observable (about 50%) change in carrier mobility, due to the non-parabolicity of the conduction band in PbTe, even in the absence of diffuse surface scattering. Experimentally, the Hall mobility was found to be nearly constant.

It is therefore necessary to consider whether even the rapid changes in R_H and ρ could be due to diffusion. This involves a discussion of the diffusion mechanism , which will be attempted in the next and final section of this chapter.

5.7 Diffusion mechanisms

Three possibilities will be considered :

a) Diffusion of vacancies through the lattice

b) Interstitial diffusion of oxygen

c) Diffusion via dislocations or grain boundaries .

a) Vacancy diffusion

In the lead salts, the impurity centres are singly-ionised vacancies * i.e. Schottky defects or F-centres (B9, p.28). For extrinsic n-type PbTe these are tellurium vacancies, many of which are ionised. Although much less mobile than the current carriers, they can migrate in the presence of a concentration gradient (and under an electric field, if ionised) . Since oxygen and tellurium are both in group VI of the periodic table, it seems likely that oxygen atoms could fill some of the vacant tellurium sites without altering the band structure of the semiconductor i.e. act as a compensating impurity . However, there are two possibilities :

1) Oxygen remains essentially at the surface of the PbTe film, and captures tellurium vacancies in the vicinity of the surface (e.g. by first capturing electrons and then attracting ionised vacancies, reducing their concentration at the surface) . Vacancies will then diffuse to the surface from the interior of the film. If carried to completion, this process would result in the removal of nearly all vacancies from the film, leaving the semiconductor intrinsic.

2) Oxygen enters tellurium vacancies and diffuses into the bulk of the film. This diffusion would involve the motion of both oxygen atoms (or O^- ions) and vacancies.

Mechanism 1) corresponds to the self-diffusion of tellurium in PbTe , assuming that this does take place by a vacancy mechanism (as for many other semiconductors, F.C.C. metals, alkali halides etc.) . The speed of the process can

---

* except in n-type PbSe and PbS , where the donor centres are believed to be interstitial lead

therefore be estimated, using the measured diffusion coefficient of Te in PbTe (see table 5.2) . The conductivity change, expressed as a surface quantity , is approximately (see eqn.(5.1) and fig. 5.16 a) :

$$\Delta[\sigma] = \tfrac{1}{2} q \mu_n n_b (Dt)^{\frac{1}{2}} \qquad (5.4)$$

giving $\Delta[\sigma] \sim 1{\cdot}5 \times 10^{-7}\ \Omega^{-1}$ after 10 seconds

$\sim 0{\cdot}5 \times 10^{-3}\ \Omega^{-1}$ after 1 month

Since the conductivity change for the highly n-type samples was about $3 \times 10^{-3}\ \Omega^{-1}$ and took place in less than a minute, process 1) is not fast enough to explain the rapid change, but might be sufficient to account for the long-term effects when samples were stored in air.

Process 2) will be either slower or faster than this, depending on whether the binding energy of oxygen at tellurium sites is higher or lower than that of tellurium. Although 'foreign' atoms in a lattice are often more weakly-bound, this may not be true in the present case . Therefore the diffusion rate cannot be estimated.

There is in any case some doubt about the mechanism of self-diffusion in PbTe . The fairly low activation energies for Pb and Te (see table [5.2]) may be due to diffusion via interstices (B9) .

5.7 b Interstitial diffusion

If atoms (or ions) can diffuse via interstices in the lattice, the activation energy is often low and the diffusion coefficient high (especially at low temperatures) . This process is responsible for the high diffusion rates of (for example) copper in germanium and hydrogen in steel ; it is also the mechanism for copper and nickel in p-type lead sulphide, which was studied by Bloem and Kröger (B7).

Cu or Ni atoms diffuse interstitially through PbS until they meet a lead vacancy, when they are immediately

captured due to the high binding energy. In the case of Cu , the atom becomes ionised with a single positive charge upon filling a vacancy, giving no change in carrier concentration :

$$V'_{Pb} + Cu^{x}_{i} \longrightarrow Cu'_{Pb} \qquad (5.5)$$

(the notation is defined in reference K10)
Nickel, however, becomes doubly-ionised (B7) , resulting in the removal of a hole from the valence band of the PbS :

$$h^{\bullet} + V'_{Pb} + Ni^{x}_{i} \longrightarrow Ni^{x}_{Pb} \qquad (5.6)$$

When all the vacancies in a given volume of semiconductor are filled, excess Cu or Ni atoms can remain in the interstices, becoming singly-ionised (B7) :

$$Cu^{x}_{i} + h^{\bullet} \longrightarrow Cu^{\bullet}_{i} \quad \text{and} \quad Cu^{x}_{i} \longrightarrow Cu^{\bullet}_{i} + e' \qquad (5.7)$$

$$Ni^{x}_{i} \longrightarrow Ni^{\bullet}_{i} + e' \qquad (5.8)$$

Electrons are thereby liberated into the conduction band, turning the semiconductor n-type.

The mechanism for oxygen in n-type PbTe will be assumed to be similar to Ni in PbS , but with the sign of the charges reversed. Oxygen atoms therefore diffuse interstitially to fill tellurium vacancies :

$$V^{\bullet}_{Te} + e' + O^{x}_{i} \longrightarrow O^{x}_{Te} \qquad (5.9)$$

By itself, this would result in an almost intrinsic semiconductor, A second stage is therefore necessary to account for the fact that PbTe is actually driven p-type. This may be the ionisation of interstitial oxygen :

$$O^{x}_{i} \longrightarrow O'_{i} + h^{\bullet} \qquad (5.10)$$

$$\text{or} \qquad O^{x}_{i} \longrightarrow O''_{i} + 2\,h^{\bullet} \qquad (5.11)$$

The extent of this process (and also the rate) will be limited by the interstitial solubility of oxygen, which may be low if the binding energy is small. Alternatively, an oxygen atom which fills a vacant tellurium site may create an associated lead vacancy.

The mechanism for oxygen might also be expected to apply to PbSe , but at a slower rate (due to the smaller lattice constant) . In fact, it provides a reasonable explanation of the kinetics measured by Jones (J3) . He observed a rapid decrease in conductance when a freshly-prepared n-type PbSe film was exposed to oxygen. But after reaching a minimum (which was believed to correspond to an intrinsic semiconductor) , the conductance increased at a rate which could easily be measured. There was evidence that this increase was controlled by a diffusion process, for which the activation energy (from fig. 3 Of ref. J3) appears to be 0·26 eV . This low value suggests an interstitial mechanism, and is close to the value for Cu in PbS (see table [5.2]) .

It is not possible to estimate the diffusion rate in PbTe without knowing the surface concentration of oxygen, which depends on the solubility. However, if the diffusion coefficient is comparable with that of Cu in PbS , it is reasonable to expect large conductivity changes within a period of seconds.

A requirement for low activation energy is that the diffusing atom (or ion) must be small enough to fit into the interstices of the lattice. Bloem and Kroger (B7) argue that this is the case for copper in lead sulphide, at least for the ionised (Cu^+) form . The oxygen atom is smaller than a Cu^+ ion (see table [5.3]) and would therefore be expected to diffuse interstitially in all three of the lead salts. The oxygen ions, however, have larger radii , particularly O^- . Therefore it is unlikely that O^- can exist at even the largest interstitial site ; a more probable ionisation product is O^{2-} (equation (5.11)) , which has a smaller radius (see table 5.3).

Table [5.2] DIFFUSION COEFFICIENTS (in cm^2 / sec)

$$D = D_o \exp (- E_D / kT)$$

material	diffusant	E_D (eV)	D_o	D (300^oK)
PbTe	Pb	0·6	$2·9 \times 10^{-5}$	1×10^{-15}
	Te	0·75	$2·7 \times 10^{-6}$	$2·5 \times 10^{-19}$
PbS	Pb	1·82	1·3	5×10^{-28}
	Cu	0·31	5×10^{-3}	$3·7 \times 10^{-8}$
	Ni	0·96	17·8	$1·5 \times 10^{-15}$

Table [5.3] Approximate atomic and ionic radii (A^o)

		Cu	= 1·3		Cu^+	= 0·96	
O	= 0·6			O^-	= 1·76	O^{2-}	= 1·3
		Te	= 1·4		Te^{2-}	= 2·1	
		Pb	= 1·7		Pb^{2+}	= 1·3	
		Ni	= 1·25		Ni^{2+}	= 0·69	

Fig. 5.16 b Interstitial diffusion of oxygen

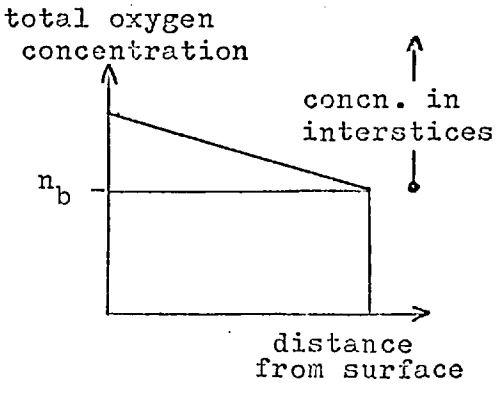

Fig. 5.16 a Diffusion of tellurium vacancies

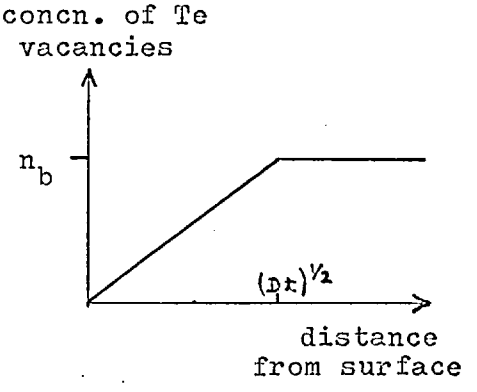

5.7 c Dislocation and grain-boundary diffusion

It is well-known that diffusion along high-angle grain boundaries proceeds more rapidly than in the bulk of a solid. Low-angle boundaries and dislocations are also regions of atomic misfit, giving a lower activation energy for diffusion. The presence of boundaries or a high density of dislocations commonly found in thin films can therefore lead to an increased diffusion rate for any of the mechanisms discussed previously. From observations on an epitaxial PbSe film, Zemel (Z4) concluded that the self-diffusion coefficient of lead in this material was higher than the bulk value by a factor of 10^4.

The experimental results (section 5.4 a) indicate very little change in Hall mobility when epitaxial PbTe films were initially exposed to oxygen. If diffusion takes place down low-angle or double-positioning boundaries, this might be expected to reduce the mobility, by analogy with polycrystalline films of PbTe and PbSe, where oxygen exposure decreased μ_H by a factor of 2 to 5 (S17) due to the creation of space-charge barriers. A similar effect could give rise to increased scattering from dislocations.

However, energy barriers and a density of dislocations should be detectable from electrical measurements (see 4.5), even in the absence of oxygen. The fact that these did not show up in the present films (even at low temperatures) may mean that conduction is not affected by them.

- - - - - - - - - - - -

The discussion in this section (5.7) suggests that diffusion rates in epitaxial films of the lead salts can be quite high. The treatment has neglected the possible formation of molecular complexes, which appear to be a common feature in semiconductors. A further requirement of a diffusion process is that the surface layer should not become appreciably p-type for an n-type film, otherwise μ_H would be reduced owing to

compensation of Hall voltage. The only mechanism which guarantees this is that of tellurium vacancy migration (5.7 a (1)).

Possible experiments which might distinguish between adsorption and diffusion processes in the lead salts are as follows :

1) Observation of the change in surface potential upon exposure to oxygen (e.g. by contact potential measurements).

2) Measurement of the diffusion coefficient of oxygen (e.g. from the depth of a p - n junction in bulk single crystals).

CHAPTER 6

FIELD-EFFECT MEASUREMENTS

6.1 The surface space-charge region

An experimental arrangement for observing the field effect in a semiconductor is shown in fig. 6.1 . A voltage V_g is applied between the semiconductor sample and an electrode (known as the field plate or 'gate') parallel to one of its surfaces, producing an electric field within the dielectric layer. Because of the lower density of charge carriers in a semiconductor compared with a metal, the field also penetrates some distance into the sample, instead of being terminated abruptly by charges at the surface. The volume of semiconductor in which the electric field lines are terminated is called the surface space-charge region.

For practical values of applied field, the band structure of the semiconductor is assumed to be unaltered right up to the surface. The field merely causes the energy bands (drawn against distance) to bend in the vicinity of the surface ; this is known as the field effect. Moreover, as soon as equilibrium is established , the Fermi energy remains constant throughout the semiconductor. The band picture for an n-type semiconductor with a positive voltage applied to the field plate is shown in fig. 6.2 .

There are two parameters, either of which can be used to describe the amount of band bending at a point within the space-charge region :

$$u = \frac{q}{kT} (E_f - E_i) \qquad (6.1)$$

$$v = u - u_b \qquad (6.2)$$

Here, E_f is the Fermi energy, and E_i is an energy which remains fixed with respect to the conduction and valence bands and is equal to the Fermi energy in the interior of the intrinsic (undoped) semiconductor. u is therefore the potential (in units of kT) referred to the intrinsic material, and u_b is the value

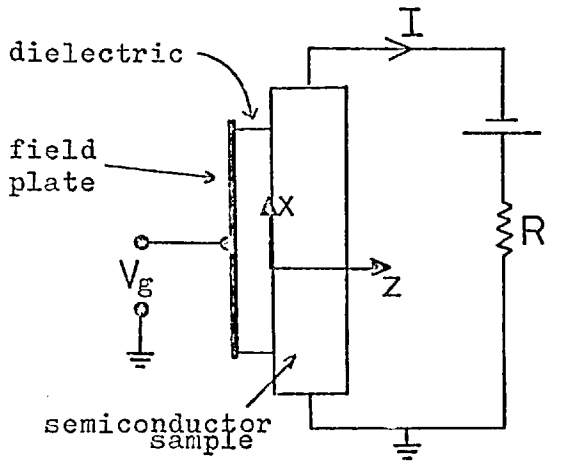

Fig. 6.1 Measurement of the field effect

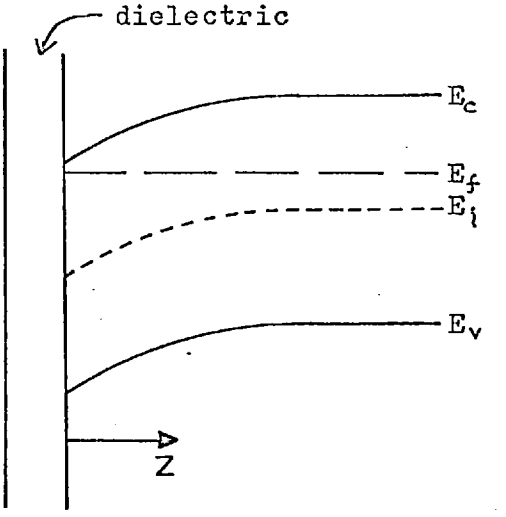

Fig. 6.2 Band bending at the surface of an n-type semiconductor

of u in the 'bulk' of the semiconductor, i.e. outside the space-charge region, when the bands are effectively flat. v is then the potential (in units of kT) measured with respect to the bulk. Since it is the energy of an electron which is measured upwards on a band diagram, a downward band bending (as in fig. 6.2) implies $v_s > 0$, where v_s is the value of v at the surface.

When there is an increase in majority carrier concentration with respect to the bulk value, the space-charge region is called an accumulation layer ; this is shown in figs. 6.3a and 6.3b . Where the majority carrier density is reduced but the minority carrier concentration remains less than the majority carrier density in the bulk, the space-charge region is termed a depletion layer. But if the bands are bent further, so that there is a layer where the minority carrier density exceeds the bulk majority carrier concentration, this region is known as an inversion layer (see figs. 6.3c and 6.3d)

The form of the potential variation with distance can be found by solving Poisson's equation :

$$\frac{d^2 V}{dz^2} = - \frac{\rho}{\kappa \epsilon_0} \qquad (6.3)$$

Fig.6.3 ACCUMULATION, DEPLETION AND INVERSION LAYERS for n- and p- type semiconductors

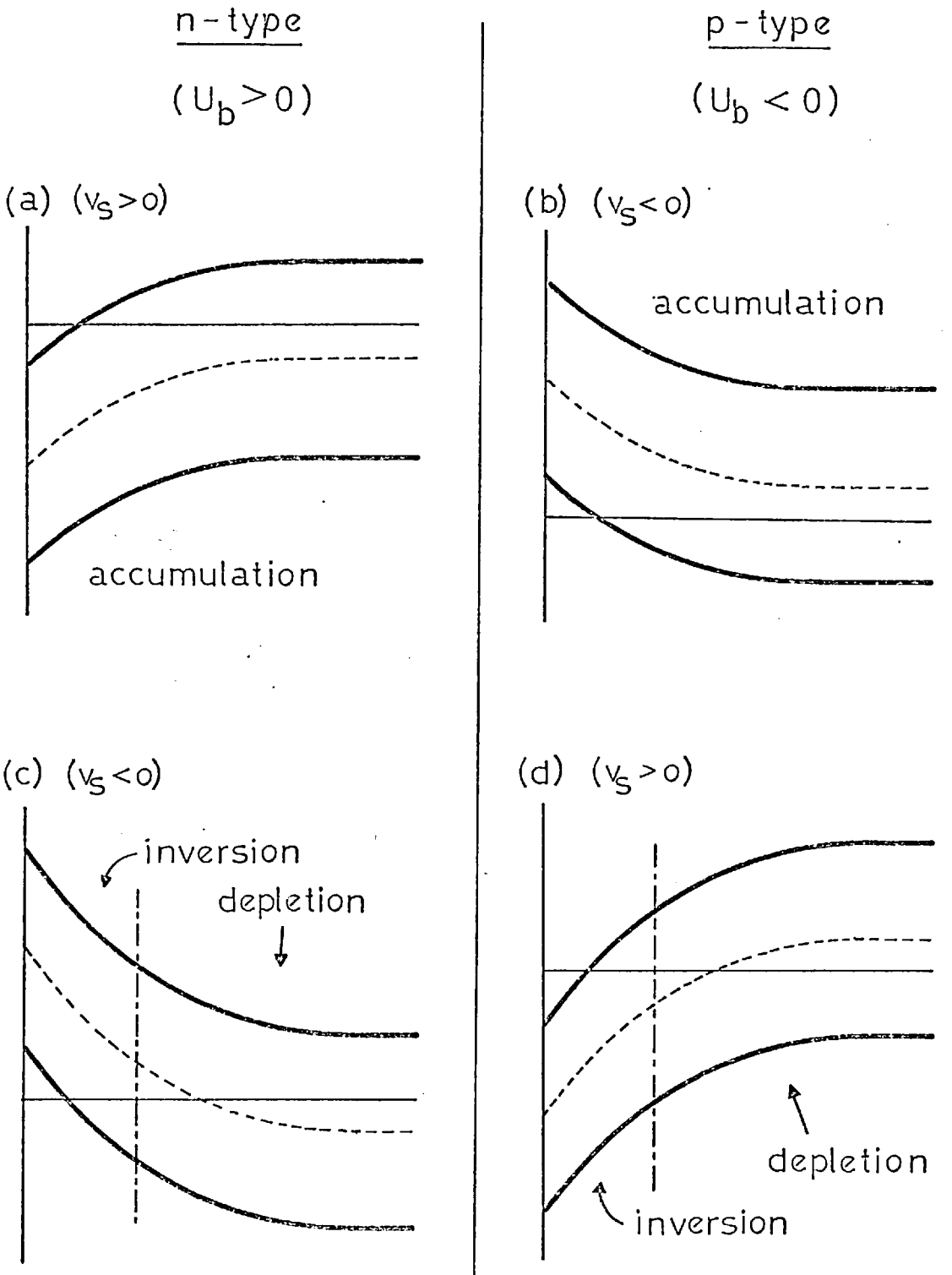

where V is the electrostatic potential

z is the distance from the semiconductor surface

and κ is the static relative permittivity

ρ is the space charge density, and is given by :

$$\rho = q (N_D^+ + p - N_A^- - n) \qquad (6.4)$$

Here, N_D^+ and N_A^- are the densities of ionized donor and acceptor impurities.

Schrieffer (S8) and Kingston and Neustadter (K6) solved equations (6.3) and (6.4) under two assumptions :

1) Complete ionization of impurities,

i.e. $N_D^+ = N_D = n_b$, $N_A^- = N_A = p_b$ (6.5)

where n_b and p_b are the bulk electron and hole densities

2) Carriers obey Boltzmann statistics. (B5) .

This allows n and p to be written :

$$n = n_i \exp(u) = n_b \exp(v) , \quad p = n_i \exp(-u) = p_b \exp(-v) \qquad (6.6)$$

where n_i is the intrinsic carrier concentration

Under these assumptions, (6.3) can be written (M5) :

$$\frac{d^2V}{dz^2} = \frac{1}{L^2} \left[\frac{\sinh (u_b + v)}{\cosh u_b} - \tanh u_b \right]$$

$$\text{where} \quad L = \left(\frac{\kappa \epsilon_o kT}{q^2 (n_b + p_b)} \right)^{\frac{1}{2}} \qquad (6.7)$$

is known as the Debye length, and is a measure of the space-charge penetration (under certain conditions) .

Integration gives $\frac{dv}{dz} = \frac{F}{L} = \frac{q}{kT} E \qquad (6.8)$

where E is the electrostatic field , and

$$F (u_b, v) = \pm \sqrt{2} \left[\frac{\cosh (u_b + v)}{\cosh u_b} - v \tanh u_b - 1 \right]^{\frac{1}{2}} \qquad (6.9)$$

The +ive sign applies for $v < 0$, and the -ive sign for $v > 0$

Applying Gauss's Law to the surface gives :

$$E_s = \frac{kT}{q} \cdot \frac{F_s}{L} = \frac{Q_{sc}}{\kappa \epsilon_o}$$

where E_s is the field just beneath the surface,
F_s is the value of the function F at the surface
and Q_{sc} is the total net charge (per unit surface area) in the space-charge region, and is therefore given by :

$$Q_{sc} = q\,(n_b + p_b)\,L\,F_s \qquad (6.10)$$

Further integration of (6.8) is possible only under special conditions (M5, p. 141).

It can be useful to define surface excesses of electrons and holes, ΔN and ΔP, with respect to the flat band condition :

$$\Delta N = \int_0^\infty (n - n_b)\,dz \quad , \quad \Delta P = \int_0^\infty (p - p_b)\,dz \qquad (6.11)$$

Using (6.6), these expressions can be re-written :

$$\Delta N = n_b L \int_{v_s}^{0} \frac{\exp(v) - 1}{F(u_b, v)}\,dv \quad , \quad \Delta P = p_b L \int_{v_s}^{0} \frac{\exp(-v) - 1}{F(u_b, v)} \qquad (6.12)$$

Except for an intrinsic semiconductor, the integrals in these expressions must be evaluated numerically ; they are termed G-functions and are given, together with values of the F-function, as a function of v_s by Many (M5, pp. 146-8, 154-5).

Seiwatz and Green (S9) also solved equations (6.3) and (6.4), allowing for partial ionization of impurities and using Fermi-Dirac statistics. Their F- function (defined by eqn. 6.8) differs from (6.9) whenever part of the semiconductor becomes degenerate.

Juhasz (J4) extended this treatment further to include non- parabolicity in one of the bands of the semiconductor. Brief details of his calculation are given in Appendix B.

The above treatments all neglect quantum effects, which become important when carriers are confined to a deep potential well at the surface. As the width of an accumulation or inversion layer is reduced, the momentum of carriers in the z-direction becomes quantized. The initial effect of this is to reduce the

average density of states in momentum-space, so there are fewer carriers in the space-charge region for a given surface potential. Conversely, the band bending is larger for a given space charge Q_{sc} which implies that the F-function is again modified. Greene (G6) has shown that this correction becomes significant when

$$E_s \sim 6 \times 10^4 \left(m_d/m_o\right)\left(\frac{T}{300}\right)^{3/2} \text{ volt cm}^{-1}$$

Applying this to PbTe, where $m_d/m_o \sim \frac{1}{4}$, $\kappa \sim 400$, gives

$$E_s \sim 1{\cdot}5 \quad 10^4 \text{ volt cm}^{-1}$$
$$Q_{sc} \sim 10^{12} \text{ charges / cm}^2 \quad \text{at room temperature}$$

This value of E_s can just be reached by applying an external field through a mica dielectric, assuming $\kappa = 6$ and a breakdown strength of 10^6 volt/cm for mica. The effect of quantization will be more important at low temperatures and for semiconductors with lower values of dielectric constant.

Quantization also lessens the degree of mobility reduction due to surface scattering (see Appendix C); for more severe band bending, however, the existing theories of surface transport break down. Carrier transport in inversion layers, including quantization, has been treated in detail by Stern and Howard (S27).

6.2 Surface states

In the previous discussion, it is not necessary to assume that the surface potential v_s is zero when there is no externally-applied field. In fact, in the majority of semiconductors which have been studied so far, there is spontaneous band bending at the free surface.

This was first recognised by Bardeen (B1), who attributed the effect to the existence of surface states. These have an effect which is similar to that of impurity states in the bulk, and were used to explain the rectification effects at a metal-semiconductor junction, which were found experimentally to be largely independent of the metal used.

Surface states had been previously predicted theoretically by Tamm (T1) and by Shockley (S14) ; these were localised states at an interface, with energies within the forbidden gap of the semiconductor. They owe their origin to the sudden termination of the crystal field, and can be thought of as being due to 'dangling bonds' at the surface.

By analogy with those in the bulk, states at the surface can become charged by trapping carriers ; this leads to band bending in the absence of applied field. Moreover, the amount of band bending produced by a given external field is reduced, as follows. Total neutrality of charge requires :

$$Q_g + Q_{sc} + Q_{ss} = 0 \qquad (6.13)$$

where Q_g is the charge applied to the gate, given by $Q_g = C V_g$
Q_{sc} is the charge in the space-charge region, given by (6.10)
and Q_{ss} is the charge which is trapped in surface states.
(6.13) can also be written :

$$Q_{sc} + Q_{ss} = Q_s$$

where $Q_s = -Q_g$ is the total charge carried by the semiconductor, per unit area of surface.

For a single energy E_t and density N_t of surface states (per unit area), Fermi-Dirac statistics give :

$$* \quad Q_{ss} = -N_t f(E_t) = -N_t \left(1 + \exp(E_t - E_f/kT) \right)^{-1} \qquad (6.14)$$

If $Q_g = 0$, $Q_{sc} = -Q_{ss}$ and in the presence of surface states, v_s is finite.
With an applied charge Q_g, Q_{sc} and Q_{ss} will both alter, but the change will be mainly in Q_{ss} if N_t is large. In this case, the induced charge goes mainly into the surface states and there is little change in surface potential.

---

* This neglects the change in degeneracy between an empty (g_o) and a full (g_1) energy level. This can be included by writing $Q_{ss} = -N_t f(E_t^f)$, where $E_t^f = E_t + kT \ln(g_o/g_1)$ (M5).
In this chapter, E_t is used to indicate the effective energy E_t^f.

Surface states of a given density N_t and energy $(E_t - E_f)$ with respect to the Fermi level are characterised by a time constant τ_{ss}, which is a measure of the time needed for Q_{ss} to reach a new equilibrium value when there is a small change in the applied field. States are referred to as fast or slow, depending on whether τ_{ss} is less or greater than about 10^{-2} seconds.

The theoretical calculations which have been carried out suggest that for an ideal surface, N_t should be approximately equal to the number of surface atoms, i.e. about 10^{15} /cm^2. So-called 'clean' surfaces of silicon and germanium have been prepared by cleaving or annealing samples in ultra-high vacuum (M5, Ch. 3) and are found to have fast states with densities of this order. These high values allow very little change in surface potential by means of an applied field.

On the other hand, 'real' surfaces, which have been etched or exposed to the atmosphere and are covered by an oxide, are generally found to have a lower density of fast states, possibly because the dangling bonds are absorbed by the oxide layer. However, they are usually found to have a high density of slow states which may be located within the oxide, giving time constants of seconds or hours.

6.3 Surface transport

If the bands at a semiconductor surface are bent by means of an external field, the conductance of the sample (for current flowing parallel to the surface) will be altered, due to the change in carrier densities within the space-charge region. This is known as conductivity modulation, and is the principle utilised in the field-effect transistor.

The average conductivity (σ) of the semiconductor, measured by passing a current between the ends of the sample as in fig. 6.1, is given (see Appendix A, eq$^{n.}$ A9) by:

$$\sigma t = \sigma_b t + \Delta\sigma \quad \text{for } t \gg L \qquad (6.15)$$

where σ_b is the conductivity of the bulk semiconductor,

t is the sample thickness (in the z-direction)

and $$\Delta\sigma = \int_0^\infty (\sigma - \sigma_b)\,dz \qquad (6.16)$$

is known as the surface conductance, and is effectively the sheet conductance of the space charge layer, since it is measured with respect to the flat-band condition. The dimensions of $\Delta\sigma$ are $(\text{Ohm})^{-1}$.

If the carriers within the space-charge region have the same mobility as those in the bulk, the surface conductance will be given by :

$$\Delta\sigma = q \int_0^\infty (p\mu_p + n\mu_n - p_b\mu_p - n_b\mu_n)\,dz$$

where μ_n and μ_p are the electron and hole mobilities.

From (6.11), $$\Delta\sigma = q(\mu_p \Delta P + \mu_n \Delta N) \qquad (6.17)$$

$\Delta\sigma$ can be calculated from (6.17) as a function of v_s (using eqns. 6.12) and as a function of Q_{sc} (using also eqn. 6.10) . The type of variation obtained for n- and p-type semiconductors is shown in fig. 6.4 . Since ΔN and ΔP have opposite signs for a given v_s, and the magnitudes vary in opposite directions, $\Delta\sigma$ goes through a minimum value. At this point, v_s is approximately $-2u_b$ (M5, p. 212); for $|v_s| > |2u_b|$, an inversion layer forms at the surface (when v_s and u_b are of opposite sign) .

The space-charge region will also cause a change in the Hall coefficient of the semiconductor, measured in the y-direction. The effective Hall coefficient R is given (Appendix A, eqn. A.10) by :

$$R\sigma^2 t = R_b \sigma_b^2 t + \Delta R\sigma^2 \qquad \text{for } t \gg L$$

where R_b is the Hall coefficient of the bulk semiconductor and $\Delta R\sigma^2$ is defined by

$$\Delta R\sigma^2 = \int_0^\infty (R\sigma^2 - R_b\sigma_b^2)\,dz \qquad (6.18)$$

$$= q \int_0^\infty (p\mu_p^2 - n\mu_n^2 - p_b\mu_p^2 + n_b\mu_n^2)\,dz$$

$$= q\left[\mu_p^2 \Delta P - \mu_n^2 \Delta N\right] \qquad (6.19)$$

again assuming that carriers in the space-charge region have bulk values of mobility.

Figure 6.4 CONDUCTIVITY MODULATION CURVES

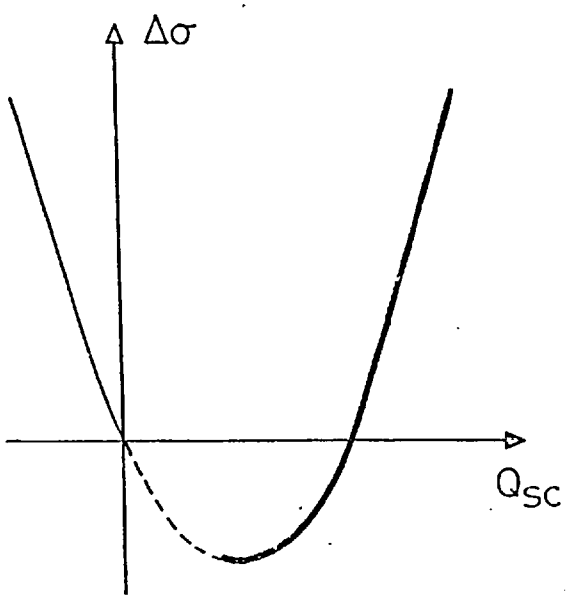

(a) n-type semiconductor

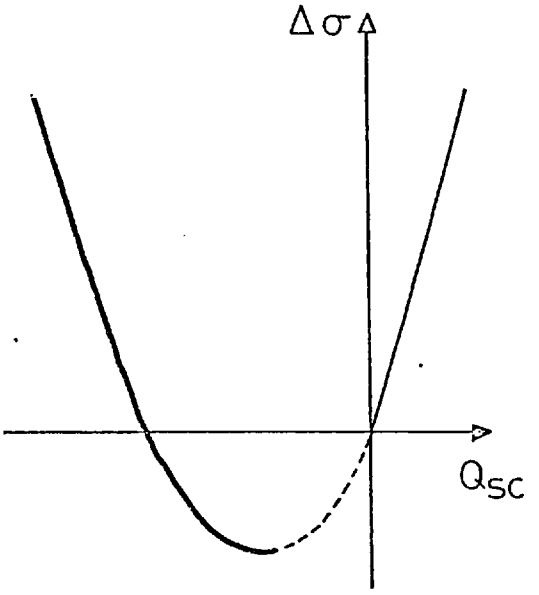

(b) p-type semiconductor

——— accumulation layer

---------- depletion layer up to the surface

▬▬▬ inversion and depletion layers present

However, carriers which collide with the surface may have part of their drift momentum destroyed (see appendix C). Carriers whose distance from the surface is comparable with their mean free path will then have a lower effective mobility. This surface scattering can be taken into account by defining surface mobilities μ_{ns} and μ_{ps} for electrons and holes by means of the equations :

$$\Delta\sigma = q (\mu_{ps} \Delta P + \mu_{ns} \Delta N) \qquad (6.20)$$

$$\Delta R\sigma^{-2} = q (\mu_{ps}^{2} \Delta P + \mu_{ns}^{2} \Delta N) \qquad (6.21)$$

μ_{ns} and μ_{ps} have been calculated as a function of v_s (see appendix C).

Although surface scattering affects all carriers which are sufficiently near to the surface, the surface mobilities are averages over excess carriers alone. Because of this, μ_{ns} and μ_{ps} become negative in the limit of small band bending.

If the drift momentum of a carrier is completely destroyed upon collision with the surface, the latter is described as completely diffuse. But if drift momentum parallel to the surface is conserved, the surface is said to be specular ; for semiconductors with isotropic energy surfaces, this implies zero mobility reduction.

Field-effect mobility

A quantity which is useful experimentally is the field-effect mobility, defined by

$$\mu_{fe} = - \frac{d(\Delta\sigma)}{d Q_g} = \frac{d(\Delta\sigma)}{d Q_s} \qquad (6.22)$$

This is the gradient of the conductivity modulation curve (fig 6.4) and is measured by means of a small a.c. signal applied to the field plate. It has dimensions of mobility (e.g. cm^2 $volt^{-1}sec^{-1}$) and incorporates the combined effedts of surface states and surface scattering. In the absence of surface states, $\mu_{fe} = \mu_{ps}$ or μ_{ns} for a p-type or n-type semiconductor surface respectively, provided that the surface conductance is sufficiently far from the minimum (fig. 6.4). If surface states are present, μ_{fe} is

frequency-dependent and is a complex quantity, since Q_g and may be out of phase.

6.4 Experimental methods

The aim of surface measurements on semiconductors is to obtain information about the surface scattering (i.e. degree of specularity) or the surface-state parameters (density, energy, time constant, capture cross-sections) or both. To achieve this, some means of varying the surface potential is required. Various methods have been used, mainly in connection with silicon and germanium surfaces (M5, F3). The methods which are of particular relevance to the present work are discussed below.

a) Gaseous ambients

Ambients such as oxygen, ozone and water vapour have been used to change the surface potential of Germanium. This method can be used in conjunction with the normal field effect, to cover a larger range of v_s. However, there is always the possibility that the surface state structure is modified by the different gases used.

The measurements described in section 5.4 could be considered in this category if the possibility of oxygen diffusion did not exist.

b) Large-signal field effect

This is usually carried out by applying an a.c. signal to a field plate near the surface, the frequency being sufficiently low so that the period of the waveform is much greater than the time constant of the surface states being investigated. The conductivity modulation is normally measured by passing a d.c. current through the sample, as in fig. 6.1 .

The aim is to produce an inversion layer at the semiconductor surface i.e. to reach the minimum in $\Delta\sigma$; only then can the surface potential be indexed. The magnitude of the external field which must be applied to obtain inversion increases with the

carrier concentration and dielectric constant of the semiconductor. The lead salts (particularly PbTe) all have large permittivities, and the carrier concentrations tend to be high. The large signal method is therefore considerably more difficult in these materials than for silicon or germanium.

The following calculation gives an estimate of the carrier concentration needed to obtain inversion in PbTe . The maximum electric field which can be applied to the surface is limited by the breakdown strength of the dielectric. For a good material such as mica, this is about 10^6 volt/cm (in the experiments described in section 6.5 , reversible breakdown effects occurred , which limited the field to about $6 \quad 10^5$ volt/cm) . With a relative permittivity $\kappa = 6$ for mica, the maximum surface charge density is 3×10^{12} charges / cm^2 .
If there are few surface states, so that $Q_s \doteqdot Q_{sc}$, the band bending produced at the semiconductor surface is :

$$\Delta v_s \doteqdot \Delta Q_{sc} \Big/ \frac{dQ_{sc}}{dv_s}$$

A typical value for $\frac{dQ_{sc}}{dv_s}$ in PbTe is -7×10^{11} cm^{-2}
(for $n_b \sim 10^{17}$ cm^{-3})

This gives $\Delta v_s \doteqdot 4$,
i.e. $4kT$ of band bending .

Making the (arbitary) assumption that the bands are flat with no applied field, the band bending required to reach the conductivity minimum is $\Delta v_s \doteqdot -2 u_b$

Assuming Boltzmann statistics, $n = n_i \exp(u_b)$
$p = n_i \exp(-u_b)$ from (6.6)

and the minimum value of n or p for inversion is :

$$n_i \exp(2) = 7 n_i = \underline{10^{17} \ cm^{-3}}$$

This value will be lower still if there is an appreciable density of surface states (section 6.2) .

This is a considerable restriction, since the majority of evaporated samples (soon after preparation) had carrier densities

higher than 10^{17} cm^{-3}. Where the carrier concentration was lower, this was usually due to the effect of oxygen (e.g. after storing n-type PbTe samples in air) and these films almost certainly contained impurity gradients (see chapter 5). Since Hall measurements give a value of the carrier concentration which is averaged over the thickness of the film (provided only one type of carrier is present; see appendix A) whereas the concentration relevant to the field effect is the value near to the surface being investigated, the value obtained from the Hall coefficient will be misleading when doping gradients are present. If p- and n-type layers exist within the film, this will give compensation of Hall voltages and the carrier mobility obtained from Hall measurements will also be inaccurate. Because values of mobility and carrier concentration are required in the field effect calculations, the results will be of doubtful validity under these conditions.

c) Small-signal field effect

For the present films, this has considerable practical advantages. Samples with larger carrier concentrations can be used (provided that the conductivity modulation is large enough to be measured) and carrier concentration gradients are less serious.

The field-effect mobility can be measured using small a.c. voltages or voltage pulses applied to the gate, but to obtain significant information about the surface states, it is necessary to make measurements as a function of several parameters such as frequency, temperature, and surface potential (varied by some other means).

The conductivity modulation is normally measured by passing a d.c. current through the sample, although an a.c. current of the same or of a different frequency to the gate signal can be used, employing a galvanometer or a wave analyser as the detector. These last two methods were tried on a number of the present films, but gave unreliable results at high frequencies.

d) Differential capacitance method

In this method, the differential surface capacitance, defined by :

$$C_s = \frac{-1}{kT} \cdot \frac{dQ_s}{dv_s}$$

is measured as a function of v_s. This is done by using a small gate signal of high frequency (where the period of the waveform is assumed to be small compared to the surface-state time constants) and the surface potential is varied by means of an a.c. signal of large amplitude and low frequency.

An advantage of this technique is that it does not involve the surface mobility ; the surface states can therefore be examined without making assumptions about the surface scattering. However, measurement is only practicable when the capacitance of the dielectric is comparable with or larger than C_s. This means that a very thin dielectric must be employed, which is not feasible using mica. The method has been applied successfully to polycrystalline films of PbTe and InSb by Lile (L8), using anodised aluminium layers less than 200 A° thick for the dielectric. It is also a convenient technique for the routine characterisation of silicon and germanium surfaces.

6.5 Large-signal measurements

a) Sample

The type of field-effect sample employed is shown in fig. 6.5 . The normal Hall sample shape (fig. 4.1) was used for the semiconductor, but the mica substrate was cleaved down to between 5 and 15 microns thickness and a field plate of copper or nickel evaporated on to the back of the mica. The capacitance between the field plate and the semiconductor could be measured accurately using a (Wayne-Kerr) capacitance bridge. The sample dimensions were measured by means of a travelling microscope.

b) Measuring circuit.

The basic circuit used for both large- and small-signal field-effect measurements is shown in fig. 6.6 . A constant d.c. current (typically 100 μA) was supplied from a battery and passed between the ends of the sample (contacts 1 and 4) via resistors R_1 and R_2 . An a.c. voltage (up to 2 kV) was applied to the field plate and to the input of a (Tektronix 536) oscilloscope. The conductivity modulation was measured as a voltage between contacts 2 and 3 of the Hall sample, and applied to a differential Y-input of the oscilloscope. If required, the Hall voltage between contacts 2 and 5 could be measured in a similar way, with the sample in a magnetic field.

The circuit could be balanced so that the displacement current induced through the field plate had no effect on the Y-deflection of the oscilloscope. This was achieved by adjusting the resistors R_1 and R_2 until the oscilloscope trace was a horizontal line with the battery disconnected. Two small capacitors C_1 and C_2 could also be adjusted to correct for any stray capacity.

c) Method of analysis

Having obtained a suitable sample, in which an inversion layer could be induced at the semiconductor surface, the trace of conductivity voltage V_σ against field-plate (gate) voltage V_g

Fig. 6.5 Field - effect sample

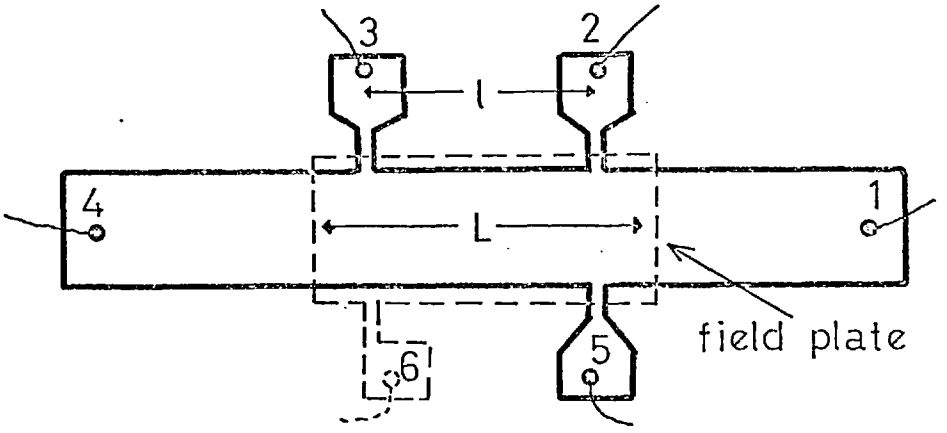

Fig. 6.6 Circuit for field-effect measurements

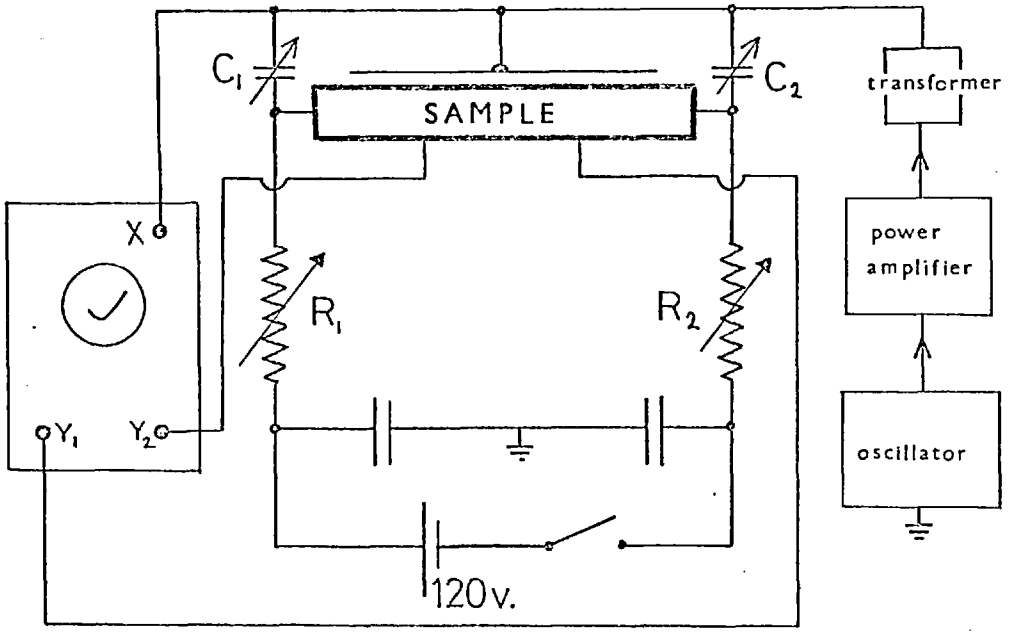

was photographed from the oscilloscope screen. The total applied charge Q_s per unit area, and the parameter $\Delta\sigma'$, which is the surface conductance relative to the $V_g = 0$ condition, can then be calculated from the equations :

$$Q_s = -Q_g = -C_g V_g \qquad (6.23)$$

$$\Delta\sigma' = \frac{1}{w} I \times \left[\frac{1}{V_\sigma} - \frac{1}{V_\sigma^\circ}\right] \qquad (6.24)$$

where C_g is the gate capacitance per unit area and V_σ° is the value of V_σ at $V_g = 0$.
$\Delta\sigma'$ is related to the surface conductance $\Delta\sigma$ by :

$$\Delta\sigma = \Delta\sigma' + \Delta\sigma^\circ$$

where $\Delta\sigma^\circ$ is the surface conductance at $V_g = 0$.

The mobility and carrier concentration of the sample can be obtained from Hall measurements in the absence of field applied to the surface, on the assumption that $\Delta\sigma^\circ \ll \sigma_b t$ i.e. that the measured conductance is mainly due to the bulk of the film rather than the space-charge region. This is justified for large sample thickness or small intrinsic band bending. Using these values, a theoretical curve of $\Delta\sigma$ against Q_{sc} may be calculated (for a range of v_s) as described in section 6.3 . In the present case, this was done using the computer program outlined in appendix B . If required, the reduction in surface mobility due to diffuse scattering can be incorporated into this calculation.

The experimental $\Delta\sigma'$ v. Q_s curve and the theoretical $\Delta\sigma$ v. Q_{sc} curve will be of different shape, since the former includes the effect of surface states and the latter does not. However, the conductance minima in both cases correspond to the same surface potential ($v_s = -2u_b$) and the same surface conductance . The two curves can therefore be superimposed, with their minima at the same vertical co-ordinate, as shown in fig. 6.7 . Points with the same ordinate then correspond to the same surface potential, and the difference in horizontal co-ordinate between the two curves is the charge $Q_{ss} = Q_s - Q_{sc}$ in surface states at this particular value of surface potential.

Figure 6.7 Large-signal A.C. field effect analysis

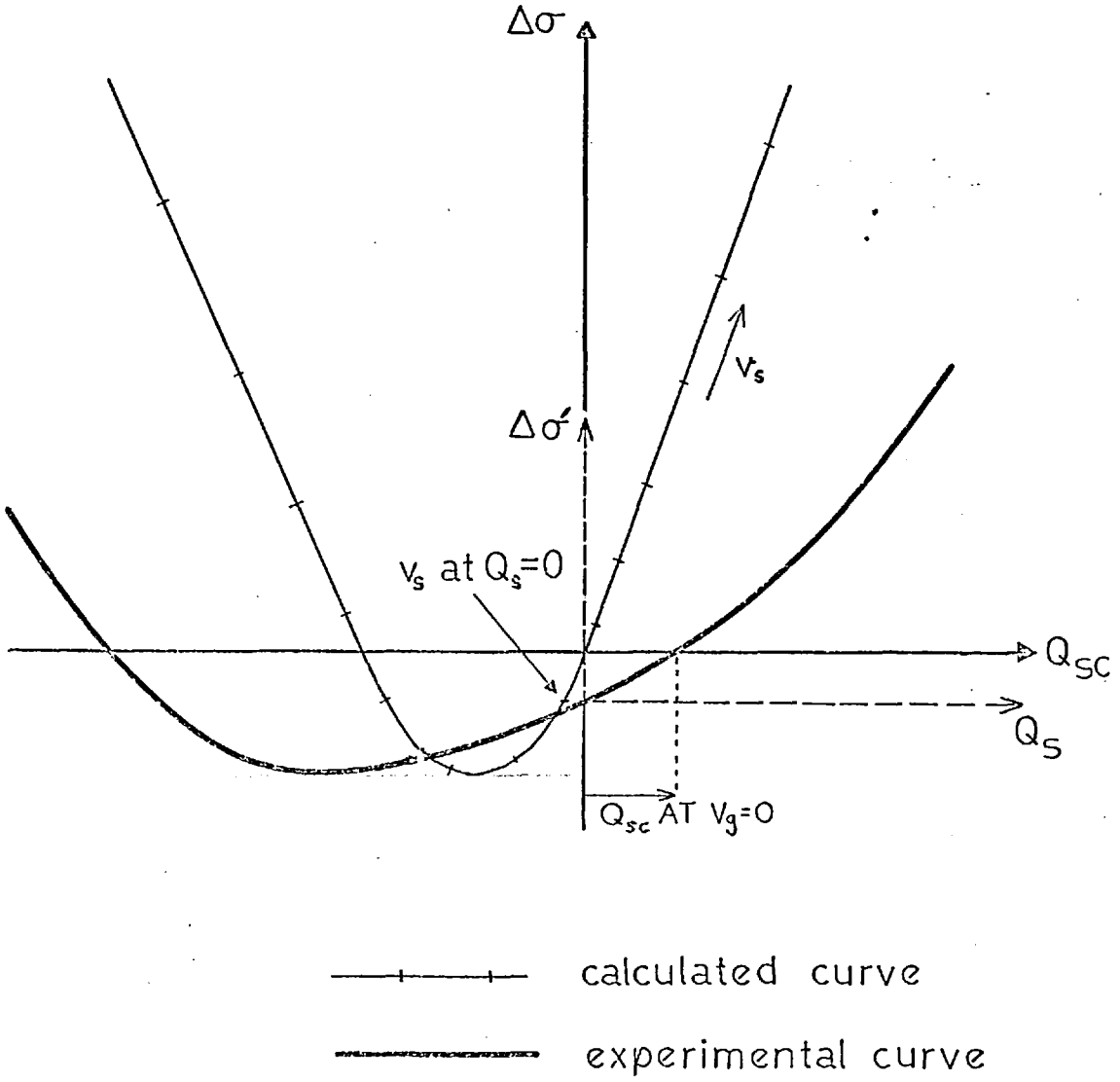

By subtracting the two curves in this manner, the trapped charge Q_{ss} can be plotted against surface potential v_s. If the range of v_s is sufficient, the resulting curve can be fitted with one or more Fermi functions (equation 6.14). The values of N_t and E_t which give the best fit to the experimental points are then taken to be the required surface-state parameters.

d) Results

The experimentally-derived curve of $\Delta\sigma'$ against Q_s for a PbTe film on mica is shown in fig. 6.8 . This sample had an n-type doping ($n_b - p_b$) of 9×10^{15} cm^{-3} and a room-temperature Hall mobility of 615 $cm^2/v.s$.

The calculated curve of $\Delta\sigma$ against Q_{sc} , assuming no mobility reduction due to surface scattering, is shown in fig. 6.9 . The case of perfectly diffuse scattering at the surface (calculated from the results of Greene, Frankl and Zemel ; see appendix C) is also shown (dotted) . However, there is little difference in shape between the two curves.

Values for the specular case have been subtracted from the experimental curve (as described in the previous section) to give the graph of surface state charge against surface potential shown in fig. 6.10. This is virtually a straight line, with a slope of 5×10^{11} charges cm^{-2} $(kT)^{-1}$.

Figure 6.8 also shows the experimental Hall coefficient as a function of gate charge. R_H/t (where t is the film thickness) reaches a maximum, corresponding to the minimum in $\Delta\sigma'$.

6.6 Small-signal measurements

The same measuring circuit (fig. 6.6) was used, the gate voltage being kept down to a level where the percentage conductivity modulation was small. The field effect mobility is then given by :

$$\mu_{fe} = \frac{I}{\Delta V_g} \frac{\Delta V_\sigma}{(V_\sigma^\circ)^2} \frac{1\,L}{C_i} \qquad (6.25)$$

Figure 6.8 Measured field effect for PbTe (sample 2) at room temperature (frequency = 70 Hz)

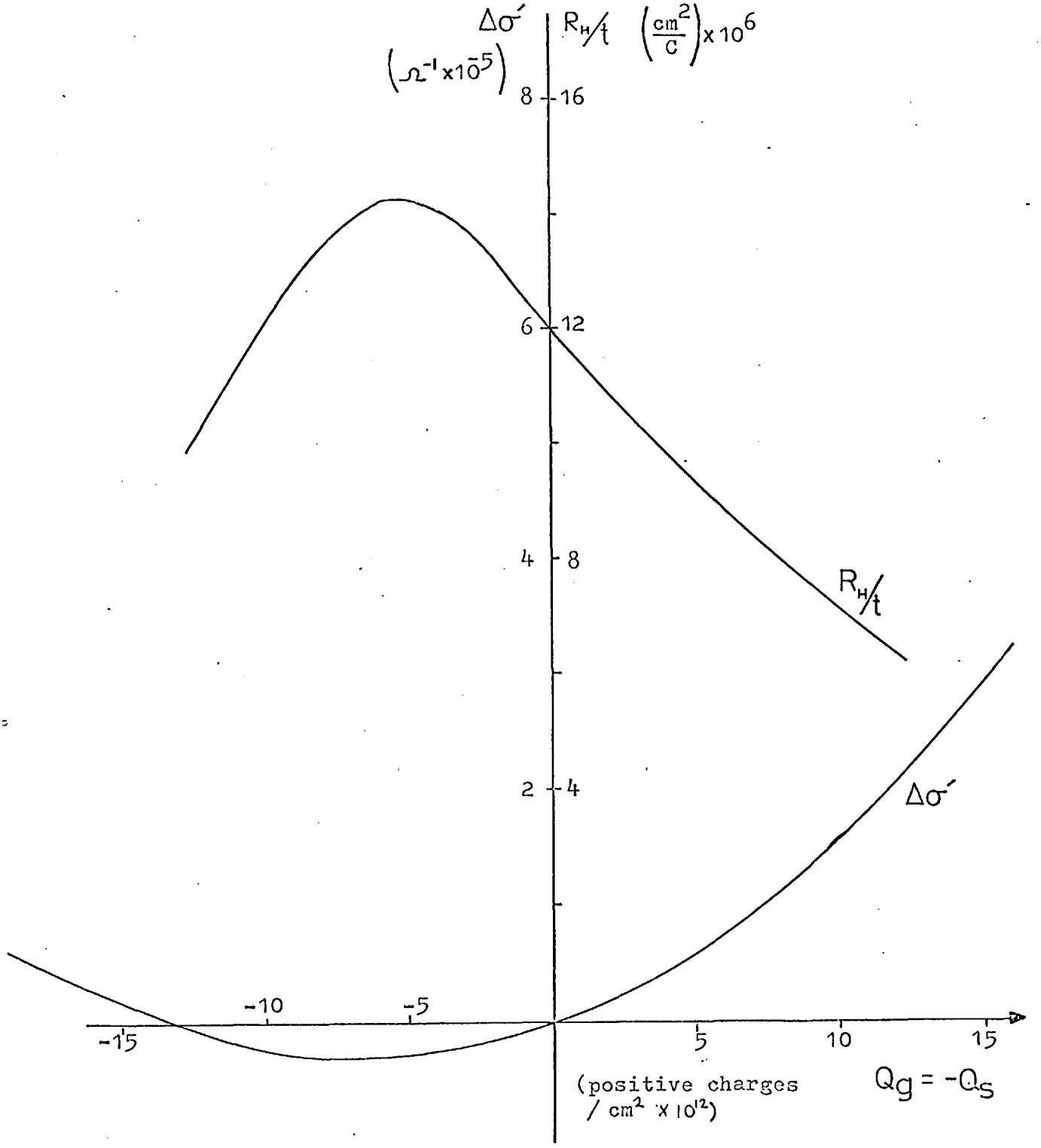

Figure 6.9 Calculated surface concuctance against surface space charge density for PbTe sample 2.

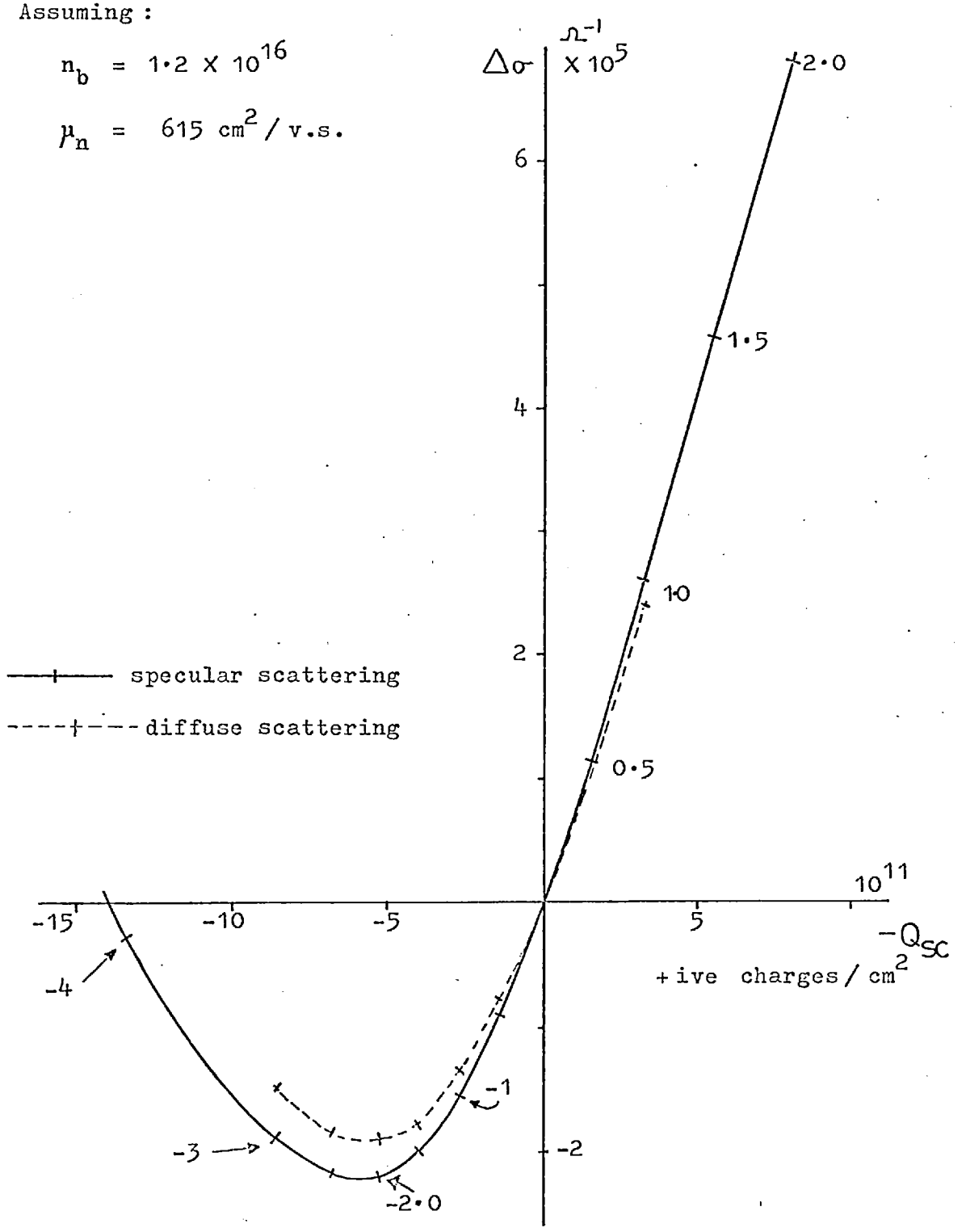

Figure 6 . 10 Charge in surface states, as a function of surface potential for PbTe sample 2 .

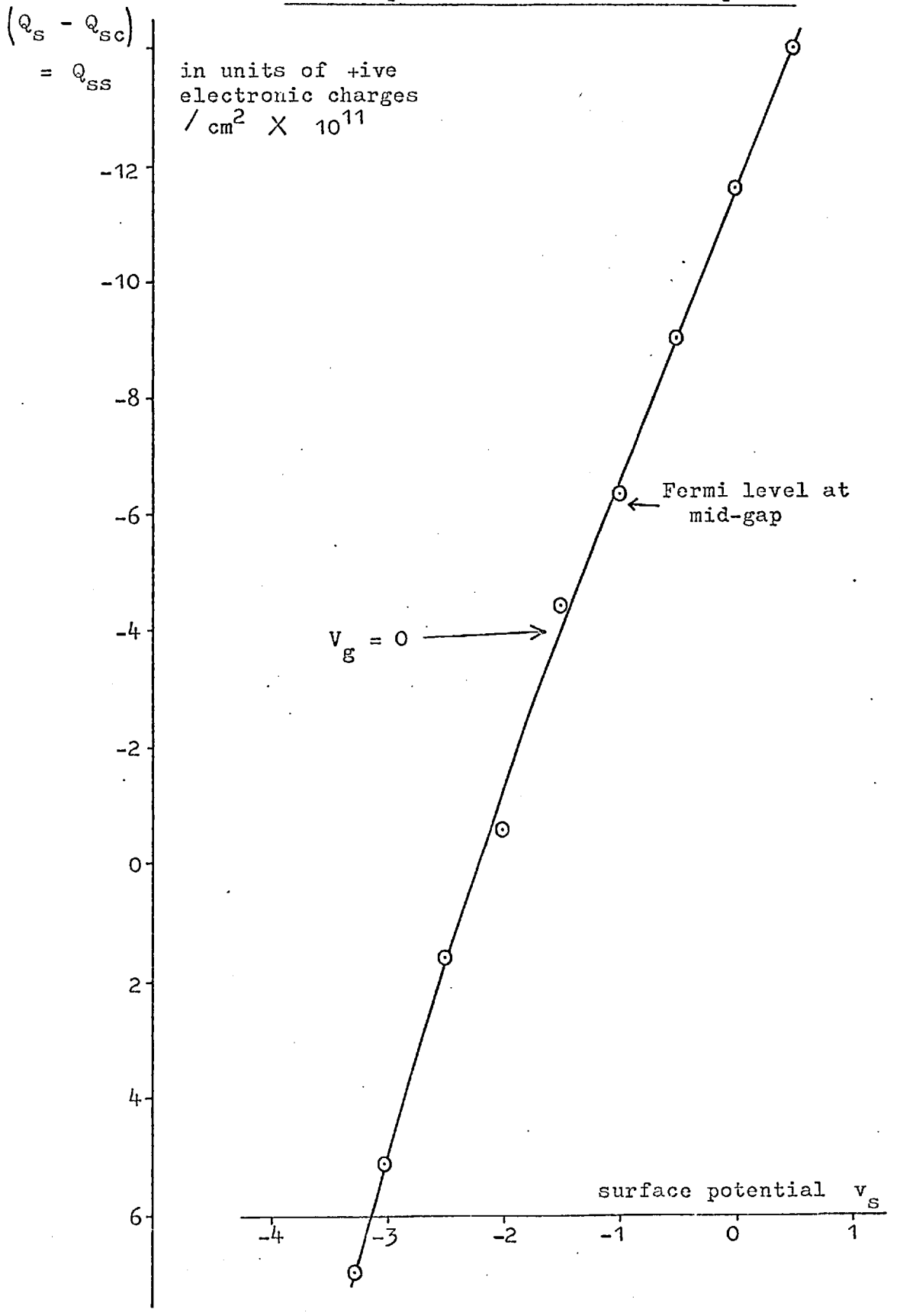

(from equations 6.22 and 6.24)

where I is the current flowing through the sample

ΔV_g is the gate voltage modulation (peak-to-peak)

ΔV_σ is the conductivity voltage modulation (p-p)

V_σ° is the conductivity voltage with $V_g = 0$

C_t is the total gate capacitance

and l, L are the sample dimensions shown in fig. 6.5

a) Field-effect mobilities

Table [6.1] shows values of μ_{fe} for a number of PbTe samples at room temperature, obtained using a measuring frequency of between 30 Hz and 100 Hz with a Hall sample configuration (fig. 6.5). Hall mobilities and carrier concentrations are also given; where these are thought to be misleading due to compensation effects (section 4.5g), the values are shown in brackets. Ignoring these cases, μ_{fe} is normally between 50% and 90% of μ_H, which reflects a reasonably low effective density of surface states.

Table 6.1 Field-effect mobilities for PbTe films on mica

(at room temperature)

SAMPLE	TYPE	CARRIER CONCENTRATION	μ_H	μ_{fe}
A 11	n	7×10^{17}	910	-790
A 14 b	n	1×10^{18}	1100	-670
A 15	n	3×10^{17}	740	-430
A 13 a	p	$1{\cdot}2 \times 10^{17}$	315	260
A 18	p	$(2{\cdot}5 \times 10^{16})$	(450)	650
A 43 a	p	(4×10^{16})	(150)	180
A 50 a	p	$1{\cdot}7 \times 10^{17}$	310	200
		cm^{-3}	$cm^2\ volt^{-1}\ sec^{-1}$	

Figure 6.11 Hall mobility and field-effect mobility as a function of temperature for PbSe sample B 11 a

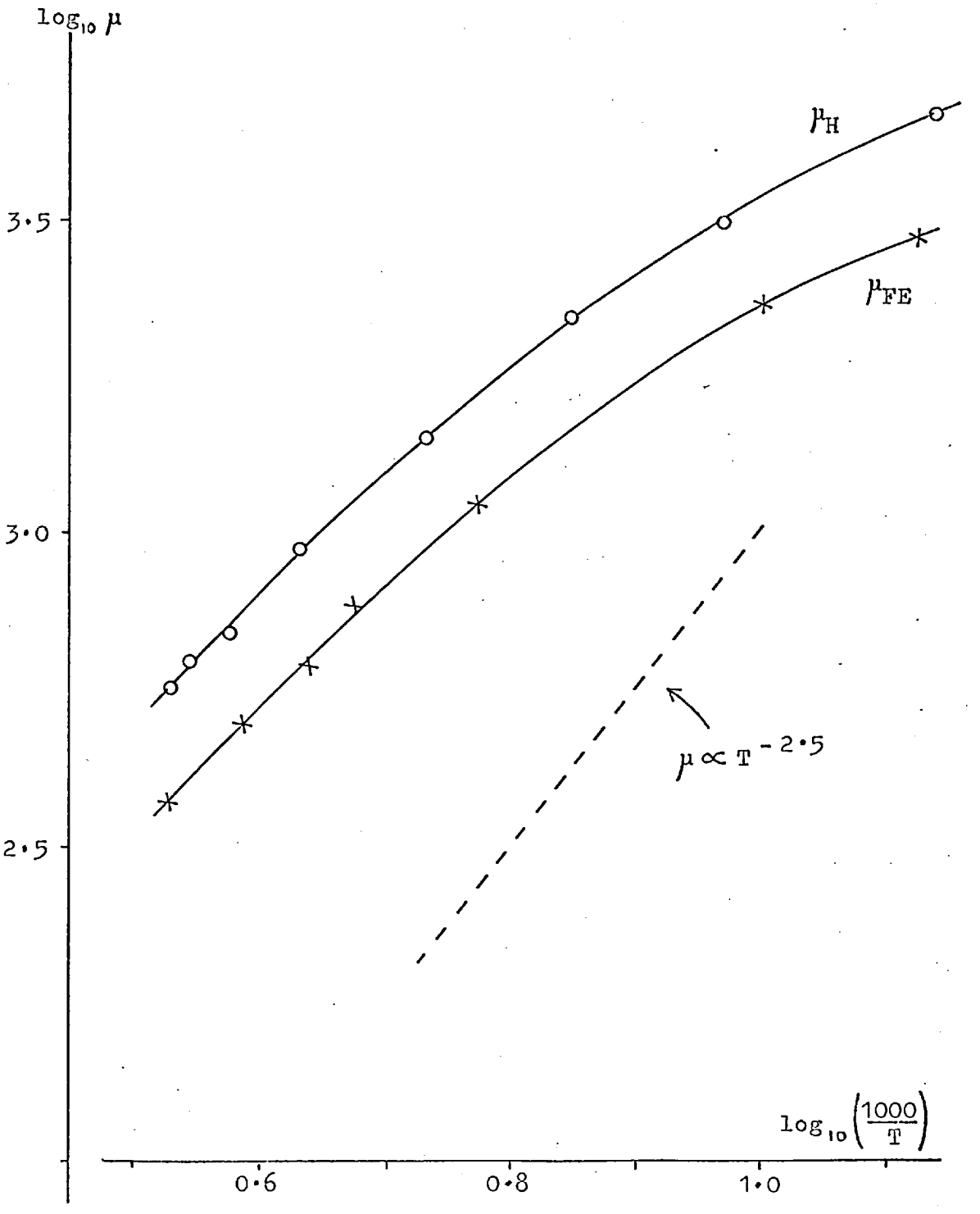

Figure 6.12 Hall and field-effect mobilities as a function of temperature

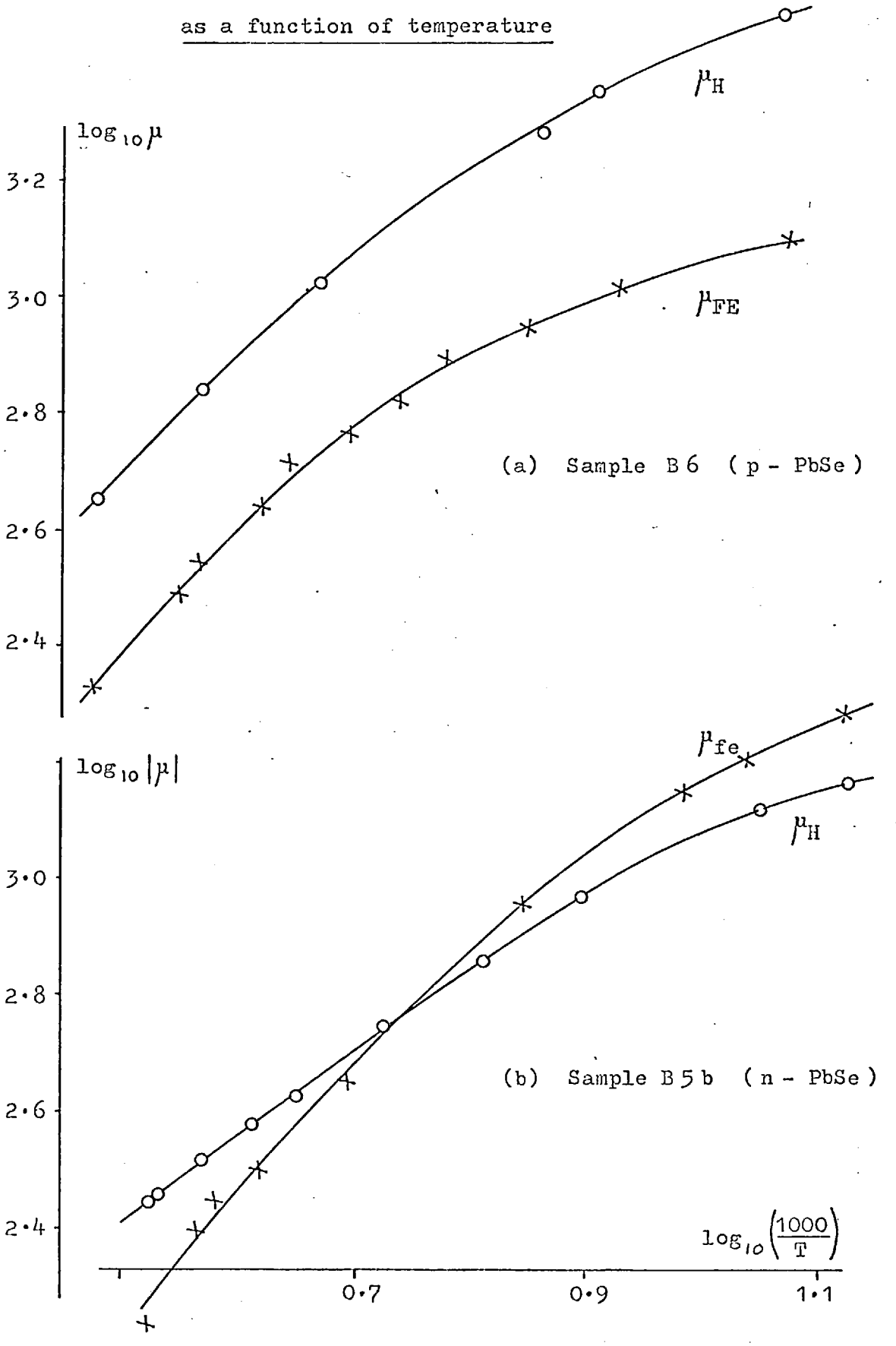

6.6 b Variation with temperature

Figure 6.11 shows μ_{fe} and μ_H for a p-type PbSe sample (B11a) plotted as a function of temperature between 77°K and 300°K . The ratio of these two mobilities is approximately independent of temperature, with $\mu_{fe}/\mu_H \doteqdot \frac{2}{3}$

Similar measurements on two other PbSe samples are given in fig. 6.12 . In the case of (B6) (p-type) , μ_{fe} increases less rapidly with (1/T) than μ_H , especially at low temperatures, whereas for sample (B5b) (n-type) the curves cross over, with $\mu_{fe} > \mu_H$ near 77°K .

These samples were coated with an evaporated layer of Si O and annealed in air to try to remove possible impurity gradients.

The change in Hall voltage with applied electric field was also measured for sample (B11a) at room temperature. The magnetic field (5·5 Kgauss) was supplied by an electro-magnet, and the change in Hall coefficient and $\Delta\sigma$ were both linear with gate voltage . Assuming that only one type of carrier is present at the surface , i.e. $\Delta P \gg \Delta N$, the surface Hall mobility for holes is given by :

$$\mu_{Hps} = \frac{d\,\Delta R\sigma^2}{d\,\Delta\sigma} = \quad 600 \quad cm^2/v.s. \quad \text{for sample (B11a).}$$

(from eqns. 6.20 , 6.21)

6.6 c Variation with frequency

To enable μ_{fe} to be measured up to higher frequencies, the dimensions of the sample were reduced to those shown in fig. 6.13 . This provides a small length of semiconductor ('source-drain gap' in transistor terminology) , which reduces the time constant of the gate equivalent circuit. This narrow channel length was produced by evaporating nickel or aluminium past a $2\frac{1}{2}$ thou-diameter nickel wire held close to the semiconductor surface. The mica substrate was cleaved down to about 10 micron thickness, and a gate electrode soldered on to the back, using

Figure 6.13 Sample for high-frequency field-effect measurements

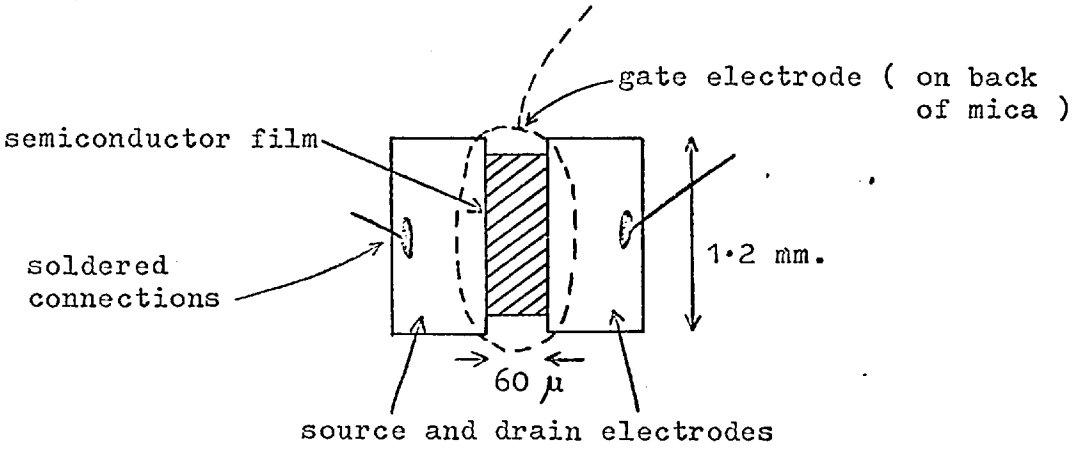

Figure 6.14 Measurement of field-effect mobility and phase angle

$$\mu_{fe} = \mu_{fe}' + i\mu_{fe}'' = \left|\mu_{fe}\right| \exp(i\theta) \quad , \quad i = \sqrt{-1}$$

$\sin\theta = \frac{\delta V_\sigma}{\Delta V_\sigma}$; μ_{fe} is given by equation (6.25) with $l = L = 60\mu$, provided that contact resistance is small.

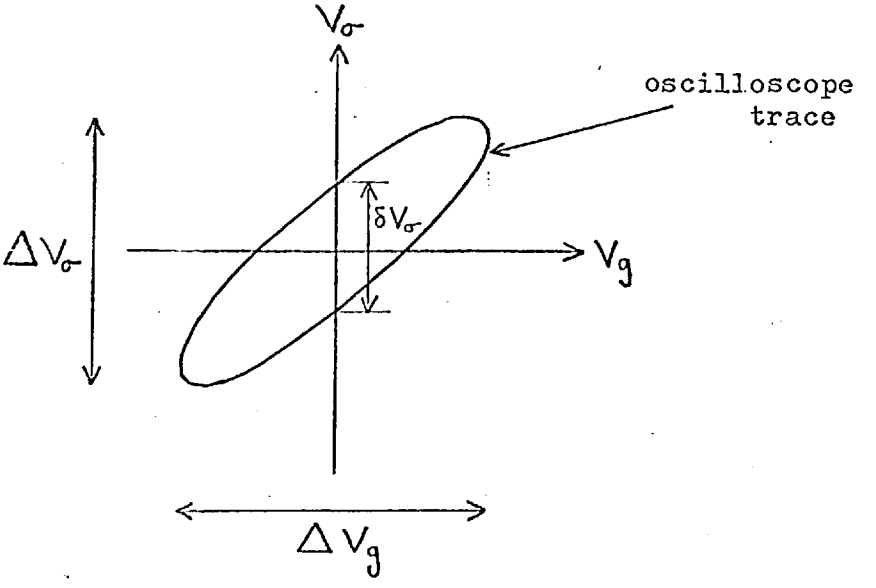

6.6 c

In / Bi alloy .

The field-effect circuit (fig. 6.6) was modified slightly to enable it to function up to higher frequencies. Resistors R_1 and R_2 were changed to 2 K values, and the battery to 9 volts. The input impedances of the differential inputs to the oscilloscope were equalised. The power amplifier and transformer were replaced by a generator giving about 100 volt R.M.S. between 30 Hz and 100 K Hz .

By adjusting R_1 and R_2 , the circuit was balanced so that the trace on the oscilloscope screen was horizontal and linear at 100 K Hz , with no current flowing through the sample. With a sample current of about 2 mA , the real part μ'_{fe} and the phase angle θ of the field effect mobility could be measured from the oscilloscope trace, as shown in fig. 6.14 .

Figures 6.15 and 6.16 show results obtained with p-type PbSe samples (T 1) and (T 2) at room temperature. μ'_{fe} increases with frequency over the range 100 Hz to 10 K Hz , the 'centre frequency' f_1 being about 1·5 K Hz . The same sort of behaviour was observed for an n-type PbTe sample (T 3) (fig. 6.17) .

The rise in μ'_{fe} at higher frequencies is due to a decreasing amount of charge entering surface states, as the period of the applied signal becomes less than the time needed for charge trapping to take place.

6.6 d Pulsed field effect

By applying voltage pulses to the gate, it is possible to obtain values for the surface state time constant τ_{ss} and the fraction α of charge which enters the surface states.

The same kind of sample (fig. 6.13) was employed, and the same circuit (fig. 6.6) except that the gate signal was supplied by a square-wave generator , which gave output voltages up to 100 v. R.M.S. .

Figure 6.15 Field-effect mobility and phase angle as a function of frequency, for sample T 1 (p - PbSe)

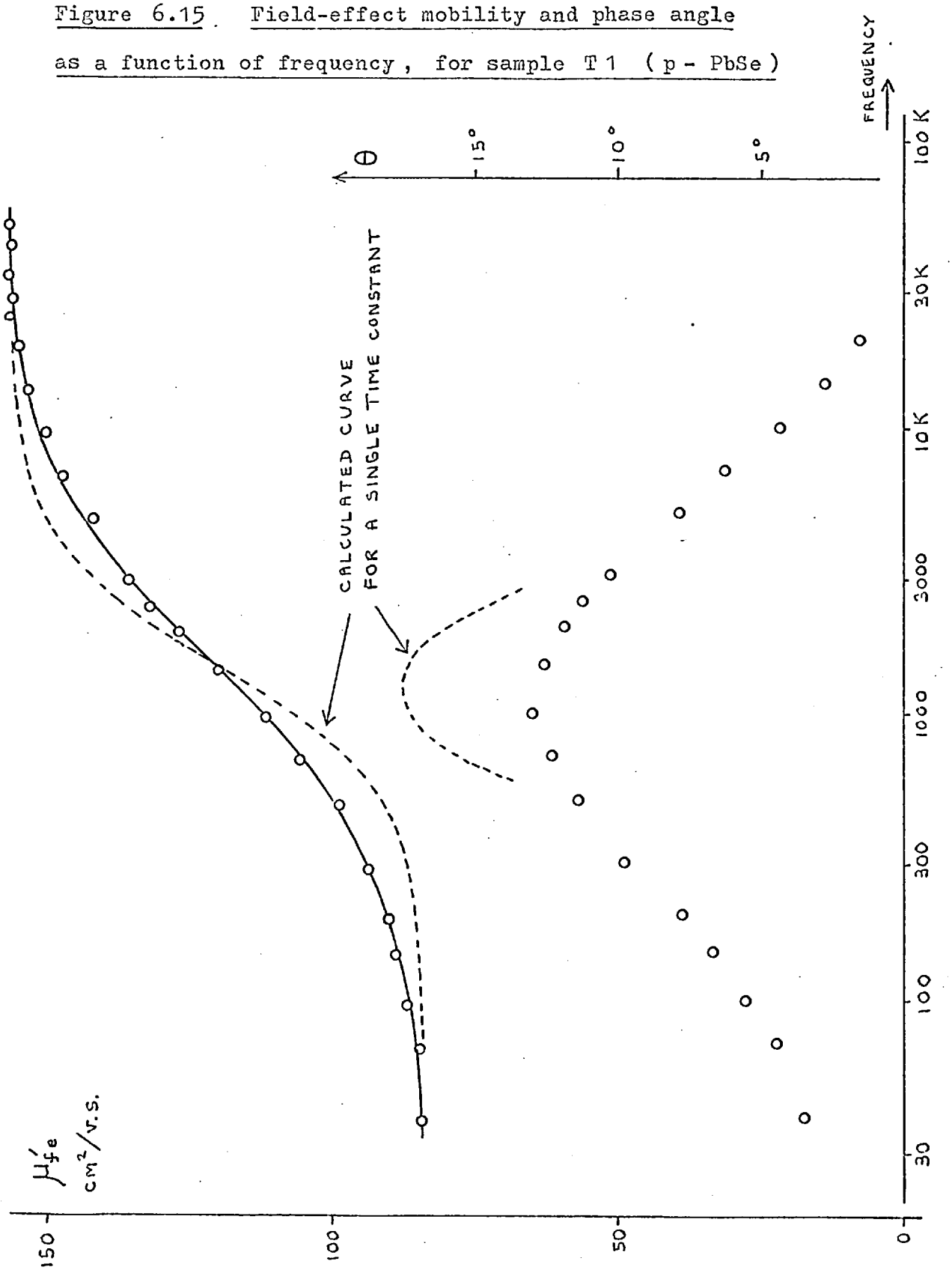

Fig. 6.16 μ_{fe}' and θ against frequency for sample T 2 (p-PbSe)

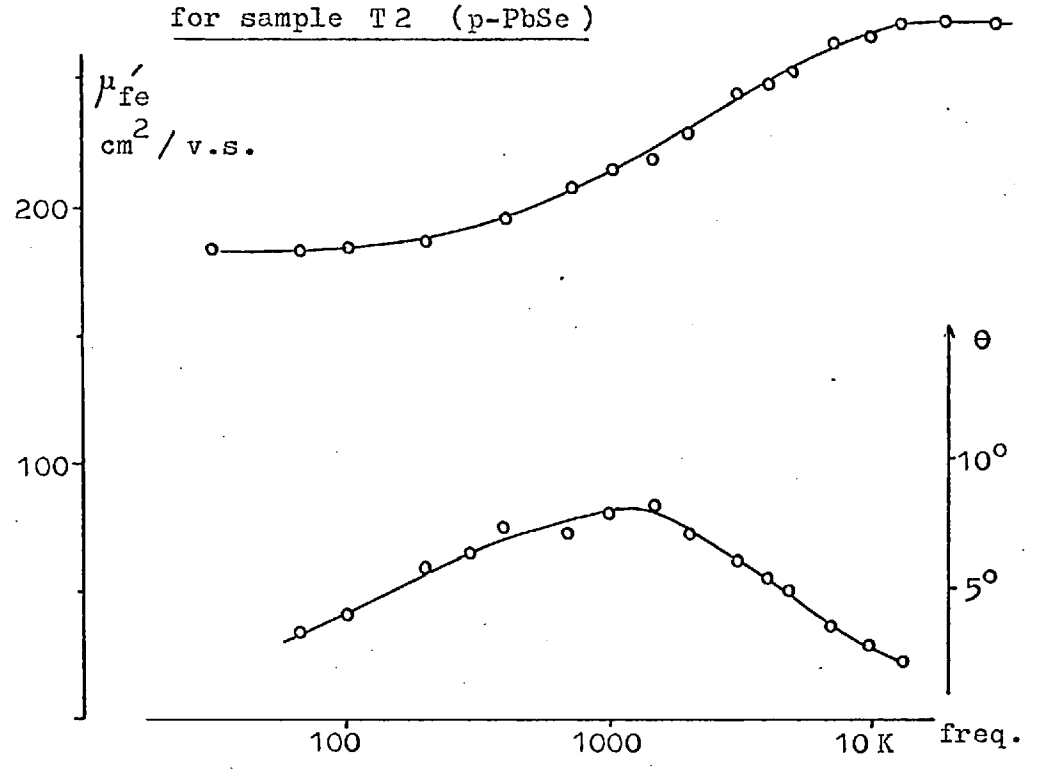

Fig. 6.17 μ_{fe}' and θ against frequency for sample T 3 (n-PbTe) at room temperature

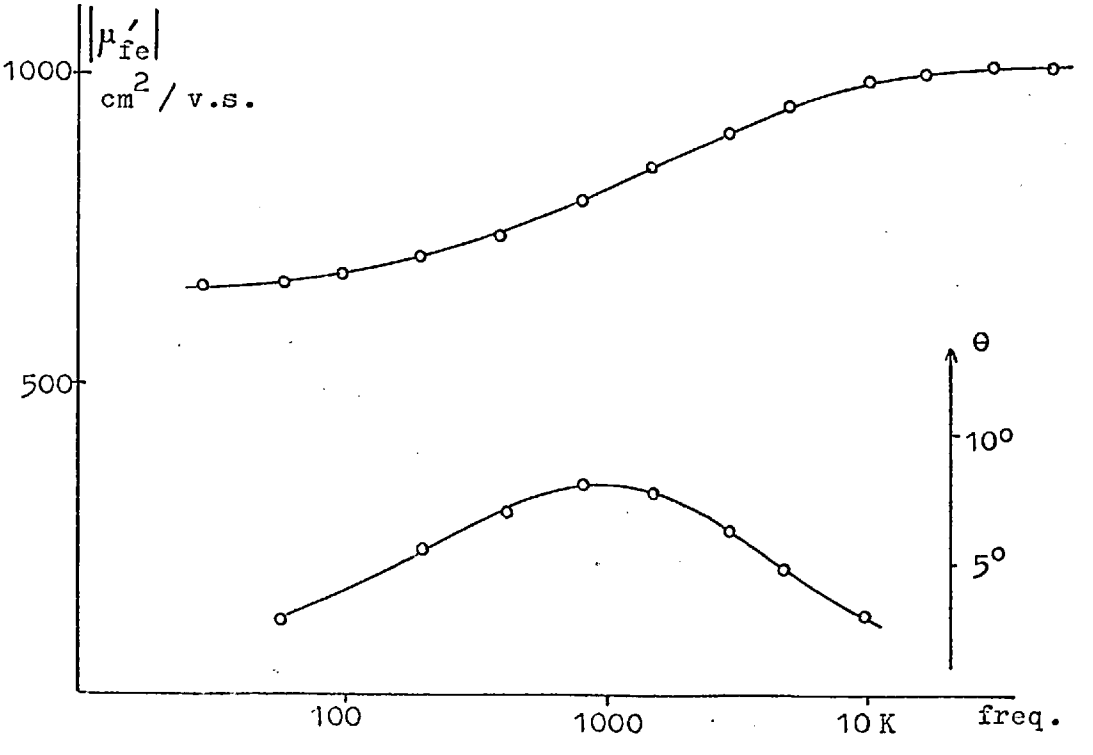

6.6 d

The kind of conductivity modulation obtained is shown in fig. 6.18 . τ_{ss} can be estimated directly from the decay of V_σ , which was observed to be approximately exponential. Near the end of the pulse, V_σ was almost constant, indicating that no more charge is entering the fast states. α can then be estimated from the ratio of the voltages (V_1 and V_2) at the beginning and end of the pulse, as shown in the diagram. This assumes that V_1 represents the full amount of modulation obtainable from the induced charge, none of which has yet become trapped by surface states. This is correct provided that there are no states with time constants less than about 10^{-6} seconds, because the rise-time of the pulse generator and the response time of the amplifiers were both less than 1 μ sec. .

The sample was enclosed in a holder made of thick copper which could be cooled by liquid nitrogen to enable measurements to be made as a function of temperature. The results are given in fig. 6.19 . τ_{ss} increased rapidly with decreasing temperature , following approximately an exponential law :

$$\tau_{ss} \propto \exp (E_{ss} / kT)$$

Values of E_{ss} for the PbSe and PbTe samples are shown in fig. 6.19 . In contrast to τ_{ss} , α was found not to vary much with temperature.

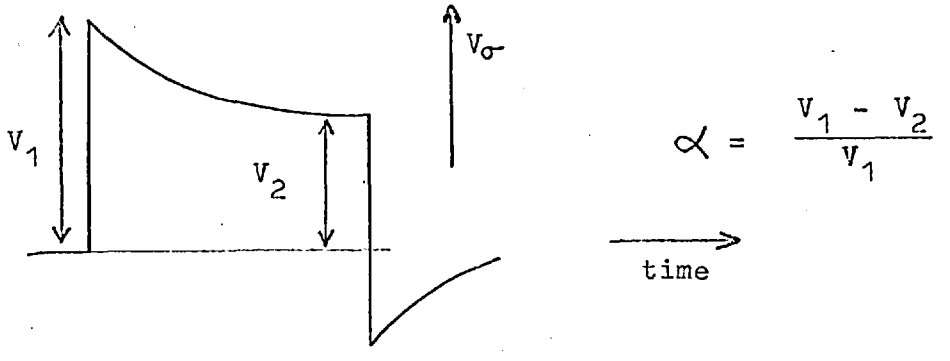

Figure 6.18 Pulsed field effect modulation

(a) Sample T3 (n-PbTe)

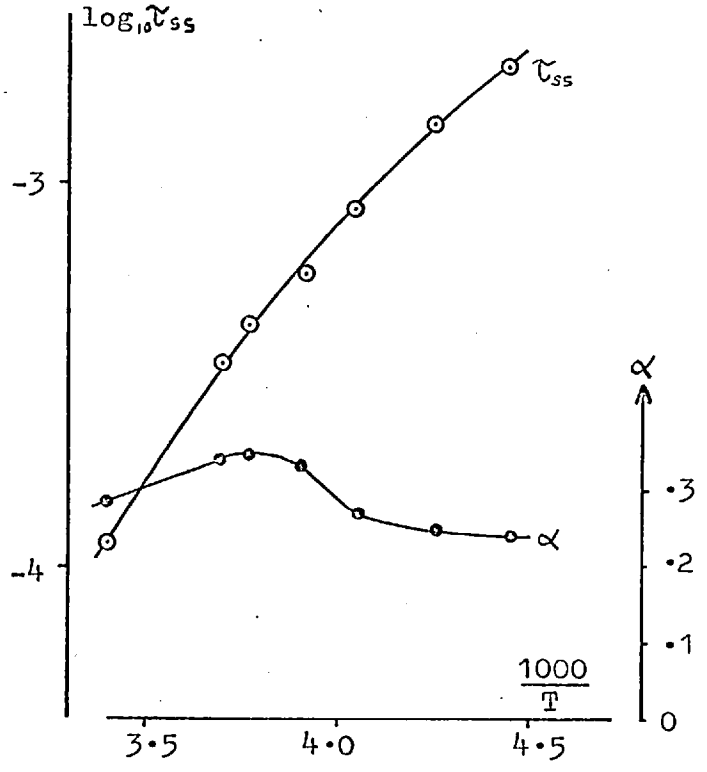

Figure 6.19 τ_{ss} and α, measured between 300°K and 210°K, plotted against 1/T.

(τ_{ss} in seconds)

Values obtained from pulse measurements

sample	$(\tau_{ss} \times 10^4)$ at 300°K ↓	α ↓	E_{ss} (eV) ↓
T2	·72	·27	·19
T3	1·15	·29	·26
T4	1·0	·20	·18

(b) Sample T2 (p-PbSe)

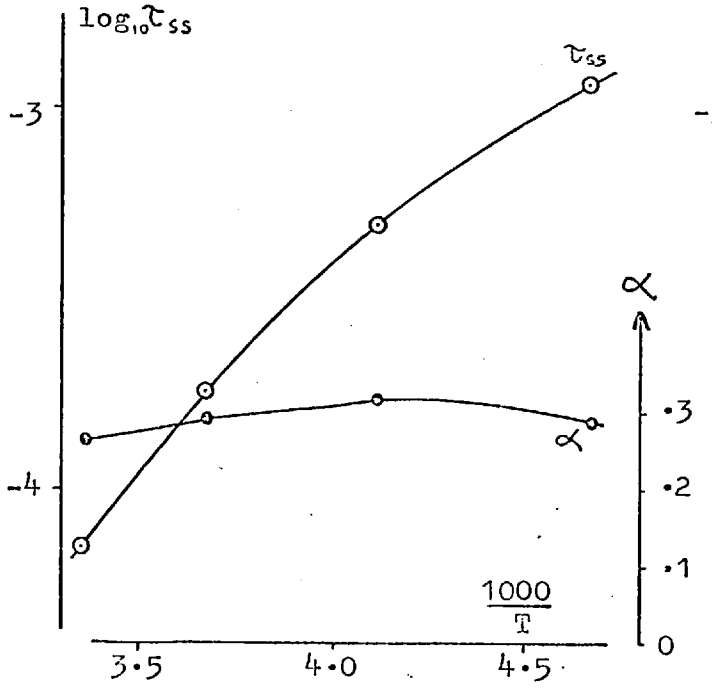

(c) Sample T4 (p-type PbSe)

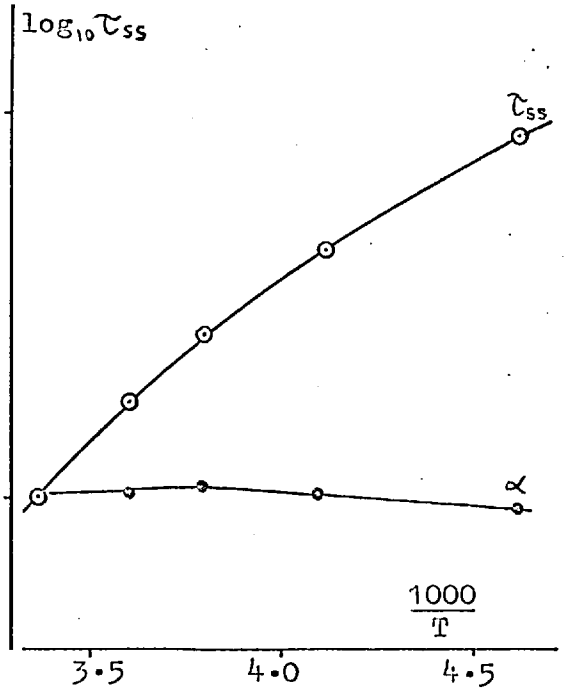

6.7 Discussion

In order to draw some conclusions about surface states at the PbTe / mica and PbSe / mica interfaces, the experimental results will be considered in turn.

a) Large-signal field effect

Comparison of the experimental and calculated field effect curves (figures 6.8 and 6.9) , as described in 6.5 c , gives the surface potential at zero applied field as $v_s = -1{\cdot}5$. This means that for a lightly-doped (n-type) PbTe sample, there is a weak depletion layer at the mica surface, as shown in fig. 6.20 .

The graph of trapped charge against surface potential (fig. 6.10) is nearly a straight line over the experimental range of v_s (about $4\,kT$) , with gradient approximately -5×10^{11} cm^{-2}. Although this does not permit curve-fitting in the normal way, various surface state models can be considered to see whether their properties are in agreement with the experimental results.

1) A single energy level

The expression for trapped charge due to a density N_t per unit area of states at a single energy E_t is (from (6.14)) :

$$Q_{ss} = -N_t f(E_t)$$

where $f(E_t) = f_n = \left(1 + \exp \frac{E_t - E_f}{kT} \right)^{-1}$ for acceptor states

and $f(E_t) = f_n - 1$ for donor levels

This does not fit the present results, since the Fermi function $f(E_t)$ is approximately linear only over about $2\,kT$, i.e. for $\left| (E_t - E_f)/kT \right| \lesssim 1$. Moreover the trapped charge (fig. 6.10) takes both positive and negative values, so that both donor and acceptor states must be present at the interface.

2) Two discrete levels

Two energy levels could account for the observed linearity in dQ_{ss} / dv_s if these are spaced about $2kT$ apart and roughly at the centre of the forbidden gap, as shown in fig. 6.21 a. To give the same gradient over the whole range of v_s, the densities $N_t(1)$ and $N_t(2)$ would have to be approximately equal. It is reasonable to suppose that one energy level would be composed of acceptors and the other of donor states, the equal numbers allowing both positive and negative values of Q_{ss} and giving $Q_{ss} \sim 0$ when the Fermi level is half-way between the levels i.e. at about mid-gap. In this case, it is not possible to decide which energy level consists of acceptor and which of donor states, since both combinations give rise to identical properties. The density $N_t(1) = N_t(2) = N_t$ of surface states can be found by differentiating the Fermi function for a single level (since the two functions operate over different ranges of energy) giving :

$$\frac{dQ_{ss}}{dv_s} = \frac{-N_t \exp(E_t - E_f / kT)}{[1 + \exp(E_t - E_f / kT)]^2} \qquad (6.26)$$

When $E_t \doteqdot E_f$,

$$\frac{dQ_{ss}}{dv_s} = -\frac{N_t}{4}$$

This can be equated with the experimental gradient, giving :

$$N_t = 2{\cdot}0 \times 10^{12} \text{ cm}^{-2}$$

In actual fact, the experimental curve (fig. 6.10) shows a change in gradient at around $V_g = 0$, which may be significant. The portion of the curve for $v_s < -1{\cdot}5$ has a gradient of $-6{\cdot}3 \times 10^{11}$ cm^{-2}. Furthermore, the charge Q_{ss} when the Fermi level is at mid-gap ($v_s \sim -1$) is not zero, but about -6×10^{11} cm^{-2}. These facts can be accounted for by assuming that the lower energy level has a higher state density of $N_t(2) \sim 2{\cdot}5 \times 10^{12}$ cm^{-2}, these being acceptors (see fig. 6.21 b). There is some further

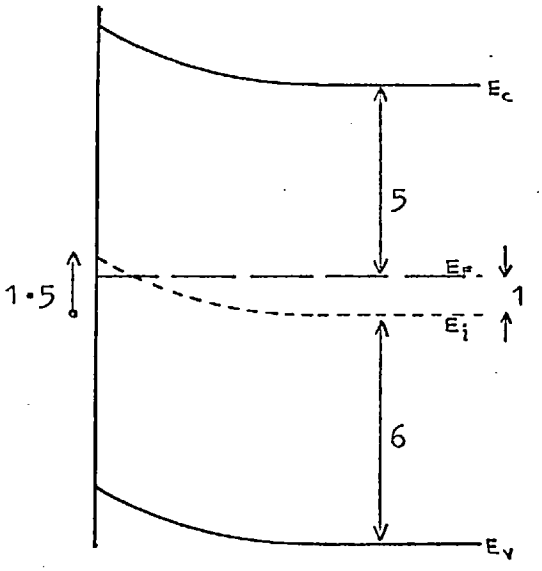

Figure 6.20

Band bending at the PbTe / mica interface for PbTe sample 2 at room temperature

(energies in units of kT)

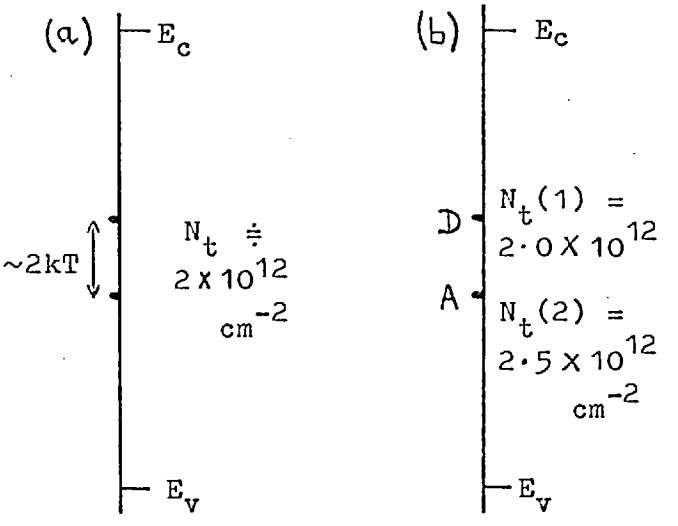

Figure 6.21

Discrete-surface-state models for the PbTe / mica interface at 300°K

Figure 6.22 Conductivity modulation in lightly-doped PbTe samples at 77°K

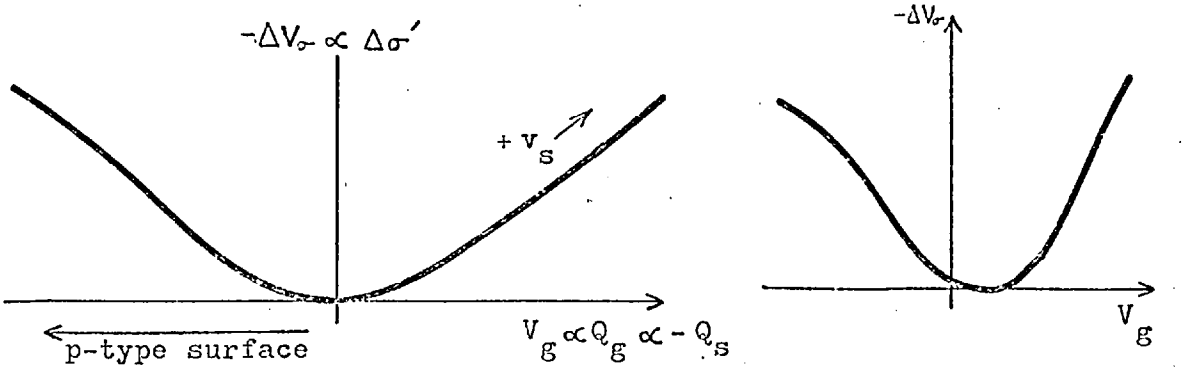

evidence for a higher density of surface states in the lower half of the energy gap from the conductivity modulation curves of near-intrinsic PbTe samples at 77°K (see fig. 6.22). These show curvature (probably due to surface states) at higher values of $\Delta\sigma$, the curvature being larger on the p-type side of the minimum.

3) Continuous distribution of states

An energy distribution of N_t' states /cm^2 /kT gives a constant value of dQ_{ss}/dv_s over the range where N_t' is constant, since the change in Q_{ss} due to a change dv_s in surface potential can be written (S15):

$$dQ_{ss} = N_t' \, dv_s$$

The experimental results would then indicate a state density of between 5×10^{11} and 6×10^{11} cm^{-2}/kT (2·0 to $2{\cdot}4 \times 10^{13}$ cm^{-2}/eV). within $\pm$ 2 kT ($\pm$ ·05 eV) of the middle of the gap. This value of N_t' is the total number of states, donor + acceptor. It is not possible to say how the state density varies outside the experimental range of v_s, except that the finite value of Q_{ss} at mid-gap suggests that there is some assymmetry in the energy distribution or else a slightly larger number of acceptor levels.

6.7 b Small-signal field effect

Field effect mobilities

The results in table 6.1 show that (at room temperature)

$$\cdot 5 \lesssim \left|\frac{\mu_{fe}}{\mu_H}\right| \lesssim \cdot 9$$

for the majority of PbTe samples.

(μ_H is the Hall mobility for the bulk of the film)

This can be expressed in terms of the fraction α of applied charge which enters the surface states (at low frequencies), since the measuring frequency was far below f_1 (defined in 6.6 c and equation (6.30)).

Equation (6.22) gives : $$\mu_{fe} = \frac{d(\Delta\sigma)}{dQ_s}$$

From (6.20) for one type of carrier at the surface : $$\mu_s = \frac{d(\Delta\sigma)}{dQ_{sc}}$$

$$\therefore \quad \mu_{fe}\,\delta Q_s = \mu_s\,\delta Q_{sc} = \mu_s\,(\delta Q_s - \delta Q_{ss}) \qquad \text{from (6.13)}$$

$$\alpha = \frac{\delta Q_{ss}}{\delta Q_s} \qquad \therefore \quad \mu_{fe} = \mu_s\,(1 - \alpha)$$

$$\alpha = 1 - \frac{\mu_{fe}}{\mu_s} \doteqdot 1 - \frac{\mu_{fe}}{\mu_H} \qquad (6.27)$$

and the values of α obtained are therefore in the range 0·1 to 0·5 .

Variation with temperature

Figures 6.11 and 6.12 indicate that μ_{fe}/μ_H does not vary much between 300°K and 77°K ; from equation (6.27) this means that α is roughly constant over this temperature range. These results can conveniently be considered with those from the pulsed field effect, where α was observed to be essentially constant down to 210° K (fig. 6.19) .

For a single discrete surface-state level, (6.14) gives

$$\delta Q_{ss} = - N_t \frac{d}{dv_s}\left[f(E_t)\right] \frac{\delta Q_{sc}}{\frac{dQ_{sc}}{dv_s}}$$

$$\text{i.e.} \quad \frac{\alpha}{1-\alpha} = - \frac{N_t \exp(E_t - E_f/kT)}{\left[1 + \exp(E_t - E_f/kT)\right]^2} \Big/ \frac{dQ_{sc}}{dv_s}$$

From (6.10) , $$\frac{dQ_{sc}}{dv_s} = q(n_b + p_b)\,L\,\frac{dF_s}{dv_s}$$

For an extrinsic semiconductor, the main temperature dependence of α would be due to $\frac{d}{dv_s}\left[f(E_t)\right]$, and for finite values of $\left|E_t - E_f\right|$ the variation with T would be quite rapid. (For $\left|E_t - E_f\right| = 1\,kT$ at room temperature, for example, $\left|\frac{d}{dv_s}\left[f(E_t)\right]\right|$

decreases by a factor of 20 upon cooling to $77^{\circ}K$). The only means of avoiding this rapid temperature dependence is to assume that $(E_t - E_f) \sim 0$. But since at least two energy levels separated by more than 1 kT must be present (from 6.7 a), this condition cannot be satisfied bor both. It therefore seems that a two-state model cannot account for the small temperature dependence of α .

If a continuous and uniform distribution of surface states is assumed, α is given by :

$$\frac{\alpha}{1-\alpha} = -N_t' \Big/ \frac{dQ_{sc}}{dv_s} = \frac{-N_t'}{q(n_b + p_b) L \frac{dF_s}{dv_s}} \qquad (6.28)$$

If the number of states per eV is assumed to be independent of temperature , then N_t' (the number of states / kT) is proportional to T . The main temperature dependence in the denominator of (6.28) is due to L , which is proportional to $T^{\frac{1}{2}}$ for an extrinsic semiconductor (eqn. (6.7)). Equation (6.28) then predicts that α should vary by no more than a factor of two between $300^{\circ}K$ and $77^{\circ}K$ and should be almost constant over the range $300^{\circ}K$ to $210^{\circ}K$, in much better agreement with the experimental results.

From (6.28) , a rough estimate of N_t' can be made. Considering PbSe sample B 11 a , $p_b = 5 \times 10^{17}$ cm^{-3}, $L = 290$ A$^{\circ}$, $\alpha = \frac{1}{3}$. dF_s/dv_s is not known accurately, because the surface potential is unknown in this case. But for $v_s = -4$, 0 , and $+12$, dF_s/dv_s is equal to 5 , 1 and 4 respectively. An approximately symmetric distribution of surface states with comparable numbers of donors and acceptors will tend to hold the Fermi level near the middle of the energy gap at the interface. This produces a depletion layer at the surface, which for sample B 11 a would give v_s +5 at room temperature. dF_s / dv_s can then be estimated as about 2 , giving $N_t' \sim 14 \times 10^{11}$ cm^{-2} / kT . This is of the same order

as the value (5×10^{11} cm^{-2} / kT) obtained from large-signal measurements on PbTe at room temperature.

For sample B 11 a , the surface Hall mobility was measured at 300°K giving $\mu_{Hs} \sim 600$ cm^2 / v.s. (section 6.6 b). This may be compared with the Hall mobility, $\mu_H \sim 530$ cm^2 / v.s., for the bulk of the film and the field effect mobility of $\mu_{fe} \sim 380$ cm^2 / v.s. Although μ_{Hs} could not be obtained very accurately, the values suggest that $\mu_{Hs} \doteqdot \mu_H$ i.e. there is no reduction in carrier mobility near the surface. This does not necessarily mean that surface scattering is specular, because if there is a depletion layer at the surface, the mobility reduction due to diffuse scattering is expected to be small. Unfortunately the change in Hall voltage with applied electric field is very small, and could only be measured reliably on this one sample.

Variation with frequency

The increased value of field-effect mobility at higher frequencies is due to the fact that trapping states become inoperative. These traps are assumed to be surface states at the mica interface, although in principle they could be bulk states distributed within the semiconductor.

Assuming that for frequencies of around 100 K Hz all the applied charge goes into the space-charge region i.e. that there are no states with time constant much less than 10 μsec., the fraction α of applied charge which becomes trapped at low frequencies is given by :

$$\alpha = 1 - \frac{\mu_{fe}^{l}}{\mu_s} = 1 - \frac{\mu_{fe}^{l}}{\mu_{fe}^{h}} \qquad (6.29)$$

from (6.27)

where μ_{fe}^{l} and μ_{fe}^{h} are the low- and high-frequency values of field-effect mobility.

The effective time constant of the surface states can be taken (M5 , p. 246) as :

$$\tau_{ss} = (2\pi f_1)^{-1} \qquad (6.30)$$

f_1 being the frequency at which $\mu'_{fe} = \frac{1}{2}(\mu^h_{fe} + \mu^l_{fe})$

Values of α and τ_{ss} calculated from (6.29) and (6.30) are shown in table [6.2], for PbSe and PbTe samples at room temperature. The values are in reasonable agreement with those obtained from pulse measurements on the same samples (fig. 6.19).

Table [6.2]

SAMPLE	MATERIAL	MODULATION TYPE	α	τ_{ss}
T 1	PbSe	p	·47	1·03
T2	PbSe	p	·33	0·89
T 3	PbTe	n	·35	1·20
A 55 a	PbTe	n	·31	0·84
A 56 a	PbTe	p	·24	0·40
				X 10^{-4} sec.

If the assumption is correct, that there are no states with much shorter time constants, the high-frequency value of μ_{fe} (μ^h_{fe}) should be essentially equal to the bulk carrier mobility, in the absence of significant surface scattering. An attempt was made to verify this by measuring the bulk Hall mobility in the field-effect sample. Although this cannot be done by the usual method, μ_H can be estimated from the change in sample resistance in a magnetic field (Corbino effect). Because of the sample geometry, the source and drain contacts effectively short-circuit the Hall voltage, which then appears as an increase δV_σ in the voltage V_σ between these two contacts in the presence of a magnetic field B, where (B2):

$$\frac{\delta V_\sigma}{V_\sigma} = \mu_H^2 B^2 + \left(\frac{\Delta\rho}{\rho}\right)_m \qquad (6.31)$$

$\left(\frac{\Delta\rho}{\rho}\right)_m$ is the normal magnetoresistance of the semiconductor, which

was undetectable in the present films. Equation (6.31) therefore gives the magnitude of the Hall mobility, provided that V is a true measure of the resistivity of the semiconductor i.e. that contact resistance is negligible.

Values of μ_H and μ_{fe}^h for two p- PbSe samples are given below.

sample	$\mu_H(C)$	μ_{fe}^h
T 1	280	160
T 2	445	280

$cm^2 / v.s.$

The values of μ_{fe}^h are substantially less than the Hall mobility $\mu_H(C)$ estimated from Corbino measurements. However, all the mobilities are below the values expected for PbSe epitaxial films. This suggests that contact resistance may be significant in these samples. It would have a greater effect on μ_{fe} than on $\mu_H(C)$, since (from (6.25) and (6.31)) $\mu_{fe} \propto V^{-2}$ whereas $\mu_H(C) \propto V^{-\frac{1}{2}}$. Owing to the small resistance of the sample (due to the small channel length), a resistance of about 20Ω at each contact would be sufficient to account for the discrepancy between $\mu_H(C)$ and μ_{fe}^h. Contact resistance should not affect the ratio of μ_{fe}^l to μ_{fe}^h ; this is borne out by the fact that values of α calculated from (6.29) are consistent with those obtained from measurements in section 6.6 b , where the sample shape used eliminates contact resistance.

For surface states at a discrete energy level, with a single time constant τ_{ss} , the in-phase component of the field-effect mobility at an angular frequency $\omega = 2\pi f$ is given (M5 , p. 246) by :

$$\mu_{fe}' = \mu_{fe}^h \left(1 - \frac{\alpha}{1 + \omega^2 \tau_{ss}^2} \right) \qquad (6.32)$$

Using values of α and τ_{ss} obtained from (6.29) and (6.30) ,

μ_{fe}' was calculated using (6.32) as a function of frequency for sample T 1 and the result is shown in fig. 6.15 (dotted curve). For the single-energy-level model, the change in μ_{fe}' occurs over a narrower range of frequency than the experimental curve. Also, the calculated maximum in phase angle θ is larger than the observed value. These results indicate that there must be at least two energy levels, with different time constants. It is not possible to analyse the experimental curves with sufficient accuracy to determine the number of energy levels or their separate densities and time constants.

Pulse measurements

Although α was approximately constant over the range $300^{\circ}K$ to $210^{\circ}K$, τ_{ss} increased rapidly with decreasing temperature, according to :

$$\tau_{ss} \propto \exp\left(E_{ss}/kT\right)$$

with $E_{ss} \sim .18$ to $.26$ eV .

For a single surface state level and a p-type semiconductor where holes predominate at the surface, the relaxation time for small-signal pulses is given (L13) by :

$$\frac{1}{\tau_{ss}} = \frac{4\, p_b}{C_p\, \bar{c}} \left\{ \left[1 + \frac{\alpha}{(1-\alpha) f_p} \right] \times \exp(-v_s) + \exp(-v_o) \right\} \qquad (6.33)$$

where p_b is the bulk hole concentration

C_p and $\bar{c}$ are the capture cross-section and mean thermal velocity of holes

f_p is the Fermi function for holes, given by :

$$f_p = \left[1 + \exp -(E_t - E_f / kT)\right]^{-1}$$

and $v_o = \frac{E_t - E_f}{kT} + v_s$. Similar equations apply to the case of electrons in an n-type semiconductor.

The activation energy for τ_{ss} is therefore either v_s or v_o (depending on which is the smaller) .

6.7 b

From field-effect measurements on polycrystalline PbS films, Zemel and Varela (Z6) obtained activation energies of between ·12 and ·24 eV , but attributed this to the temperature dependence of the capture cross-section C_p .

For a distribution of energy levels, which the previous results in this chapter seem to require, $1/\tau_{ss}$ would be given by a sum of terms similar to the R.H.S. of equation (6.33) for different energies, each weighted according to the number of states at the particular energy. In this case, it is difficult to see how the large value of E_{ss} can occur, because states with a large value of $|E_t - E_f|$ will have little effect on the trapping processes unless their density is very high. It may therefore be necessary in the present case to assume that C_p has a large temperature dependence. But without further information about the surface potential and the surface-state energy distribution, the temperature dependence of τ_{ss} cannot be interpreted unambiguously.

Some of the conclusions from field-effect data are summarised in chapter 7 .

CHAPTER 7

SUMMARY AND CONCLUSIONS

The following chapter contains a summary of the main results of the present study, with reference to those of previous workers.

7.1 Structure and growth of epitaxial PbTe, PbSe, and PbS films

The electron diffraction patterns of PbTe deposited on to mica show that the films are well-oriented, with {111} parallel to the substrate, and with good azimuthal alignment. This is also true of PbSe deposited at room temperature. However, films of PbS on mica give a more complicated diffraction pattern, except at high growth temperatures, where the deposit appears to have {100} parallel to the substrate.

Shadowed replicas of discontinuous PbTe films show that the nuclei are triangular pyramids (tetrahedra) with {111} base and {100} sides, which occur in two twinned orientations (double positioning) . As the film grows, these nuclei coalesce, leaving a system of double-positioning boundaries. These boundaries are still present in 3000 A^{o} films, although their number decreases with increasing film thickness.

Up to about 300 ^{o}C , the number of boundaries and other defects in continuous films decreases with increasing deposition temperature, corresponding to a rise in the measured Hall mobility (figures 3.12 and 3.17) .

Above 300 ^{o}C growth temperature, the Hall mobility starts to fall, possibly due to the formation of cracks in the film upon cooling.

At about 400 ^{o}C , the film surface breaks up into a system of {100} faces, and appears dull when viewed by the naked eye. Above this temperature, re-evaporation from the substrate becomes considerable. Also, the surface mobility of PbTe molecules becomes very high, and even films whose actual (average)

thickness is 1000 A^{o} consist of isolated nuclei.

The nucleation and growth of PbSe on mica appears to be similar, except that more than one orientation is present, as discussed in ref. (P 13).

Although there is a reasonable amount of previously-published work on the electrical properties of epitaxial PbTe, PbSe and PbS films (see section 1.5), their growth and structure has been less well-studied.

Spot electron-diffraction patterns have been reported for these semiconductors when deposited on a variety of substrate materials (E 5, M 3, P 1, S 12, L 7).

The nature and behaviour of dislocations in epitaxial PbSe and PbS on NaCl were investigated by Matthews (M 8, M 9).

Palatnik et al (P 1) studied the nucleation of PbTe on NaCl as a function of deposition temperature, but the evaporation was carried out in a relatively poor vacuum (5×10^{-4} torr) and the film structure appeared to be dominated by the presence of a large number of cleavage steps on the substrate.

Nucleation of PbTe on rocksalt was studied more recently by Lewis and Stirland (L 7), who observed {100} orientation at all substrate temperatures. At 200 °C, the nuclei were square in outline due to {100} faces, although more complicated shapes were generated when islands started to coalesce. At temperatures of 100 °C and below, dendritic growth occurred, and this was explained in terms of a large interchange of PbTe molecules between islands. Just before films became completely continuous, filling of the remaining channels produced lines of dislocations, some of which remained during subsequent growth.

Certain structural differences are therefore apparent between PbTe films on mica and those on alkali halide substrates.

1) In {100} films on cleaved alkali halides, there can be

no double-positioning boundaries, because the symmetries of the film and substrate surface are the same. However, there appear to be boundaries or dislocation arrays of some sort, which are effective in scattering current carriers (Z 7, Z 4) . These may be low-angle boundaries, or regions of misfit due to the difference in lattice spacing between film and substrate.

2) {100} appears to be the surface of lowest free energy for PbTe . Effects of surface break-up (as observed in {111} films at high temperatures) are therefore not to be expected with films on rocksalt.

There are several advantages and disadvantages between the two kinds of substrate material.

Sodium chloride and other alkali-halides have the advantage that the substrate can be dissolved (in water, for example) without attacking the film ; this is convenient for electron microscopy.

Mica can be cleaved easily to give large surface areas (square centimetres) which are free from optically-visible cleavage steps. This provides a good surface for nucleation studies and also gives films with reliable electrical properties.

Mica is crystallographically not a well-defined substance; it contains loosely-bound water molecules, some of which are evolved upon heating in vacuum. However, it is chemically unreactive and provides a more practical substrate material for commercial applications e.g. thin film circuits.

7.2 Electrical properties of epitaxial films

In the present study, Hall measurements were made (in air) on a large number of films, to determine the carrier concentration and the Hall mobility over the temperature range 300 ^{o}K to 77 ^{o}K . Carrier concentrations were mainly within the range 10^{17} to 10^{19} cm^{-3} , but showed considerable variation between

samples. It was not possible to control the carrier concentration accurately by varying the deposition conditions.

In the case of PbS, only n-type films could be grown. The carrier concentrations were high and the mobilities appreciably below bulk values. This suggests that dissociation in the evaporation source occurs to a greater extent with PbS than for PbSe and PbTe. This is understandable because the equilibrium vapour pressure of sulphur over PbS is higher than for tellurium over PbTe at the same temperature (C 5), despite the stronger bonding in PbS. It might be possible to grow lead sulphide films of better stoichiometry by evaporating lead and sulphur separately in a three-temperature method (G 10) as used previously for InSb and CdSe.

The Hall mobilities of the films were generally comparable with bulk values for the three lead compounds (at room temperature) and increased with decreasing temperature, though not quite so rapidly as in the bulk. The best electrical mobilities were obtained for n-type PbTe, with μ_H = 1300 $cm^2/v.s.$ at room temperature (bulk value is 1600) and up to 17,000 $cm^2/v.s.$ at 77 ^oK (approximately two-thirds of the bulk value). These values are similar to the ones obtained for n-type PbTe on mica by Makino (M 4). The present results for PbSe and PbS on mica are also comparable with those for similar films on NaCl (Z 7, B 19, G 3).

From analysis of the Hall mobility as a function of temperature, the departure from bulk mobility values appears to be due to additional carrier scattering, probably from double-positioning boundaries. By analogy with polycrystalline films, these boundaries might be expected to act as potential barriers, reducing the conductivity at low temperatures. However, this effect was not observed, possibly due to the high dielectric constant of the semiconductors, particularly PbTe. This would reduce the potential barrier height for a given charge at the interface, and might account for the high mobility values obtainable.

Because of the high electrical mobilities, epitaxial films of the lead salts could be suitable for use in thin-film circuits, e.g. for a thin-film field-effect transistor. In the latter case, the parameter of importance is the field-effect mobility, and the results given in chapter 6 show that this can be quite high, at least at the PbTe / mica interface. For this application, however, the electrical properties of the films are required to be stable over long periods of time.

The present results (chapter 5) show that for unprotected films the conductivity changes over a period of months when samples are stored in an oxygen environment. This is in contrast with previously-reported results for epitaxial PbTe and PbSe on NaCl, where long-term ageing effects were not observed (S 11, B 13). The only differences appear to be in the substrate material (and consequent orientation of the film) and in the film thickness. In the present case, the thickness was of the order of 3000 A° (cracking effects were sometimes observed with thicker samples), whereas the previous workers have used film thicknesses of a few microns. The interaction with oxygen resembles the effects observed in polycrystalline films, which suggests that the crystal structure of the present films may be less perfect than for {100} films on rocksalt. The mobility values do not support this conclusion, though the latter may not be a sensitive test of film quality, due to the high dielectric constants.

The present results do, however, show that encapsulation of the semiconductor film by an evaporated layer of insulator can reduce the effects of the atmosphere.

7.3 Interaction of the lead salts with oxygen

In the experiments described in section 5.4, the room-temperature Hall coefficient and resistivity of epitaxial PbTe films were measured in vacuum (directly after deposition) and upon exposure to air or oxygen. Oxygen was found to change

the conductivity towards p - type , and large changes in surface conductance ($2 \times 10^{-2} \Omega^{-1}$ for certain n-type PbTe samples) were observed, but with very little change in Hall mobility. The effect was fairly rapid, occurring within less than a minute after sudden exposure to atmospheric pressure, and was partly reversible (over a period of hours) is vacuum conditions were restored.

The results were considered (section 5.5) in terms of two possible mechanisms :

1) Adsorption of oxygen on the surface of the film, procucing a surface space-charge region within the semiconductor.

2) Bulk doping of the semiconductor by oxygen, which might diffuse into the film.

Investigation of the kinetics of the reaction and the effect of temperature (section 5.6) failed to discount either of these two possibilities. However, mechanism (1) seems unlikely, since it would involve very large surface charge densities (10^{14} cm^{-2}) and it is difficult to account for the small magnitude of the variation in Hall mobility. Another reason for doubting the existence of a strong space-charge region within films exposed to air is that several samples showed high Hall coefficients, which would be impossible in the presence of a degenerate layer near the surface.

Mechanism (2) rests on the assumption that diffusion is sufficiently rapid to account for a major part of the change in conductance. By comparison with other related systems (section 5.7) , there is a possibility that this is so.

Previous work on the effect of oxygen on the lead salt semiconductors has not established any exact reaction mechanism. Measurements have been performed on polycrystalline films and (more recently) on crushed powders and single-crystal films.

The early experiments on polycrystalline films were made in an attempt to explain the mechanism of oxygen-induced photoconductivity. Changes in thermoelectric power and resistivity (B 8)

and of Hall mobility (S 17) were measured during initial exposure of freshly-deposited films to oxygen. The resistance of n-type PbTe films was found to increase by several orders of magnitude and subsequently to decrease, corresponding to the change to p-type conduction. The Hall mobility decreased by a factor of about 5. These effects were attributed (B 8) to the adsorption of oxygen at crystallite surfaces inside the film, which would remove electrons from the crystallites and also create space-charge barriers, thus reducing the mobility.

The effect of oxygen on the conductance and photoconductance of polycrystalline PbS films was studied by Harada and Minden (H 3). Oxygen was assumed to trap electrons by creating surface states of two different energies at intercrystalline surfaces.

Jones (J 3) investigated the effect of oxygen on the resistivity of polycrystalline PbSe films, and from the reaction kinetics obtained evidence of a diffusion process with an activation energy of about 0·26 eV. The reaction was very slow at room temperature, but was appreciable over a period of hours above 100 °C. Re-evacuation did not cause significant change in the resistivity, but the original values could be restored by annealing at 350 °C in vacuum.

Berezhnaya (B 4) examined the effect of oxygen and carbon monoxide on the resistivity and Hall coefficient of polycrystalline n-type films of PbS. Oxygen increased the resistivity during the course of a few hours (at room temperature), with little change in Hall mobility. Carbon monoxide was also effective over a period of hours and acted to reverse the effect of oxygen. But after prolonged exposure to oxygen (for several days), the change was irreversible, possibly due to the formation of a stable oxide.

The kinetics of the reaction of oxygen with PbS were also studied by Hillenbrand (H 6), who measured the uptake of oxygen gas by crushed material. Temperatures of 150 °C or 200 °C were necessary for reasonable reaction rates; the rate was found

to be proportional to the oxygen pressure and inversely proportional to the amount of oxygen already reacted. This was explained by assuming that an oxide layer (up to a few atomic layers in thickness) is formed at the surface, the rate-limiting process being the diffusion of S^{2-} ions through the oxide film. Sulphur was shown to be liberated from the surface in the form of SO_2, which could be detected by mass spectrometry.

Similar experiments on crushed PbTe were carried out by Green and Lee (G 4). They concluded that up to 0·7 monolayer coverage there was a single reaction mechanism, probably the formation of a surface peroxide layer.

Experiments on epitaxial PbS films (On NaCl) (B 17, C 12) showed that exposure to oxygen caused a change in conductance and the appearance of a certain amount of photoconductivity, over a period of minutes. Electron paramagnetic resonance detected the presence of peroxide radicals at the surface.

Brodsky and Zemel (B 13) measured the change in Hall coefficient and resistivity when epitaxial PbSe films (previously exposed to air) were placed under vacuum. There was not much change in Hall mobility (see section 5.5 a). The changes in R_H and ρ were thought to be due to a space-charge layer created when oxygen is adsorbed on the surface.

More recently, Zemel (Z 5) has suggested that this space-charge region might arise from the formation of a defected oxide layer at the surface, rather than from ionisation of oxygen at surface states. The surface-state model appeared less probable because the high surface charge densities required would give a spread in energy levels (due to Coulomb interaction) exceeding the band gap of the semiconductor. The existence of a surface oxide film provides a possible explanation for the small magnitude and large temperature dependence of the 'sticking coefficient' (G 4), since the rate of reaction could be limited by diffusion within the oxide layer.

However, this model does not explain the experimental results of the present study (e.g. the constant value of Hall mobility and the irreversible effects discussed in section 5.5 b)

because the changes in conductivity (and Hall coefficient) are still assumed to occur within a space-charge region inside the semiconductor.

7.4 Surface states at lead-salt surfaces

Previous surface measurements on the lead salts have mainly been performed with polycrystalline films, in air, and have given some information about surface states present at oxidised surfaces.

Petritz et al (P 11) measured the Hall coefficient and resistivity of polycrystalline PbS films as a function of temperature, and inferred the existence of electron trapping states approximately 0·1 eV above the valence band. These were believed to be created by oxygen at intercrystalline boundaries. Pulsed field-effect measurements at the external surface (P 11) also showed evidence of trapping states, with a time constant of about 250 μsec . In addition, the D.C. field effect indicated the presence of slow states, with a time constant of the order of 3 minutes (Z 1) .

The field effect and photoconductivity in polycrystalline PbS films were measured by Zemel and Varela (Z 6) . The field-effect mobility increased with frequency between 100 and 3000 Hz indicating a time constant of 200 to 300 μsec at 300 ^{o}K . The time constant increased rapidly with decreasing temperature. Trap densities were believed to be of the order of 10^{13} per cm^2 of film surface, with capture cross-sections about 10^{-21} cm^2 at room temperature.

Nesterenko et al (N 1) examined the field effect in polycrystalline layers of PbS and obtained evidence of fast states with a density greater than 10^{12} cm^{-2} and time constant less than 5 μsec . There was also a slow relaxation over a period of minutes.

The D.C. field effect at the PbTe / mica interface was measured in vacuum at 84 ^{o}K by Müser et al (M 17). Lead telluride was flash-evaporated on to mica at 0 ^{o}C , and the electric field applied through the substrate. There was evidence of slow states,

with relaxation times of the order of 1 minute. Anomalous effects were observed with high applied fields, which were later explained as being due to ion bombardment of the film from the electrodes (M 6).

The field effect in epitaxial PbTe films on sodium chloride has been demonstrated using thin-film transistor structures by Skalski (S 19). The transconductance and percentage modulation obtained were low, possibly due to the high carrier concentration in the semiconductor ; field-effect mobilities are not quoted.

Surface states in polycrystalline PbTe films were investigated by Lile (L 8) by means of differential surface capacitance measurements on the PbTe / alumina interface at 77 ^{o}K. The trapped charge was obtained as a function of surface potential over a range covering most of the semiconductor band gap. The results imply a continuous energy distribution of surface states, of about 2×10^{13} cm^{-2} eV^{-1} at mid-gap, rising to values in excess of 2×10^{14} cm^{-2} eV^{-1} near the band edges.

The measurements described in chapter 6 were made on epitaxial films of PbTe and PbSe by applying an electric field through the mica substrate.

The large-signal A.C. field effect at room temperature showed that (with zero applied field) the Fermi level at the PbTe / mica interface is near the centre of the energy gap of the semiconductor. The charge trapped in surface states varied linearly with surface potential over the range of measurement (about 4 kT). This is in agreement with similar measurements made by Lee (L 4).

These results suggest two possible models for the surface-state distribution at the PbTe / mica interface at room temperature.

(1) Two discrete energy levels (acceptors and donors), each within about ·025 eV (1 kT) of the centre of the band gap and of density roughly 2×10^{12} cm^{-2}.

(2) A continuous energy distribution of states, which is of approximately uniform density 2×10^{13} cm^{-2} eV^{-1} within

± · 05 eV of the centre of the band gap. This is also the density found by Lile (L 8) within ± ·04 eV of mid-gap (for PbTe / Al_2O_3 at 77 °K).

Although theoretical results for ideal surfaces (T 1, S 14) predict that surface states should have discrete energies, this may not be the case for real systems. Results for Ge and Si surfaces (M 5 , pp. 390 - 392) have usually been fitted to a model involving discrete energy levels (often four), but the data is not usually sufficiently accurate to distinguish between a discrete and a continuous distribution.

Small-signal field-effect measurements for PbSe and PbTe (section 6.6) showed that the fraction of applied charge which becomes trapped in surface states is typically one-third and is independent of temperature. This supports model (2) rather than (1) .

The field-effect mobility increased with frequency over the range 100 to 10,000 Hz , suggesting a surface-state time constant of about 100 μ sec at room temperature. The time constant increased to more than 1000 μ sec at 210 °K . These results are similar to those of Zemel and Varela (Z 6) on the oxidised PbS surface. This similarity might be due to the fact that in both cases the bonding at the interface is between lead and oxygen atoms (page 72) .

Slow states with time constants of a few seconds were detected in some of the present samples. The decay in conductivity modulation appeared to be non-exponential.

The change in Hall coefficient with applied electric field (pages 175, 188) suggests that surface scattering at the PbSe / mica interface may be specular, but this result requires further confirmation.

- - - - - - - -

APPENDIX A

The Hall coefficient of an inhomogeneous semiconductor

Expressions are derived below for the measured Hall coefficient and conductivity of a semiconductor sample where the carrier concentration or mobility varies in a direction parallel to the magnetic field and perpendicular to the current flow. The semiconductor is assumed to be isotropic, and the magnetic field to be small ($\mu B \ll 1$) . More general treatments are given in references (H 5, B 2, H 11) .

The sample geometry is shown in fig. A.1 . For a thin slab of material (as shown) over which the semiconductor properties are approximately uniform, the Hall and conductivity voltages are given (eqns. (4.1)) by :

$$V_{Hi} = B \frac{R_i I_i}{t_i} \qquad (A.1)$$

$$V_\sigma = \frac{1}{w} \frac{I_i}{\sigma_i t_i} \qquad (A.2)$$

The total current passing through the sample is :

$$I = \sum_i I_i = \sum_i \frac{w}{l} \sigma_i t_i V \qquad (A.3)$$

(V_σ is the same for all slabs)

But the measured conductivity of the whole sample is given by :

$$\sigma = \frac{l I}{w t V} \qquad \text{from (4.1)}$$

$$\therefore \sigma = \frac{\sum \sigma_i t_i}{t} \qquad (A.4)$$

from (A.3) & (A.2)

Equivalent circuits for the Hall voltages due to a single slab are shown in fig. A.2 a , b .
Since the Hall generators are electrically in parallel, the equivalent circuit for the whole sample is as shown in fig. A.2 c .

Figure A.1

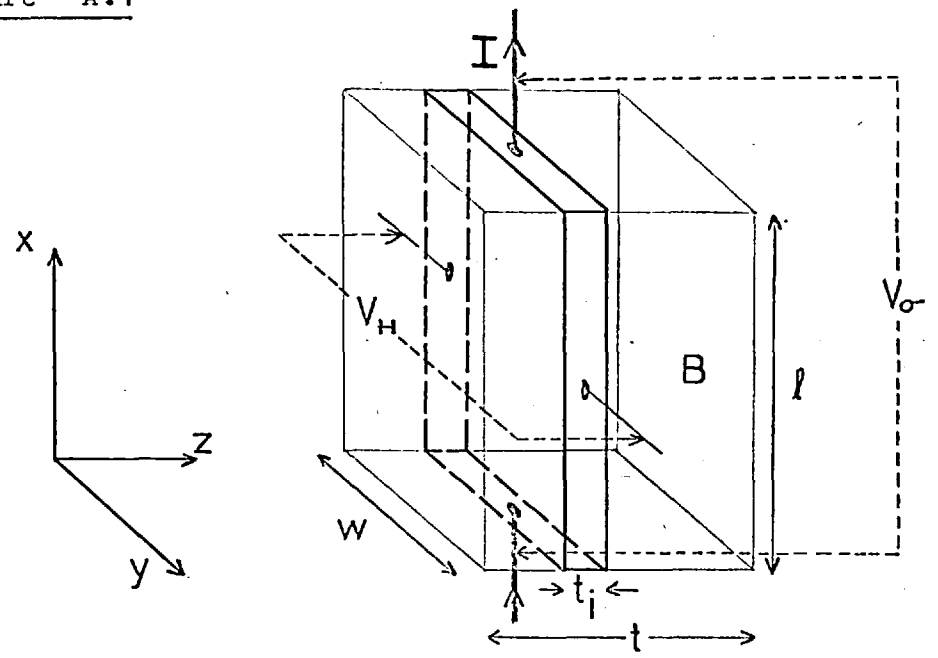

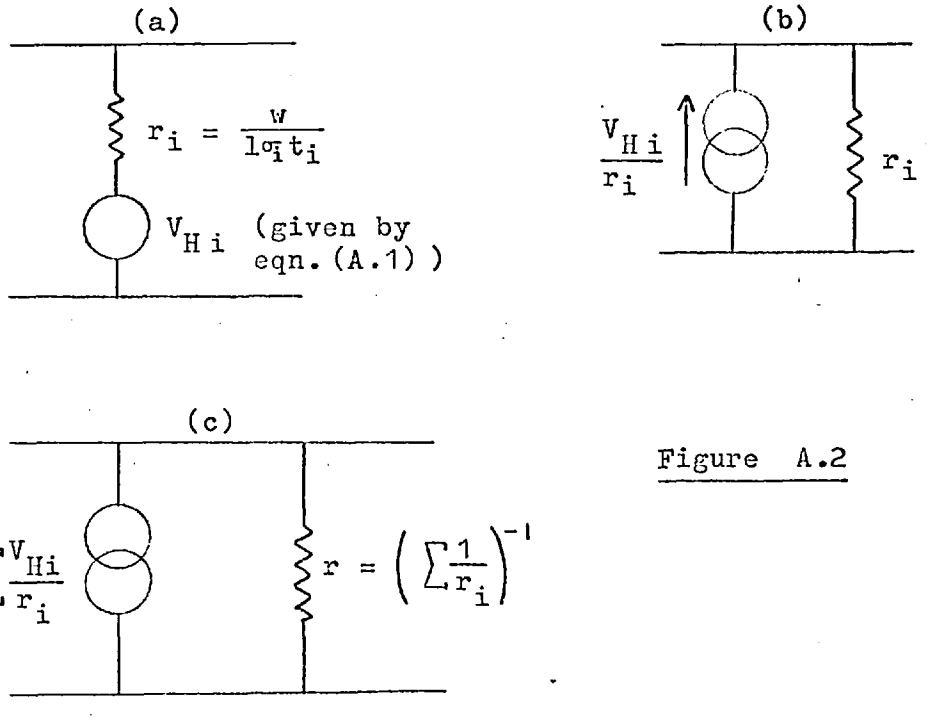

Figure A.2

A.

The Hall voltage is given by :

$$V_H = \sum_i \frac{V_{H\,i}}{r_i} \times r = \frac{\sum V_{H\,i}/r_i}{\sum 1/r_i}$$

Substituting for $V_{H\,i}$ and r_i ,

$$V_H = \frac{B\frac{l}{w}\sum R_i \sigma_i I_i}{\frac{1}{w}\sum \sigma_i t_i} = \frac{B\frac{w}{l} V_\sigma \sum R_i \sigma_i^2 t_i}{\sum \sigma_i t_i}$$

(using A.2)

The measured Hall coefficient is $R = \frac{V_H t}{B I} = \frac{V_H t}{B} \cdot \frac{l}{w t V_\sigma \sigma}$

$$\therefore \quad R = \frac{\sum R_i \sigma_i^2 t_i}{\sigma \sum \sigma_i t_i} = \frac{\sum R_i \sigma_i^2 t_i}{\sigma^2 t} \qquad (A.5)$$

For a continuous variation of R and σ in the z-direction, equations (A.4) and (A.5) become :

$$\sigma t = \int_0^t \sigma_i \, dz \qquad (A.6)$$

$$R \sigma^2 t = \int_0^t R_i \sigma_i^2 \, dz \qquad (A.7)$$

a) If only one type of carrier is present in the sample, and the mobility μ is independent of z ,

For holes, $R_i = \frac{r f}{q p_i}$, $\sigma_i = q p_i \mu$ (A.8)

(A.6) and (A.7) give :

$$R = \frac{\int_0^t R_i \sigma_i^2 \, dz}{1/t\left[\int_0^t \sigma_i \, dz\right]^2} = \frac{r f \; q\mu^2 \int p_i \, dz}{\frac{q^2\mu^2}{t}\left[\int_0^t p_i \, dz\right]^2}$$

i.e. $R = \frac{r f \, t}{q \int_0^t p_i \, dz} = \frac{r f}{q \, \bar{p}}$.

A.

where $\bar{p} = \int_0^t \frac{p\,dz}{t}$ = mean value of p

Therefore the Hall coefficient gives the mean value of carrier concentration, averaged over the thickness of the film.
(The same applies if only electrons are present in the sample.)

Under these conditions (one carrier type , constant μ), the Hall voltages V_{Hi} in all the layers (fig. A.1) can be shown to be equal. This is not so when the mobility is a function of z ; circulating currents then flow in the x — z plane, but provided these are small compared with I , equations (A.6) and (A.7) should still be valid.

b) Where there is band bending, e.g. at the surface of a semiconductor, the integrals in (A.6) and (A.7) can be taken separately over the carriers present under flat-band conditions and over excess carriers in the space-charge region.

$$\therefore \quad \text{from (A.6)} \quad \sigma t = \int_0^t \sigma_b\,dz + \int_0^t (\sigma - \sigma_b)\,dz$$

$$= \sigma_b t + \Delta\sigma \qquad \text{if } t >> L \qquad (A.9)$$

using the definition of $\Delta\sigma$ (eqn. 6.16) .

$$\text{From (A.7)}, \quad R\sigma^2 t = \int_0^t R_b \sigma_b^2\,dz + \int_0^t (R\sigma^2 - R_b\sigma_b^2)\,dz$$

$$= R_b\sigma_b^2 t + \Delta R\sigma^2 \qquad (A.10)$$

(for $t >> L$)

where $\Delta R\sigma^2$ is defined by equation (6.18) .

c) Equation (A.7) also gives correctly the formula for the 2-carrier Hall coefficient in a homogeneous semiconductor, by integrating separately over holes and electrons between the same limits (0 to t) :

$$R\sigma^2 t = rf\left[\int_0^t p\mu_p^2 - \int_0^t n\mu_n^2\right] \quad \text{from (A.7) and (A.8)}$$

$$R = rf \cdot \frac{p\mu_p^2 - n\mu_n^2}{(p\mu_p + n\mu_n)^2} \qquad (A.11)$$

APPENDIX B

Computer program for surface data analysis

The computer program which was used to interpret some of the results in chapters 5 and 6 calculates bulk and space-charge parameters for a semiconductor with a uniform concentration of impurity centres, using Fermi-Dirac statistics and assuming non-parabolic bands and the absence of surface states.

Input data

The input data are read in the following order :

1) E_D E_V E_A $\left(\frac{m_{dn}}{m_o}\right)^{3/2}$ $\left(\frac{m_{dp}}{m_o}\right)^{3/2}$ B κ

(where E_D, E_V and E_A are the energies of the donor levels, valence band edge and acceptor levels, in eV referred to the conduction band edge ; m_{dn} and m_{dp} are the density-of-states effective masses for electrons and holes ; B is a non-parabolicity factor for the valence or conduction band, defined below ; κ is the static relative permittivity of the semiconductor)

2) μ_n $(b)^{-1}$ T

(where μ_n is the bulk electron mobility in cm^2 / volt sec , $b = \mu_n / \mu_p$ and T is the temperature in ^oK)

3) $v_s(u)$ $v_s(l)$ Δv_s

(the upper and lower limits of surface potential and the increments required)

4) Surface mobility reduction, as a function of v_s (if required)

5) N_A N_D

(bulk acceptor and donor impurity concentrations)

B.

Output data

$$E_i \qquad n_i \qquad E_F \qquad n_b \qquad p_b$$

(intrinsic Fermi level and carrier concentration, bulk Fermi level and bulk electron and hole concentrations)

As a function of v_s : Q_{sc} ΔN ΔP $\Delta\sigma$ $\Delta R\sigma^{-2}$

(surface space-charge parameters defined by equations (6.10), (6.11), (6.16) and (6.18). Q_{sc}, ΔN and ΔP in units of +ive charges / cm^2, $\Delta\sigma$ in $(ohm)^{-1}$ and $\Delta R\sigma^{-2}$ in $cm^2\ volt^{-1}\ sec^{-1}\ ohm^{-1}$)

Method of computation

Allowing for partial ionisation of impurities and using Fermi-Dirac statistics, equation (6.4) can be written :

$$\rho = q\,(N_D^+ + p - N_A^- - n) \qquad (B.1)$$

with

$$N_D^+ = N_D \left[1 + 2\exp(v - w_{DF}) \right]^{-1} \qquad (B.2)$$

$$N_A^- = N_A \left[1 + 2\exp(-v - w_{FA}) \right]^{-1} \qquad (B.3)$$

$$n = n_o \left[A_c F_{\frac{1}{2}}(v - w_{CF}) + B_c F_{\frac{3}{2}}(v - w_{CF}) \right] \qquad (B.4)$$

$$p = n_o \left[A_v F_{\frac{1}{2}}(-v - w_{FV}) + B_v F_{\frac{3}{2}}(-v - w_{FV}) \right] \qquad (B.5)$$

where

$$n_o = \frac{4\pi}{h^3} (2 m_o kT)^{3/2}$$

$$w_{pq} = (E_p - E_q) / kT$$

$$F_r(w) = \int_0^\infty \frac{\varepsilon^r \, d\varepsilon}{1 + \exp(\varepsilon - w)}$$

v is defined by equation (6.2)

A and B are defined (J 4) by the density-of-states function (eqn. (1.5)) :

B.

$$g(\varepsilon) = kT\, g(E) = n_o \left(A \varepsilon^{1/2} + B \varepsilon^{3/2} \right)$$

where $\varepsilon = E / kT$, E being the energy from the conduction or valence band edge, measured into the appropriate band.

The suffices C , V , F , D , A denote conduction and valence bands, Fermi level and donor and acceptor levels .

A and B are given by the following formulae :

$$A = \left(m_d / m_o \right)^{3/2}$$

For parabolic bands, B = 0

For spherical, non-parabolic bands (K 3) e.g. InSb :

$$B = \frac{5}{2} \left(\frac{m_d}{m_o} \right)^{3/2} \frac{kT}{E_g^*} \qquad (K\,8,\ J\,4)$$

For ellipsoidal, non-parabolic bands (C 2) e.g. PbTe :

$$B = \frac{5}{3} \left(\frac{m_d}{m_o} \right)^{3/2} \left(1 + \frac{u}{5} \right) \frac{kT}{E_g^*} \qquad (A\,7,\ R\,4)$$

where $u = \dfrac{m_L(\text{conduction band edge})}{m_L(\text{valence band edge})}$

E_g^* is the effective interaction energy gap (D 3)

Equation (B.1) is first of all solved (by iteration) for the bulk of the semiconductor (flat bands), with $\rho = 0$. The intrinsic Fermi level E_i is found by setting $N_A = N_D = 0$. With given values of N_A and N_D , the actual Fermi level E_F is then calculated. n_i , n_b and p_b are next obtained, using equations (B.4) and (B.5) with $v = 0$.

Using Poisson's equation (6.3) and integrating with respect to z , eqn. (B.1) (with B.2 to B.5) becomes :

$$\frac{dv}{dz} = \frac{F(v)}{L} = \frac{1}{L} \left\{ \frac{N_D}{n_o} \ln \left[\frac{1 + \frac{1}{2} \exp(w_{DF} - v)}{1 + \frac{1}{2} \exp(w_{DF})} \right] \right.$$

$$\left. + \frac{N_A}{n_o} \ln \left[\frac{1 + \frac{1}{2} \exp(w_{FA} + v)}{1 + \frac{1}{2} \exp(w_{FA})} \right] + \frac{2}{3} A_v \left[F_{\frac{3}{2}}(-v - w_{FV}) - F_{\frac{3}{2}}(-w_{FV}) \right] \right.$$

contd.

$$+ \frac{2}{5} B_V \left[F(-v - w_{FV}) - F(-w_{FV}) \right] + \frac{2}{3} A_C \left[F(-v - w_{CF}) - F(-w_{CF}) \right]$$

$$+ \frac{2}{5} B_C \left[F(v - w_{CF}) - F(-w_{CF}) \right] \qquad \text{(B.6)}$$

For a given value of v_s, the space charge parameters are then evaluated.

Q_{sc} is obtained from equation (6.10), using eqn.(B.6) with $v = v_s$.

From equations (6.11) and (6.8),

$$\left.\begin{aligned} \Delta N &= L \int_0^{v_s} \frac{n - n_b}{F(v)} \, dv \\ \Delta P &= L \int_0^{v_s} \frac{p - p_b}{F(v)} \, dv \end{aligned}\right\} \qquad \text{(B.7)}$$

ΔN and ΔP are computed using equations (B.7) by numerical integration; the values of n, p, and F(v) for each value of v are obtained from equations (B.4), (B.5), and (B.6).

$\Delta\sigma$ and $\Delta R\sigma^{-2}$ are calculated using equations (6.20) and (6.21).

The space charge parameters are re-calculated at intervals of Δv_s over the required range of surface potential.

Further details of the theory and computer calculation are given by Juhasz (J 4).

APPENDIX C

Surface transport theory

The following is a brief summary of the theories put forward to account for the motion of current carriers near the surface of a metal or a semiconductor.

When a carrier collides with an external surface, its energy is conserved (on the average). But if the surface acts as a scattering centre, the thermal momentum of the carrier may be randomised in direction. When carriers in the bulk of the material have a net component of momentum (drift momentum) parallel to the surface (e.g. due to an externally-applied electric field) this is wholly or partially destroyed by surface scattering, leading to a reduced electrical mobility for carriers near the surface.

The magnitude of this effect was first calculated by J.J. Thomson (T 3) for metals, using the Drude (kinetic) theory of conduction. He assumed that the drift momentum of an electron is completely destroyed (diffuse scattering) upon collision with the surface, and obtained the following formula for the conductivity of a film of thickness t :

$$\frac{\sigma}{\sigma_b} = \frac{t}{2\,l}\left[\log_e \frac{l}{t} + \frac{3}{2}\right] \qquad (C.1)$$

where σ_b and l are the bulk conductivity and mean free path.

The problem was treated more rigourously by Fuchs (F 6) by solving the Boltzmann transport equation (B 2) :

$$\underline{a} \cdot \mathrm{grad}_c f + \underline{c} \cdot \mathrm{grad}_r f = -\frac{f - f_o}{\tau} = -\frac{f_1}{\tau} \qquad (C.2)$$

where f and f_o are the distribution functions with and without current flow, τ is the (bulk) relaxation time, $\underline{a}$ is the acceleration and $\underline{c}$ the total velocity of an electron.

Diffuse surface scattering is included as a boundary condition, i.e. $f_1(c_z, z) = 0$ for $c_z > 0$, $z = 0$

C.

The solution can be written approximately :

$$\frac{\sigma}{\sigma_b} = 1 - \frac{3}{8k} \quad \text{for} \quad k = \frac{t}{l} >> 1$$
$$\frac{\sigma}{\sigma_b} = \frac{3}{4k} \log\left(\frac{1}{k}\right) \quad \text{for} \quad k << 1 \qquad (C.4)$$

The solution was later generalised to include partially-specular reflection, the boundary condition being :

$$f_1 (c_z > 0 , \; z = 0) = p \; f_1 (c_z < 0 , \; z = 0) \qquad (C.5)$$

giving solutions :

$$\frac{\sigma}{\sigma_b} = 1 - \frac{3}{8k} \cdot (1 - p) \quad \text{for} \quad k >> 1$$
$$\frac{\sigma}{\sigma_b} = \frac{3}{4} \cdot \frac{1 + p}{1 - p} \cdot k \log k \quad \text{for} \quad k << 1 \qquad (C.6)$$

Verification of these expressions is difficult, because very thin films must be used, which normally contain a high density of defects. But in 1949, Andrews (using Sn foil and Hg wires below $4\,^{\circ}K$) obtained good agreement with equations (C.6), assuming that $p = 0$ i.e. perfectly-diffuse scattering.

The theory was extended by Sondheimer (S 24) to include the effect of a magnetic field on the conductivity and Hall coefficient, as a function of film thickness. His conclusions were verified by Babinski and Siebermann (with Na wire at $1\,^{\circ}K$).

To obtain a solution of (C.2) which applies to semiconductors, a correct form of the equilibrium distribution function f_o must be chosen, and allowance made for band bending at the surface. This was done for diffuse surface scattering by Schrieffer (S 8), using Boltzmann statistics for f_o and considering only carriers which are confined to a potential well (accumulation or inversion layer) near the surface. An effective conductivity mobility $\mu(\text{eff})$ for these carriers was obtained, assuming a linear potential variation, and also for the exact potential variation given by Poisson's equation. In the former case,

$$\frac{\mu(\text{eff})}{\mu_b} = 1 - \exp(\alpha^2) \; (1 - \text{erf} \, \alpha)$$

C.

where $\alpha = \dfrac{\sqrt{2\, m_i\, kT}}{q\, E_s\, \tau}$

These equations received some experimental confirmation (M 5) but for Si and Ge surface scattering was found to be only partly diffuse (see M 5) .

This treatment was extended by Zemel (Z 2) to include the Hall coefficient and Hall mobility μ_H . For the case of a linear potential well, he obtained :

$$\frac{\mu_H(\text{eff})}{\mu_{Hb}} = \left[1 - \frac{2\alpha}{\sqrt{\pi}} - (1 - 2\alpha^2)\exp(\alpha^2)\,(1 - \operatorname{erf}\alpha)\right]^{\frac{1}{2}}$$

For large α (small potential gradient) , $\mu_H(\text{eff}) \doteqdot \mu(\text{eff})$
For $\alpha \leqslant 1$, $\mu_H(\text{eff}) \doteqdot \frac{\sqrt{\pi}}{2}\,\mu(\text{eff}) \doteqdot 0{\cdot}87\,\mu(\text{eff})$

In 1960 , Greene, Frankl and Zemel (G 8) solved the Boltzmann equation in terms of the surface mobility μ_s (see page 159) for the Poisson potential, using non-degenerate statistics but including scattering of 'bulk' carriers not confined to a potential well. μ_s / μ_b was obtained as a function of u_s and u_b ; it has also been given in terms of v_s and u_b (M 5) . Greene, Frankl and Zemel also considered partially specular scattering, and the case of very thin films where the thickness is comparable with the Debye length. Amith (A 11) obtained solutions for the Hall and field-effect mobilities, using a truncated linear potential.

Flietner (F 2) has pointed out that the solution of Greene, Frankl and Zemel implies a mobility cusp (discontinuity in $d\mu_s / d\,v_s$) at $v_s = 0$. However, this could not be observed experimentally (Davis, 1964). Greene (G 7) modified the Fuchs boundary condition (equation C.5) to allow variation of the reflectivity parameter p with direction relative to the surface; this enables the absence of a mobility cusp to be explained. The parameter p has also been shown (G 7, G 9) to be different from the kinetic specularity w (the probability of specular reflection).

C.

The above treatments all assume Maxwell-Boltzmann (non-degenerate) statistics, that effective mass is independent of energy (parabolic bands) and direction (spherical constant-energy surfaces), and that the relaxation time τ is energy-independent.

However, Greene has solved the Boltzmann equation for a degenerate semiconductor (with isotropic, energy-independent m^* and τ). Juhasz (J 4) obtained a solution for a degenerate semiconductor with a non-parabolic but spherical band, such as the conduction band in InSb . A solution has also been attempted for non-spherical energy surfaces (H 2, P 15) ; in this case, mobility can be reduced even for a perfectly specular surface, since momentum but not velocity parallel to the surface is conserved. The results were confirmed experimentally (F 4) .

Calculations have also been carried out using an energy-dependent bulk relaxation time (G 6) .

BRIT. J. APPL. PHYS., 1967, VOL. 18. PRINTED IN GREAT BRITAIN

Epitaxial films of PbTe, PbSe and PbS grown on mica substrates

R. F. EGERTON and C. JUHASZ

Materials Section, Department of Electrical Engineering, Imperial College, London

MS. received 13*th March* 1967

Abstract. High-mobility (111) films of PbTe, PbSe and PbS were obtained by evaporation on to mica, followed in some cases by annealing beneath a layer of insulator. Long-term changes in the electrical properties have been investigated during storage in air.

Thin films of PbS giving a single-crystal diffraction pattern were reported by Elleman and Wilman (1948). More recent investigations (Makino 1964, Zemel *et al.* 1965, Bylander and Rodolakis 1965) have established that epitaxial films of PbS, PbSe and PbTe can be grown, having semiconducting properties closely approaching those of the bulk compounds. Because of the high values of carrier mobility obtainable these materials offer interesting possibilities for use in thin-film transistors (Pennebaker 1965, Skalski 1965). This note reports on single-crystal films of (111) PbTe, PbSe and PbS prepared by evaporation on to freshly-cleaved mica.

Small lumps of the compound were sublimed *in vacuo* from a small silica tube surrounded by a spiral heater of tantalum wire. The substrate temperature was controlled by radiation from an electrically heated strip of Mo foil, the back of the mica having been painted with a colloidal suspension of graphite, in which was embedded the tip of a wire thermocouple. Most of the films were deposited at a rate of 4 Å sec^{-1} to a thickness of about 4000 Å, the pressure during evaporation being below 5 μtorr.

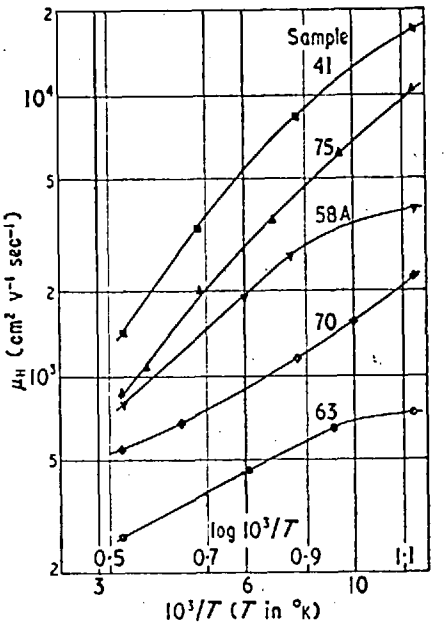

μ_H plotted against log ($10^3/T$) for different films.

The films were scratched through to form a bridge pattern for Hall-effect measurements and connecting wires soldered with In or In–Bi alloy. Samples were mounted, in air, between the pole pieces of a 2 kG magnet, and d.c. conductivity and Hall voltages measured between room temperature and 77°K. The Hall coefficient and Hall mobility, defined by $\mu_H = R_H\sigma$, were calculated.

In most of the films R_H was approximately constant over the whole temperature range. The figure shows μ_H plotted against reciprocal temperature for 5 samples of different types. Carrier concentrations and substrate thermocouple temperatures for these particular specimens are given in the table.

Sample	Material	Carrier conc. (cm^{-3})	Substrate temp. (°c)	Comments
41	PbTe	$n = 5{\cdot}0 \cdot 10^{17}$	260	Annealed under SiO
70	PbTe	$p = 1{\cdot}9 \cdot 10^{17}$	260	
75	PbSe	$n = 4{\cdot}7 \cdot 10^{17}$	300	Annealed under SiO
58A	PbSe	$p = 5{\cdot}0 \cdot 10^{17}$	250	
63	PbS	$n = 6{\cdot}0 \cdot 10^{18}$	230	

The values of μ_H are comparable with those achieved for similar films on NaCl substrates (Zemel *et al.* 1965) and for n-type PbTe on mica (Makino 1964), and at room temperature are within a factor of 2 of some of the best bulk specimens (Allgaier and Scanlon 1958). Carrier concentrations are generally lower than those obtained previously.

Some of the films were covered with a protective layer of evaporated SiO and annealed at 400°C for several minutes, as described elsewhere (Juhasz and Anderson 1967). This has the effect of improving the mobility, which in many cases follows a $T^{-5/2}$ law near room temperature, with some decrease in the magnitude of the exponent at lower temperatures.

Changes in the value of R_H have been observed in unprotected films over a period of several months after deposition. In the case of n-type films, R_H increases and the sample eventually appears p-type. For p-type films the change is generally less, and may be in either direction. Storing the specimens in a chamber evacuated by a rotary pump has no effect on this ageing. The most probable explanation would seem to be that the films gradually absorb oxygen, which is known to be a p-type dopant in PbTe (Bode and Levinstein 1954) since it is likely that the surface is covered by a monolayer of oxygen atoms, even at pressures of about 0·1 torr (Green and Lee 1966). Preliminary experiments suggest that these changes do not occur when a film is kept in a high vacuum system.

In the case of initially n-type PbSe films which have been stored for some time, R_H changes from positive to negative values as the temperature is lowered. This has been observed recently by Zemel (1966), and appears to be explicable only if an impurity (e.g. oxygen) gradient exists within the film.

Films protected with a SiO layer show R_H practically unaltered after six months storage in air, the only significant change being in μ_H, usually a decrease of the order of 10–20% over the whole temperature range.

Field-effect measurements are being carried out to investigate the mica–PbTe interface. The conductivity minimum can be reached on some of the purest films, the surface-state density being low enough to permit appreciable conductivity modulation.

Acknowledgments

The authors wish to acknowledge the assistance of the Science Research Council who provided a grant for this work, and the continuous encouragement of Professor J. C. Anderson. One of us (C.J.) would like to thank Dr. J. N. Zemel for many stimulating discussions on the lead salts.

References

ALLGAIER, R. S., and SCANLON, W. W., 1958, *Phys. Rev.*, **111**, 1029–37.
BODE, D. E., and LEVINSTEIN, M., 1954, *Phys. Rev.*, **96**, 259–65.
BYLANDER, E. G., and RODOLAKIS, A. S., 1965, *Proc. Inst. Elect. Electron. Engrs*, **53**, 395–6.
ELLEMAN, A., and WILMAN, H., 1948, *Proc. Phys. Soc.*, **61**, 164–74.
GREEN, M., and LEE, M. J., 1966, *J. Phys. Chem. Solids*, **27**, 797–804.
JUHASZ, C., and ANDERSON, J. C., 1967, *Proc. 3rd Int. Vacuum Congr., Stuttgart*, 1965 (London: Pergamon).
MAKINO, Y., 1964, *J. Phys. Soc. Japan*, **19**, 1242.
PENNEBAKER, W. B., 1965, *Solid-State Electron.*, **5**, 509–15.
SKALSKI, J. F., 1965, *Proc. Inst. Elect. Electron. Engrs*, **53**, 1792.
ZEMEL, J. N., JENSEN, J. D., and SCHOOLAR, R. B., 1965, *Phys. Rev.*, **140**, 330–42.
ZEMEL, J. N., 1966, *The Use of Thin Films in Physical Investigations* (London: Academic Press), p. 341.

REFERENCES

(A 1) AIGRAIN, P. and BALKANSKI, M., 'Constantes Sélectionées Relatives aux Semiconducteurs', Pergamon Press, 1961

(A 2) AIRAPETYANTS, S.V. et al, Soviet Phys.- Solid State, 8, 1069 (1966)

(A 3) ALEKSEEVA, G.T. et al, Soviet Phys.- Solid State 8, 2258 (1967)

(A 4) ALLGAIER, R.S., Phys. Rev. 112, 828 (1958)

(A 5) ALLGAIER, R.S., Proc. Int. Conf. Semic. Phys., Prague, 1960. p. 1037

(A 6) ALLGAIER, R.S., J. Appl. Phys. 32, 2185 (1961)

(A 7) ALLGAIER, R.S., Phys. Rev. 152, 808 (1966)

(A 8) ALLGAIER, R.S. and HOUSTON, B.B., Proc. Int. Conf. Semic. Phys., Exeter, 1962. p. 172

(A 9) ALLGAIER, R.S. and HOUSTON, B.B., J. Appl. Phys. 37, 1 (1966)

(A 10) ALLGAIER, R.S. and SCANLON, W.W., Phys. Rev. 111, 1029 (1958)

(A 11) AMITH, A., J. Phys. Chem. Solids 14, 271 (1960)

(A 12) ANDREEV, A.A., Soviet Phys.- Solid State 8, 2256 (1967)

(A 13) AVERKIN, A.A. and DERMENZHI, P.G., Soviet Phys.- Solid State 8, 79 (1966)

(A 14) AVERKIN, A.A. et al, Soviet Phys.- Solid State 3, 1354 (1961)

(A 15) AVERKIN, A.A. et al, Proc. Int. Conf. Semic. Phys., Exeter, 1962. p. 690

(B 1) BARDEEN, J., Phys. Rev. 71, 717 (1947)

(B 2) BEER, A.C., 'Galvanomagnetic Effects in Semiconductors' Solid State Physics (Suppl. 4), Academic Press, London (1963)

(B 3) BELL, D.G. et al, Proc. Roy. Soc. A 217, 71 (1953)

(B 4) BEREZHNAYA, I.A., Russian J. Phys. Chem. 36, 1500 (1962)

(B 5) BERZ, F. Proc. Phys. Soc. 71, 275, 458 (1958)

(B 6) BIS, R.F. and ZEMEL, J.N., J. Appl. Phys. 37, 1 (1966)

(B 7) BLOEM, J. and KRÖGER, F.A., Philips Res. Rep. 12, 281, 303 (1957)

(B 8) BODE, D. and LEVINSTEIN, H., Phys. Rev. 96, 259 (1954)

(B 9) BOLTAKS, B.I. 'Diffusion in Semiconductors', Infosearch Ltd., London (1963)

(B 10) BRAUN, F., Ann. Phys. Chem. 153, 556 (1874)

(B 11) BREBRICK, R.F. and SCANLON, W.W., Phys. Rev. 96, 598 (1954)

(B 12) BREBRICK, R.F. and STRAUSS, A.J., J. Phys. Chem. 40, 3230 (1964)

(B 13) BRODSKY, M.H. and ZEMEL, J.N., Phys. Rev. 155, 780 (1967)

(B 14) BROUDY, R. and LEVINSTEIN, H., Phys. Rev. 94, 285, 290 (1954).

(B 15) BURSTEIN, E., Proc. Int. Conf. Phys. of Semic., Paris (1964) p. 1066

(B 16) BURSTEIN, E. et al, Proc. Int. Conf. Phys. of Semic., Paris (1964). p. 1065

(B 17) BYKOVA, T.T., Soviet Phys. - Solid State 8, 959 (1966)

(B 18) BYKOVA, T.T. and VINOKUROV, I.V., Soviet Phys. - Solid State 7, 2103 (1966)

(B 19) BYLANDER, E.G. and RODOLAKIS, A.S., Proc. I.E.E.E. 53, 395 (1965)

(C 1) CHASMAR, R.P., Nature (London) 161, 281 (1948)

(C 2) COHEN, M.H., Phys. Rev. 121, 387 (1961)

(C 3) CONKLIN, J.B. et al, Phys. Rev. A 137, 1282 (1965)

(C 4) CROCKER, A.J., J. Phys. Chem. Solids, 28, 1903 (1967)

(C 5) CROCKER, A.J., Private Communication

(C 6) CROCKER, A.J. and ROGERS, L.M., Brit. J. Appl. Phys. 18, 563, (1967)

(C 7) CUFF, K.F. et al , J. Appl. Phys. 32 , 2179 (1961)

(C 8) CUFF, K.F. et al , Proc. Int. Conf. Semic. Phys., Exeter , 1962 . p. 316

(C 9) CUFF, K.F. et al , Proc. Int. Conf. Semic. Phys., Paris , 1964 . p. 677

(D 1) DEVYATKOVA, E.D. and SMIRNOV, I.A. , Soviet Phys. - Solid State 3 , 1675 (1962)

(D 2) DEXTER, D.L. and SEITZ, F. , Phys. Rev. 86 , 964 (1952)

(D 3) DIMMOCK, J.O. and WRIGHT, G.B. , Phys. Rev. 135 , A 821 (1964)

(D 4) DIXON, J. and RIEDL, H. , Proc. Int. Conf. Semic. Phys., Exeter , 1962 . p. 179

(D 5) DIXON, J. and RIEDL, H. , Phys. Rev. 138 , A 873 (1965)

(D 6) DUBROVSKAYA, I.N. and RAVICH, Yu.I. , Soviet Phys. - Solid State 8 , 1160 (1966)

(E 1) EARLY, J.W. , Amer. Min. 35 , 338 (1950)

(E 2) EHRENBERG, W. , 'Electric Conduction in Semiconductors and Metals' , Clarendon Press, Oxford (1958)

(E 3) EHRENBERG, W. and HIRSCH, J. , Proc. Phys. Soc. B 64 , 700 (1951)

(E 4) EHRENREICH, H. and OVERHAUSER, A.W., Phys. Rev. 104 , 331, 649 (1956)

(E 5) ELLEMAN, A. and WILMAN, H. , Proc. Phys. Soc. 61 , 164 (1948)

(E 6) EVANS, R.C. , 'An Introduction to Crystal Chemistry' , Cambridge University Press (1939)

(F 1) FINLAYSON, D. and GRIEG, D., Proc. Phys. Soc. B 69 , 796 (1956) .

(F 2) FLIETNER, H. , Physica Status Solidi 1 , 484 (1961)

(F 3) FRANKL, D.R. , 'Electrical Properties of Semiconductor Surfaces' , Pergamon Press , 1967

(F 4) FRIEDMAN, A.N. and KOENIG, S.H. , I.B.M. J. Res. and Dev. 4 , 158 (1960)

(F 5) FRÖHLICH, H. and MOTT, N.F. , Proc. Roy. Soc. A171 , 496 (1939)

(F 6) FUCHS, K. , Proc. Camb. Phil. Soc. 34 , 100 (1938)

(G 1) GERSHSTEIN, E.Z. et al , Soviet Phys. - Technical Physics 2 , 2302 (1957)

(G 2) GIBSON, A.F. , Proc. Phys. Soc. B 65 , 378 (1952)

(G 3) GOBRECHT, H. et al , Zeit. Phys. 187 , 232 (1965)

(G 4) GREEN, M. and LEE, M.J. , J. Phys. Chem.Solids 27 , 797 (1966) .

(G 5) GREENE, R.F. , Phys. Rev. 131 , 592 (1963)

(G 6) GREENE, R.F. , Surface Science 2 , 101 (1964)

(G 7) GREENE, R.F. , Phys. Rev. 141 , 687, 690 (1966)

(G 8) GREENE, R.F. et al , Phys. Rev. 118 , 947 (1960)

(G 9) GREENE, R.F. and O'DONNELL, R.W. , Phys. Rev. 147 ,599 (1965)

(G 10) GÜNTHER, K-G. , in 'The Use of Thin Films in Physical Investigations' , ed. J.C. Anderson . Academic Press, 1966 .

(H 1) HALPERN, V. , Brit. J. Appl. Phys. 18 , 163 (1967)

(H 2) HAM, F.S. and MATTIS, D.C. , I.B.M. J. Res. and Dev. 4 , 143 , (1960)

(H 3) HARADA, R.H. and MINDEN, H.T. , Phys. Rev. 102 , 1258 (1956)

(H 4) HERRING, C. , Bell Syst. Tech. J. 34 , 237 (1955)

(H 5) HERRING, C. , J. Appl. Phys. 31 , 1939 (1960)

(H 6) HILLENBRAND, L.J. , J. Phys. Chem. 41 , 3971 (1964)

(H 7) HINTENBERGER, H. , Z. Phys. 119 , 1 (1942)

(H 8) HIRAHARA, E. and MURAKAMI, M. , J. Phys. Soc., Japan 9 , 671 (1954)

(H 9) HIRSCH, P.B. et al , 'Electron Microscopy of Thin Crystals' Butterworths , London (1965)

(H 10) HIRTH, J.P. et al , in 'Single-Crystal Films' (page 9) Ed. M.H. Francombe and H. Sato , Pergamon Press (1964)

(H 11) HLÁSNIK, I. , Solid State Electronics 8 , 461 (1965)

(H 12) HOWARTH, D. and SONDHEIMER, E. , Proc. Roy. Soc. A 219 , 53 (1953) .

(H 13) HUMPHREY, J.N. et al , Phys. Rev. 90 , 111 (1953)

(H 14) HUNG, C. and GLIESSMAN, J. , Phys. Rev. 96 , 1226 (1954)

(J 1) JACOBS, M.H. et al , Phil. Mag. 13 , 129 (1966)

(J 2) JOHNSON, G.W. , J. Electronics & Control 12 , 421 (1962)

(J 3) JONES, R.H. , Proc. Phys. Soc. B 70 , 704 (1957)

(J 4) JUHASZ, C. , Ph. D. Thesis , London University (1967)

(J 5) JUHASZ, C. and ANDERSON, J.C. , Trans. 3rd Vacuum Congress, Stuttgart , 1965

(K 1) KANAI, Y. and SHOHNO, K. , Jap. J. Appl. Phys. 2 , 6 (1963)

(K 2) KANAI, Y. et al , J. Appl. Phys. suppl. 32 , 2146 (1961)

(K 3) KANE, E.O. , J. Phys. Chem. Solids 1 , 249 (1957)

(K 4) KAY, D.H. , 'Techniques for Electron Microscopy' , Blackwell , 1965

(K 5) KEHOE, R.B. et al , Phil. Mag. 1 , 783 (1956)
Brit. J. Appl. Phys. 7 , 29 (1956)

(K 6) KINGSTON, R.H. and NEUSTADTER, S.F. , J. Appl. Phys. 26 , 718 (1955)

(K 7) KOBAYASHI, A. et al , J. Phys. Chem. Solids 14 , 37 (1960)

(K 8) KOLODZIEJCZAK, J. , Acta Phys. Polon. 20 , 289 (1961)

(K 9) KOVAL'CHIK, T.L. and MASLAKOVETS, I.P. , Soviet Phys. - Technical Physics 1 , 2337 (1957)

(K 10) KRÖGER, F.A. , 'The Chemistry of Imperfect Crystals' , North Holland (1964)

(L 1) LASSER, M.E. and LEVINSTEIN, H., Phys. Rev. 96, 47 (1954)

(L 2) LAWSON, W.D., J. Appl. Phys. 22, 1444 (1951)

(L 3) LAWSON, W.D., J. Appl. Phys. 23, 495 (1952)

(L 4) LEE, M.J., Private Communication

(L 5) LEHOVEC, K. and SLOBODSKOY, A., Solid State Electronics 3, 45, (1961)

(L 6) LEWIS, B. and CAMPBELL, D.S., J. Vacuum Science and Technology 4, 209 (1967)

(L 7) LEWIS, B. and STIRLAND, D.J., 'Growth and Morphology of Epitaxial PbTe Deposits on Rocksalt', to be published

(L 8) LILE, D.L., Ph.D. Thesis, London University (1968)

(L 9) LIN, P.J. and KLEINMAN, L., Phys. Rev. 142, 478 (1966)

(L 10) LINDLEY, D.H. and BANBURY, P.C., Proc. Phys. Soc. B 74, 359 (1959)

(L 11) LOW, F. and PINES, D., Phys. Rev. 98, 414 (1955)

(L 12) LOW, G.G.E., Proc. Phys. Soc. B 68, 1154 (1955)

(L 13) LOW, G.G.E., Proc. Phys. Soc. B 69, 1331 (1956)

(L 14) LYDDANE, R. et al, Phys. Rev. 59, 673 (1941)

(M 1) MACKINTOSH, I., Proc. Phys. Soc. B 69, 115 (1955)

(M 2) MACKINTOSH, I.M., J. Electronics 1, 554 (1956)

(M 3) MAKINO, Y., Jap. J. Appl. Phys. 19, 580 (1964)

(M 4) MAKINO, Y. and HOSHINA, T., J. Phys. Soc., Japan 19, 1242 (1964)

(M 5) MANY, A. et al, 'Semiconductor Surfaces', North Holland Publ. Co., 1965.

(M 6) MARSCHALL, N., Physics Letters 24, A 73 (1967)

(M 7) MARTIN, D.P., Ph.D. Thesis, London University (1967)

(M 8) MATTHEWS, J.W., Phil. Mag. 6, 1347 (1961)

(M 9) MATTHEWS, J.W. and ISEBECK, K., Phil. Mag. 8, 469 (1963)

(M 10) van der MERWE, J.H. in 'Single-Crystal Films', (page 139) ed. M.H. Francombe and H. Sato, Pergamon, 1964

(M 11) MILLER, E. et al, J. Appl. Phys. 32, 2457 (1961)

(M 12) MOCHAN, I.V. and SMIRNOVA, T.V., Soviet Phys. - Solid State 3, 1936 (1962)

(M 13) MONTGOMERY, H.C., Phys. Rev. 106, 441 (1957)

(M 14) MOSS, T.S., Proc. I.R.E. 43, 1869 (1955)

(M 15) MOSS, T.S., 'Optical Properties of Semiconductors', Butterworth Scientific Publications, 1959

(M 16) MOTT, N.F. and GURNEY, R.W., 'Electronic Processes in Ionic Crystals', Clarendon Press, Oxford, 1940

(M 17) MÜSER, H.A. et al, Physics Letters 11, 283 (1964)

(N 1) NESTERENKO, B.A., Soviet Physics - Solid State 5, 2341 (1964).

(N 2) NII, R., J. Phys. Soc., Japan 19, 58 (1964)

(N 3) NORRIKOVA, S.I. and ABRIKOSOV, N.Kl., Soviet Phys. - Solid State 5, 1397 (1964)

(P 1) PALATNIK, L.S. et al, Soviet Phys. - Solid State 7, 1374, (1965)

(P 2) PALIK, E.D. et al, Phys. Rev. 135, A 763 (1964)

(P 3) PAPARODITIS, C., 'Single-Crystal Films' (page 79) Ed. M.H. Francombe and H. Sato, Pergamon, 1964

(P 4) PASHLEY, D.W. and STOWELL, M.J., Phil. Mag. 8, 1605 (1963)

(P 5) PAUL, W. et al, Proc. Int. Conf. Semic. Phys., Exeter, 1962. p. 712

(P 6) PEARSON, G.L., Phys. Rev. 76, 459 (1949)

(P 7) PETRITZ, R.L., Phys. Rev. 104, 1508 (1956)

(P 8) PETRITZ, R.L., Phys. Rev. 110, 1254 (1958)

(P 9) PETRITZ, R.L. and LUMMIS, F., Phys. Rev. 105, 502 (1957)

(P 10) PETRITZ, R.L. and SCANLON, W. , Phys. Rev. 97 , 1620 (1955)

(P 11) PETRITZ, R.L. et al , in 'Semiconductor Surface Physics' , ed. R.H. Kingston , University of Pennsylvania Press, 1956 . p. 229

(P 12) PIPPARD, A.B. , 'The Dynamics of Conduction Electrons' , Blackie & Son , London (1965)

(P 13) POH, K.J. , M.Sc. Thesis , London University (1968)
D. I. C. Thesis , Imperial College (1968)

(P 14) PORTER, R.F. , J. Chem. Phys. 34 , 583 (1961)

(P 15) PRICE, P.J. , I.B.M. J. Res. & Dev. 4 , 152 (1960)

(P 16) PUTLEY, E.H. , Proc. Phys. Soc. B 65 , 388, 389 (1952)

(P 17) PUTLEY, E.H. , Proc. Phys. Soc. B 65 , 736 (1952)

(P 18) PUTLEY, E.H. , Proc. Phys. Soc. B 65 , 993 (1952)

(P 19) PUTLEY, E.H. , Proc. Phys. Soc. B 68 , 22 (1955)

(P 20) PUTLEY, E.H. , 'The Hall Effect and Related Phenomena' , Butterworths , London . (1960)

(R 1) RABII, S. , Phys. Rev. 167 , 801 (1968)

(R 2) RAVICH, Yu.I. , Soviet Phys - Solid State 7 , 1466 (1965)

(R 3) REDIKER, R.H. and CALAWA, A.R. , J. Appl. Phys. suppl. 32 , 2189 (1961)

(R 4) ROGERS, L.M. , Brit. J. Appl. Phys. 18 , 1227 (1967)

(S 1) SAAKYAN, V.A. et al , Soviet Phys. - Solid State 7 , 2541 , (1966)

(S 2) SATO, Y. et al , Jap. J. Appl. Phys. 2 , 11 (1963)

(S 3) SATO, Y. et al , J. Phys. Soc., Japan 19 , 24 (1964)

(S 4) SCANLON, W.W. , Phys. Rev. 92 , 1573 (1953)

(S 5) SCANLON, W.W. , in 'Semiconductor Surface Physics' , ed. R.H. Kingston , University of Pennsylvania Press, 1956 . p. 238

(S 6) SCANLON, W.W. , Phys. Chem. Solids , 423 (1959)

(S 7) SCANLON, W.W. , Phys. Rev. 126 , 509 (1962)

(S 8) SCHRIEFFER, J. , Phys. Rev. 97 , 641 (1955)

(S 9) SEIWATZ, R. and GREEN, M. , J. Appl. Phys. 29 , 1304 (1958)

(S 10) SELLA, C. and TRILLAT, J.J. in 'Single-Crystal Films' , ed. M.H. Francombe and H. Sato , Pergamon (1964) . p. 201

(S 11) SEMILETOV, S.A. , Soviet Phys. - Crystallography 9 , 65 (1964) .

(S 12) SEMILETOV, S.A. and VORONINA, I.P. , Soviet Physics - Crystallography 9 , 405 (1964)

(S 13) SEMILETOV, S.A. and VORONINA, I.P. , Soviet Physics - Doklady 8 , 960 (1964)

(S 14) SHOCKLEY, W. , Phys. Rev. 56 , 317 (1939)

(S 15) SHOCKLEY, W. and PEARSON, G.L. , Phys. Rev. 74 , 232 (1948)

(S 16) SHOGENJI, K. and UCHIYAMA, S. , J. Phys. Soc., Japan 12 , 252 (1957)

(S 17) SILVERMAN, S.J. and LEVINSTEIN, H. , Phys. Rev. 94 , 871 (1954) .

(S 18) SIMPSON, O. , Nature 160 , 791 (1947)

(S 19) SKALSKI, J. , Proc. I.E.E.E. 53 , 1792 (1965)

(S 20) SMIRNOV, I.A. , Soviet Phys. - Solid State 2 , 1793 (1960)

(S 21) SMITH, R.A. , Advances in Physics 2 , 321 (1953)

(S 22) SMITH, R.A. , Physica 10 , 910 (1954)

(S 23) SMITH, R.A. , 'Semiconductors' , Cambridge University Press, 1964

(S 24) SONDHEIMER, E.H. , Advances in Physics 1 , 1 (1952)

(S 25) SOULE, D.E. and CASHMAN, R,J. , Phys. Rev. 93 , 635 (1954)

(S 26) STARIK, P.M . , Soviet Phys. - Solid State 7 , 1812 (1966)

(S 27) STERN, F. and HOWARD, W.E. , Phys. Rev. 163 , 816 (1967)

(S 28) STILES, P.J. et al , J. Appl. Phys. suppl 32 , 2174 (1961)

(S 29) STILES, P.J. et al , Proc. Int. Conf. Semic. Phys., Exeter, 1962 . p. 577

(S 30) STOWELL, M.J. and LAW, T.J. , Phys. Status Solidi 16 , 117 (1966) .

(S 31) STREL'CHENKO, E.G. , Soviet Phys.-Solid State 8 , 772 (1966)

(S 32) SUNDQUIST, B.E. , Acta. Met. 12 , 585 (1964)

(T 1) TAMM, I.E. , Z. Phys. 76 , 849 (1932)

(T 2) TAUBER, R. et al , J. Appl. Phys. 37 , 4855 (1966)

(T 3) THOMSON, J.J. , Proc. Camb. Phil. Soc. 11 , 120 (1901)

(T 4) TOLPYGO, K.B. and FEDORCHENKO, A.M. , Soviet Phys. - J.E.T.P. 4 , 713 (1957)

(T 5) TORREY, H.C. and WHITMER, C.A. , 'Crystal Rectifiers' ; McGraw - Hill , New York (1948)

(U 1) UCHIYAMA, S. and SHOGENJI, K. , J. Phys. Soc., Japan 12 , 431 (1957)

(W 1) WAGNER, C. , Z. Chem. Phys. B 11 , 163 (1930)
B 22 , 195 (1933)

(W 2) WALTON, D. , J. Chem. Phys. 37 , 2182 (1962)

(W 3) WAXMAN, A. et al , J. Appl. Phys. 36 , 168 (1965)

(W 4) WEINBERG, I. , J. Chem. Phys. 36 , 1112 (1962)

(W 5) WILCOCK, D. , Ph. D. Thesis , London University (1967)

(W 6) WILCOCK, D. , Private Communication

(W 7) WILMAN, H. , Proc. Phys. Soc. 60 , 117 (1948)

(W 8) WYCKOFF, R.W.G. , 'Crystal Structures' , Interscience, New York.

(Z 1) ZEMEL, J.N. in 'Semiconductor Surface Physics' , ed. R.H. Kingston , University of Pennsylvania Press, 1957 . p. 193

(Z 2) ZEMEL, J.N. , Phys. Rev. 112 , 762 (1958)

(Z 3) ZEMEL, J.N. , Proc. Int. Conf. Phys. of Semic. , Paris , 1964 . p. 1061

(Z 4) ZEMEL, J.N. in 'The Use of Thin Films in Physical Investigations' , ed. J.C. Anderson , Academic Press, London (1966) . p. 319

(Z 5) ZEMEL, J.N. , 'Interaction of Oxygen at Pb Salt Surfaces', To be published .

(Z 6) ZEMEL, J.N. and VARELA, R. , J. Phys. Chem. Solids 14 , 142 (1960)

(Z 7) ZEMEL, J.N. et al , Phys. Rev. 140 , 330 (1965)

(Z 8) ZHITINSKAYA, M.K. et al , Soviet Phys. - Solid State 8 , 246 (1966)

(Z 9) ZIMAN, J.M. , 'Principles of the Theory of Solids' , Cambridge University Press , 1964 .